CLATHRIN - MEDIATED ENDOCYTOSIS, POST ENDOCYTIC TRAFFICKING AND THEIR REGULATORY CONTROLS IN PLANTS

by

MADHUMITHA NARASIMHAN

DECEMBER 2018

A thesis presented to the
Graduate School
of the
Institute of Science and Technology Austria, Klosterneuburg, Austria
in partial fulfillment of the requirements
for the degree of
Doctor of Philosophy

The dissertation of *Madhumitha Narasimhan*, titled *Clathrin-Mediated Endocytosis, post-endocytic trafficking and their regulatory controls in plants*, is approved by:

Supervisor: Jiri Friml, IST Austria, Klosterneuburg, Austria

Signature: _____

Committee Member: Eva Benkova, IST Austria, Klosterneuburg, Austria

Signature: _____

Committee Member: Daniel Van Damme, VIB/ Universiteit Gent, Belgium

Signature: _____

Exam Chair: Johann Danzl, IST Austria, Klosterneuburg, Austria

Signature: _____

I hereby declare that this dissertation is my own work and that it does not contain other people's work without this being so stated; this thesis does not contain my previous work without this being stated, and the bibliography contains all the literature that I used in writing the dissertation.

I declare that this is a true copy of my thesis, including any final revisions, as approved by my thesis committee, and that this thesis has not been submitted for a higher degree to any other university or institution.

I certify that any republication of materials presented in this thesis has been approved by the relevant publishers and co-authors.

Signature: _____

[Student Name]

February 4, 2019

Abstract

Clathrin-Mediated Endocytosis (CME) is an aspect of cellular trafficking that is constantly regulated for mediating developmental and physiological responses. The main aim of my thesis is to decipher the basic mechanisms of CME and post-endocytic trafficking in the whole multicellular organ systems of *Arabidopsis.* The first chapter of my thesis describes the search for new components involved in CME. Tandem affinity purification was conducted using CLC and its interacting partners were identified. Amongst the identified proteins were the Auxilin-likes1 and 2 (Axl1/2), putative uncoating factors, for which we made a full functional analysis. Over-expression of Axl1/2 causes extreme modifications in the dynamics of the machinery proteins and inhibition of endocytosis altogether. However the loss of function of the *axl1/2* did not present any cellular or physiological phenotype, meaning Auxilin-likes do not form the major uncoating machinery.

The second chapter of my thesis describes the establishment/utilisation of techniques to capture the dynamicity and the complexity of CME and post-endocytic trafficking. We have studied the development of endocytic pits at the PM – specifically, the mode of membrane remodeling during pit development and the role of actin in it, given plant cells possess high turgor pressure. Utilizing the improved z-resolution of TIRF and VAEM techniques, we captured the time-lapse of the endocytic events at the plasma membrane; and using particle detection software, we quantitatively analysed all the endocytic trajectories in an unbiased way to obtain the endocytic rate of the system. This together with the direct analysis of cargo internalisation from the PM provided an estimate on the endocytic potential of the cell. We also developed a methodology for ultrastructural analysis of different populations of Clathrin-Coated Structures (CCSs) in both PM and endomembranes in unroofed protoplasts. Structural analysis, together with the intensity profile of CCSs at the PM show that the mode of CCP development at the PM follows 'Constant curvature model'; meaning that clathrin polymerisation energy is a major contributing factor of membrane remodeling. In addition, other analyses clearly show that actin is not required for membrane remodeling during invagination or any other step of CCP development, despite the prevalent high turgor pressure. However, actin is essential in orchestrating the post-endocytic trafficking of CCVs facilitating the EE formation. We also observed that the uncoating process post-endocytosis is not immediate; an alternative mechanism of uncoating – Sequential multi-step process – functions in the cell.

Finally we also looked at one of the important physiological stimuli modulating the process – hormone, auxin. auxin has been known to influence CME before. We have made a detailed study on the concentration-time based effect of auxin on the machinery proteins, CCP development, and the specificity of cargoes endocytosed. To this end, we saw no general effect of auxin on CME at earlier time points. However, very low concentration of IAA, such as 50nM, accelerates endocytosis of specifically PIN2 through CME. Such a tight regulatory control with high specificity to PIN2 could be essential in modulating its polarity.

Acknowledgments

To my life coach – my dad. I owe you my success! I got up everyday - even on the toughest days of my life, simply because you could make me laugh about it all. You made the toughest goals easier; sometimes 'Riddikulus!'

To my darling mother and sister, Pri – you are just so pretty!

To my best friend, Lesia – you just made my life eventful by being part of my everyday. And to my dearest, Arun – for taking the Zen path instead of me. Maybe one day we will travel together; not yet.

To my mentor, Jiri Friml. I, forever, will wonder what you saw in me when you signed up to make me part of your science; and I forever am grateful for it.

My sincere gratitude to Roshan Prizak, Maciek Adamoski and Lanxin Li. We grew together throughout this remarkable scientific journey. Maciek, without those endless discussions with you, my science would have never evolved. Thanks for pushing my limits. And Lanxin, thanks for the essential discussions whenever I needed a parallel brain. I couldn't have done without you. Prizak, you have been my intellectual pillar; it has been an incredible learning experience. I am eternally grateful to you.

I thank Chai, Michal, Apurva and Keerthi. I could always count on you. With a special mention to Michal – for being a wonderful partner. We have waltzed, and watched each other grow; I thank you for making my life tolerable and meaningful.

I thank all my lab mates and ex-lab mates. I have consciously and unconsciously learnt from all of you. With special mention to Xixi, Shutang, Bin and Lesia – you have inspired me to work harder. I would never have persevered through my PhD, if I had not learnt how to from you. And thanks to Barbara and Lenka, you girls showed me how to be tough without a hint of bitterness. Also thanks for consistently rendering your scientific consult (with no fee).

I have had so many wonderful moments – scientific and non-scientific through my life at IST. I would like to specially mention Zusana - for being my partner for one of the best performances I had the opportunity to bring forth for the IST charity event; Lesia and Maciek - for organizing the finest parties to celebrate the best moments of my life.

I thank Fernando Aniento for his enthusiastic collaborations. I thank Eva Benkova and Daniel Van Damme for all the discussions and constructive criticisms. My eternal gratitude lies with Walter Kaufmann and the whole EM facility for their expert assistance; and also with the BIF for the consistent support.

My sincere gratitude to Alexandra Mally, Monika Hrtyan, Dorota Jaworska, Vlad Cozac, Ulrike Seiss and many more people from the Academic affairs and SSU who have rendered outstanding support that made my scientific career feasible.

I finally thank all my family members, friends and colleagues who have been part of my life in so many ways.

About the Author

Madhumitha Narasimhan completed her bachelors in Biotechnology at Kamaraj College of Engineering and Technology, and completed her Master1 (M1 level) in Interdisciplinary Approaches to Life Science (AIV) Master Program at Université Paris Diderot - Centre de Recherches Interdisciplinaires. She then joined IST Austria in September 2013. She did her rotations exploring the fields of Cell biology and Evolutionary biology before joining the group of Plant cell and developmental biology, headed by Prof. Jiri Friml. Her main research focus had been studying various aspects of clathrin-mediated endocytosis processes and trafficking pathways. She has presented her work in three international conferences. She has established Metal-Replica procedure to study clathrin-coated cesicles in planta with a close collaboration with the electron microscopic facility at IST.

List of Publications Appearing in Thesis

1. Adamowski, M., Narasimhan, M., Kania, U., Glanc, M., De Jaeger, G. and Friml, J., 2018. A Functional Study of AUXILIN-LIKE1 and 2, Two Putative Clathrin Uncoating Factors in Arabidopsis. *The Plant Cell*, pp.tpc-00785.
   http://www.plantcell.org

Manuscripts under preparation:

Narasimhan, M., Johnson, A., Kauffmann, W., Prizak, R., Matejovicova, L., Friml, J., A comprehensive study of clathrin-cediated endocytosis and trafficking *in planta*

Narasimhan, M., Johnson, A., Tan, S., Li, L., Verstraeten, I., Casillas-Perez, B., Rodriguez, Han, H., L., Himschoot, E., Sanchezs, J., Aniento, F., Friml, J., Regulation of PIN2 polarity by auxin through clathrin-mediated endocytosis

Table of Contents

List of Figures

List of Tables

List of Symbols/Abbreviations

ABA - Abscisic acid
AFCS - Alexa Fluor 647 – castasterone
AFM - Atomic Force Miscroscopy
ANTH - AP180 N-Terminal Homology
ATP - Adenosine Triphosphate
BAR - Bin/Amphiphysin/Rvs domain family
BFA - Brefeldin A
BiFC -Bimolecular Fluorescence Complementation
BR – Brassinolide
CCP – Clathrin-Coated Pit
CCSs - Clathrin-Coated Structure
CCV - Clathrin-Coated Vesicle
CLEM- Correleative Light-Electron Microscopy
CME - Clathrin-Mediated Endocytosis
COP1 - Coat Protein 1
DAPI - 4',6-diamidino-2-phenylindole
DMSO - Dimethyl Sulphoxide
dSTORM - direct Stochastic Optical Reconstruction Microscopy
EE – Early endosome
ENTH - EpsinR/CLINT/Enthoprotein
EtOH - ethanol
FCHo1/2 - Fer/Cip4 homology domain-only proteins 1 and 2
GA - Giberelic Acid
GA - Gluteraldehyde
GTP – Guanosine Triphosphate
IAA - Indole -3 Acetic Acid
Jasp - Jasplakinolide
LatB - Latrunculin B
LE - Late Endosome
LLSM - Lattice Light-Sheet Microscopy
LSM - Light-Sheet Microscopy
MVB - Multi Vesicular Body
NA -Numerical aperture
NAA - Naphthaleneacetic acid
NaCl - Sodium chloride
ns - not significant
PAMP - Pathogen-Associated-Molecular-Patters
PH - Pleckstrin homology
PI - Propidium iodide
PIns(4)P - Phosphotidyl Inositol (4) Phosphate
PIns(4,5)P_2 - Phosphotidyl Inositol (4,5) bis -phosphate
PM - Plasma membrane
pol-TIRF - Polarisation - Total Internal Reflection Fluorescence
PRR - Pattern Recognition Receptors
qRT-PCR - Real-Time Quantitative Reverse Transcription PCR
RAM - Root Apical Meristem

ROI - Region of interest
SA - Salicylic Acid
SEM - Scanning Electron Microscopy
SIM - Structured Illumination Microscopy
TEM - Transmission Electron Microscopy
TGN - Trans-Golgi Network
TIRF - Total Internal Reflection Fluorescence
TPC - TPLATE complex
VAEM - Variable Angle Epifluorescence Microscopy

Proteins often mentioned
ABD - Actin Binding Domain
Arf1 - ADP-Ribosylation Factor1
Axl - Auxilin-like
BRI - BR-INSENSITIVE
CHC - Clathrin Heavy Chain
CLC - Clathrin Light Chain
Drp - Dynamin related protein
FAPP1 - Four-phosphate-adaptor protein 1
Flg - Flagellin
FLS - Flagellin sensing
HSC - Heat-shock cognate protein
mKO - mKusabira Orange
PEPR - pep1 Receptor
PIN - PIN-FORMED
ST - Sialyl- Transferase
VHA-a1 - vacuolar ATPase a1

1 Introduction

Clathrin-Mediated Endocytosis is the major endocytic pathway for transporting cargos from the plasma membrane into the cell, although several parallel pathways are observed to be responsible. Clathrin is the key protein that gives the characteristic shape and geometry for the basket, hence the name for the endocytic pathway. Several studies have been conducted and are still ongoing in figuring out the fascinating construction of the basket itself – on how the clathrin polymerises and arranges around a membrane. Many players involved in developing the pit have been identified. And the search still goes on. Post-endocytic trafficking of the fully-coated vesicle and the Early-endosomal formation are also under continuous study. My thesis aims at studying different aspects of this pathway *in planta*. Clathrin-Mediated Endocytosis would also be termed as CME or simply endocytosis in this paper for the sake of convenience and readability.

CME is a highly dynamic process and there are several stages of progression. Understanding such a complicated process of membrane bending and folding into a vesicle, carrying the targeted proteins and delivering into the targeted endomembrane structures requires creating a myriad of techniques. Several electron microscopic procedures have been exploited into ultra structurally observing the Clathrin-Coated Structures, CCSs (refers to both Clathrin-Coated Pits or CCPs, and Clathrin-Coated Vesicles or CCVs). Many different live imaging techniques that are being developed are utilized and adapted for observing the process with high spatial and temporal resolution. CME is also a very conserved process in structure composition and therefore the distinct developmental stages are highly conserved among the eukaryotes. The exchange of knowledge and also techniques in studying different model organisms is the basis of such a rapid development in the field. The widely studied cellular systems are of *Saccharomyces* yeast and of mammalian cell lines. This has led to a huge gap in our understanding between the plant cellular systems and these systems. Here, I would discuss different techniques that are available and the crucial knowledge we gained using them, extending it to unexplored territories *in planta*.

One of the aims of my thesis is to decipher the basic mechanisms constituting CME and post-endocytic trafficking in the whole multicellular organ systems of *Arabidopsis*. Within a cell, there is a constant influx and efflux of membrane maintaining its homeostasis between the Plasma membrane and the Endomembrane. And there exists a balance between endocytosis and secretion of proteins. All the developmental stimuli in an organ system, stress signaling, nutrition uptake, osmotic regulation, wounding and infection constantly shift this equilibrium. CME is one of the basic processes, which is regulated by several physiological stimuli, which we will go over in detail later on. Therefore focusing on developing techniques and studying the basic endocytic pathway is a prudent start.

1.1 Structure of the CCPs and CCVs

The structure of clathrin-coated pits and vesicles has been studied for 30 years and still the fascination over it continues. The important aspect of studying them is the requirement of super-resolution microscopy. Electron microscopic techniques like Transmission Electron Microscopy (TEM), Scanning Electron Microscopy (SEM), and recent advancement with Atomic Force Microscopy (AFM) offer very high spatial resolution to study their structures.

Parallelly, several approaches have been developed to access the vesicles, either directly observing them in the cell or by building them *in vitro*. The most common approaches are:

1.1.1 Unroofing the cells and observing the topological details

Unroofing of cells is one of the most common procedures used, where the cells are adhered to a base or a grid. Later the membrane is torn off and its cytosolic side is imaged. Alternatively, the cells are sonicated or detergent-extracted to remove the cytosolic contents and the *en face* view of the membrane bound organelles is imaged. Metal shadowing replica or cryo EM procedure of these structures enables capturing their native conformation (Makihara et al., 2016). The morphological characterisation such as their sizes and shapes, and their interaction with cytoskeletal components were performed using such techniques. The studies revealed that, typically in a cell, the CCVs are of varying sizes and are made of varying combinations of clathrin lattice arrangement patterns, such as, pentagons, hexagons and, occasionally, heptagons (Cheng et al., 2007; Heuser and Kirchhausen, 1985). CCVs from calf brain have a basket diameter of ~65nm and those from chick fibroblast cells have a diameter of 150nm. A typical mammalian cell is known to possess spherical CCVs of ~ 100nm diameter (Kaksonen and Roux, 2018). Several physiological conditions were tested using this technique. Human and chicken fibroblast cells were shown to form microcages at pH 6.3. K+ depletion and hypertonic conditions caused the CCPs to disappear and empty microcages started developing, causing an inhibition of endocytosis.

1.1.2 Observing the cross-sections of the cell:

An alternative to unroofing technique is to preserve the sample and section. Samples are preserved by high pressure freezing and freeze substitution followed by embedding and sectioning; alternatively, samples are chemically fixed and embedded at room temperature. Thin sections of about 40-100 nm enable us to observe cross-sections of the invaginating membrane. Such studies on yeast have helped us characterize the size of the invaginating pits and vesicles. Typically yeast cells have invaginating neck of greater than 100nm developing into an ellipsoidal vesicle of size 30x150nm (Buser and Drubin, 2013; Idrissi et al., 2008; Kaksonen and Roux, 2018).

1.1.3 Isolating the CCVs from tissues and observing the topological details

Instead of observing the CCSs in their native state, CCVs were isolated from the tissues and freeze-dried. TEM imaging performed on CCVs isolated from calf brain gave our earlier understanding on the structural details of the clathrin triskelion and the basket assembly. This was one of the extensive studies conducted by Heuser and Kirchaussen. They also looked at the enclosed membrane after disintegrating the coat (Heuser and Kirchhausen, 1985). A similar approach was re-adapted and the isolated CCVs were embedded in vitreous ice. Cryo-electron tomography of those revealed details on the membrane versus coat orientation. There were vesicles as small as 31nm with just 36 triskelions that had membrane in it (Cheng et al., 2007).

1.1.4 Reconstituting the CCVs from purified clathrin:

In vitro polymerisation is also a popular technique utilised to study the structural details of CCP formation. Clathrin molecules were purified and polymerised *in vitro*. Various stages of polymerization revealed the details on pit development (Heuser and Kirchhausen, 1985). Recently, Saleem et al., performed similar experiments to answer different questions. They calculated clathrin polymerization energy and the depth of invagination by polymerizing the molecules of clathrin with its adaptors on GUVs of varying tonicity (Saleem et al., 2015).

1.1.5 In plants – state of the art and scope of my thesis

Several studies were conducted in different plant species over the past three decades. Using techniques like freeze-etching, serial thin sectioning and negative staining, several individual studies found that the structure of the CCVs is very comparable to animal systems. First sighting of CCSs *in planta* was in radish protoplast (Bonnett and Newcomb, 1966). Another extensive study in carrot protoplasts showed pits and vesicles of around 100nm and 80 nm in diameter respectively. The isolated CCVs, after detergent treatment to release the coat, had intact preserved membrane. Studies conducted on carrot cell suspension yielded similar results (Coleman et al., 1987; Hawes and Martin, 1986). Onion protoplasts had plenty of CCSs preserved at the PM, varying from 40-100nm diameter (Doohan and Palevitz, 1980), and the average diameter of the CCSs in tobacco protoplasts was found to be 100nm with a density of 8 pits/sq.um (Fowke, 1980). Another extensive study on unroofed root hair cells of several species gave much less density of pits and they reported the typical diameter of the pit to be 72-96 nm in diameter (Emons and Traas, 1986).

There were several more studies until the 90s (Beevers, 1996) but none of them were conducted on the model organism Arabidopsis. There is not enough ultra structural evidence for the existence of clathrin pits in Arabidopsis, except for a whole organ freeze-fracture procedure done on the root tip (Dhonukshe et al., 2007) uncovering a few developing pits coated with clathrin. But no further comprehensive study was performed. However, there are several other microscopic studies done with florescent-tagged clathrin and other machinery proteins, in addition to biochemical and genetic studies (Fan et al., 2013; Gadeyne et al., 2014a; Konopka et al., 2008). Most of the work on endocytosis and trafficking these years is being conducted in Arabidopsis sp. Ultra structural characterisation of CCSs at the plasma membrane is the basis for studying endocytosis. This makes it a compulsion to focus on reviving these obsolete techniques developed *in planta* for Arabidopsis research again.

In my thesis, I have attempted unroofing technique with detergent based solubilisation of cytosolic contents in Arabidopsis protoplasts. I have made metal (gold and platinum) replica of the plasma membrane and the associated structures, and further characterized different populations of CCSs based on the sizes and shapes using SEM. This is so far the first report on Arabidopsis *thaliana*. This technique could pave way for better analysis of plant endocytosis.

1.2 Development of CCP at the plasma membrane

Clathrin pits develop into vesicles through a series of stages, which is conserved across Eukaryotes. However, the precise events leading to their development, the timescale, the

proteins involved, the forces to withstand, the rate and the amount of endocytosis are a few of the features that vary among cell types within a tissue system and at species level across kingdoms (also see review by Kaksonen and Roux, 2018). Some of the key aspects of CCP developments are discussed below.

1.2.1 Stages of CCP development

The clathrin pit development is a very dynamic process, which involves tracking multiple proteins with temporal resolution. The arrival and departure of some of the key proteins with respect to one another has so far been elucidated in good detail. And such studies have marked the progression of CME through the following key developmental stages: Initiation and cargo selection; Maturation; Vesicle scission and removal.

Most of the advancement in CME research could be attributed to Total Internal Reflection Fluorescence (TIRF) imaging. And there are more recent developments in microscopic techniques that are being used to further elucidate finer aspects of CME (Picco and Kaksonen, 2018). One such notable advancement is the polarized TIRF microscopy using which one could monitor membrane bending by labeling the membrane with special probes. Scott et al., have succeeded in labeling the membrane with DiL probes and by creating a special field of polarized light excited the probe and observed the topological changes of the bending membrane (Scott et al., 2017). Correlative EM (CLEM) imaging of clathrin pits is getting attention recently. Utilising integrative microscopic techniques combining EM and fluorescent imaging gives a better understanding on the role of machinery proteins in pit development (Avinoam et al., 2015; Kukulski et al., 2012; Scott et al., 2017). Lattice Light-Sheet Microscopy (LLSM) enables a high speed 3-D scanning over samples of big volume SIM with better axial resolution, thus creating a first step towards studying multi-cellular complex systems. Amongst the promising super-resolution techniques, SIM offers both spatial resolution (80nm) and the temporal resolution in live samples. TIRF-SIM has rendered a far better experience in imaging the dynamic endocytic sites (Li et al., 2015).

Our knowledge on the molecular mechanisms during CCP initiation and development arose by employing, in addition to microscopy, genetic and biochemical tools in yeast and animal systems. The developmental process has a regulated temporal structure. The dynamics of the machinery proteins transitioning the developmental stages have been studied with temporal resolution by tracking their assembly and movement at the endocytic site (Brach et al., 2014; Cocucci et al., 2012; Kaksonen et al., 2005; Picco et al., 2015; Taylor et al., 2011). The whole process from the initiation of pit, coat assembly and maturation, up until scission of the vesicle takes between 60s and 120s in yeast and animal cellular systems.

Initiation: There are continuous changes in the type of phosphoinositides in the membrane undergoing endocytosis and this controls the binding property of wide range of machinery proteins. Thus metabolism of phosphoinositides is crucial for CCP development. Phosphotidyl Inositol (4) Phosphate ($PI(4,5)P_2$) has been proven to be involved in initiation, as its depletion resulted in loss of CCPs from the membrane (Kaksonen and Roux, 2018; Zoncu et al., 2007). In BSC cells, it has been shown that the heteroterameric adaptor protein, AP2 and clathrin are together recruited to the endocytic site during the initial times. FCHo - Fer/Cip4 homology domain-only - proteins has been proven to be important in sustenance of CCP development, though not in initiation itself (Cocucci et al., 2012). And

this is because FCHo recruits F BAR proteins that are regulators of curved membranes, which is essential during invagination and maturation (Henne et al., 2010). Both FCHo1/2 and its yeast homologue syp1 reach the endocytic site ahead of both clathrin and AP2. And in the same study, decrease in FCHo levels by RNAi against FCHo1+2, was found to cause complete loss of CCP from the PM; and over-expression caused an increase. This suggests that FCHo acts as a nucleating factor. Together, it is hard to interpret the precise role of FCHo. $PI(4,5)P_2$ binding to three different binding sites of AP2, thus bringing about the conformational change and further activation by cargo binding, had been proven to be required for initiation and stabilized maturation of developing pits (Kadlecova et al., 2017; Kelly et al., 2014).

Cargoes and Cargo loading: Many receptors have been shown to be endocytosed in a clathrin mediated way. One of the common approaches to study Receptor-mediated endocytosis (RME) is to observe the clathrin dynamics after modifying the expression levels of the receptors or the ligands. Colocalisation studies of the receptor and clathrin by dual – colour TIRF imaging is also common. Transferrin receptor tetrameric complexes and GPCR cargoes were followed this way and were shown to be internalised only through a sub-set of CCPs. Ligand dependent induction of endocytosis of the receptor, in an otherwise abortive clathrin pit was clearly shown by (Puthenveedu and von Zastrow, 2006). Also ligand activation of chemokine receptor, CCR5 was observed to be constitutively recruited into stable Flat Clathrin Lattices (FCLs) at the PM by dSTORM and dual-colour TIRF imaging (Grove et al., 2014).

Maturation and scission: During the pit development, the membrane curvature develops and continuously changes. Three huge classes of Bin-Amphiphysin-Rvs (BAR) domain proteins – BAR, N-BAR and F-BAR - have been attributed in recognizing and maintaining the membrane changes (Dawson et al., 2006). Co-ordinated endocytic waves have been shown to establish polarity during cortical propagation. For such a co-ordination, a feedback of F-BAR proteins has been shown to be inevitable (Yang et al., 2017). Recently, using pol-TIRF technique, Brandon et al., showed that clathrin assembly lymphoid myeloid leukemia (CALM), an ANTH domain protein accumulates at the onset of membrane bending, suggesting its role in initiating membrane curvature (Scott et al., 2017). Scission of the vesicle from the membrane occurs by GTP hydrolysis of the GTPase Dynamin that assembles at the neck of the vesicle. In yeast, an interaction between dynamin and actin has been shown to be important in scission (Palmer et al., 2015), and so have been the BAR domain proteins. However the mechanism of scission is not clear (Hurley and Hinshaw, 2012; Pawlowski, 2010; Roux, 2014). In addition, dynamin has been shown to drive pit maturation (Loerke et al., 2009).

1.2.1.1 In plants: state of the art and scope of my thesis

So far the different developmental stages have not been temporally mapped *in planta*. This would require temporal mapping of recruitment profiles of a few tens of endocytic machinery markers with respect to one another; alternatively, developing techniques like pol-TIRF or CLEM would enable mapping the machinery proteins with respect to membrane topology (flat to curved), which would unravel the stage-by-stage CCP developmental process. Nevertheless, the basic clathrin pit ultrastructural analysis in many plant species (as discussed in previous section) together with all the recent cell biological and genetic studies

conducted in Arabidopsis pertaining to endocytic machinery proteins, do ascertain the conservation of CME *in planta*.

Initiation: Reduced density of pits at the PM was observed in double mutants of the Phosphatidyl Inositol 4-Phosphate 5-Kinases – *pip5k1 pip5k2* (Ischebeck et al., 2013) and over-expression of PIP5K6 resulted in excessive invaginations in pollen tube tip (Zhao et al., 2010), meaning that Pins(4,5)P2 is important for CCP initiation. TPLATE complex (TPC) is a set of closely associated proteins that is hypothesized to possess early-adaptor function. Through Tandem Affinity Purification (TAP) experiments, TPC was found interacting with several endocytic machinery proteins like clathrin, sub-units of AP2 and Dynamin related proteins (DRP). TPLATE COMPLEX MUNISCIN-LIKE or TML, a monomeric adaptor protein part of the TPC, is evolutionarily close to muniscin family of proteins and the yeast syp1. Also, it is to be noted that there are no homologues of FCHo identified in plants so far. Co-localisation studies of TPLATE and clathrin with dual-colour TIRF imaging show that TPLATE arrives earlier to the endocytic pit (Gadeyne et al., 2014a). Mutation of *ap2 σ* mutant, a subunit of in AP2 complex, leads to a 50% reduction in clathrin pits (Fan et al., 2013). In a recent study, it was shown that AP2 sub-units are not all recruited at the same time. AP2µ spikes in the beginning of the development of CCP whereas the AP2A1 sub-unit comes later and persists, meaning the µ sub-unit is involved during the initiation phase (Johnson and Vert, 2017a). Also it was shown that depletion of the activity of both TPC and AP2 resulted in total abolishment of membrane clathrin, but just the presence of TPC could re-establish membrane clathrin. This proves that TML is inevitable in CCP initiation, though AP2 is not the major adaptor in plants (Kim et al., 2013; Wang et al., 2016). TWD40-2, a putative subunit of the TPLATE complex, plays a significant role and a co-operative role together with AP2 at the endocytic pit. *ap2m-1 twd40-2-3* double mutant caused increased CESA particle density, implying defective endocytosis and trafficking of CESA leading to inefficient cellulose biosynthesis in the cells (Bashline et al., 2015). Together, it has been established that AP2 and TPC function in initiation of endocytic events in plants. However, we do not know how PIP2 and AP2 and Tplate activate initiation. Thorough genetic mutational studies of AP2 and TML might lead to a better understanding of this.

Cargo selection: CME of several cargoes have been indirectly shown. For example, PIN2 endocytosis have been observed to be defective in dominant-negative (DN) version of CLATHRIN HEAVY CHAIN (CHC) (Dhonukshe et al., 2007). BOR1 receptor endocytosis was inhibited by over-expressing the dominant-negative form of DRP1A protein (DN-DRP1A) in plant root cells; similarly, endocytosis of PEPR was inhibited by over-expressing the putative plant uncoating factor Auxilin-like (Ortiz-Morea et al., 2016; Yoshinari et al., 2016). But none of the studies had a direct co-localisation by dual-colour TIRF, which would offer a better understanding on the dynamics and the specificity of the internalisation process. Alternatively, varying the concentration of the ligand/receptor and subsequently analyzing the dynamics of the machinery proteins could be insightful.

Maturation and scission: Membrane bending sensors that are essential for invagination and maturation of CCPs have not been properly characterized in plants. AP180, an ENTH domain protein, has been identified and has been shown to possess clathrin-assembling property (Barth, 2004). Also two other ANTH domain proteins – CAP1 and ECA4 have been identified

to function together with TPC (Gadeyne et al., 2014b). Their localisation is known, however their dynamics and their functionality in a maturing CCP have not been studied yet (Zouhar and Sauer, 2014). Six families of plant dynamins have been identified so far and only Drp2 and Drp1 family of dynamins have been associated to endocytosis. Drp2 family has the Pleckstrin homology - PH and Proline rich - PR domains, that are necessary for binding to other membrane binding and modulating proteins. However Dpr1 family of proteins that lack these domains have been observed to be functional at the endocytic pits in concert with Drp2 (Fujimoto et al., 2010; Konopka et al., 2008). Moreover, DN-DRP1A expression in cells resulted in arrested CCPs (Yoshinari et al., 2016). All these studies point towards potentially important machinery proteins, but thorough recruitment dynamics studies need to be carried out to place their function in endocytic pit development.

Some isolated studies on the lifetime distribution of the clathrin foci (CCP residence time at the PM) show the mean lifetime to be around 20 seconds (Johnson and Vert, 2017a; Konopka et al., 2008; Stefano et al., 2018). This is fascinating, as most animal cells and yeast have a much longer lifetime: 60-120s. This proves that evolution of developmental mechanisms has diverged *in planta*. Several co-localisation studies so far have continuously indicated only partial co-localisation of the machinery proteins with one another. For example, only 50% of TPLATE foci co-localise with AP2 (Gadeyne et al., 2014b; Johnson and Vert, 2017b). Also AP2 and TPLATE are not simultaneously needed in a developing pit, with AP2 tetrameric composition being dispensable (Kim et al., 2013; Wang et al., 2016). This denotes that there are different kinds of clathrin pits, which might be functionally distinct. This needs to be further explored.

Most of my studies have been conducted in multicellular whole organ system of root and hypocotyl. This offers a better understanding on endocytic properties of complex multi-cellular organ. Utilising the power of LLSM would definitely be the next step.

1.2.2 Modes of CCP development: membrane-bending models

The function of clathrin, in clathrin-mediated endocytosis is proposed to be modulating the membrane topology. Clathrin polymerization energy has been claimed to feed the bending energy during the pit development. The opposing forces of the process are the turgor/hydrostatic pressure of the cytosol, the membrane tension and the rigidity/elasticity of the membrane. As discussed before, several membrane-modulating proteins are involved in the process. However, the question as to how clathrin polymerisation changes the membrane topology during development of the endocytic pit has been debated over several years. The two favourite models so far proposed are (Kaksonen and Roux, 2018; Lampe et al., 2016; Sochacki and Taraska, 2018):

Model 1 - Constant surface area model: The size of the pit is pre-determined. Clathrin molecules polymerise into a flat lattice initially. Hence, the surface area and the amount of clathrin at the pit remain constant, while continuous remodeling of the polygonal structures develops the pit. Basically, clathrin molecules are constantly re-organised at the pit developing the bud into a vesicle.

Model 2 - Constant curvature model: The pit develops as the clathrin molecules are added to it, while the radius of curvature of the developing pit stays constant. During

the course of development, the clathrin constantly polymerises in the pit, and not as an initial flat lattice, thus developing the pit into a complete vesicle

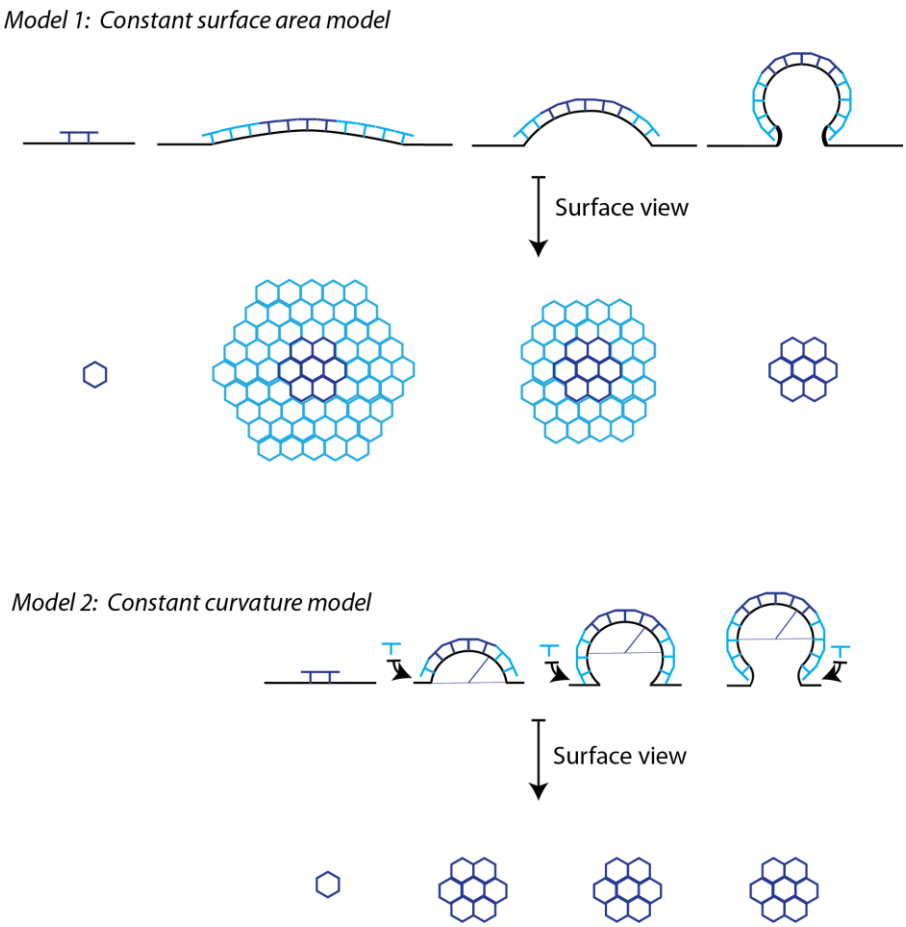

Figure 1: Models elucidating the mode of membrane bending during CCP development
The cross-view and the surface view of different stages of development of the pit are shown. Polymerised clathrin lattice is shown in blue. In dark blue, the central lattice viewed during ultrastructural analysis of CCPs is shown. Model 1: The constant surface area – The initial surface area is set by polymerised clathrin lattice. Later the membrane bends and the surface view of the clathrin lattice diminishes. Polymerised clathrin lattice is shown in blue. In dark blue, the central lattice viewed during ultrastructural analysis of CCPs is shown. Model 2: The membrane bends as the clathrin molecules polymerise and the surface view of the lattice stays the same with the radius of curvature remaining constant.

There are evidences for the existence of both the modes of development. Recently Avinoam et al., performed CLEM on the developing membrane by fluorescently tagging the machinery proteins and EM observation of the membrane topology, and proved that CCP development in human cells follows model 1 (Avinoam et al., 2015). In addition, the isolated clathrin pit intensity profile over time (the progression profile) could depict the mode of development (Loerke et al., 2009). Based on the duration of the assembly, maturation and departure phases in the progression, Avinoam et al., further validated their CLEM observation. In such a mode of development, it has been proposed that the transition from the assembly of clathrin lattice into membrane bending and invagination could be the rate-limiting step, and membrane tension is a major factor that could stall the transition (Bucher et al., 2018). Recently Bucher et al., and Brandon et al., through independent studies proved

the existence of CCPs developing by following model 2. Curiously, they observed that there is a fraction of CCPs that develop by model 1, as well. In addition, they identified a third mode of membrane bending.

Model 3 - Mixed model: clathrin initially polymerises in a flat lattice and after a point, the membrane starts remodeling with continuous clathrin exchange. Later on, additional clathrin molecules assemble at the pit (with an established radius of curvature) further developing the pit into a vesicle (Bucher et al., 2018; Scott et al., 2017).

Thus they permanently resolved the question whether these models are mutually exclusive. In conclusion, in a given cell, there could be multiple modes of membrane bending during CCP development. The local tension, the binding machinery proteins, the composition of the membrane etc. could be influencing the mode of development. The factors influencing the decision over the mode of CCP development is yet not clear in animal cells.

However, in yeast, membrane-bending dynamics is different. Due to high turgor pressure the development of the CCP does not necessarily follow the above models. Though similar to model 1, the clathrin molecules and other coat proteins initially assemble to form a flat lattice, it is predominantly the actin remodeling force that develops the pit, not the clathrin polymerisation energy (Dmitrieff and Nédélec, 2015; Kaksonen and Roux, 2018; Picco et al., 2015).

1.2.2.1 In plants: state of the art and scope of my thesis

As discussed previously, many studies have been conducted in different species to observe the basic clathrin pit architecture. However, nobody has actually studied the membrane remodeling in plants during CCP development. This requires characterizing hundreds of pits in various stages of development. In my thesis, I have characterized the *en fac*e surface view of the CCSs at the plasma membrane and further analysed the stages of CCSs development, in order to figure out the model of development.

1.2.3 CCP developmental rate: Rate of endocytosis

The rate of development of the endocytic pit at the plasma membrane determines the endocytic rate of cell. The duration of development of a pit could be measured by following the lifetime of the fluorescent machinery marker lines by TIRF time-lapse imaging. The distribution of lifetime measurements of the entire population of clathrin pits is the conventional method of understanding the rate of endocytosis in a cell.

In yeast and mammalian systems, several studies have been conducted in faithfully obtaining the lifetime distribution. The first milestone is selecting the marker lines for following the developing pits; the second is to image them without gaps and with high accuracy of detection; the third is to develop an automated tracking software to follow the CCP developmental trajectories (Mettlen and Danuser, 2014). Lifetimes of CCPs in yeast are more or less constant with less probability for abortion, owing to the modular recruitment of machinery proteins, which ensures uniformity in CCP development (Kaksonen et al., 2005). However, in mammalian systems, there exists a huge variability and this demands complex data mining and analysis. Methodologies for detection and tracking CCP dynamics are constantly upgrading. Aguet et al., and Loerke et al., came up with an analytical method

for eliminating the 'abortive pits' and obtaining a distribution of 'productive pits' (Aguet et al., 2013; Loerke et al., 2009; Mettlen and Danuser, 2014).

1.2.3.1 In plants: state of the art and scope of my thesis

In the plant system, the major drawback is the choice of marker lines that would faithfully represent all the endocytic events. Though CLC-GFP (Konopka et al., 2008) is the basic line of choice, there is no alternative way of tracking the 'real' endocytic events; for example, there is no established methodology to eliminate the non-productive pits based on dynamin co-localisation or based on employ master/slave approach by co-localising with AP2 (Aguet et al., 2013). As discussed before, AP2 and TPLATE both act as adaptors independently. And the functionality of plant dynamins – Drp, has not been solved yet.

Only recently automated detection and tracking of CCPs have been adapted over kymographs (an ImageJ algorithm) of a few selective CCPs. Alexander Johnson and Gergory vert have tracked CCPs in root epidermal cells and obtained the lifetime distribution of thousands of trajectories (Johnson and Vert, 2017b). Interestingly, the distribution resembles closer to mammalian cellular systems and not yeast. The lifetime data obtained by following all the developmental events at the PM, formed a complex distribution incorporating trajectories of both abortive and productive pits. Unfortunately, there are no further studies discerning the productive pits form the rest. Nevertheless, this study proves the closer evolutionary path between mammalian (but not yeast) and plant cellular systems.

The average lifetime (γ) of pit at the PM determines the specific rate of endocytosis ($1/\gamma$) of the cell. The overall endocytotic rate of the cell however depends on the total number of pits or the density of the pits (∂) at the PM ie. ∂/γ. Therefore, in my studies we have considered both the density and the average lifetime of the developing pits.

Though following the CCPs enables quantification of endocytosis in a cell, most of the cellular studies utilised direct visualization of cargoes. Uptake of transferrin and ferritin, internalisation of fluorescent ligands like A488-factor have been commonly used to quantify endocytosis in mammalian and yeast cellular systems (Fujimoto et al., 2000; Toshima et al., 2006). However, in the past decade, almost all the endocytosis studies in Arabidopsis have utilized the FM dyes – FM4-64 or FM 1-43 – that stain the PM and further quantify the amount of labeling of endosomes after several min. Another widely used method was quantifying the endocytosed cargoes in the endosome, after aggregating them in the form of BFA body, post treatment by the fungal toxin Brefeldin A or BFA (Dhonukshe et al., 2007; Gadeyne et al., 2014a; Paciorek et al., 2005; Zwiewka et al., 2015). Alternatively, fluorescently tagged ligands that undergo endocytosis were developed eg. TAMRA pep1 and AFCS, which could also be visualized in endosomes (Irani et al., 2012; Ortiz-Morea et al., 2016). Such quantifications are not a direct indication of the endocytic potential of the cell as measurement of endocytosis occurs at the endosomal stage; but it definitely is a trustable indicator.

The above methods have certain disadvantages as quantifying endosomal signal also incorporates the additional factors of post-endosomal trafficking and more, which I have discussed in my thesis. This has forced us to look for alternative ways of testing the internalisation potential of a cell. Many plasma membrane receptors – eg. BOR1, PEPR, BRI1

- and other cargoes have been identified to undergo endocytosis. Following the loss of PM signal of the fluorescently tagged cargoes have gained some attention recently (Jásik et al., 2016; Ortiz-Morea et al., 2016; Takano et al., 2005). In my studies, I have utilised such lines to test the overall rate of endocytosis in the whole organ system – root meristem.

1.3 Role of actin in CCP development

Alongside clathrin and membrane bending sensors and modulators like ANTH/ENTH and BAR domain proteins, actin is also considered to be important for membrane deformation. Actin is inevitable for CME in yeast system. The pushing force generated by the polymerizing actin filaments promotes membrane bending and invagination, which take place approximately in the final 15 seconds. (Picco et al., 2015; Sun et al., 2015). But the role of actin is variable across several mammalian lines studied; and in some cases, the same cell type requires actin during only certain conditions like higher membrane tension during polarized development (Boulant et al., 2011; Fujimoto et al., 2000).

The detailed mechanism of how the proteins get activated and subsequently promote actin polymerisation has been worked out in the past two decades using several biochemical and genetic studies. After the initiation and assembly phases of early module proteins including clathrin and AP2, middle and late module proteins that are essential for actin-membrane interaction assemble and further promote nucleation of actin. Sla1-End3-Pan1, the late module trio has been attributed to the actual transition from coat to actin assembly. Deletion of Pan1 resulted in delay in this transition. Sla2 is an essential linker transforming the actin forces to the plasma membrane. Sla2 and Pan1 could regulate arp2/3 complex and interactions with myosins. Myosins together with Las17/WASP are located both at the PM and the tip of the invagination. Las17/WASP potentially could bind both actin monomers and arp2/3 complex thus facilitating actin polymerisation (Carlsson, 2018; Girao et al., 2008; Goode et al., 2014).

Parallelly, many theoretical studies, membrane tension and osmotic perturbation studies have been carried out to understand the mechanics of membrane modification. It has been proposed that in yeast, to overcome the turgor pressure, actin polymerisation force is absolutely essential, but it acts in consort with other coat proteins and membrane modifying factors (Carlsson and Bayly, 2014). In yeast cells, decreasing the turgor pressure using sorbitol rescued the defective endocytic phenotype in mutants of actin bundling proteins (Aghamohammadzadeh and Ayscough, 2009).
In a recent study conducted in mammalian cells, they showed that actin dynamics was essential for complete membrane deformation, particularly under high membrane tension conditions – induced by high osmolarity or by artificially stretching the membrane. After actin perturbation, TEM images revealed incomplete CCPs and the lifetime distribution indicated arrested and delayed development of pits (Boulant et al., 2011).

Several other studies have been conducted to directly observe actin organization during endocytosis. Actin forms a clear focus of polymerisation at the endocytic site. The dynamics of recruitment of actin to the endocytic site along with coat proteins, the nucleation promoting factors and other machinery proteins have been studied using TIRFM both in

animal and yeast cells (Kaksonen et al., 2005; Merrifield et al., 2004; Picco et al., 2015). However resolving the spatial organization of actin is even more challenging. SIM and, to an extent, dual colour TIRF imaging has helped us resolve actin architecture around the CCPs (Li et al., 2015; Yarar, 2004). Utilising unroofing techniques (discussed before) and visualizing the actin architecture around the CCSs at the PM using TEM and AFM helped us understand their spatial interaction to much higher degree (Fujimoto et al., 2000; Usukura et al., 2016). Huge plaques of clathrin associated to focal adhesion proteins and actin in skeletal muscles have been structurally resolved to study contractile forces (Vassilopoulos et al., 2014). Collins et al, beautifully showed the changes in actin arrangement from small peripheral patches to comet like tail through various developmental stages of clathrin pit. This was a thorough study utilising CLEM, clearly establishing the role of acto-myosin network in CME, in mammalian cell (Collins et al., 2011).

1.3.1 In plants: state of the art and scope of my thesis

Function of actin in endocytosis for membrane remodeling in high turgor pressure systems has been established by several methods, but only in yeast as the model system. *In planta* analysis could have definitely offered more insights.

The role of actin in endocytosis has not been directly studied in plants. Konopka et al., pharmacologically inhibited actin and analysed the lifetime distribution of the developing pits at the PM. The observed increase in lifetime, meaning a delay in pit development in addition to arrested pits, imply that actin plays a role in CCP development in Arabidopsis. However the observation was not based on extensive unbiased measurement and analysis of CCP lifetimes which is to be obtained by automated tracking of all the CCP trajectories; the results consisted a subset of trajectories from kymographs (Konopka et al., 2008).

The homologues of yeast late coat proteins - Sla1, Sla2- that have been implied to function in actin nucleation at the pit, have not yet been identified in Arabidopsis. Homologues of yeast WASP do not exist in Arabidopsis, but there are related proteins identified as At SCAR1-4, which activate Arp2/3 complex (Frank et al., 2004). Arp2/3 complex and its functions are highly conserved in Arabidopsis; however its role in CME is not understood yet. SH3P, a family of proteins proposed to be functionally similar to the membrane tabulating protein - yeast Rvs167, was shown to be localised at the PM and the vesicles and further bind to actin (Lam et al., 2001). Moreover, a total of 17 Myosins have been identified in Arabidopsis. It is clear that Arabidopsis myosins do not belong to Myosin1 family of yeast, which contains myo3/5 required for membrane bending. Nevertheless, these myosins have not yet been characterised with respect to CCP development; except for one attempt, where ATM1, one of the plant myosins, was found to be localised at the plasma membrane and EE (Golomb et al., 2008; Reddy and Day, 2001). Most importantly, the localisation of actin at the pit has not yet been confirmed. Unroofing studies conducted in protoplasts in the 1980s (discussed before) have revealed thin filaments of actin and microtubules adjacent to the clathrin pits, but the structural preservation of actin had been a challenge.

Though there are so many gaps, slowly the pieces are coming together. The questions that remain to be answered are: a) Actin has been unanimously claimed to be inevitable for membrane remodeling in high turgor pressure systems. Does it hold true for plant cells as well? b) If so, when and how does actin localise at the pit? We have tried to answer these

questions in my thesis using Arabidopsis multi-cellular root and hypocotyl systems. We have directly looked at cortical actin localisation in epidermal cells. We have further tested membrane uptake and cargo internalisation after pharmacologically perturbing actin, using LatB and Jasplakinolide. We have also quantitatively analysed all the endocytic trajectories in an unbiased way to obtain the endocytic rate of the system after actin perturbation. This is the first thorough study on understanding the endocytic role of actin *in planta.*

1.4 Post-endocytosis

Two key features of post-endocytosis are 1) uncoating and 2) Early-endosomal formation. After scission, the coated vesicles disassemble the coat proteins and fuse to an early endosome releasing the contents of the vesicle. This is the first step in endomembrane trafficking; from there, further protein sorting towards recycling and degradation occur. Several studies have been conducted in understanding the uncoating machinery and trafficking processes.

1.4.1 Uncoating

A fully formed vesicle releases the coat proteins and fuses to the endosome. That requires the action of the uncoating machinery. It mainly consists of Heat shock cognate 70 (HSC70), that possesses ATPase activity, and its co-factor containing DnaJ domain, Auxilin. HSC70 ATPase activity was shown to increase 5-fold in the presence of Auxilin (Jiang et al., 1997; Prasad et al., 1993). Studies have been conducted in different animal cellular systems. A highly selective activity of HSC70 on uncoating brain-derived CCVs was shown using biochemical studies involving high-speed centrifugation assays. Auxilin is the functional co-factor for HSC70 in neuronal cells, and cyclin-G dependent kinase (GAK) in the non-neuronal cells (Buxbaum and Woodman, 1995; Greener et al., 2000). Swa2, the Auxilin homologue in yeast, also possess HSC70 activation property; and its mutation results in growth defects (Gall et al., 2000). In addition, Prk1 is the GAK homologue in yeast, and hampering its kinase activity resulted in clamps of vesicles containing all the coat module proteins along with abnormal, excessive actin assembly (Sekiya-Kawasaki et al., 2003). Mutation of Synaptojanin (a protein involved in phosphorylation of lipids), resulted in 100% lethality of knock out pups in mice due to neuronal degeneration. Moreover, similar to prk1 inhibition phenotype in yeast, s*ynaptojanin* mutant also exhibited abnormal clustering of coated CCVs in actin matrix in neurons (Cremona et al., 1999).

Auxilin dynamics studies conducted using TIRF have shown that a burst of Auxilin at the end of an endocytic event marks the beginning of the uncoating process. And it is tightly correlated to dynamin function, meaning that the vesicle should have reached a certain level of completion (Massol et al., 2006). However the exact mechanism of how Auxilin and the ATPase activity of Hsc70 bring about the disassembly of the coat proteins is not well understood. There are competing models proposed (Kaksonen and Roux, 2018).

There is one more unresolved question. Is the disassembly a non- cooperative two-step process or a sequential cooperative process? In other words, does the disassembly of the coat happen all-at-once, with no intermediates; or does the clathrin coat disassemble bit-by-bit? This question was answered independently in mammalian and yeast system using

two different methods. Krantz et al used a novel technique called Burst Analysis Spectroscopy (BAS) and looked at the size distribution of fluorescently labeled clathrin baskets isolated from S. *cerevisiae* under different conditions. Each clathrin basket produces a burst of fluorescent intensity. Based on the distribution of intensity, size distribution of the clathrin basket could be inferred. They observed that in the presence of the ATPase and its co-factor Swa2p, the coat disassembles extensively indicating a co-operative two-step model with no partial intermediates. Bocking et al., independently addressed the same question by single particle visualization of clathrin structures using TIRF. They monitored the fluorescent intensity of the clathrin coat under different conditions. The uncoating kinetics in the presence of HSC70 and Auxilin clearly indicated a very rapid transition characteristic of co-operative model. The coat was disassembled all at once (Böcking et al., 2011; Krantz et al., 2013). There exists still a competing theory, where uncoating of CCVs should not be complete and there should be residual coat protein in order to dock to an Early Endosome (EE) and subsequently fuse (Trahey and Hay, 2010).

1.4.1.1 In plants: state of the art and scope of my thesis

Kirsch and Beevers made initial discoveries of the plant uncoating machinery in pea plants in 1993. They characterized the ATPase and uncoating activity of HSC70 *in vitro*. They showed that pea HSC70 could uncoat the isolated CCVs from both the bovine brain cells and pea plants, proving conservation functionality of the uncoating machinery over different kingdoms. Two Auxilin-like proteins, which have the characteristic DnaJ domain were identified and studied in Arabidopsis. Auxilin-likes were co-immunoprecipitated along with CLC and their interaction with both SH3P1 and SH3P2 was proved. Furthermore, Lam et al., proved the uncoating property of Arabidopsis Auxilin-like in the presence of animal HSC70 *in vitro*. Using TIRF microscopy, we observed bursts of Auxilin-likes at the end of the lifetime of CCP. Furthermore, its over-expression resulted in the complete loss of CCP formation at the PM. Both these observations are very similar to the ones made in mammalian and yeast systems, further asserting the role of plant Auxilin-likes in CME. Surprisingly, the double knock out of both the Auxilin-likes did not incur any apparent phenotype. Also only 5% of the total CCPs at the PM had Auxilin-likes arriving at the end of their development (Adamowski et al., 2018; Kirsch and Beevers, 1993; Lam et al., 2001). This shows that the essential HSC70-Auxilin duo observed in both yeast and mammalian systems is not strictly required in plants. Overall, one could conclude that the uncoating machinery is not strongly conserved *in planta*. There might be an alternative pathway enabling disassembly of the coat and further fusion to the EE.

HSC70 is not studied well in Arabidopsis. However, in my thesis we have addressed uncoating by following the CCVs, that scission from the PM. We observed the CCVs reaching the EE and the time frame of uncoating. Also, given the fact that Auxilin-like is not widely functional, we have addressed the mechanism of disassembly to check if it is co-operative or sequential. Nevertheless, one has to conduct a thorough study including HSC70, and in parallel, look for an alternative uncoating mechanism.

1.4.2 Trafficking to form Early Endosomes (EE):

The endocytosed CCVs reach the EE to release the endocytosed proteins for subsequent sorting and also to recycle the membrane. There are few studies available on the vesicular trafficking process. There are two ways for the endocytosed CCVs to reach the EE: 1) Actin

independent trafficking towards an EE, 2) Active transport along actin towards an EE. There are evidences for both mechanisms.

There is unusual evidence in a human cell line for the existence of myo6 motor activity upon nascent uncoated vesicles, enabling shuffling of vesicles out of the actin mesh. In this case, the actin mesh was hindering the CCV motility, which was rescued by myo6 activity and by actin depolymerisation treatment (Buxbaum and Woodman, 1995). Most of the other evidences point towards actin driving the scissioned vesicle away from the PM, most likely to the EE (Barroso-González et al., 2009; Collins et al., 2011; Merrifield et al., 1999; Yarar, 2004). Actin polymerisation aiding the membrane deformation further develops into a comet-tail like structure driving of the CCVs into the cytoplasm. In one exceptional case as shown my Merrifield et al, actin polymerises like a tail right after vesicle scission to propel the pinosome away from the membrane. In yeast, there was a thorough study conducted on trafficking where they showed that both the vesicles and the EE move along actin. They used a combination of TIRF and wide-field imaging to follow both the PM endocytic events and deeper tracking of EE trafficking. They found that either EE is transported to pick up vesicles form the point of vesicle release or the CCVs reach the EE mid-way. Lack of actin resulted in misregulation of the cargoes (Toshima et al., 2006).

1.4.2.1 In plants: state of the art and scope of my thesis

The trafficking of endocytosed vesicles has never been studied in plants before. We have utilised unroofing technique, as mentioned below, to directly look at the ultrastructural evidence of cortical actin transporting vesicles. Also we utilised VAEM to observe the dynamics between actin marker line and clathrin vesicles at a deeper angle, in addition to directly observing the dynamics of EE/TGN system with respect to CCPs. With such tools at hand, we have tried to understand the trafficking of CCVs and formation of EE for the first time in plants.

1.5 Regulation of endocytosis in plants: state of the art and scope of my thesis

CME is a highly regulated process. It accommodates multiple molecular regulatory parameters to decide ‘what’, ‘when’, ‘how much’ to endocytose. Molecular regulatory parameters encompass a huge field understanding protein modifications like ubiquitination and phosphorylation of cargoes and so on. But, I would discuss some of the regulatory signaling occurring, not at the molecular level, but at the physiological level that could potentially alter the endocytic rate of specific proteins.

Endocytosis of some proteins occur constitutively at a basal rate in resting condition, whereas other proteins require certain signals – endogenous or exogenous that function as a ‘GET SET - GO’ code to get endocytosed. More notably, such regulatory signals could potentially modulate or further attenuate the existing endocytic rate. Exogenous cues that have been suggested to influence plant endocytosis are: gravistimulation, phototropism, pathogen stress, nutrient availability, salt and osmotic stress. Endogenous signaling that is still being studied extensively is Hormonal regulation of its carriers and receptors; also signaling peptides that are required to elicit specialised response are secreted to regulate

endocytosis. Both exogenous and endogenous signals go hand in hand in plant growth and developmental regulation.

1.5.1 Endogenous signaling - Hormonal and other peptide-mediated regulation

Plants produce local and global signaling molecules to elicit various responses. Some small peptides have been identified to be secreted locally to induce RME and to trigger subsequent signaling. On the other hand, hormonal signaling covers long distances and possess multi-level regulatory controls over development. Such a massive expanse in distribution is mainly possible because of ubiquitous multiple transporters expressed across several cell types. Therefore, a crucial part of hormonal signaling involves regulating endocytosis and trafficking of its own transporters and receptors. It is to be noted that generally crosstalk exists between hormones, thus regulation of alternate receptors and signaling pathways is highly prevalent. auxin and its effect on endocytosis have been studied for over a decade. Therefore I have discussed it in detail over others.

1.5.1.1 Auxin

Auxin is imported and exported through AUX/LAX and PIN-FORMED (PINs) family proteins respectively (Adamowski and Friml, 2015; Swarup and Péret, 2012). PIN2 has been shown to undergo clathrin-mediated constitutive endocytosis (Dhonukshe et al., 2007; Kleine-Vehn et al., 2011). Several evidences have been accumulated over the decade on auxin regulating endocytosis of PIN proteins. auxin regulates levels and distribution of CLC and CHC proteins in both the PM and EE/TGN, and clathrin mutants show defective Polar auxin Transport and gravitropism (Wang et al., 2013a, 2016). Short-term auxin treatment inhibits PIN accumulation in BFA bodies; and this has been shown to happen only in the absence of AUXIN BINDING PROTEIN 1, ABP1. That is, auxin binding to ABP1, relieves it off the membrane further inhibiting endocytosis of PINs over long period (>3h), auxin has shown to increase degradation of PINs, and a heavy loss of PIN from the plasma membrane could be clearly observed. At the same time, auxin depletion also causes heavy PIN degradation (Baster et al., 2013; Paciorek et al., 2005; Robert et al., 2010; Zwiewka et al., 2015). Amongst all the hormones, auxin is considered special because it has been shown to inhibit the general endocytic rate of the cell, in addition to controlling the endocytosis and recycling of its exporters, PINs (Paciorek et al., 2005; Robert et al., 2010).

However there are recent debates occurring over these claims on effects of auxin. Jasik et al., has recently showed by photo-convertible PIN2 Dendra that the PM PIN2 population gets endocytosed normally in the presence of all the homologues of auxin with no exceptions (Jásik et al., 2016). His work has put all the known endocytosis studies done with auxin-BFA debatable. Thus whether or not auxin inhibits endocytosis in general and PINs in particular is a huge question now. Moreover, the effects of auxin on cellular clathrin distribution and their impacts on endocytosis remain to be explored.

In my thesis, I have tried to clarify these gaps and debates, and I have compiled a possible working model for auxin and its regulation of CME.

1.5.1.2 Other hormones

Crosstalk between auxin and cytokinin has been studied in different ways. It was found that cytokinin perception through AHK4 is required for PIN1 degradation and LRP development through regulation of auxin distribution (Marhavý et al., 2011). Also strigolactone has been shown to regulate shoot branching by enhanced endocytosis of PIN1 in vascular tissues (Shinohara et al., 2013). Salicylic acid (SA) also has been shown to generally affect endocytic machinery proteins. Just like auxin, SA reduces the PM localisation of clathrin, but in addition also reduces the AP2 levels. Moreover, SA was shown to reduce PIN2 endocytosis, however not of flagellin uptake (Du et al., 2013; Wang et al., 2016).

Brassinosteroid (BR) signaling requires binding of BR to BRI1 receptor. Tyrphostin A23 treatment (which inhibits cargo being sorted into the CCPs) mediated blockage together with other means of inhibition of endocytosis resulted in retention of BRI1 at the PM, which increased BR1 signaling. Thus attenuation of BR signaling requires endocytosis and removal of the BR1 receptor from the PM, thus curtailing continuous transmission of signals (Irani et al., 2012). Also knockout of AP2 genes resulted in reduced endocytosis of BRI1 (Di Rubbo et al., 2013). Similarly, abscisic acid binds to its receptors PYRABACTIN RESISTANCE1 (PYR1)/PYR1-LIKE (PYL)/ REGULATORY COMPONENTS OF ABA RECEPTORS (RCAR). Belda-Palazon et al have done an extensive proteomic analysis on the co-immunoprecipitated PYR/PYL/RCAR receptors with several CME machinery proteins bound to them. Furthermore, they showed that ABA binding to PYR/PYL/RCAR receptors mediates their ubiquitination and endocytosis (Belda-Palazon et al., 2016).

An essential aspect of hormonal signaling is that several physiological responses are manifested through it. That is, several growth and developmental responses to exogenous signaling happen via manipulation of hormonal signaling pathway. As separate topics, I would highlight three well-characterised physiological responses to external signals – gravitropism, phototropism and halotropism (comes under osmotic and salt stress). These indeed form special cases on auxin mediated endocytic regulation of PINs.

1.5.1.3 Peptides

Apart from direct hormonal regulation, endogenous peptides also could indirectly control endocytosis of proteins. Small peptides called Golvens, which are transcriptionally regulated by auxin, are likely to be secreted out to apoplasts. And these secreted peptides in turn regulate auxin distribution in tissues, gravity response, and further accelerate PIN2 endocytosis. But exogenous auxin could over-ride this regulation (Whitford et al., 2012). There is another family of peptides called *At*Peps that are released locally after wounding. It has been shown to trigger immune response (Huffaker et al., 2006).

1.5.2 Gravitropism and Phototropism

Plants, through receptors and signaling pathways, sense gravity and light. In response, plants exhibit directional bending and growth as required. Such a responsive development ensues several upstream growth and developmental signaling cascades. One such extensively studied signaling pathway is the asymmetric distribution of auxin that facilitates root and hypocotyl bending. This requires differential PIN trafficking signals occurring across cell files.

After 2 h of gravistimulation, auxin concentration increases in the lower cell files and gets depleted in upper cell files. At the same time, PIN2 abundance at the PM of the lower cell files and an increased PIN2 degradation at the upper cell files could be observed. Proteosomal degradation of PIN2 in the upper cell files is important in establishing this asymmetry in its localisation. Moreover PIN2 endocytosis and trafficking is inevitable in establishing the PIN2 asymmetry. PM stabilized non-endocytosable PIN2*wav6-52* (a mutant allele of PIN2 with a glycine to glutamate substitution) is agravitropic with defective PIN2 asymmetry after gravistimulation. The stabilization of PIN2 at the lower side could be attributed to auxin-mediated inhibition of endocytosis. On the other hand, auxin treatment greater than 2h increases loss of PINs from the membrane and subsequent degradation. This could be a concentration and time-dependent effect of auxin in regulating PIN abundance at the PM (Abas et al., 2006; Baster et al., 2013).

It has been clearly shown that retromer-mediated PIN2 exocytosis is required for PIN abundance at the PM. Mutants of SORTING NEXIN 1 and VPS29 show enhanced vacuolar degradation of PINs and also showed defective gravitropic response (Kleine-Vehn et al., 2008). Gibberellic acid has been shown to fasten the retromer-mediated recovery of PINs. Like auxin, it is also asymmetrically distributed with high concentration at the lower side, in addition it could influence auxin distribution in cells after gravistimulation (Löfke et al., 2013; Salanenka et al., 2018). This result proves that auxin and Gibberellic acid function together in gravistimulation. And it is impossible to eliminate the possibility that not auxin, but Gibberellic acid actually is regulating the PIN abundance at PM, particularly of PIN2 after gravistimulation.

Like gravity, light regulates PIN trafficking. Concomitantly, loss of PINs from the PM and enhanced vacuolar degradation were observed when light grown seedlings were shifted to darkness. Notably, this dark induced degradation is not specific to PINs; even BRI1 and PIP2 undergo enhanced vacuolar targeting (Kleine-Vehn et al., 2008; Laxmi et al., 2008). Also Laxmi et al., showed that red light and not blue increases PIN2 endocytosis and vacuolar targeting; and this light mediation of PIN trafficking is dependent on phytochrome signaling. Recently, blue light has been shown to accelerate apical hook opening. And this most likely requires PIN3 asymmetry and a corresponding asymmetric auxin distribution. Regulation of this whole process is clathrin dependent (Yu et al., 2016).

1.5.3 Pathogen response

Involvement of CME in plant immune response has only recently been deciphered (Žárský, 2016). Pathogen-Associated-Molecular-Patters or PAMP related response is the preliminary response elicited by plants (Chisholm et al., 2006). Only a few Pattern Recognition Receptors (PRRs) have been identified to be regulated by CME that elicit immune response. Flagellin triggered PAMP response is widely studied and well characterised. Flagellin in bacteria is recognised by the receptor FLS2 in plants. FLS2 has been shown to undergo endocytosis both in the activated and inactivated form. That is, FLS2 gets constitutively endocytosed and recycled back in the Flagellin unbound state. Upon Flagellin binding, it undergoes endocytosis and trafficking to degradative pathway (Beck et al., 2012). Flagellin binding to FLS2 activates the co-receptor BAK1 and this regulates downstream MAP Kinase mediated response conferring resistance to both bacterial and fungal pathogens (Asai et al., 2002; Chinchilla et al., 2007). Another set of PRRs that has been recently characterised are the

PEPRs. The cells, when wounded by pathogen to boost immunity release a family of peptides, *At*Peps. These peptides bind to PEPRs and activate the co-receptor BAK to trigger an immune response. Upon pep1 binding, PEPRs undergo endocytosis and subsequent vacuolar degradation (Huffaker et al., 2006; Ortiz-Morea et al., 2016). Furthermore, an infection resistance study conducted on mutants of the clathrin machinery protein, *chc2,* showed that clathrin is essential for immunity against certain bacterial infections. *chc2* mutants under-performed in flg22-triggered stomatal immune response (Mbengue et al., 2016).

1.5.4 Nutrient signaling

Plants absorb essential micro and macro elements from the soil. Some of the nutrient transporters have been studied in detail in low/deprivation and high abundance conditions of the respective nutrients in order to understand various stress responses of the plants. AtAMT1;1, AtAMT1;2 and AMT1;3 have been attributed to 90% N uptake in Arabidopsis (Yuan et al., 2007). The question to what happens to these transporters at the PM in low, medium and high Ammonium concentration was studied by Fluorescent correlation spectroscopy and TIRF-VAEM techniques. They observed clustering and subsequent endocytosis of AtAMT1;3 under high Ammonium stress. They also demonstrated that endocytosis of the clustered receptors could be both clathrin-mediated and membrane microdomain-associated (Wang et al., 2013b). Localisation studies and transport assays have been conducted on Boron (B) importers and exporters. Nodulin 26-like intrinsic protein 5;1 (NIP5;1), a boron importer that functions as Boric acid channel was shown to be repressed under high B conditions. Wang et al., demonstrated that its polar localisation is dependent on CME and its localisation is important for B translocation. Takano et al., showed that BOR1 exporter is expressed in low B condition and its polar localisation is also clathrin-dependent. Also, BOR1 is lost from the PM and gets degraded at the vacuole at high B conditions (Takano et al., 2005; Yoshinari et al., 2016).

Another transporter – IRON-REGULATED TRANSPORTER1 (IRT1) and its non-transcriptional regulation was studied by fluorescent imaging and biochemical studies. Barberon et al., reported that over-expression of IRT1 resulted in accumulation of iron and other metals leading to oxidative stress. Furthermore, they found that IRT1 is almost non-existent at the PM and they appear only on iron deprivation. This scenario is maintained by mono-ubiquitination of the transporter and by subsequent constitutive-endocytosis, recycling and degradation. Tyrphostin A23 treatment and also mutations hindering the ubiquitin interaction increased the concentration of IRT1 at the PM leading to afore-mentioned oxidative stress response (Barberon et al., 2011, 2014). Similar studies have been conducted on phosphate transporter. Lin et al., showed that PHOSPHATETRANSPORTER1 (PHT1), which was previously shown to be upregulated during Pi deprivation, is PM localised and NLA, an E3 ligase is its interactor at the PM. Moreover *nla* mutants contained increased concentration of PHT1 protein at the PM, proving that NLA induces the endocytosis and degradation of PHT1.They also observed PHT1-YFP localised in EE/TGN, which was absent after CME inhibition by Tyrphostin (Lin et al., 2013). Such studies show that endocytosis and protein turnover is key in maintaining metal homeostasis

1.5.5 Osmotic and salt stress response

Generally osmotic pressure is handled by modulating the amount of membrane at the PM through endo- and exo- cytosis. This response could be aimed to reduce membrane surface area, that potentially contributes to water loss through aquaporins and other means (Baral et al., 2015). Several studies have been conducted to test endocytosis – both clathrin-mediated and independent regulation by varying the parameters such as membrane tension, turgor pressure, osmolarity etc. Generally, in all systems including plants, higher osmolarity resulted in enhanced endocytosis and vice versa. Zwiewka et al., has clearly shown enhanced CME together with increased membrane internalisation through FM4 - 64 uptake experiments. However, in plants, salt stress, ie., stress with respect to Na+ ions, has been of special interest; and notably, salt response does not always concur with general hyperosmotic stress. Plants are much more sensitive to salt (and not always to hyperosmolar condition induced by mannitol, for example) and possess a multitude of signaling pathways to regulate Na+ induced stress. Thus, apart from broadly enhancing endocytosis, cells respond also by tuned CME controlled responses to NaCl (Zwiewka et al., 2015).

Na+ has been shown to regulate a heterotrimeric G protein complex to mediate growth response. The plants, to survive Na^+ stress, need to activate the G-protein via clathrin-mediated endocytosis of RGS1. High Na+ resulted in increased endocytosis of the PM RGS1, thus activating Gα and releasing Gβγ. This confers tolerance to NaCl (Colaneri et al., 2014). High concentration of NaCl also causes accelerated recycling of Aquaporins, PIP2. Nevertheless, it is not clear why Aquaporins are not permanently lost from the PM to prevent water loss, and is always continuously recycled back (Luu et al., 2012). The most notable NaCl mediated response is halotropism. And this goes hand in hand with endogenous hormonal signaling, specifically through establishing asymmetric auxin distribution and by endocytic-trafficking regulation of PIN2. auxin redistribution after high salt response has been shown recently. They have shown that Phospholipase gets activated at high NaCl concentration, concomitantly enhancing endocytosis of PIN2 protein at the side facing high salt concentration. auxin accumulates at the other end and an increased PM localisation of PIN2 could be observed on this side, probably by an inhibitory effect of auxin on endocytosis. Such an asymmetrical auxin distribution triggers increased cell division on the side facing the salt (auxin depleted side), thus enabling a directional bending away from salt. Importantly, external application of auxin (10nM IAA) abolishes halotropism entirely due to lack of asymmetry in auxin distribution between tissues (Galvan-Ampudia et al., 2013). Such studies show that CME plays a role in regulating very specific stimulus by salt ions conferring physiological growth response to stress, in addition to overall osmotic regulation.

Several plant responses to exogenous stimuli like halotropism, gravitropism and phototropism depend on auxin distribution and its heavily debated inhibitory effect on PIN endocytosis. It is wise to clarify and connect together the observations made so far. This is the aim of the final part of my thesis. We have tested the direct effect of both the widely used synthetic analogue of auxin – NAA and the natural auxin – IAA, on endocytosis of its exporter PINs and on completely unrelated receptors like PEPR. Also, we tested the effect of auxin directly on the endocytic machinery at the PM and looked for changes in their

endocytic rate. Importantly, we have tested BFA, the widely used tool for studying endocytosis and the effect auxin holds on it. Based on these tests, we have come up with a possible role for auxin in endocytosis.

1.6 Aims and scope of my thesis: summary

Clathrin-mediate endocytosis is a highly regulated process in the cell. The scope of my thesis is to understand the basic mechanisms behind CCP development and CCV formation and also to understand the regulatory role of the phyto-hormone, auxin in the whole organ system.

One of the aims of my thesis is to directly visualize the CCSs in the cell. We developed the metal replica technique in unroofed protoplasts to perform an ultrastructural analysis on the developing CCPs and the CCVs at the plasma membrane and the endomembrane systems. This, for the first time in plants, enabled us to understand the mechanism of membrane bending and CCP formation.

An unresolved question that still remains in plants is, if actin-pulling force is essential for membrane being and remodeling during CCP formation. To address this question, we have utilised TIRF microscopic observation of endocytic events at the plasma membrane following actin perturbation. In addition, we quantitavely analysed the endocytic potential of the cell to decipher the role of actin in endocytosis in high turgor pressure whole organ systems.

Post-endocytic trafficking of the endocytosed CCV is not understood in plants. How do the vesicles reach the EE? When and how uncoating of CCVs occur? How does the clathrin cage disassemble before fusion to the EE? Using TAP-MS analysis on CLATHRIN LIGHT CHAIN, we identified putative uncoating co-factors Auxilin-likes, and further characterised them. By following the disassembly of two different proteins of a single clathrin cage, we have proposed the functioning disassembly model. Also we followed the dynamics of the EE/TGN and actin with respect to the endocytosed CCVs. This enabled us to understand the mechanism of EE formation.

Finally, we checked if the developmentally crucial hormone, auxin, can regulate endocytosis in cells. To begin with, we carefully chose the right tools for the study. Finally we directly followed the endocytosis of a few cargoes to check for specificity of auxin in regulating endocytosis.

Through my thesis, I would describe in detail the methods we developed to study CME, new results we obtained that sheds light into various steps along the process and many more open questions that need to be resolved.

2 A Functional Study of AUXILIN-LIKE1 and 2, Two Putative Clathrin Uncoating Factors in Arabidopsis

2.1 Introduction

The endomembrane system provides a spatial organization for plant cell activities by compartmentalising distinct biochemical processes. The endomembrane system compartments, including the plasma membrane (PM), endoplasmic reticulum (ER), Golgi stacks, trans-Golgi network/early endosome (TGN/EE), multi-vesicular body (MVB) and vacuole perform distinct, specialised functions. At the cell periphery, endocytosis internalises PM-localised proteins, lipids, and extracellular material. The best-characterised endocytic mechanism in plants depends on the coat protein clathrin. More than 20 years ago, clathrin-coated pits and vesicles were observed in plant cells by electron microscopy and vesicles were purified from plant tissues (Tanchak et al., 1984; Mersey et al., 1985; Emons and Traas, 1986; Galway et al., 1993). With the advent of Arabidopsis thaliana as a model system and the availability of mutants and live imaging techniques in recent times, CME has been further investigated (e.g. Dhonukshe et al., 2007; Kitakura et al., 2011; Wang et al., 2013; Konopka et al., 2008, Gadeyne et al., 2014). Despite these advances, detailed descriptions of the events that comprise CME in plants are still often based on the more advanced studies of CME in animal and yeast systems (reviewed in McMahon and Boucrot, 2011).

In non-plant systems, the endocytic process is initiated by the adaptor protein complex AP-2, which acts by interacting with specific PM lipids and endocytotic cargoes and through clathrin recruitment. Proteins of the FCH domain only (FCHo) family were also proposed to be initiation factors (Henne et al., 2010). In plants, two candidates for initiation factors are the conserved AP-2 complex (Di Rubbo et al., 2013; Kim et al., 2013; Yamaoka et al., 2013; Bashline et al., 2013; Fan et al., 2013) and the recently identified TPLATE adaptor protein complex (Gadeyne et al., 2014; Zhang et al., 2015). A family of genes encoding monomeric adaptors of the AP180 N-Terminal Homology and Epsin N-Terminal Homology (ANTH/ENTH) type is present in plant genomes as well (reviewed in Zouhar and Sauer, 2014). Clathrin-coated pits grow via the recruitment, by adaptors, of clathrin triskelions. These are three-legged units of the clathrin coat, and are composed each of three clathrin light chains and three clathrin heavy chains (CLCs and CHCs, respectively). Clathrin triskelions assemble into a regularly shaped lattice surrounding the forming lipid vesicle. The scission (separation) of a completed vesicle from the PM is mediated by dynamins, i.e., molecular scissors that mechanically constrict the neck between the clathrin-coated vesicle (CCV) and the PM. In non-plant systems, upon scission, the CCV recruits uncoating factors, which are the molecular chaperone Hsc70 and its cochaperones auxilin/cyclin G-associated kinase (GAK) (Gao et al., 1991; Ahle and Ungewickell, 1990; Ungewickell et al., 1995; Massol et al., 2006; Xing et al., 2010). The uncoating step releases the vesicle for its subsequent fusion with endosomal compartments and allows the CME machinery components to be recycled for further rounds of endocytosis. The CCV-uncoating process is virtually uncharacterised in plants, although an auxilin-like protein of A. thaliana is thought to have an uncoating function (Lam et al., 2001).

So far, endocytosis has been manipulated in plants through the use of clathrin mutants and a dominant negative version of CHC (Kitakura et al., 2011; Dhonukshe et al., 2007), lines with downregulated expression of the endocytic adaptors (Gadeyne et al., 2014, Di Rubbo et al., 2013; Kim et al., 2013; Bashline et al., 2013; Fan et al., 2013), and mutants defective in dynamins (Yoshinari et al., 2016; Collings et al., 2008) and early endosomal components (Tanaka et al., 2013). These and similar tools allowed the roles of CME in processes such as plant immunity (reviewed in Khaled et al., 2015), establishment of polar auxin transport through the polarised subcellular localization of PIN-FORMED (PIN) auxin transporters (reviewed in Adamowski and Friml, 2015; Łangowski et al., 2016), and brassinosteroid signalling to be identified (Irani et al., 2012; Di Rubbo et al., 2013).

Here, our aim was to search for new proteins involved in CME in plants. To this end, we screened for proteins that bind to CLC, a fundamental component of the clathrin coat, in Arabidopsis. Based on several confirmed interactors, this study focused on two putative homologues of the uncoating factor auxilin. We found that overexpression of AUXILIN-LIKE1 and AUXILIN-LIKE2 caused an arrest of growth and development and inhibition of endocytosis, likely by preventing clathrin recruitment to endocytic pits initiated by the adaptor proteins. In contrast, loss of AUXILIN-LIKE1/2 function did not visibly interfere with development, or endocytosis, under optimal growth conditions.

2.2 Results

2.2.1 Identification of CLC1-associated proteins

To search for new proteins involved in CME, we employed Tandem Affinity Purification coupled with Mass Spectrometry (TAP-MS, Van Leene et al., 2014) using CLATHRIN LIGHT CHAIN1 (CLC1) as bait. We first expressed C- and N-terminal CLC1-TAP tag fusions in A. thaliana cell suspensions, which was followed by protein isolation, affinity purification, and identification of clathrin-bound proteins by mass spectrometry. Using this technique, we identified a small number of clathrin-binding proteins with sequence features indicating possible endocytic functions (Figure 1A).

The first proteins identified were two highly homologous proteins containing DNAJ domains at their C termini. As such, they bear limited similarity to auxilins and GAKs, which also contain C-terminal DNAJ domains that are needed for Hsc70 recruitment and activation leading to clathrin uncoating (Ungewickell et al., 1995). We named the putative auxilin homologues AUXILIN-LIKE1 (AT4G12780) and AUXILIN-LIKE2 (AT4G12770). These two proteins belong to a family of seven proteins in A. thaliana with C-terminal DNAJ domains, which can all therefore be called auxilin-likes. AUXILIN-LIKE1 is identical to the auxilin-like protein identified previously as a putative uncoating factor in A. thaliana (Lam et al., 2001).

Second, we found CAP1, a monomeric adaptor protein that, together with its closest homologue ECA4 (Song et al., 2012), was identified based on interactions with the TPLATE endocytic adaptor protein complex (Gadeyne et al., 2014). CAP1 and ECA4 are part of a family of ANTH/ENTH adaptors that may be involved in the generation of coated vesicles at various sites of the endomembrane system (Zouhar and Sauer, 2014)

Third, we found SH3P2, a protein consisting of a central BAR domain and a C-terminal SH3 domain, the first of which acts in membrane curvature generation, while the second functions in protein-protein interactions. In animals, proteins with a similar BAR-SH3 domain composition are called endophilins and have been shown to act in a clathrin-independent endocytic pathway (Boucrot et al., 2014; Renard et al., 2014). SH3P2 belongs to a family of three proteins in A. thaliana, the other two being SH3P1 and SH3P3 (Lam et al., 2001). SH3P2 has been implicated in the autophagy pathway (Zhuang et al., 2013, 2015), cell plate formation (Ahn et al., 2017) as well as vacuolar trafficking of ubiquitinated cargoes (Kolb et al., 2015; Nagel et al., 2017). Apart from AUXILIN-LIKE1/2, CAP1 and SH3P2, our TAP approach also identified the thioesterase DHNAT2, a peroxisome-localised enzyme (Widhalm et al., 2012), but we did not follow up on this finding. Finally, and as expected, we also identified both CHC homologues of A. thaliana as well as two of the three homologues of CLC.

To confirm the interactions of the two auxilin-likes, CAP1, and SH3P2 with clathrin, we utilized bimolecular fluorescence complementation (BiFC), also known as the split-GFP assay (Kerppola, 2009). In this approach, two proteins of interest are fused to two complementary fragments of the green fluorescent protein (GFP) molecule and transiently co-expressed in wild tobacco (Nicotiana benthamiana) leaves via Agrobacterium tumefaciens injection. The physical proximity, or a direct interaction, of the two assayed proteins results in reconstitution of the GFP molecule and fluorescence, which is captured by confocal laser scanning microscopy (CLSM). Using this method, we confirmed the interactions of AUXILIN-LIKE1, AUXILIN-LIKE2, CAP1, and SH3P2 with CLC1 (Figure 1B). As a negative control, we probed for interactions of all these proteins with PHOSPHATIDYLINOSITOL 4,5-BISPHOSPHATE KINASE1 (PIP5K1; Tejos et al., 2014; Ischebeck et al., 2013), a peripheral PM-localised protein, and found no reconstituted GFP fluorescence (Supplemental Figure 1A). We also tested for interactions between our CLC-interacting proteins and observed interactions of AUXILIN-LIKE1/2 with SH3P2 and CAP1, but no interaction between SH3P2 and CAP1 (Supplemental Figure 1B). A summary of all BiFC interactions is presented in Figure 1C. The localisation of the interacting pairs in wild tobacco cells appeared to be cytosolic. However, this is expected for soluble proteins, and we think it may not be indicative of the real interaction site of these proteins, as it is likely that reconstitution of a GFP molecule in the BiFC assay binds the two partners into stable dimers that subsequently don't exhibit normal localisation and activity. Finally, SH3P2 was recently shown to interact with CHC (Nagel et al., 2017), while AUXILIN-LIKE1 was reported to interact with clathrin and with SH3P1, an SH3P2 homologue (Lam et al., 2001). These additional observations clearly support our interaction data.

In conclusion, our TAP and splitGFP data demonstrate interactions between clathrin, AUXILIN-LIKE1/2, CAP1 and SH3P2, suggesting a common function of these proteins.

A

AGI code	Protein name	Isolated with (no. exp.)	
		C-terminal tag	N-terminal tag
AT4G12780 / AT4G12770	AUXILIN-LIKE1/2	2	-
AT4G32285	CAP1	2	-
AT4G34660	SH3P2	1	-
AT5G48950	DHNAT2	2	2
AT3G08530	Clathrin Heavy Chain1	2	2
AT3G11130	Clathrin Heavy Chain2	2	2
AT2G20760	Clathrin Light Chain1	2	2
AT2G40060	Clathrin Light Chain2	2	-

B

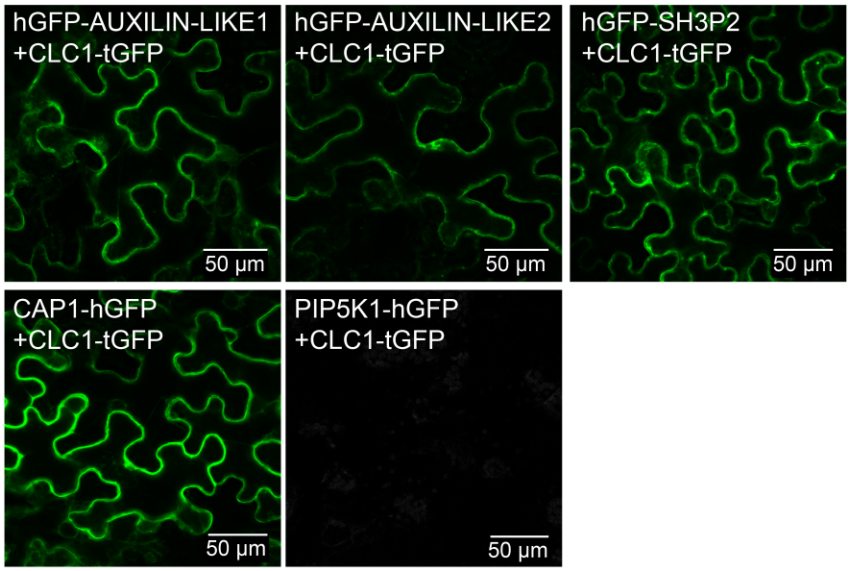

C

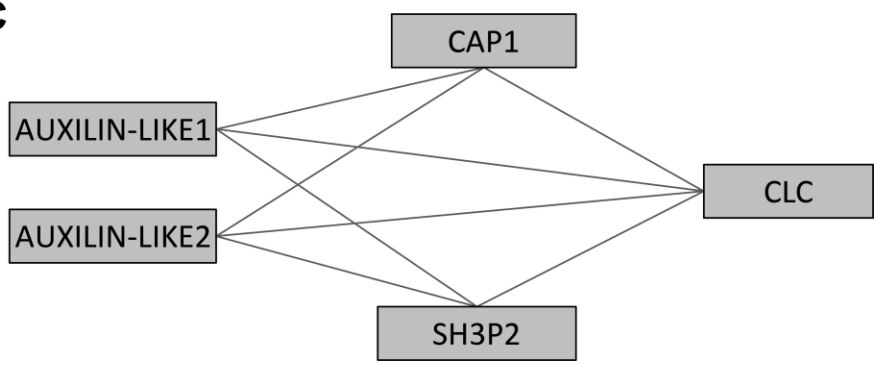

Figure 1. Identification of CLC-interacting proteins.

(A) Tandem Affinity Purification-Mass Spectrometry (TAP-MS)-based isolation of proteins associated with clathrin. CLATHRIN LIGHT CHAIN1 (CLC1) in C- and N-terminal fusions with TAP tags was used as bait. Two repetitions with each construct were performed.

(B) BiFC-based interactions between CLC1 and selected interactors identified with TAP-MS. Pairs of proteins of interest fused with halves of the GFP molecule were transiently expressed in wild tobacco leaves and reconstituted GFP fluorescence was imaged in epidermis on the abaxial leaf side. PIP5K1 did not interact with any of the proteins tested and was used as a negative control.

(C) Schematic representation of all interactions detected with BiFC. Additional interactions are presented in Supplemental Figure 1.

2.2.2 Subcellular localisation of clathrin-associated proteins

Next, we addressed the subcellular localisation of the newly identified clathrin interactors (Figure 2 and Supplemental Figure 2). We used CLSM on fluorescent protein fusions expressed in stable transgenic lines of A. thaliana. We used a common model system for endomembrane trafficking studies, the epidermis of the seedling root apical meristem (RAM). To detect CAP1 localisation, we cloned *CAP1pro:CAP1-mCherry* and *35Spro:CAP1-RFP* constructs and in both cases observed PM and cell plate binding (Figure 2A, B and Supplemental Figure 2A). Rarely, in approx. 10% of seedlings, CAP1 also showed binding to endosomal compartments (Supplemental Figure 2A). For SH3P2 localisation, we utilized the previously published *UBQpro:SH3P2-GFP* line and cloned a 35Spro:SH3P2-GFP construct. Here too we observed PM and cell plate binding, as well as endosomal-like intracellular signals, which were larger and more pronounced upon strong overexpression driven by the 35S promoter (Figure 2A, B and Supplemental Figure 2A). Our observations of SH3P2 localisation are consistent with other recent reports (Ahn et al., 2017; Kolb et al., 2015; Nagel et al., 2017). We failed to clone the AUXILIN-LIKE1/2 locus promoter region and instead prepared *UBQ10pro:GFP-AUXILIN-LIKE1* as well as 35Spro:RFP-AUXILIN-LIKE1 and *35Spro:RFP-AUXILIN-LIKE2* constructs. Both auxilin-likes localised to the PM and cell plates, like CAP1 and SH3P2 (Figure 2A, B). Furthermore, all proteins of interest showed background cytosolic staining, while SH3P2 and CAP1 additionally weakly stained the nucleus. In summary, the localisation patterns are consistent with a function of AUXILIN-LIKE1/2, CAP1, and SH3P2 in CME at the PM as well as clathrin-mediated processes at the cell plate. Additionally, SH3P2 functions at the endosomes, as has been demonstrated (Nagel et al., 2017), and the rarely observed endosomal localisation of CAP1 suggests it may function there as well.

In animal cells, auxilins and GAKs are briefly recruited to clathrin-coated pits (CCPs) at the end of their lifetimes on the PM during the transition to vesicle budding (Massol et al., 2006; Lee et al., 2006). Apart from this late burst of auxilin recruitment, small and variable amounts of auxilin are present at earlier stages of CCP growth (Massol et al., 2006). Such events can be observed with Total Internal Reflection Fluorescence (TIRF) microscopy, a method that allows live imaging of the PM surface at high magnification. We wanted to address the recruitment of AUXILIN-LIKE1/2 to newly forming clathrin-coated vesicles in a similar manner. We generated a double fluorescent reporter line, *CLC2pro:CLC2-GFP* x *UBQ10pro:mCherry-AUXILIN-LIKE1*, and employed Variable Angle Epifluorescence Microscopy (VAEM), a plant cell specific TIRF-like method that allows the PM surface through plant cell walls to be imaged, although it does not completely remove the cytoplasmic background below the PM (Konopka and Bednarek, 2008). In the epidermis of etiolated hypocotyls, AUXILIN-LIKE1 appeared as highly dynamic PM foci (Figure 2C, Supplemental Movie 1). With kymograph analysis, we observed events of brief AUXILIN-LIKE1 recruitment at the end of the lifetime of clathrin-coated pits, as previously described in non-plant systems. However, notably, we only observed this in a small fraction of all CCPs (estimated at around 5%), while the majority of clathrin-positive foci apparently did not recruit AUXILIN-LIKE1 (Figure 2C). We also regularly observed events of brief AUXILIN-LIKE1 recruitment at sites not containing clathrin. Based on these observations, we performed a control to assure that the observed colocalisation events indeed represent specific late recruitment to coated pits. We looked at the kymographs for events where AUXILIN-LIKE1 signal appears not at the end, but around the beginning of a CLC2-GFP trace, which we

consider to represent accidental colocalisation. We found such events to be much more rare (16 versus 100 events in a single TIRF movie), which confirms that AUXILIN-LIKE1 is indeed specifically recruited at the end of the PM lifetime for at least a subpopulation of CCPs.

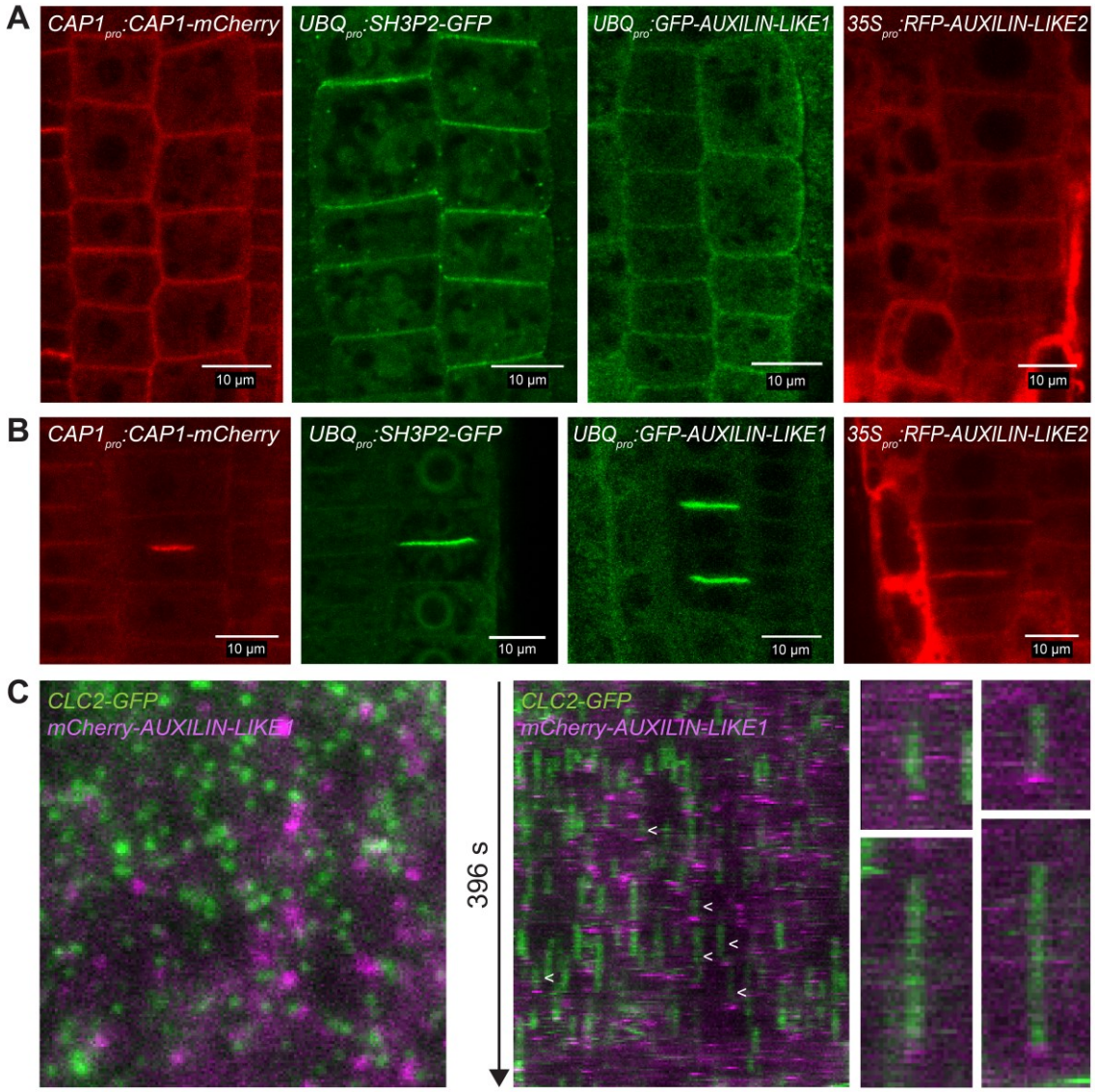

Figure 2. Subcellular localizations of the identified clathrin interactors.
PM (A) and cell plate (B) localisation of CAP1, SH3P2, AUXILIN-LIKE1 and AUXILIN-LIKE2 fluorescent protein fusions in the seedling root epidermis of stable transformants. Background cytosol staining can be observed in all lines, while CAP1 and SH3P2 also show faint nuclear staining. 35Spro:RFP-AUXILIN-LIKE1 was identical to 35Spro:RFP-AUXILIN-LIKE2. Additional localisation data, including co-localisations with PM markers, is presented in Supplemental Figure 2B.
(C) VAEM colocalisation of clathrin (*CLC2pro:CLC-GFP*) and AUXILIN-LIKE1 (*UBQpro:mCherry-AUXILIN-LIKE1*) in the hypocotyl epidermis. Kymographs (middle and right) show examples of auxilin-like1 recruitment at the end of CCP lifetime, which was observed in a small subset of all endocytic events (arrowheads). The majority of clathrin foci were lacking AUXILIN-LIKE1, and AUXILIN-LIKE1 foci without clathrin could be observed. See also Supplemental Movie 1.

This observation might indicate that the majority of clathrin-coated vesicles do not use AUXILIN-LIKE1/2 for uncoating. Alternatively, perhaps AUXILIN-LIKE1/2 recruitment often takes place later after scission, when the vesicles had already moved away from the PM, and thus moved away from the variable region of VAEM detection. Some brief recruitment events could have also been missed because our method uses sequential imaging of the two fluorescent channels.

2.2.3 Seedling phenotypes of AUXILIN-LIKE1/2 overexpressors

While generating transgenic lines expressing fluorescent protein fusions of the clathrin-associated proteins, we observed that overexpressing AUXILIN-LIKE1 and AUXILIN-LIKE2 under the control of the 35S promoter was associated with deleterious phenotypes (Supplemental Figure 3B). In the T2 generation of *35Spro:RFP-AUXILIN-LIKE1* and *35Spro:RFP-AUXILIN-LIKE2* lines, we saw many seeds that did not germinate, even after prolonged culturing. Seeds that did germinate often developed slowly and exhibited relatively weak and patchy expression of RFP-AUXILIN-LIKE1/2 signals. In the T3 generation, a virtually complete silencing of the transgenes was observed. These observations indicate that we selected against high AUXILIN-LIKE1/2 expression levels, which was of interest to us, because overexpressing auxilins in non-plant systems can inhibit endocytosis (Zhao et al., 2001). In contrast, overexpression of CAP1 and SH3P2 in 35S-promoter-driven lines did not interfere with seed germination or seedling development (Supplemental Figure 3A). Therefore, we chose to follow up on the effects of AUXILIN-LIKE1/2 overexpression as a possible way to elucidate a clathrin-associated function of these two putative uncoating factors.

To circumvent the deleterious effects of constitutive AUXILIN-LIKE1/2 overexpression, we generated stable transgenic A. thaliana lines overexpressing AUXILIN-LIKE1/2 under the control of chemically inducible promoters. We prepared estradiol-inducible transactivation lines overexpressing untagged AUXILIN-LIKE1 and AUXILIN-LIKE2 (XVE»AUXILIN-LIKE1 and XVE»AUXILIN-LIKE2), as well as a tamoxifen-inducible transactivation line overexpressing GFP-tagged AUXILIN-LIKE1 (*INTAM»GFP-AUXILIN-LIKE1*). Depending on the strength of a particular transgenic line, upon chemical induction, we observed a spectrum of seedling phenotypes ranging from weak reduction in the rates of growth and development to a strong delay or inhibition of germination, as well as the complete inhibition of seedling growth and development if the transgene was activated later (Figure 3A, B, Supplemental Figure 4). Overexpression of auxilin-like genes in the lines with strong phenotypes was confirmed with qRT-PCR (Supplemental Figure 5). Using long-term, time-lapse confocal microscopy with automated root tracking (TipTracker; von Wangenheim et al., 2017), we directly compared root growth rates with AUXILIN-LIKE1 expression levels in the root tips of induced *INTAM»GFP-AUXILIN-LIKE1* seedlings (Supplemental Figure 6). GFP-AUXILIN-LIKE1 expression was first observed 1 h after induction and gradually increased until approximately 15 h. Following GFP-AUXILIN-LIKE1 expression, we observed a sharp decrease in growth between the 4th and 11th h of induction. Therefore, growth inhibition appears to be a relatively direct effect of AUXILIN-LIKE1/2 overexpression.

Using light microscopy, we found that the morphology of cells in the RAM in AUXILIN-LIKE1/2 overexpressing seedlings was drastically different from that of the wild-type controls. RAM epidermis cells of XVE»AUXILIN-LIKE1/2 lines exhibited enlarged vacuoles that filled major parts of the cell volume, while the cytosol content was reduced and the nucleus was displaced from its central location (Figure 3C and D). This phenomenon was typically observed after approximately 1 day of induction and became progressively more pronounced after 2-3 days.

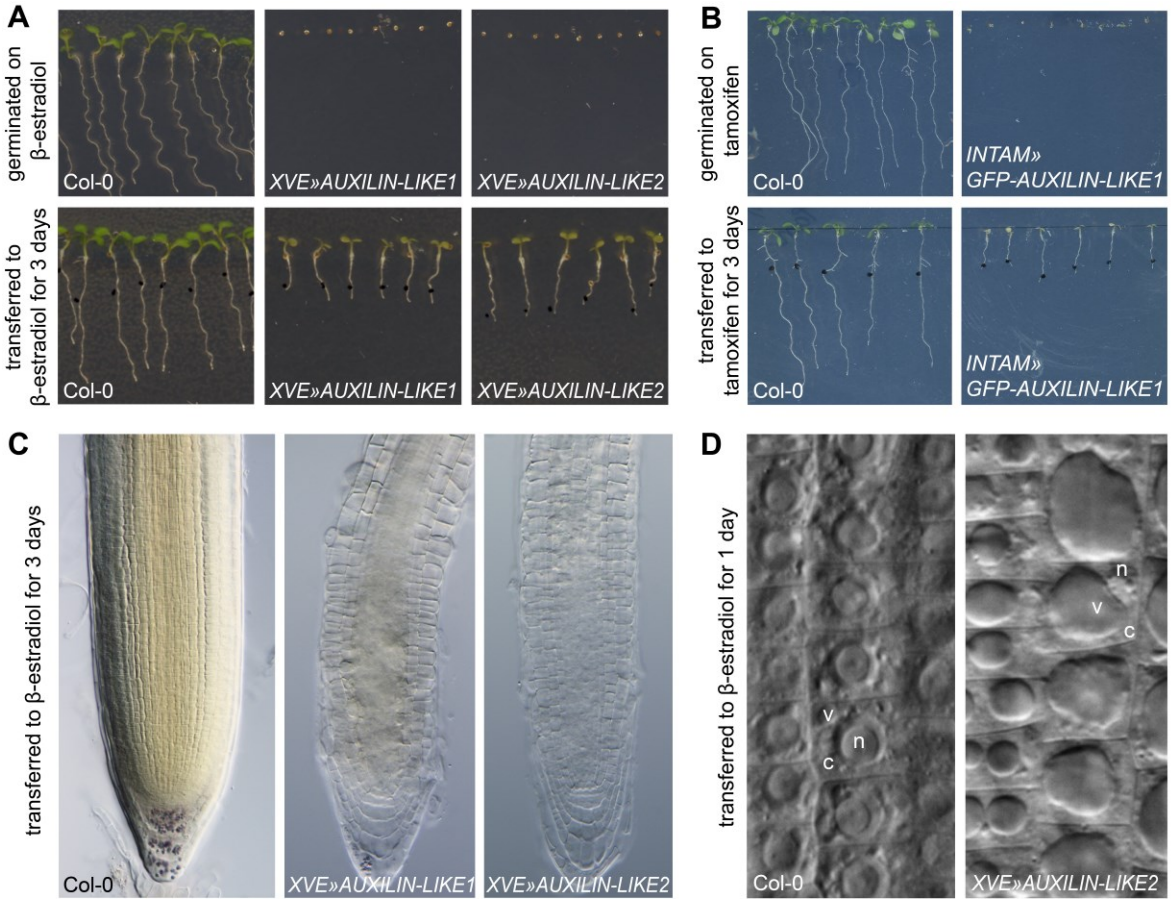

Figure 3. AUXILIN-LIKE1/2 overexpression causes an arrest of seed germination and seedling growth and alterations in cell morphology.
Overexpression of auxilin-likes in *XVE»AUXILIN-LIKE1/2* (A) or *INTAM»GFP-auxilin-like1* (B) lines inhibits or strongly delays seed germination, and inhibits seedling growth if the transgene is induced post-germination. The RAMs of AUXILIN-LIKE1/2 overexpressing seedlings appear semi-transparent (C) due to enlargement of vacuoles and reduction of the cytoplasmic volume (D). V, vacuole; c, cytoplasm; n, nucleus

2.2.4 Inhibition of endocytosis by AUXILIN-LIKE1/2 overexpression

Using our inducible overexpressing lines, we then assayed the effect of AUXILIN-LIKE1/2 overexpression on endocytosis. Three lines of evidence support the notion that overexpression of AUXILIN-LIKE1 and AUXILIN-LIKE2 leads to the inhibition of endocytosis: (i) imaging of the endocytic cargoes, (ii) imaging of the molecular endocytic machinery, and (iii) the distribution of membranes within the cell.

As a basic experiment to assay the general rates of endocytosis, we monitored the uptake of FM4-64, a membrane dye commonly used in studies of endocytosis (Aniento and Robinson, 2005; Bolte et al., 2004; Jelínková et al., 2010). After pulse staining of A. thaliana seedlings with FM4-64, the dye is gradually taken up by the cell through the endocytic process, and over time it can be observed first at endosomal compartments and then at the tonoplast (vacuolar membrane). XVE»AUXILIN-LIKE1/2 lines induced overnight (approx. 16-24 h) showed an inhibition of FM4-64 uptake in a majority of the seedlings and RAM epidermis cells observed (Figure 4A). Considering the alteration of cell morphology – the enlargement of vacuoles – we monitored the cells closely in the visible light channel to recognise areas still containing the cytosol, and therefore also endosomes that FM4-64 could reach, and saw that staining was either absent from these areas or endosomes were only weakly stained compared to the controls (Supplemental Figure 7A). In these experiments, we also observed that FM4-64-stained PMs in XVE»AUXILIN-LIKE1/2 lines often lost the normal, smooth appearance and were instead thicker and uneven, which will be explained below. We then repeated the FM4-64 uptake experiment in the *INTAM»GFP-AUXILIN-LIKE1* line at earlier stages of induction. In this line, we could monitor AUXILIN-LIKE1 expression directly due to the GFP fluorescence. We observed inhibition of FM4-64 uptake into RAM epidermis cells as early as 8 h after transgene induction (Figure 4B). The rate of endocytic tracer uptake was inversely correlated with GFP expression levels on a cell to cell basis, confirming that the endocytic inhibition by auxilin-like overexpression is cell-autonomous. Importantly, at these early stages of overexpression, the epidermal cells still exhibited normal morphology, with abundant cytosol and small, fragmented vacuoles. Finally, at an even earlier time point of 5h of expression induction, *GFP-AUXILIN-LIKE1 levels* were already high in the lateral root cap, and we observed inhibition of FM4-64 uptake specifically in this tissue (Supplemental Figure 7B).

Next, we corroborated these findings by monitoring known CME cargoes, including the auxin efflux transporters of the PIN family (Nodzyński et al., 2016; Adamowski and Friml, 2015) and the syntaxin KNOLLE (Lauber et al., 1997). The endocytic trafficking of PIN proteins is classically assayed via Brefeldin A (BFA) treatments. BFA treatments lead to the deactivation of ADP-ribosylation factors (ARFs), components of the vesicle formation machinery in the endomembrane system, by directly targeting a subset of ARF activators, the guanine nucleotide exchange factors for ARFs (ARF-GEFs). As a result, certain endomembrane trafficking pathways, including GNOM ARF-GEF-dependent polar recycling of PINs to the PM, are inhibited, while other, including PIN endocytosis, are not. As a related phenomenon, agglomeration of endosomal compartments into large structures called ‘BFA bodies’ or ‘BFA compartments’ occurs. Therefore, after BFA treatments, the continuously internalized PIN proteins can be observed inside BFA bodies, from which they can’t be recycled back to the PM (Naramoto et al., 2014). In RAMs of *XVE»AUXILIN-LIKE1/2* seedlings induced for 16-24 h, immuno-labelled PIN1 was rarely found in BFA bodies in the stele, while in the epidermis, PIN2-GFP was not observed in BFA bodies at all (Figure 5A, B), indicating that PIN1 and PIN2 endocytosis was inhibited. To assure that BFA bodies still form after auxilin-like overexpression and that they can be observed despite the enlarged vacuoles, we visualised the BFA body structures themselves using CLC2-GFP as a marker of aggregating endosomal populations (Figure 5C).

To confirm these observations without the use of BFA and to more clearly distinguish the internalisation of PIN2 from its biosynthesis and secretion, we monitored the cellular turnover of PIN2 over the long term using PIN2 fused to Dendra (a green-to-red photoactivatable fluorescent protein induced by blue light). After 6 h of XVE»AUXILIN-LIKE2 induction, we converted PIN2-Dendra from the green into the red form in whole root tips. 18 h later, AUXILIN-LIKE2 overexpressing seedlings retained significant amounts of the red PIN2-Dendra form at the PMs (Figure 5D), demonstrating inhibition of PIN2 endocytosis. In control seedlings, virtually all of the red form became internalized and degraded and was replaced by newly synthesised, green PIN2-Dendra.

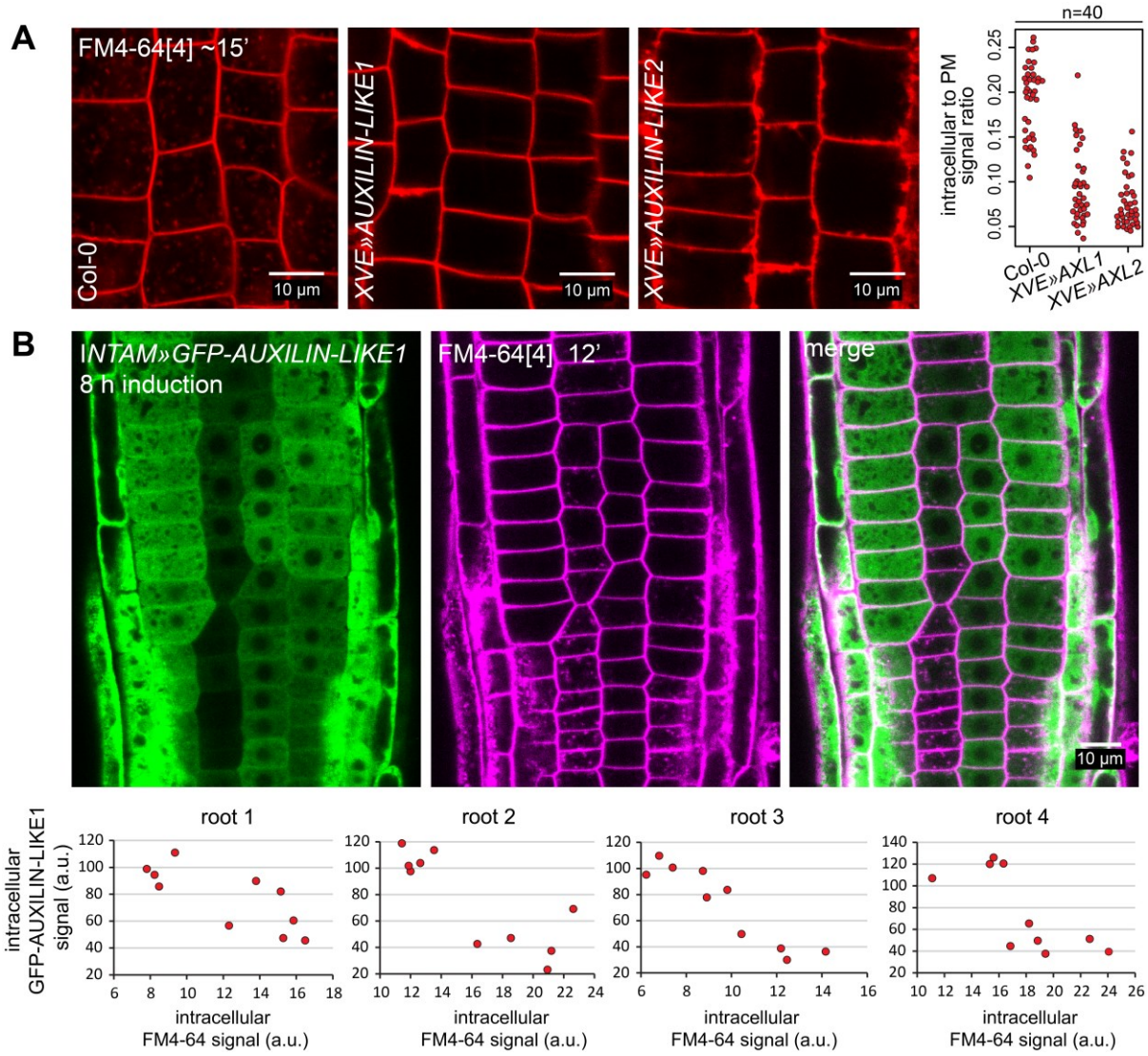

Figure 4. Inhibition of FM4-64 endocytic tracer uptake by AUXILIN-LIKE1/2 overexpression
(A) The uptake of the endocytotic tracer FM4-64 into RAM epidermal cells *in XVE»AUXILIN-LIKE1/2* seedlings induced for 16-24h is strongly reduced. At least 10 roots per genotype were imaged in three repeated experiments. The graphs shows quantification of intracellular-to-PM FM4-64 signal ratio from 40 cells coming from 4 roots in a representative experiment.
(B) FM4-64 uptake at early stages (8h) of *INTAM»GFP-AUXILIN-LIKE1* induction. The degree of FM4-64 uptake correlated with GFP-AUXILIN-LIKE1 levels in individual root meristem epidermal cells. Graphs show examples of this correlation in four roots. Each data point represents an individual cell. Notice that at this stage of AUXILIN-LIKE1 overexpression, cell morphology remains normal, with abundant cytosol illuminated by GFP-AUXILIN-LIKE1 expression, and small, fragmented vacuoles seen by negative staining. a.u., arbitrary units.

In addition to PIN1 and PIN2, we monitored the endocytosis of KNOLLE. KNOLLE is a SNARE protein that is specifically expressed during cell division, and targeted to the growing cell plates, where it is retained for some time after cell division is completed. The specific localisation of KNOLLE to the newly formed cell membranes is dependent on the endocytic process, as inhibition of endocytosis is associated with lateral spreading of KNOLLE to the 'old' PMs after the completion of cell division (Boutté et al., 2010). Similar to previous observations, overexpression of AUXILIN-LIKE1/2 also caused diffusion of KNOLLE out of the newly completed cell membranes and into the 'old' PMs, demonstrating that endocytosis of KNOLLE was inhibited (Figure 5E).

In summary, our imaging of FM4-64 dye, as well as known CME cargoes: PIN1, PIN2 and KNOLLE, supported the notion that overexpression of AUXILIN-LIKE1/2 inhibits endocytosis.

2.2.5 AUXILIN-LIKE1/2 overexpression inhibits endocytosis at the clathrin recruitment step

Next, we visualized the effect of auxilin-like overexpression on the molecular components of the endocytic machinery itself. For this analysis, we crossed the XVE»AUXILIN-LIKE1 line with fluorescent reporter lines for subunits of the adaptor protein complexes AP2 and TPLATE (AP2A1-TagRFP and TPLATE-GFP), for clathrin (CLC2-GFP), and for dynamins (DRP1C-GFP). We then performed live imaging after 1 day (16-24 h) of AUXILIN-LIKE1 induction.

Through CLSM of seedling roots, we observed that clathrin signals were absent from the PMs of epidermal cells in a majority of AUXILIN-LIKE1 overexpressing seedlings (Figure 6A). These observations were confirmed in the hypocotyl epidermis, where we employed VAEM. Upon AUXILIN-LIKE1 overexpression, normal, densely distributed clathrin-positive PM foci were not observed (Figure 6B). However, we did observe CLC2 signals that were very sparse, larger than normal endocytic pits, and often laterally mobile (Supplemental Movie 2). We cannot determine whether these were clathrin structures that were attached to the PM or localised to the cytosol.

Apart from endocytosis at the PM, clathrin participates in vesicle formation at other compartments of the endomembrane system, where it likely acts with AP-1, AP-3 and AP-4 complexes to function in vacuolar, and potentially secretory, trafficking (Richter et al., 2014; Park et al., 2013; Wang et al., 2013b, 2014; Feraru et al., 2010; Fuji et al., 2016; Robinson and Pimpl, 2014; Zwiewka et al., 2011). Interestingly, it appears that the endosomal clathrin pools were not affected by auxilin-like overexpression, as CLC2-GFP signals were still bound to endosomes (observed as large, intracellular bodies) in both roots and hypocotyls (Figure 6A, B, Supplemental Movie 2).

The presence of dynamin (DRP1C) at the PM was also reduced, although the reduction was less pronounced than that of clathrin. In most roots, very weak PM signals of DRP1C-GFP could still be observed (Figure 6C), while VAEM in the hypocotyl epidermis showed DRP1C-positive foci of normal appearance, but at much reduced densities compared to the control (Figure 6D). These remaining DRP1C foci did not show normal dynamics in most of the cells observed, but instead exhibited very long lifetimes, suggesting that these DRP1C-containing structures may have been non-functional (Figure 6E).

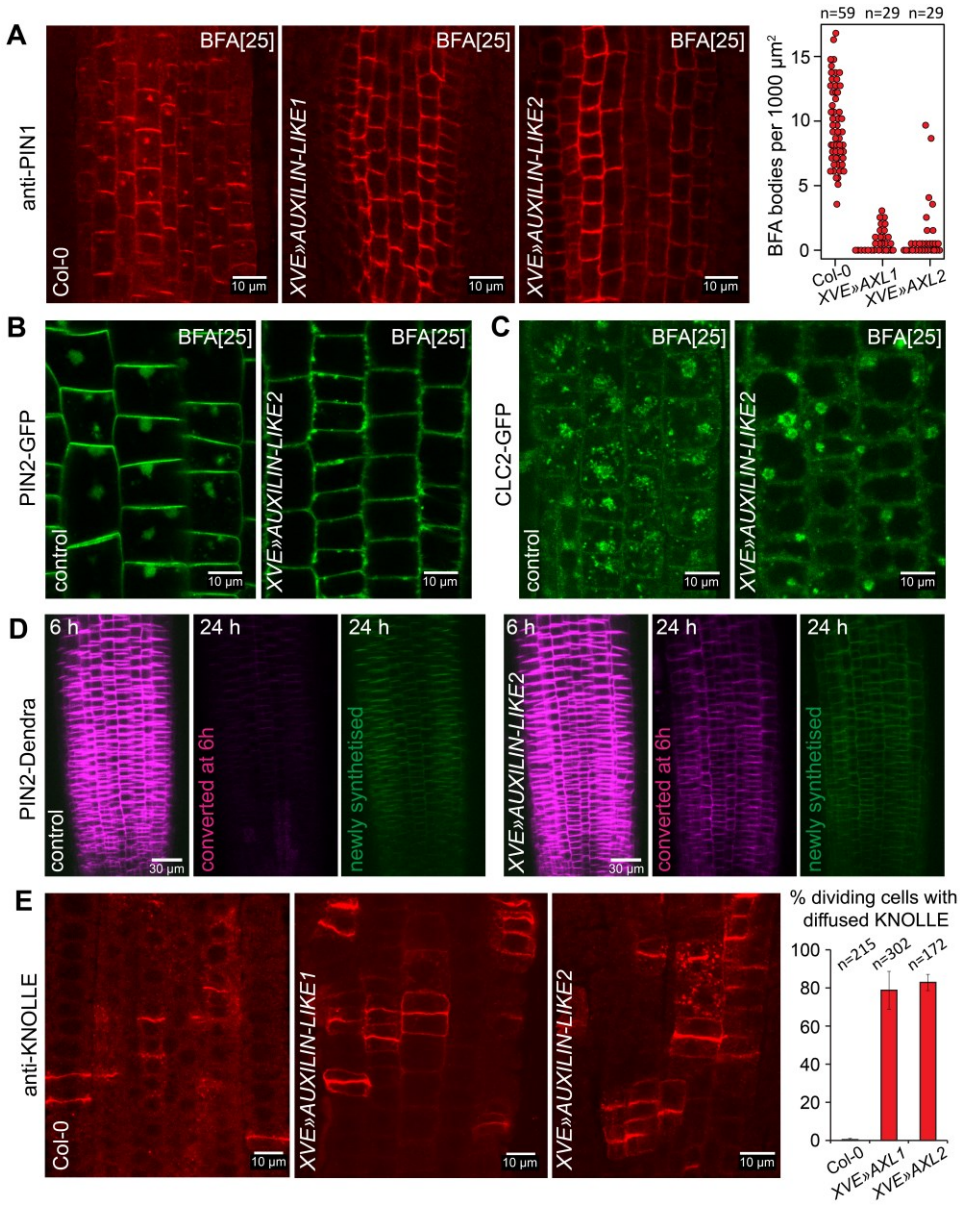

Figure 5. Inhibition of protein cargo endocytosis by AUXILIN-LIKE1/2 overexpression

(A) Immunolocalization of PIN1 in the RAM stele after 90 min of BFA (25 µM) treatment. The BFA body number is markedly reduced, indicative of inhibition of PIN1 endocytosis. The graph shows collated results from three repetitions of the experiment. Each data point represents one root.

(B) Following AUXILIN-LIKE2 overexpression, PIN2-GFP does not localise to BFA-induced bodies in RAM epidermis after 90 min of BFA (25 µM) treatment. Control experiment with CLC2-GFP used as an endosome marker (C) shows that BFA bodies can be easily observed in auxilin-like overexpressing seedlings despite the enlarged vacuoles. (D) Long-term PIN2 turnover monitoring in *XVE»AUXILIN-LIKE2* with photoconvertible PIN2-Dendra fusion. PIN2-Dendra has been converted from green into red form in whole root tips at 6h of AUXILIN-LIKE2 induction. At the 24h time point, significant amounts of the red form have been retained at the PMs of auxilin-like overexpressing seedlings, while the protein has been internalised and degraded in the mock-treated controls. Panels at 6h show merged green and red channels, while panels at 24h show green and red channels separately. (E) Immunolocalization of KNOLLE in the RAM of *XVE»AUXILIN-LIKE* lines showing diffusion of KNOLLE out of the completed cell plates and into the 'old' PM in late cytokinetic cells. The graph show % of cells with diffused KNOLLE signals; error bars indicate standard deviation between 3 experiments. Experiments in A, B, C, E were performed after 16-24h of XVE»AUXILIN-LIKE1/2 induction.

Interestingly, in contrast to clathrin and dynamin, the endocytic adaptor complexes AP2 and TPLATE were not only present at the PMs of *XVE»AUXILIN-LIKE1*, but their binding was consistently stronger than in control conditions. This was most clearly observed in the RAM epidermis using CLSM (Figure 7A, B), but the same phenomenon occurred in the hypocotyl epidermis, as observed by VAEM (Figure 7 C, D). Furthermore, time-resolved imaging demonstrated that these adaptor protein foci had shorter lifetimes at the PM than under control conditions (Figure 7E, F; Supplemental Movies 3 and 4).

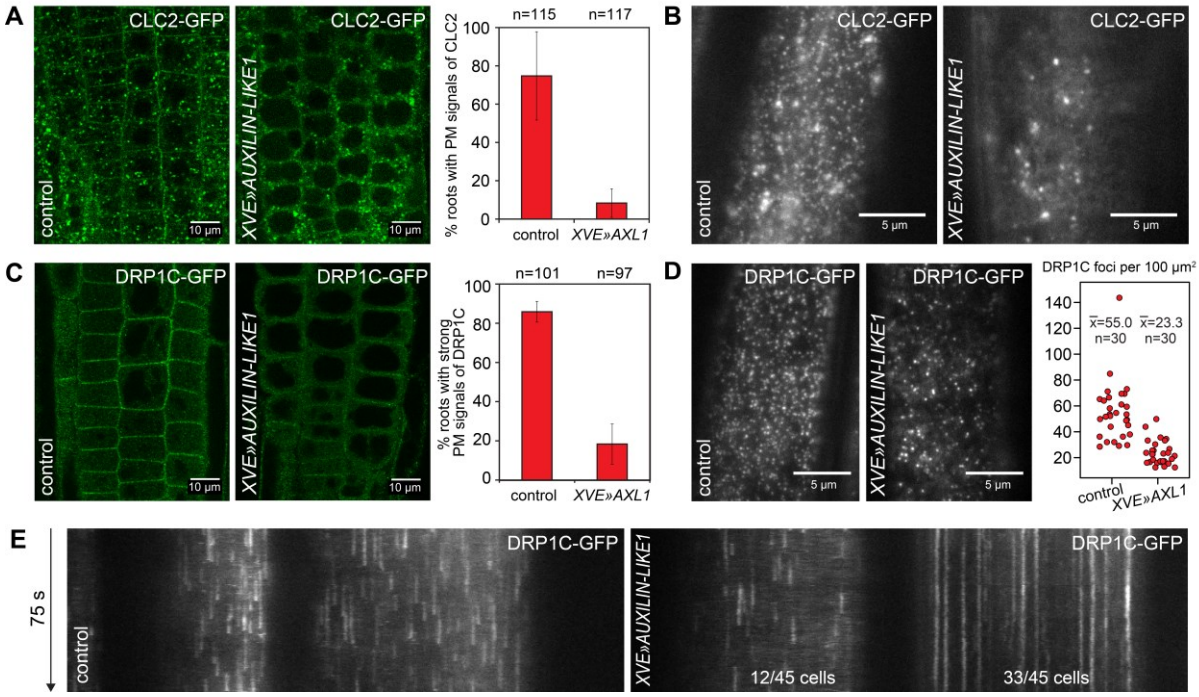

Figure 6. Loss of clathrin and dynamin from the PMs of XVE»AUXILIN-LIKE1 line.
Following AUXILIN-LIKE1 overexpression, CLC2-GFP signals were absent from the PMs of RAM epidermis cells (A) and normal CLC2-GFP endocytic foci could not be observed in hypocotyl epidermis by VAEM (B). The endosomal clathrin populations were retained in both tissues.
DRP1C-GFP PM signals were markedly reduced in RAM epidermis (C), and the density of DRP1C-positive PM foci was reduced in the hypocotyl epidermis (D). The remaining DRP1C-positive PM foci had exceptionally long lifetimes in the majority of observed cells (E).
Graphs in (A) and (C) show average ± SD percentage of roots with strong PM signals from the fluorescent markers. Graph in (D) shows collated measurements from three repetitions of the experiment. All experiments in this figure were performed after 16-24h of XVE»AUXILIN-LIKE1 induction.

In summary, live microscopy observations of clathrin, dynamin, and adaptor protein complexes suggest that auxilin-like overexpression blocks endocytosis after the initial step of adaptor protein complex binding to the PM. It appears that endocytic pits are initiated by the adaptors at high frequency, but due to the lack of clathrin binding, they are not progressing and quickly become aborted. The nature of the scarce, remaining DRP1C-positive structures with long lifetimes remains unclear.

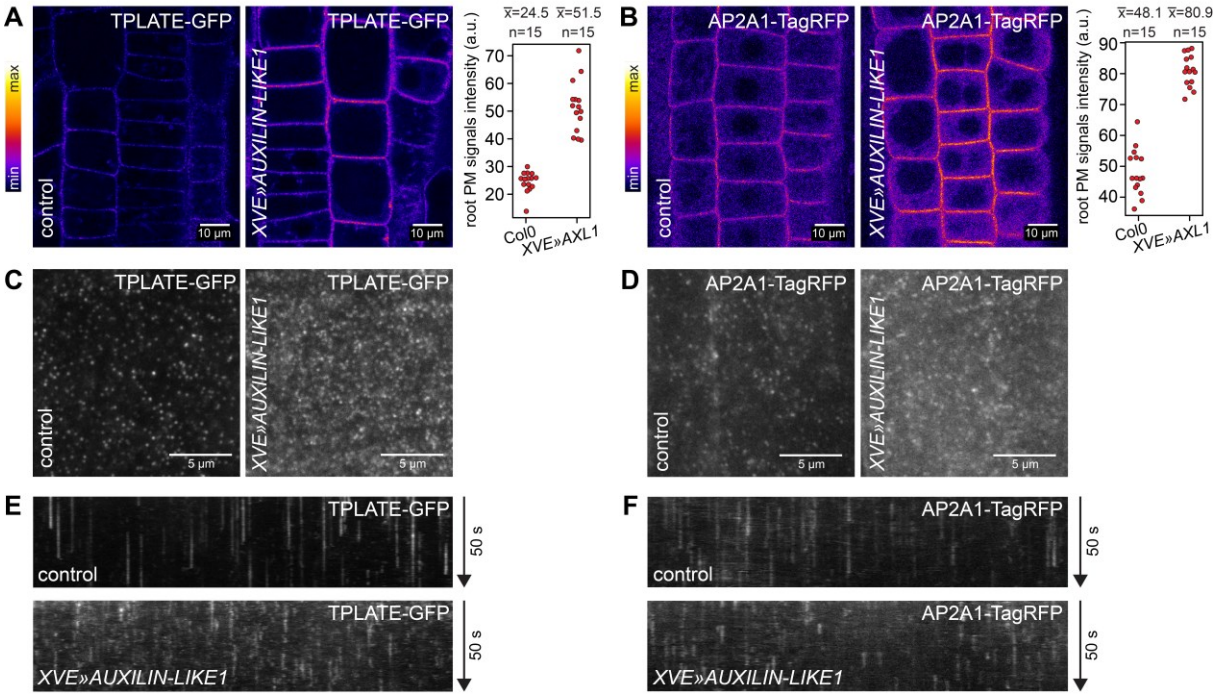

Figure 7. Increased PM binding of endocytic adaptor protein complexes in XVE»AUXILIN-LIKE1 line.
Overexpression of AUXILIN-LIKE1 caused increased PM binding of TPLATE, a subunit of the TPLATE complex, as well as AP2A1, a subunit of the AP-2 complex. CLSM images from RAM epidermis (A and B) and VAEM images from hypocotyl epidermis (C and D) are shown. Graphs in A and B show PM signal intensity measurements from a representative experiment. Kymographs (E and F) show reduced lifetimes of TPLATE and AP2A1 foci in *XVE»AUXILIN-LIKE1* line, likely indicating that endocytic pits aborted after initiation. All experiments in this figure were performed after 16-24h of *XVE»AUXILIN-LIKE1* induction.

2.2.6 Disturbance in cellular membrane distribution indicates inhibited endocytosis

Apart from cargoes and the trafficking-related molecular machinery, the endomembrane system naturally consists of the biological membranes themselves. These membranes are in a constant state of flux through the cell, moving from place to place as vesicles (e.g. secretory vesicles, CCVs, COPI and COPII-coated vesicles) and through the maturation of compartments, examples of which include the proposed maturation of TGN/EE into MVBs (Scheuring et al., 2011) and the cis-medial-trans progression of cisternae in the Golgi stack. Considering this overall membrane flow, one can imagine that interfering with a particular trafficking process could lead to broad changes in membrane distribution in the endomembrane system. Specifically, inhibited endocytosis should lead to the excess accumulation of the membrane at the cell periphery – the plasma membrane – and a concomitant loss of membranes from the cell interior, both occurring due to the now isolated, imbalanced activity of the secretory pathway. Indeed, upon staining the PMs in AUXILIN-LIKE1/2 overexpressing lines with the FM4-64 dye or with PIN2-GFP, we observed thick deposits of membrane at the cell periphery instead of the typical smooth, thin PMs (Figure 8). This observation provides more, although indirect, evidence for inhibited endocytosis due to AUXILIN-LIKE1/2 overexpression. Staining with propidium iodide (PI)

showed that the cell wall structure was also affected (Supplemental Figure 8), as thick deposits strongly binding to PI could be seen.

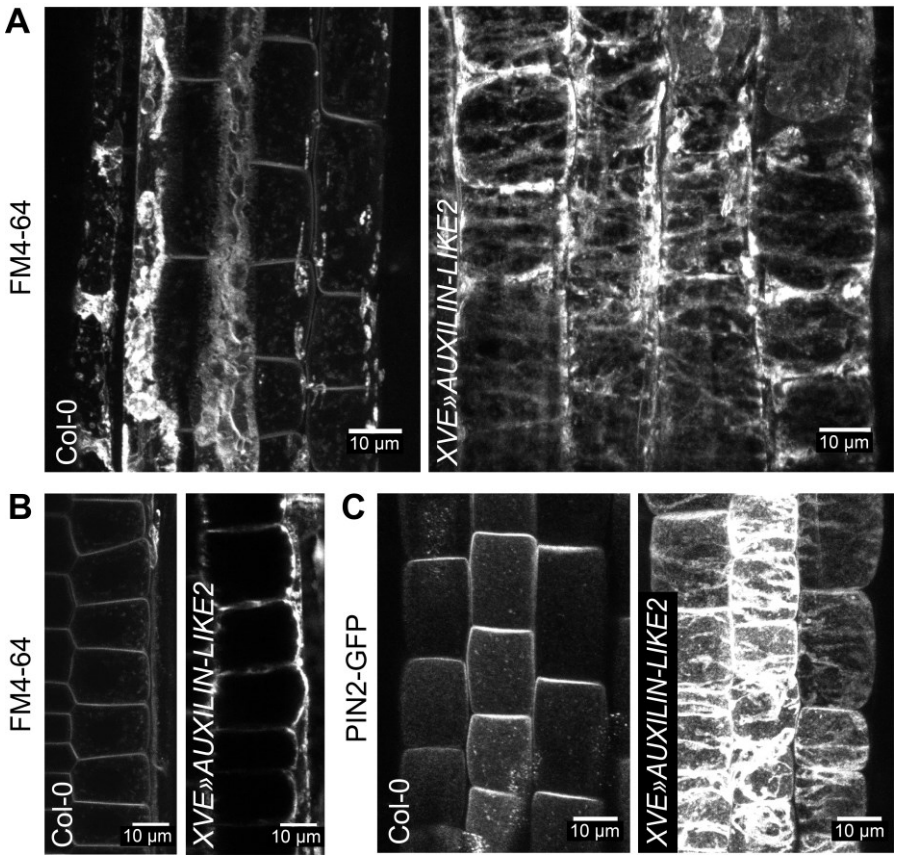

Figure 8. Excess membrane accumulation at the PM as a result of inhibited endocytosis
Overexpression of AUXILIN-LIKE2 caused excess deposition of membrane material at the PMs of root epidermis, as visualised with FM4-64 staining (A and B) or with PIN2-GFP (C). (A) and (C) are maximum intensity projections of z-stacks through outer region of the epidermis, while (B) is a longitudinal section of epidermal cells showing membrane aggregation mainly in the outer domain. FM4-64-stained deposits in Col-0 in (A) are likely remnants of apoptosed lateral root cap cells.

Taken together, the imaging of endocytic cargoes, the endocytic machinery components, and the cellular distribution of membranes all demonstrated that overexpressing AUXILIN-LIKE1/2 leads to the inhibition of endocytosis. This phenomenon is analogous to the effect of overexpression of auxilin homologues in non-plant systems. However, we do not consider these data to necessarily be indicative of a vesicle-uncoating function. The most parsimonious interpretation is that overexpressed AUXILIN-LIKE1/2 proteins may inhibit the recruitment of clathrin to initiating endocytic pits simply by binding to and retaining all available clathrin in the cytosol, although this simple model would not explain why the endosomal pools of clathrin remain intact. However, together with our protein-protein interaction and subcellular localisation data, these findings constitute strong evidence for a clathrin-related function of AUXILIN-LIKE1/2.

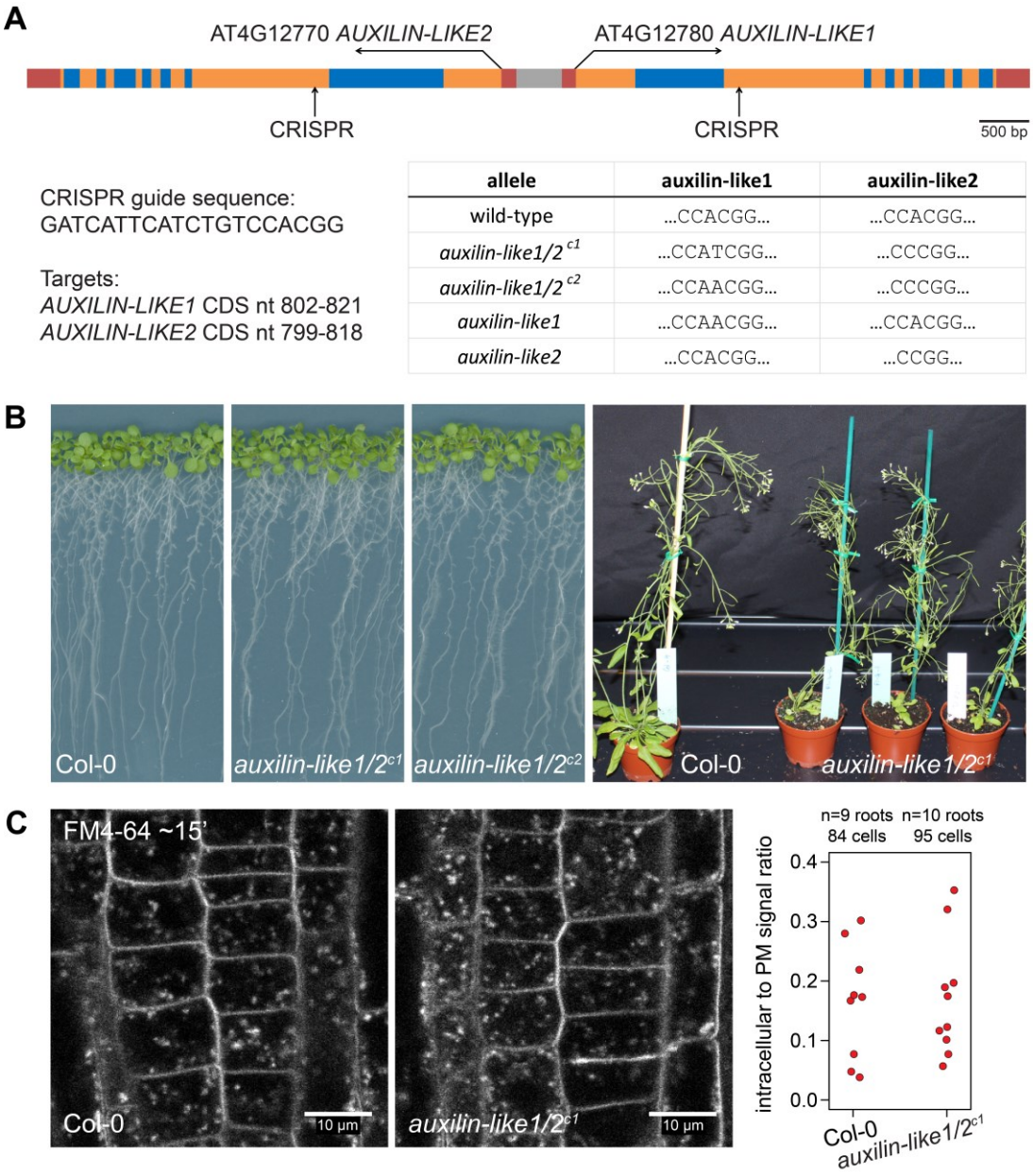

Figure 9. *auxilin-like1/2* loss-of-function mutants

(A) Isolation of *auxilin-like1/2* CRISPR mutants. Top: overview of the *AUXILIN-LIKE1/2* genomic locus showing CRISPR target sites in the 2nd exons of AUXILIN-LIKE1 and AUXILIN-LIKE2. Bottom: details of the CRISPR target sequence and the isolated mutant alleles.

(B) *auxilin-like1/2* double homozygous mutants, as well as single mutants, developed normally at both the seedling and adult stages.

(C) FM4-64 uptake into *auxilin-like1/2c1* seedlings was comparable to that of the controls, indicating functional endocytosis.

2.2.7 AUXILIN-LIKE1/2 loss of function

In an attempt to address the specific molecular function of AUXILIN-LIKE1/2, we aimed to obtain *auxilin-like1/2* knockout plants. The behaviours of the two proteins in terms of interactions, localisation, and the effects of overexpression were the same in our experiments, and the two proteins share very high sequence similarity. Therefore, we expected AUXILIN-LIKE1 and AUXILIN-LIKE2 to be functionally redundant, and so, we aimed

to obtain a double mutant. *AUXILIN-LIKE1* and *AUXILIN-LIKE2* genes occupy a common locus on chromosome 4, in which their coding sequences are inversely oriented around a short, shared promoter region (Figure 9A). The genes are therefore tightly linked, making it impossible to generate double mutants by crossing single T-DNA insertion lines. Instead, we generated double knockouts by simultaneously targeting both paralogues using CRISPR technology. The CRISPR method generates short (1-2 nt) deletions or insertions in the target sequence, thus causing open reading frame shifts and disrupting the coding sequence. Using this approach, we isolated two double mutant combinations, *auxilin-like1/2c1* and *auxilin-like1/2c2*, as well as single *auxilin-like1* and *auxilin-like2* mutants (Figure 9A). To our surprise, both the single and the double mutants were phenotypically normal under standard growth conditions at the seedling and adult stages (Figure 9B). The plants also exhibited normal fertility. Furthermore, an FM4-64 uptake experiment using the RAM epidermis of *auxilin-like1/2c1* seedlings did not indicate any defects in endocytosis (Figure 9C). This loss-of-function analysis revealed that A. thaliana auxilin-like proteins are not essential for endocytosis and development, at least under optimal environmental conditions. This finding is in contrast to the results of similar analyses in animals such as mouse (Mus musculus), worm (Caenorhabditis elegans), and zebrafish (Danio rerio), where defects in growth and development of *auxilin/GAK* mutants were reported (Yim et al., 2010; Greener et al., 2001; Bai et al., 2010; Lee et al., 2008), hinting at crucial differences in the mechanism of clathrin-mediated endocytosis between plants and animals.

2.3 Discussion

Here, we aimed to expand our knowledge of clathrin-mediated endocytosis in plants by searching for, and functionally characterising, novel clathrin-associated proteins. Using a TAP-MS approach, we identified four CLC-binding proteins with possible endocytic functions: CAP1, SH3P2, AUXILIN-LIKE1 and AUXILIN-LIKE2. We analysed the binary interactions among these proteins and revealed their localisation to the PM and the cell plate, two of the sites of clathrin action.

Our more detailed studies focused on characterising the two putative uncoating factor homologues, AUXILIN-LIKE1 and AUXILIN-LIKE2. Like auxilin homologues in non-plants, we found that overexpressing AUXILIN-LIKE1/2 led to an inhibition of endocytosis. We believe that our inducible auxilin-overexpressing lines are useful and very efficient genetic tools for specifically interfering with endocytosis, with applications in studies of various clathrin-dependent processes (e.g. Ortiz-Morea et al., 2016). Our in-depth mapping of the effects of AUXILIN-LIKE1 overexpression on the molecular components of the endocytic pathway may prove interesting for researchers interested in the endocytic process itself. We note that the effect of AUXILIN-LIKE1/2 overexpression appears to be specific for the PM pool of clathrin, as we did not observe a loss of clathrin from the endosomal compartments.

The observation that membranes accumulated at the cell periphery, which we interpret as an effect of the continuation of secretion in the absence of endocytosis, tangibly demonstrates the interdependence of distinct trafficking processes in the endomembrane system. Although highly speculative, it is tempting to hypothesise that the loss of cytoplasm in which the endomembrane compartments are embedded, together with the increase in vacuolar volume, as observed in AUXILIN-LIKE1/2 overexpressing lines, are also trafficking

homeostasis-related phenomena, as they may represent secondary effects of the bulk loss of internal endomembrane compartments.

In an attempt to address the specific molecular function of AUXILIN-LIKE1/2, we also generated *auxilin-like1/2* mutants using CRISPR technology. We found that the loss of AUXILIN-LIKE1/2 function did not visibly affect endocytosis or plant growth and development under optimal growth conditions. This is in contrast to loss-of-function alleles of other endocytic components, which exhibit various defects in growth, development, and/or reduced fertility (e.g. Gadeyne et al., 2014; Kang et al., 2001, 2003; Collings et al., 2008; Kim et al., 2013; Kitakura et al., 2011). This observation also differs from that of auxilin loss-of-function mutants in yeast, whose growth is reduced (Ding et al., 2015), and auxilin/GAK loss-of-function mutants in animals such as mouse, worm, or zebrafish, where various aspects of development are affected (Yim et al., 2010; Greener et al., 2001; Bai et al., 2010; Lee et al., 2008).

We propose several possible interpretations for the lack of mutant phenotypes in *auxilin-like1/2*. First, it appears likely that AUXILIN-LIKE1/2 function is necessary for only a small subset of all clathrin-coated vesicles that form at the PM. This can be concluded from our VAEM colocalization analysis of clathrin and AUXILIN-LIKE1, in which we observed that a vast majority of CCPs did not recruit AUXILIN-LIKE1. As discussed above, it is possible that auxilin-like recruitment often takes place in the cytosol, and such events could have been missed by our imaging system. However, it is also possible that most CCVs are in fact uncoated with the help of other factors, while the function of AUXILIN-LIKE1/2 is limited to only a specific subpopulation of vesicles. This appears consistent with the observation that knocking out the two genes does not visibly interfere with endocytosis, and it hints at the exciting possibility of the existence of functionally distinct populations of PM-derived CCVs in plant cells, only one of which uses the conserved auxilin-Hsc70 pathway for uncoating.

Second, the lack of evident phenotypes in *auxilin-like1/2* may be explained by a functional overlap between the closely homologous AUXILIN-LIKE1/2 pair and any of the five remaining auxilin-like proteins in A. thaliana. However, we and others identify these proteins as auxilin-like only due to the presence of C-terminal DNAJ domains that recruit and activate the heat shock protein. The remaining portions of auxilin-likes have different lengths and bear little or no sequence similarity when comparisons are made between the closely homologous AUXILIN-LIKE1/2 pair and AUXILIN-LIKE3-7 (Supplemental Figure 9). The lack of sequence similarity, together with the specific detection of AUXILIN-LIKE1/2 but not AUXILIN-LIKE3-7 in our CLC-TAP assay, suggest a possible diversification in the functions of plant C-terminal DNAJ proteins beyond simply clathrin-related processes. An example of this is JAC1 (AUXILIN-LIKE6), which was identified in a forward genetic screen for regulators of light-dependent chloroplast relocations in the leaf (Suetsugu et al., 2005) – a process, to our knowledge, not regulated by clathrin. An analysis of the effects of AUXILIN-LIKE3-7 overexpression, as well as clathrin binding assays, may help to address with more certainty whether any of these proteins could function in the endocytic process together with AUXILIN-LIKE1/2. At the moment, we hypothesise that plant cells recruit the chaperoning function of Hsc70 at various cellular locations using a suite of auxilin-like DNAJ domain proteins that act as binding adaptors between the chaperone and distinct target protein complexes.

As a final note, while it is true that some of the features of AUXILIN-LIKE1/2, such as the presence of a C-terminal DNAJ domain, the late recruitment to coated pits, and the effects of overexpression, suggest they possess a function identical to that of non-plant auxilins, our data are insufficient to draw specific conclusions about the molecular function of these auxilin-like proteins. Returning to protein sequence comparisons, when whole sequences are taken into consideration, neither AUXILIN-LIKE1/2 nor any other A. thaliana auxilin-like are similar to non-plant auxilins; interestingly, yeast auxilin is overall not similar to animal auxilins either. Although biochemical experiments have suggested that AUXILIN-LIKE1 possesses uncoating activity in vitro (Lam et al., 2001), we believe that further investigation into the molecular function of AUXILIN-LIKE1/2, and into the uncoating of CCVs in plants, may bring more clarity. The recent finding that the yeast auxilin homologue AUX1/SWA2 not only participates in the uncoating of CCVs, but also functions with COPI and COPII-coated vesicles in the early secretory pathway (Ding et al., 2015), provides a cautionary tale against assuming that distantly similar proteins found across the tree of life possess identical molecular functions.

2.4 Materials and method

2.4.1 Plant materials

The following previously published Arabidopsis thaliana lines were used: *UBQ10pro:SH3P2-GFP* (Zhuang et al., 2013), *PIN2pro:PIN2-GFP* (Abas et al., 2006), PIN2pro:PIN2-Dendra (Salanenka et al., 2018), *CLC2pro:CLC2-GFP*, *DRP1Cpro:DRP1C-GFP* (Konopka and Bednarek, 2008), INTAM:GAL4 (Friml et al., 2004), *TPLATE-GFP x AP2A1-TagRFP* (Gadeyne et al., 2014), *35Spro:PIN5-GFP* (Mravec et al., 2009).

The following lines and crosses were generated in this study: *XVE»AUXILIN-LIKE1*, *XVE»AUXILIN-LIKE2*, *XVE»AUXILIN-LIKE1×CLC2pro:CLC2-GFP*, *XVE»AUXILIN-LIKE1×DRP1Cpro:DRP1C-GFP*, *XVE»AUXILIN-LIKE1×TPLATE-GFP*, *XVE»AUXILIN-LIKE1×AP2A1-TagRFP*, *XVE»AUXILIN-LIKE2×PIN2pro:PIN2-GFP*, *XVE»AUXILIN-LIKE2×PIN2pro:PIN2-Dendra*, *CAP1pro:CAP1-mCherry*, *35Spro:CAP1-RFP*, *35Spro:SH3P2-GFP*, *UBQ10pro:GFP-AUXILIN-LIKE1*, *CLC2pro:CLC2-GFP×UBQ10pro:mCherry-AUXILIN-LIKE1*, *35Spro:RFP-AUXILIN-LIKE1*, *35Spro:RFP-AUXILIN-LIKE2*, *UAS:GFP-AUXILIN-LIKE1*, I*NTAM»GFP-AUXILIN-LIKE1 (UAS:GFP-AUXILIN-LIKE1×INTAM:GAL4)*, *auxilin-like1/2c1, auxilin-like1/2c2, auxilin-like1, auxilin-like2*.

Unfortunately, 35Spro:RFP-auxilin-like1/2 seeds are not available due to low yields and a high degree of silencing, but expression vectors for plant transformation can be provided instead.

2.4.2 Molecular cloning

All constructs used for TAP, for generating stable Arabidopsis transgenic lines, and for BiFC assays were cloned with the Gateway system. The following Gateway entry clones were generated in this study: CLC1/pDONR221, AUXILIN-LIKE1/pENTR/D-TOPO, AUXILIN-LIKE2/pENTR/D-TOPO, AUXILIN-LIKE1/pDONRP2rP3, AUXILIN-LIKE2/pDONRP2rP3, CAP1/pENTR/D-TOPO, SH3P2/pENTR/D-TOPO (all in variants with and without stop codons), PIP5K1/pDONR221, pCAP1/pDONRP4P1r. The coding sequences of *CLC1*, *AUXILIN-LIKE1*, *AUXILIN-LIKE2*, and *CAP1* were cloned from A. thaliana (accession Columbia-0) cDNA, whereas those of SH3P2 and the CAP1 promoter were cloned from A. thaliana Col-0 genomic DNA. The primers used are shown in Table 1.

Table 1: Primers for molecular cloning

construct	F primer	R primer (with stop)	R primer (without stop)
auxilin-like1/pENTR	CACCATGGATGATTTCACAGGATTGTT	TCAGAAGAGTTCTTCTGAGTTAAAC	GAAGAGTTCTTCTGAGTTAAACTTG
auxilin-like2/pENTR	CACCATGGATGATTTCACAGGATTGTT	TCAAAAGAGTTCCTCTGAGTTGAAT	AAAGAGTTCCTCTGAGTTGAATTTG
CAP1/pENTR	CACCATGGCGCTAAGCATGCGA	TCAGTAAGGGTTGTTGTAGTAATAACC	GTAAGGGTTGTTGTAGTAATAACC
SH3P2/pENTR	CACCATGGATGCAATTAGAAAACAAGC	TCAGAAAACTTCGGACACTTTG	GAAAACTTCGGACACTTTGCTA
auxilin-like1/pDONRP2rP3	GGGGACAGCTTTCTTGTACAAAGTGGCCATGGATGATTTCACAGGATTGTT	GGGGACAACTTTGTATAATAAAGTTGGTCAGAAGAGTTCTTCTGAGTTAAAC	-
auxilin-like2/pDONRP2rP3	GGGGACAGCTTTCTTGTACAAAGTGGCCATGGATGATTTCACAGGATTGTT	GGGGACAACTTTGTATAATAAAGTTGGTCAAAAGAGTTCCTCTGAGTTGAAT	-
CLC1/pDONR221	GGGGACAAGTTTGTACAAAAAAGCAGGCTCGATGGCGACTTTTGATGATGGAG	GGGGACCACTTTGTACAAGAAAGCTGGGTTTCACTCCGCCTTGGTTCCCTCGGCC	GGGGACCACTTTGTACAAGAAAGCTGGGTTCTCCGCCTTGGTTCCCTCGGCC
PIP5K1/pDONR221	GGGGACAAGTTTGTACAAAAAAGCAGGCTATGAGTGATTCAGAAGAAGA	-	GGGGACCACTTTGTACAAGAAAGCTGGGTGCCCTCTTCAATGAAGA
pCAP1/pDONRP4P1r	GGGGACAACTTTGTATAGAAAAGTTGgataggcgttcaaatcgg	GGGGACTGCTTTTTTGTACAAACTTGgattccactactacttaaggattcgaa	

The expression vectors were cloned using previously published Gateway vectors (Karimi et al., 2002; Curtis and Grossniklaus, 2003; Van Leene et al., 2014). Constructs for TAP were generated by fusing CLC1 with TAP tags and with 35S promoter sequences in pKCTAP and pKCTAP destination vectors. The following constructs were cloned and used for stable transformation of A. thaliana: *XVE»AUXILIN-LIKE1* and *XVE»AUXILIN-LIKE2* (pMDC7B(UBQ10)), 35Spro:RFP-AUXILIN-LIKE1 and 35Spro:RFP-AUXILIN-LIKE2 (pK7WGR2), *UAS:GFP-AUXILIN-LIKE1* (pK7m34GW), *UBQ10pro:GFP-AUXILIN-LIKE1* (pB7m34GW,0), *UBQ10pro:mCherry-AUXILIN-LIKE1* (pB7m34GW,0), *35Spro:SH3P2-GFP* (pH7FWG2), *35Spro:CAP1-RFP* (pK7RWG2), and *CAP1pro:CAP1-mCherry* (pK7m34GW). The constructs used for the BiFC assays were cloned in p*7m34GW and p*7m24GW2 backbones (where * indicates resistance cassettes not relevant for these constructs) and consisted of fusions of N- and C-terminal parts of EGFP fused to CLC1, AUXILIN-LIKE1, AUXILIN-LIKE2, CAP1, SH3P2, and PIP5K1, all under the control of the 35S promoter.

2.4.3 Tandem Affinity Purification

TAP using CLC1 as bait was carried out as described previously (Van Leene et al., 2014) with Arabidopsis thaliana cell cultures.

2.4.4 BiFC assays

For the BiFC assays, Nicotiana benthamiana leaves were transiently transformed with Agrobacterium tumefaciens. The Agrobacterium strains carrying the BiFC constructs were grown to OD=1, spun down, and resuspended in infiltration buffer (10 mM MgCl2, 10 mM MES, 100 µM µM acetosyringone) to OD=1.5. The suspensions were incubated at room temperature on a shaker for 2 h. Strains carrying the two assayed constructs were mixed and injected into the bottom sides of leaves. Leaves were imaged by CLSM 3-4 days after injection. Each interacting pair was assayed in three repeated experiments. Positive interactions displayed broad areas of GFP fluorescence throughout the injected leaf surface. Single pictures of GFP fluorescence were taken to document the result.

2.4.5 Growth conditions and chemical induction of transgenes

Arabidopsis thaliana seedlings were grown on ½MS medium with 1% (w/v) sucrose at 21°C under a 16h day - 8h night cycle, or in darkness for imaging in etiolated hypocotyls. Lights used were Philips GreenPower LED in deep red/far red/blue combination, intensity: 2100µW +/-10%. Estradiol induction of the *XVE»AUXILIN-LIKE1/2* lines was done by transferring 3-day-old seedlings to medium containing β-estradiol (Sigma-Aldrich) or solvent (ethanol) as a control. β-estradiol concentrations used: 2.5 µg/ml (~9.18 µM) for experiments presented in Fig. 3, 4, 5A,B,C,E, 6, 7, 8, Suppl. Fig. 7A; 2 µM for experiments presented in Fig. 5D, Suppl. Fig 5, 8. Induction of the *INTAM»GFP-AUXILIN-LIKE1* line was done analogously on medium supplemented with 2 µM tamoxifen (Sigma-Aldrich).

2.4.6 Seedling root morphology

For light microscopy of *XVE»AUXILIN-LIKE1/2* seedling roots, seedlings were stained in Lugol's solution for approximately 1 min, washed, and mounted on slides in chloral hydrate solution.

2.4.7 Immunostaining

An Intavis InsituPro VSi robot was used for immunostaining according to a previously published protocol (Sauer et al., 2006). The following antibodies were used: rabbit anti-PIN1 (1:1000, Paciorek et al., 2005), rabbit anti-PIN2 (1:1000, Abas et al., 2006), rabbit anti-KNOLLE (1:1000, Lauber et al. 1997), and Anti Rabbit-Cy3 (1:600, Sigma-Aldrich catalog no. C2306).

2.4.8 Fluorescent imaging

CLSM imaging was done with a Zeiss LSM700, LSM800 and LSM880 confocal microscopes with Plan-Apochromat 20x/0.8 and Plan-Apochromat 40x/1.2 lenses. Long-term live imaging with root growth tracking was performed on a vertical Zeiss LSM700 as previously described (von Wangenheim et al., 2017).

VAEM imaging was carried out with an Olympus IX83 inverted microscope equipped with a cell-TIRF module and an UAPON OTIRF 100x lens. For colocalisation imaging of *CLC2pro:CLC2-GFP×UBQ10pro:mCherry-AUXILIN-LIKE1*, the two channels were captured sequentially.

2.4.9 FM4-64 and FM1-43 staining

For FM4-64 uptake experiments, seedlings were stained in liquid ½MS medium with 1% (w/v) sucrose supplemented with 2 µM FM4-64 dye (ThermoFisher) for 5 min in the dark and on ice. Excess dye was washed off and the seedlings were mounted in ½MS medium with 1% (w/v) sucrose on microscopy slides at room temperature, marking the start of the internalization time measurement.
To visualise the membrane accumulation at the PMs of the *XVE»AUXILIN-LIKE2* line, and for colocalisations of fluorescent markers with PM-localised FM4-64 and FM1-43 stains, the seedlings were treated as described above but at room temperature and imaged immediately after washing. FM1-43 stain was used at 0.2 µM concentration.

2.4.10 BFA treatments

Seedlings were incubated in liquid ½MS medium with 1% (w/v) sucrose and containing Brefeldin A (Sigma-Aldrich) at a final concentration of 25 µM. The solvent (DMSO) was added to the controls.

2.4.11 Propidium iodide staining

Propidium iodide (Sigma-Aldrich) was diluted 100x in ½MS medium with 1% (w/v) sucrose and roots were stained for 2 min before CLSM imaging.

2.4.12 Fluorescence quantification

Quantification of CLSM and VAEM fluorescence images was performed using Fiji/ImageJ. FM4-64 uptake was quantified by comparing average PM and intracellular signal intensities in individual cells. BFA bodies stained by PIN1 were counted in circular areas 50 µm in diameter, placed in the middle of microscopic pictures. DRP1C-GFP foci at the PM in VAEM pictures were counted similarly in circular areas 120 pixels in diameter. PM signal intensities of TPLATE-GFP and AP2A1-TagRFP in root epidermis were measured on lines drawn along multiple PMs in individual microscopic pictures.

2.4.13 Quantitative RT-PCR

Total RNA from approximately 15 4-day-old seedlings induced with 2 µM β-Estradiol/4-Hydroxytamoxifen/solvent control (Sigma-Aldrich) for 24 h was extracted using the TRIzol reagent (Invitrogen, Carlsbad, CA, USA) and purified using an RNeasy Mini Kit (Qiagen) according to manufacturer's instructions. 2 µg of RNA was reverse-transcribed using an iScript cDNA Synthesis Kit (BioRad). qRT-PCR was performed in 5 µL reactions using the LightCycler480 SYBR Green I Master Mix in a LightCycler480 II (Ser. no. 5659, Roche) according to manufacturer's instructions. Relative gene expression was calculated with the 2-ΔΔCT method (Livak and Schmittgen, 2001). The primers used are listed in Table 2.

Table 2: Primers for qPCR

TUB2-F	TAACAACTGGGCCAAGGGACA
TUB2-R	ACAAACCTGGAACCCTTGGAGAC
EF1-F	TGCTGTTGTAACAAGATGGATGCC

EF1-R	GGGTTGTATCCGACCTTCTTCAGG
AXL1-F	GGGGAAGAAAGGGGCAGATA
AXL1-R	GTCCAATGGATCAGTACGGGA
AXL2-F	AACAATTTGGGGAAGAAAGAGAGTG
AXL2-R	TGGATCAGTGAACCCTCCTGT

2.4.14 CRISPR mutant isolation

The CRISPR construct was cloned according to a published method (Richter et al., 2018). T1 plants transformed with the CRISPR construct were selected on Basta and resistant transformants genotyped for AUXILIN-LIKE1/2 mutations by PCR-amplification and sequencing of relevant gene fragments. Plants carrying mutations in auxilin-like paralogues were propagated, and the T2 progenies were PCR-genotyped to find those that segregated out the CRISPR cassette (by amplification of the Cas9 and Bar genes). Among them, single and double auxilin-like homozygotes were selected. The primers used are listed in Table 3.

Table3: Primers for sequencing Axl CRISPR mutation

CAS9-F	TGAGAACACTCAGCTCCAGAAT
CAS9-R	TCGAAACCACCGTATTTCTTAG
BAR-F	TCTCTTACGACTCAATGACAAG
BAR-R	GTGATTTTTGCGGACTGAGCT
AXL1-CRISPR-F	GGGGAAGAAAGGGGCAGATA
AXL1-CRISPR-R	GTCCAATGGATCAGTACGGGA
AXL2-CRISPR-F	AACAATTTGGGGAAGAAAGAGAGTG
AXL2-CRISPR-R	TGGATCAGTGAACCCTCCTGT
AXL1-seq	TGCAATGTAGCATGAACTATA
AXL2-seq	AACCTAGAAGATAACTCCCAG

2.4.15 Protein sequence alignment

Auxilin-like protein sequences were aligned using the Geneious software package (www.geneious.com) with standard settings.

2.4.16 Accession numbers

Sequence data from this article can be found in the GenBank/EMBL libraries under the following accession numbers: AUXILIN-LIKE1 (At4g12780), AUXILIN-LIKE2 (At4g12770), CAP1 (At4g32285), SH3P2 (At4g34660), CLC1 (At2g20760), CLC2 (At2g40060), CHC1 (At3g08530), CHC2 (At3g11130), DRP1C (At1g14830), TPLATE (At3g01780), AP2A1 (At5g22770), KNOLLE

(At1g08560), PIN1 (At1g73590), PIN2 (At5g57090), AUXILIN-LIKE3 (At1g21660), AUXILIN-LIKE4 (At4g36520), AUXILIN-LIKE5 (At1g75310), JAC1/AUXILIN-LIKE6 (At1g75100), AUXILIN-LIKE7 (At1g30280), PIP5K1 (At1g21980), DHNAT2 (At5g48950).

2.5 Supplementary Information

Supplemental Figure 1. Additional BiFC interactions.
Supplemental Figure 2. Additional subcellular localisation data for AUXILIN-LIKEs, SH3P2 and CAP1.
Supplemental Figure 3. Growth and development of seedlings in transgenic lines constitutively overexpressing AUXILIN-LIKE1, SH3P2, and CAP1.
Supplemental Figure 4. Uninduced controls for seed germination experiments with XVE»AUXILIN-LIKE lines.
Supplemental Figure 5. qPCR of inducible AUXILIN-LIKE overexpression lines
Supplemental Figure 6. Correlation of GFP-AUXILIN-LIKE1 expression and root growth inhibition during INTAM»GFP-AUXILIN-LIKE1 induction
Supplemental Figure 7. Additional data on FM4-64 uptake in inducible AUXILIN-LIKE overexpression lines
Supplemental Figure 8. Propidium iodide staining of XVE»AUXILIN-LIKE2 roots.
Supplemental Figure 9. Protein sequence alignment of A. thaliana AUXILIN-LIKE1-7.

Supplemental Movie 1. VAEM colocalisation of CLC2-GFP and mCherry-AUXILIN-LIKE1.
mCherry-AUXILIN-LIKE1 foci briefly colocalised with a subset of the CCPs being formed at the PM.
Supplemental Movie 2. VAEM imaging of CLC2-GFP in *XVE»AUXILIN-LIKE1* line.
The movie shows loss of normal CLC2-positive endocytic pits at the PM and appearance of some larger, and often mobile, CLC signals which were either PM-attached or intracellular. Large endosomal CLC signals are still present after auxilin-like1 overexpression.
Supplemental Movie 3. VAEM imaging of TPLATE-GFP in *XVE»AUXILIN-LIKE1* line.
The movie shows TPLATE-GFP foci formed at high density and with rapid dynamic following AUXILIN-LIKE1 overexpression.
Supplemental Movie 4. VAEM imaging of AP2A1-TagRFP in *XVE»AUXILIN-LIKE1* line.
The movie shows AP2A1-TagRFP foci formed at high density and with rapid dynamic following AUXILIN-LIKE1 overexpression.

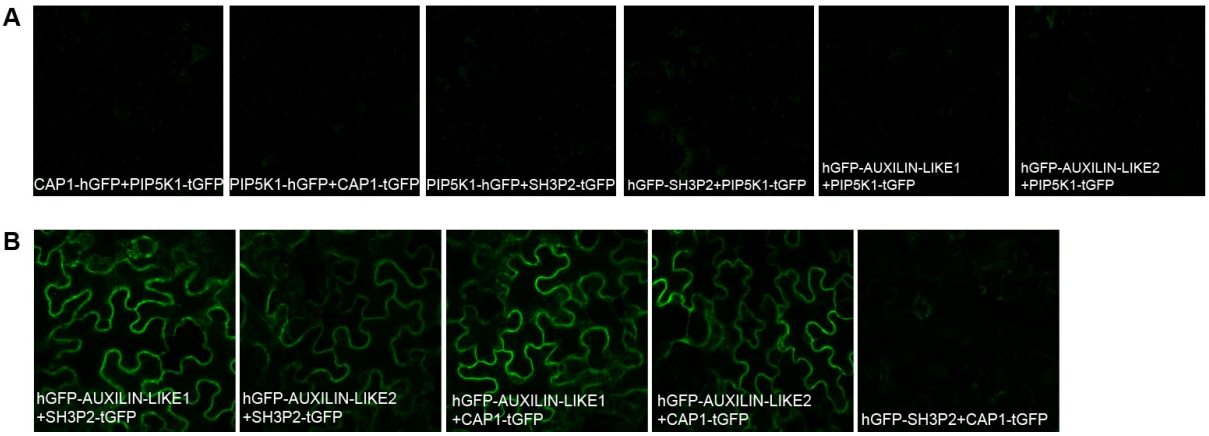

Supplemental Figure 1. Additional BiFC interactions. (Supports Figure 1) (A) Lack of interaction and GFP fluorescence upon coexpression of any CLC1 interactor with PIPK51. (B) BiFC interactions among selected CLC1 interactors. AUXILIN-LIKE1/2 interacted with CAP1 and SH3P2, but no interaction was detected between SH3P2 and CAP1.

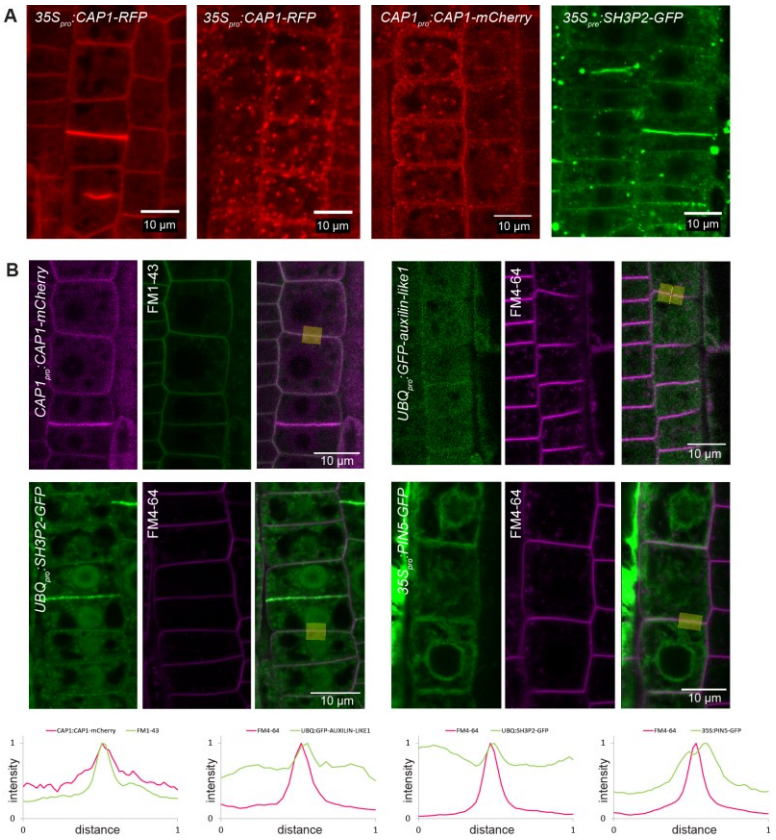

Supplemental Figure 2. Additional subcellular localisation data for AUXILIN-LIKEs, SH3P2 and CAP1. (Supports Figure 2)

(A) *35Spro:CAP1-RFP* line showed PM and cell plate localisation with faint cytosolic background signal. In both *35Spro:CAP1-RFP* and *CAP1pro:CAP1-mCherry* lines, signal was detected at the endosomes in some (~10%) of the seedlings analysed. *35Spro:SH3P2-GFP* localised to PM, cell plate and endosomes or intracellular aggregates.

(B) Colocalisation of CAP1, AUXILIN-LIKE1, and SH3P2 with the PM marked by FM4-64 and FM1-43 stains. PIN5-GFP, an ER-localised marker, was used as a negative control. Graphs show measurements of signal intensity along lines drawn across the PM and surrounding area.

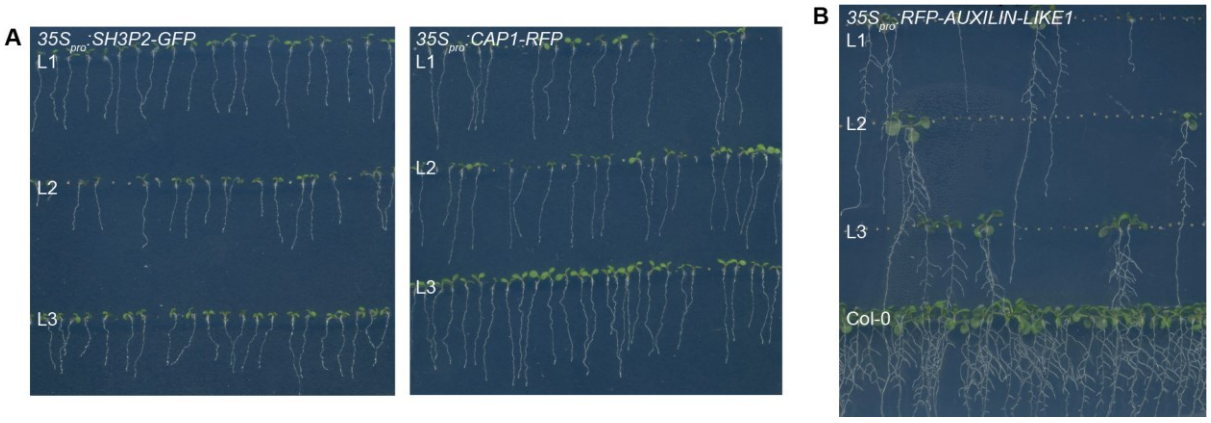

Supplemental Figure 3. Growth and development of seedlings in transgenic lines constitutively overexpressing AUXILIN-LIKE1, SH3P2, and CAP1. (A) Normal seed germination and growth in *35Spro:SH3P2-GFP* and *35Spro :CAP1-RFP lines*. (B) Germination arrest in segregating T2 populations of *35Spro:RFP-AUXILIN-LIKE1* lines. *35Spro:RFPAUXILIN-LIKE2* lines behaved similarly and are not shown. L1, L2, L3 – distinct transgenic lines.

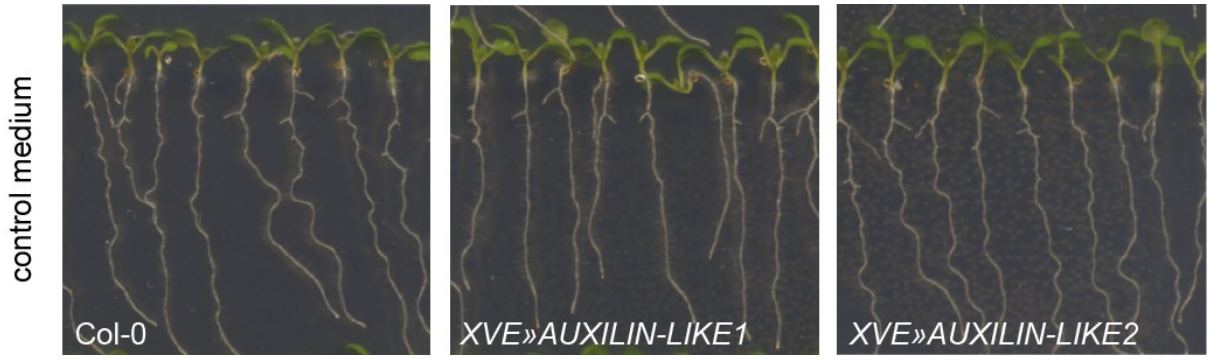

Supplemental Figure 4. Uninduced controls for seed germination experiments with XVE»AUXILIN-LIKE lines. (Supports Figure 3) Normal germination and growth *of XVE»AUXILIN-LIKE1/2* seedlings on a medium without beta-estradiol.

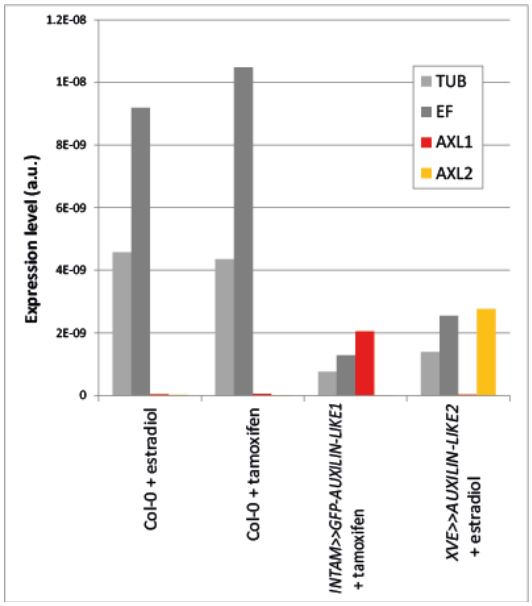

Supplemental Figure 2.5. qPCR of inducible AUXILIN-LIKE overexpression lines (Supports Figure 3). Expression level of auxilin-like1 and auxilin-like2 were scored in *INTAM»GFP- AUXILIN-LIKE1 and XVE»AUXILIN-LIKE 2* 24h after induction. Results are expressed as the average +/- standard deviation of three biological replicates (RNA isolates from three distinct pools of approx.. 15 seedlings) and three technical replicates (three qPCR reactions on each cDNA sample). Tubulin beta-chain 2 (TUB2, AT5G62690) and GTP binding Elongation factor Tu family protein (EF1, AT5G60390) were used as reference genes.

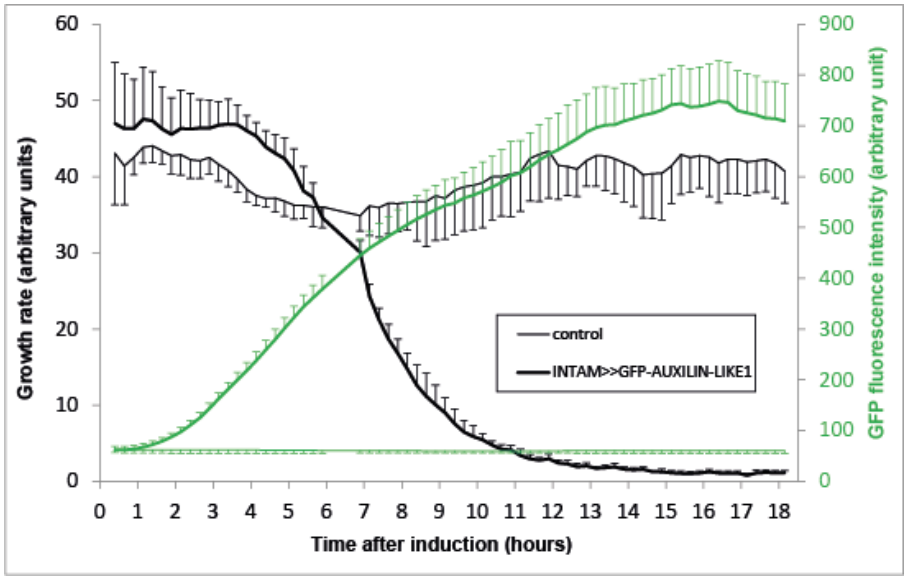

Supplemental Figure 6. Correlation of GFP-AUXILIN-LIKE1 expression and root growth inhibition during *INTAM»GFP-AUXILIN-LIKE1* induction (Supports Figure 3). Growth rates (in black) were automatically measured by TipTracker (von Wangenheim et al. 2017) during long-term live microscopy and compared with GFP-AUXILIN-LIKE1 signal intensities (in green; mean gray values of sum projections of z-stacks) in whole root tips. 6 control and 8 induced roots were analysed.
Error bars for growth and GFP intensity indicate standard deviations. Only single (upper or lower) bar is drawn for clarity.

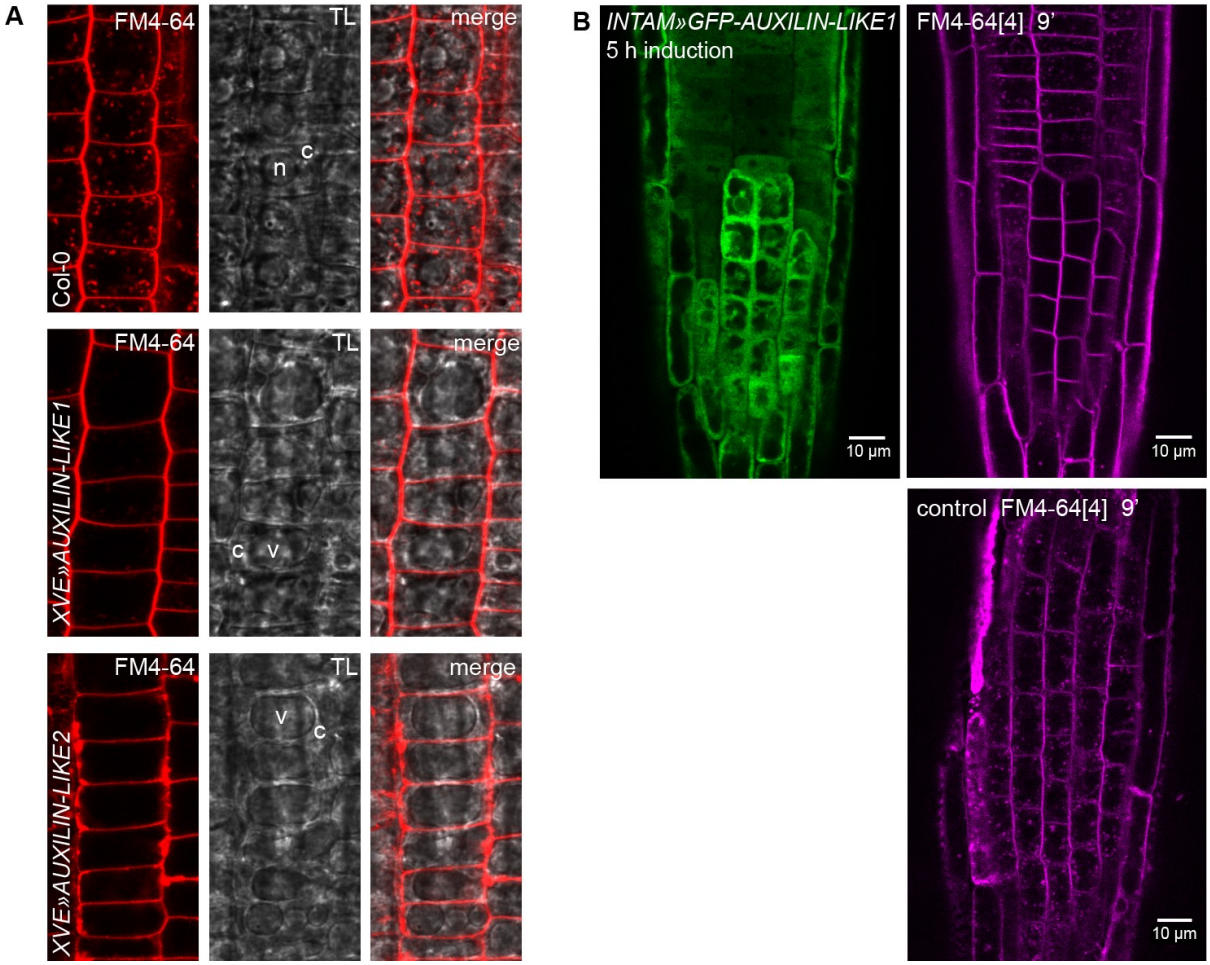

Supplemental Figure 7. Additional data on FM4-64 uptake in inducible AUXILIN-LIKE overexpression lines (Supports Figure 4) (A) Comparison of FM4-64 fluorescence and transmitted light channel showing areas of cytosol with faint or absent staining of endosomes in the auxilin-like1/2-overexpressing lines. V, vacuole; n, nucleus; c, cytoplasm. (B) FM4-64 uptake into the lateral root cap was inhibited after 5h of induction in *INTAM»GFP-AUXILINLIKE1* line concomitant with high expression of the transgene in this tissue. Control shows FM4-64 uptake into lateral root cap in the wild type.

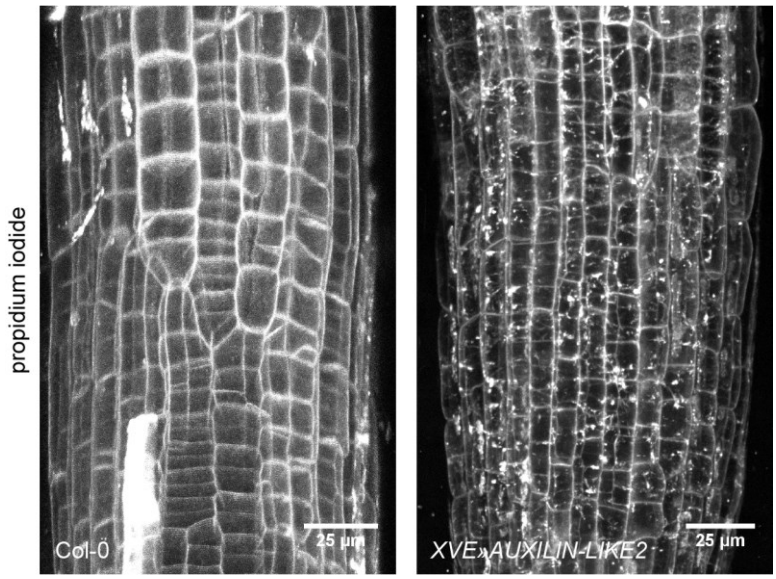

Supplemental Figure 8. Propidium iodide staining of *XVE»AUXILIN-LIKE2* roots. (Supports Figure 8) Propidium iodide staining of cell walls demonstrates aggregations in the cell wall, similar in appearance to the agglomerations of membranes observed in this line. PI staining was overall stronger *in XVE»AUXILIN-LIKE2* and the detection sensitivity had to be adjusted to achieve correctly exposed pictures.

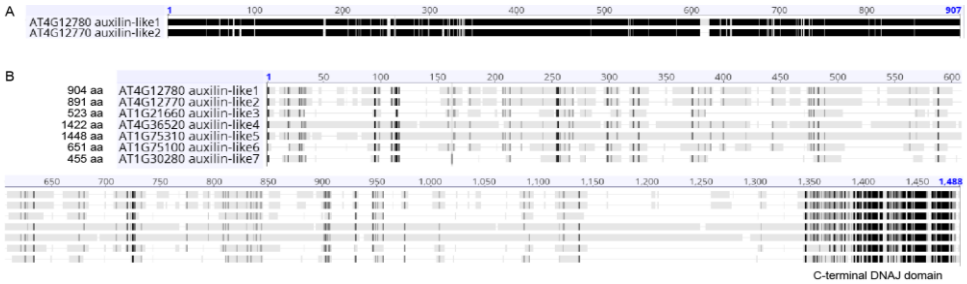

Supplemental Figure 9. Protein sequence alignment of A. thaliana AUXILIN LIKE1-7. Protein sequence alignments highlighting high overall similarity between AUXILIN-LIKE1 and AUXILINLIKE2 (A) and little similarity between AUXILIN-LIKE1/2 and AUXILIN-LIKE3-7 with the exception of the C terminal DNAJ domain (B). Gray-to-black scale represents local similarity score. Lengths of the proteins are indicated.

2.6 External contributions

The Tandem Affinity Purification was done by Dr. Ursula Kania and Prof. Geert De Jaeger, at PSB department, VIB Ghent.
Maciek Adamowski made the constructs and further characterised SH3P2, CAP1 proteins. He also made the over-expression analysis of Axl1/2.
Split GFP constructs were made by Anna Mueller and further BiFC assays were carried out by Maciek Adamowski.
qPCR assay, PI staining, root growth inhibition analyses on the axl1/2 were performed by Matous Glanc.
We would like to thank James Matthew Watson, Monika Borowska, and Peggy Stolt-Bergner at ProTech Facility, Vienna Biocenter Core Facilities for the CRISPR/CAS9 construct; Daniel Van Damme ,Sebastian Bednarek, and Liwen Jiang for sharing published material

3 Dissecting Clathrin-Coated Vesicle formation and trafficking *in planta*

3.1 Introduction

CME is the major endocytic pathway so far described *in planta.* It is an evolutionarily conserved process involved in packaging of proteins from the plasma membrane to be internalized into the cell. Clathrin-Coated Pits (CCP) develop into Clathrin-Coated Vesicles (CCVs) through a series of events: initiation, cargo-selection, clathrin assembly, scission, later undergoes uncoating and fusion to Early endosomes (EE) (McMahon and Boucrot, 2011; Sekiya-Kawasaki et al., 2003).

Each event has been studied in detail over the past decades both in yeast and mammalian systems. Most of the studies have been conducted in unicellular systems of saccharomyces and cultured mammalian cells. Several tens of machinery proteins are involved in procession of these events. Several techniques have been developed in studying these processes enabling their thorough characterisation spatially and temporally (Goode et al., 2014; Kirchhausen, 2009; McMahon and Boucrot, 2011; Mettlen and Danuser, 2014). But *in planta,* over the past few years, only a few of the machinery proteins had been identified and characterized (Fan et al., 2015). And most of the studies utilized entire organ system taking into account the higher order interactions; but the down-side being limitations in developing techniques to handle a huge organ itself.

In *Arabidopsis* system, the dynamics of adapter proteins- AP2 and TPLATE, the putative scission regulators - the DRPs, the uncoating factor Auxilin-likes, together with the coat proteins CLC and CHC have been studied. And some of these machinery proteins have found to be developmentally crucial. Loss of function of CLC1, DRP1C, TPLATE, TWD40, EH2 and TML lead to severe gametophytic defects (Adamowski et al., 2018; Van Damme et al., 2006; Fan et al., 2013; Fujimoto et al., 2010; Gadeyne et al., 2014b; Johnson and Vert, 2017b; Konopka et al., 2008; Yamaoka et al., 2013). Moreover DN-DRP1A (Dominant negative form of plant dynamin) and over expression of auxilin-likes are lethal, suggesting endocytosis to be inevitable for plant development (Adamowski et al., 2018; Yoshinari et al., 2016). Also there has been several evidences of receptors and other cargoes being endocytosed in a clathrin-mediated way with the aid of TPLATE and AP2 adaptors like – PINs, CESA, PEPR, BRI1 and a few more (Bashline et al., 2015; Fan et al., 2013; Gadeyne et al., 2014b; Di Rubbo et al., 2013). Following the machinery markers and analyzing the rate of formation/departure together with the density would give a good sense of rate of endocytosis in the cell. Alternatively, directly following the cargoes would give a better sense of functional endocytosis in the system.

Moreover, plant cellular system inherently is under high turgor pressure. This requires characterizing the involvement of opposing bending and deforming forces on the membrane during CCP development - such as action of ANTH/ENTH domain proteins (Miller et al., 2015; Skruzny et al., 2015), BAR domain proteins (Dawson et al., 2006) and actin. Animal cells under high membrane tension under special conditions like hyposmotic pressure or growth requires actin mediation of clathrin pit development. Similarly, yeast cells which are under high turgor pressure requires actin at the endocytic spot offering the opposing force for bending the membrane, alongside several other factors (Basu et al., 2014; Boulant et al.,

2011; Lemière and Berro, 2018; Watanabe et al., 2013). In plants, despite endocytosis being developmentally crucial, the mutants of *actin* and its regulators like - *arp*s and *wave* pertaining to actin branching exhibit some developmental defects, but not lethal phenotypes (Gilliland et al., 2002, 2003; Kotchoni et al., 2009; Li, 2004; Nishimura et al., 2003). This begs the question as to how actin influences endocytosis and endosomal trafficking. Role of actin in CCP development and CCV trafficking, uncoating and fusion into EE are not well understood in plants.

Despite the extending knowledge on machinery proteins involved in CCP developmental process, there is a huge gap in understanding the assembly of clathrin itself at the pit and the eventual clathrin cage development in plants. Studying the clathrin cage assembly requires developing a technique in a simpler system – like protoplasts, good enough to preserve the clathrin baskets at both the PM and the EM structures. We, for the first time, applied metal replica on unroofed Arabidopsis *thaliana* protoplasts to directly observe the CCP structure and development. We have further studied the influence of actin in dynamics of endocytic and post-endocytotic process in the entire multi-cellular organ system; we have used the epidermal cells of both root and hypocotyl systems of *Arabidopsis.* In order to eliminate the adaptation of plants towards alternative machinery in mutant condition and to get around the redundancy in roles among different types of actin, we pharmacologically for short time frames intervened with actin filament formation and function, and followed the endocytic and post-endocytic trafficking events. We have used high-resolution microscopic technique – TIRF and observed the endocytic events marked by machinery proteins at the plasma membrane of the epidermal cells *in vivo*. We have then analysed the rate of CCV formation and cargo (PIN2) internalisation to understand the role of actin in endocytosis. Based on these analyses, we have extended our understanding on the effect of actin perturbation in late endosomal (LE) and vacuolar trafficking. Furthermore, we have observed post-endocytic events such as CCV removal and Early-endosomal formation with high spatial and temporal resolution.

3.2 Results

3.2.1 Different populations of clathrin-coated structures are found at the plasma membrane and endomembrane system.

The endocytic events have not yet been understood well, *in planta*. In order to study the clathrin mediated endocytosis process, the development of Clathrin-Coated Pits (CCPs) and Clathrin-Coated Vesicles (CCVs) need to be characterised. We have, for the first time, established a method for unroofing cells to observe the plasma membrane and endomembrane structures in *Arabidopsis.* We have done extensive ultrastructural analysis of populations of Clathrin-Coated Structures (CCSs) using SEM imaging technique on metal replica on unroofed *Arabidopsis* protoplasts.

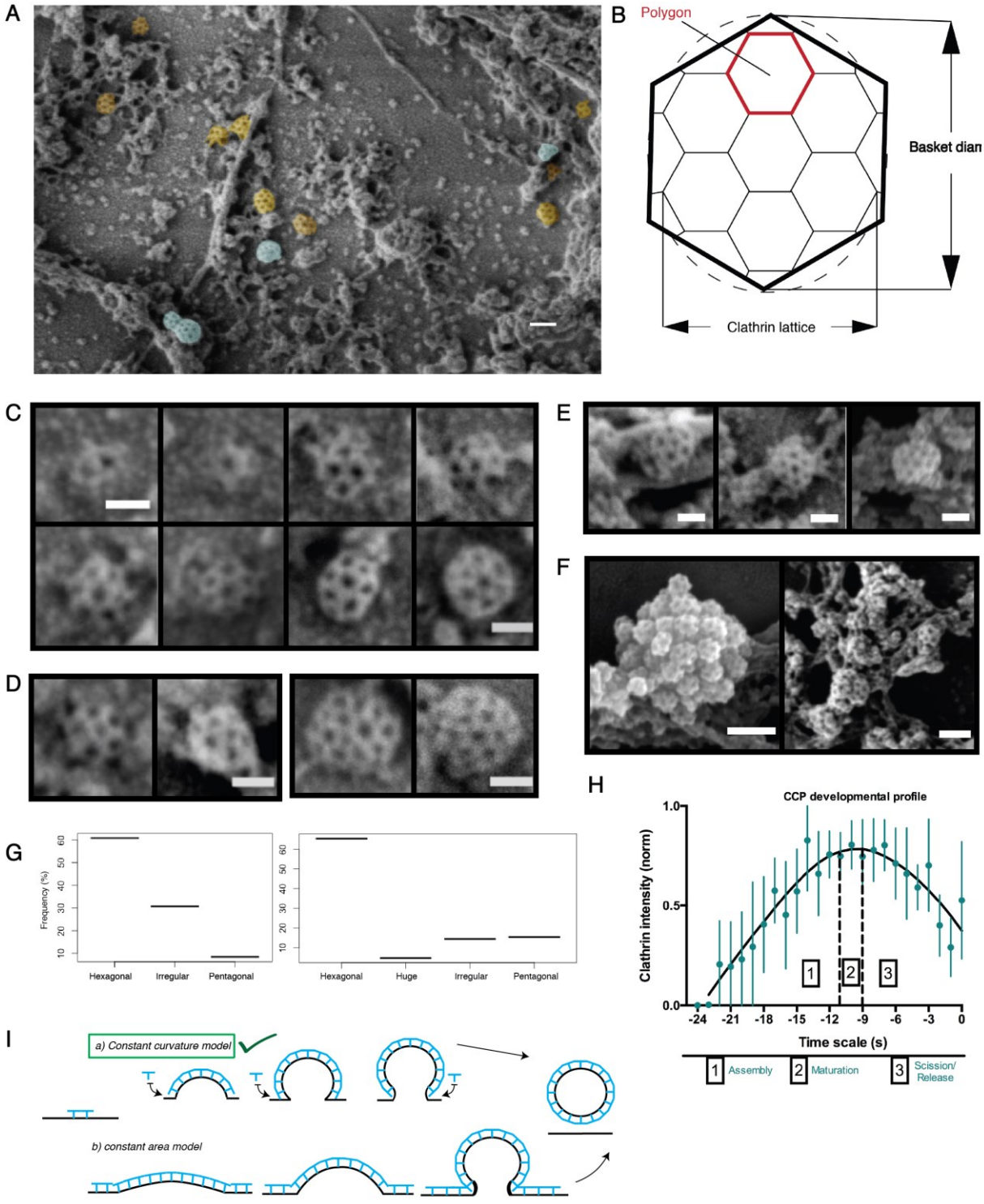

Figure 1: The ultrastructural characterisation of the clathrin-coated structures in unroofed protoplasts

A) CCSs are found associated to the flat Plasma membrane (coloured in orange) and also to the endomembrane structures (coloured in blue). Scale bar: 100 nm.

B) Illustration of a CCP. The illustration depicts the *en face* surface view of the growing 'Clathrin lattice' of most common - Hexagonal basket. The length of the projected the *en face* surface view is considered as the 'basket diameter'.

C) CCP development at the plasma membrane followed across different stages. The progress of the most common Hexagonal vesicle is shown combining several disparate events. All the images are scaled and the scale bars represent 50 nm.

D) Pentagonal (on the left) and Medium-sized/ Irregular basket types (on the right) at the plasma membrane. Scale bars: 50 nM.
E) and F) Arrangement of the CCSs in the endomembrane structures. E) Isolated CCSs of pentagonal, hexagonal and Medium-sized /Irregular basket types are shown. Scale bars: 50 nm. F) Aggregation of CCSs is shown to the left. Aggregation and partial fusion of CCPs is shown to the right. More arrangements are shown in supplementary figure S1 C, D, E. Scale bars: 100 nm.
G) Histogram of different populations of CCSs in the plasma membrane (left) and endomembrane structures (right).
H) CCP developmental profile. The time-intensity course represents combined mean fluorescence profile of CLC2-GFP. Line used: *pCLC2*::*CLC2-GFP*. The profile corresponds to different clathrin pit developmental phases – assembly, maturation and scission-release. The points represent mean ± SEM of the average intensity time-course of all the trajectories that have the lifetimes between 17-24 s. 6 cells (101,72,97,118,185,99 trajectories from each cell) of root epidermis were analysed. A smoothening lowess fit is made over the points and the phase transitions are marked.
I) Models of clathrin mediated membrane bending. Two widely discussed models are shown. Developing CCPs in *Arabidopsis* system follows the 'Constant curvature' model.

We observed well-preserved CCSs of various stages at both plasma membrane and several of them deeper inside the cells – being attached to cytoskeletal and endomembrane structures (figure 1A and supplementary figure S1A,B). CCPs develop by forming lattices of polygons (hexagons and pentagons, occasionally heptagons), which later mature into a fully coated vesicle. These CCPs that reach their maturation could be categorized into major population sets based on the basket diameter size and shape – constituting the basket type.

One of the populations of CCVs develops by forming a basic hexagonal lattice. The hexagonal lattice consists of a central polygonal ring surrounded by 6 others with more polygons getting added around it developing into a vesicle. The progress could be clearly seen at the plasma membrane (fig 1C). The final spherical vesicle has a similar hexagonal en face surface view, categorised as hexagonal basket type. A second population of CCVs consists of a basket with a pentagonal surface view with one central polygon surrounded by 5 others i.e. Pentagonal basket (figure 1D, left). Both these populations of CCSs are small and possess a basket diameter of approximately ~60 nm (15 cells, totally 190 pits measured). There exists a third irregular population of CCVs that are medium sized with a diameter ranging between 80-110 nm (15 cells, totally 72 pits measured) and are likely developed from larger lattices (figure 1D, right). Interestingly the population with a hexagonal basket type is the most occurring and it constitutes 60% of total population. The frequency distribution of the distinct population of CCSs at the plasma membrane and the endomembrane could be seen in figure 1G. The distribution is very similar in both cases, except for the occasional occurrence of huge clathrin lattice occurring in the endomembrane (Supplementary figure S1C).

Apart from the sizes and shapes of the CCSs, their arrangement is very notable. Unlike the plasma membrane where they remain separated from one another, the endomembrane structures have them arranged differently. Multiple fused CCSs are often seen in these structures, as shown in supplementary figure S1D. Deeper in the cell, a single huge lattice that remain fused to the endomembrane surface is observed occasionally (supplementary figure S1E). There are also isolated pits belonging to all three typical basket types partially fused to the endomembrane surface (figure 1E). Also aggregations of different populations of CCSs are observed, as shown in figure 1F and supplementary figure S1C. These

aggregations have been previously reported to belong to Early Endosome/Trans-Golgi Network – also known as Golgi-Associated TGN (EE/TGN) and Poly-Coated Reticulum (PCR - also known as free TGN), through different electron microscopic studies (Galway et al., 1993; Kang et al., 2011; Tanchak et al., 1988). The partially coated and fused vesicles could be either the endocytosed CCVs that are on the verge of getting uncoated while fusing to the EE. Or these vesicles, as predicted, could be budding off the EE/TGN, the putative function of which is delivering cargoes to the vacuoles and the plasma membrane (Kirchhausen, 2000; Kural et al., 2012; Robinson and Pimpl, 2014; Watanabe et al., 2014).

To summarise, metal replica of protoplasts is a useful method to study various structural aspects of the cell. SEM imaging has revealed the existence of distinct populations of CCSs that are on the plasma membrane and various endomembrane structures. However, their origin and function are not clear *in planta* (Robinson and Pimpl, 2014)

3.2.2 The clathrin-coated pit development at the PM follows 'constant curvature model'

The replica of *Arabidopsis* root protoplasts show different populations of CCSs associated to both the Plasma membrane and the endomembrane structures. However the actual mechanism of CCP development by membrane remodeling is unclear *in planta*. The mechanism of membrane bending has been studied extensively in yeast and mammalian systems. In yeast cells, after all the coat proteins initially assemble, the membrane starts bending through actin polymerisation forces acting against it. However in the mammalian systems, clathrin polymerisation energy has been attributed to membrane remodeling, in addition to other membrane modifiers like BAR domain and ANTH/ENTH. There are two major models that were proposed as to how clathrin brings about the topological changes to the membrane, as shown in figure 1G. Model 1 – 'Constant surface area' - clathrin molecules initially form a flat lattice and then through continuous exchange of polygons and additional forces from actin and other membrane modifying proteins, bend the membrane. Therefore, during membrane bending, the radius of curvature continuously decreases, in effect modifying the *en face* view from a large flat lattice to a smaller curved dome. As an extension of model 1, in mammalian systems CCPs mature and bud off the clathrin plaques and Flat Clathrin Lattices (FCLs) at the plasma membrane. These large lattices gives rise to multiple CCPs which endocytose receptors and potentially other cargoes (Avinoam et al., 2015; Grove et al., 2014; Leyton-Puig et al., 2017). Model 2 - 'Constant curvature model' - clathrin assembly to the pit directly bends the membrane and the continuous polymerisation develops the curvature. Such a mode of development maintains the radius of curvature; hence the *en face* view of the curvature stays the same (Kaksonen and Roux, 2018; Lampe et al., 2016).

As shown in figure 1A and supplementary figure 1A, ultrastructural analysis of unroofed protoplasts revealed the absence of large clathrin assemblies or FCLs in *Arabidopsis*. Most of the flat lattices found were much smaller and the curved domains of the most abundant hexagonal pits were spotted more frequently. Live imaging of the CCPs with clathrin marker line concordantly reveals smaller pits, not larger lattices (figure 2B). Also in other plant species, lack of both FCLs and plaques was shown by previous workers (Coleman and Evans, 1987; Emons and Traas, 1986).

The plasma membrane of the unroofed protoplasts showed typically smaller lattices with fewer polygons (of clathrin). These polygons have a set initial surface area and a defined curvature of a hexagonal pit. Later new clathrin polygons get added to the defined radius of curvature maintaining the enface view of a curved hexagonal pit. Thus the hexagonal pit develops displaying a constant curvature (figure 1E). Clathrin polymerization continues and the completed CCV pinches off the plasma membrane. This mechanism of CCV formation supports the canonical 'Constant curvature model'. This is the first direct evidence leading to the elucidation of the mechanism of CCP development and the final vesicle formation *in planta.* However, it is to be noted that there might be other modes of pit development still functioning. For instance medium-sized/irregular pits, which are complex, diverse and less frequent, could not be quantified by simple observation techniques, hence we cannot rule out other modes of development operating.

Apart from the direct observation of CCPs at the PM in protoplasts, the evidence is further supported by intensity measurements of clathrin pit development. The measurements of clathrin intensity profile (CLC2-GFP) were made in the entire organ system – epidermal cells of root. The intensity time course of clathrin pit development is shown in figure 1C. The intensity profile was obtained from all the clathrin trajectories belonging to the average lifetime that range ~18 – 24 s (figure 1H). The profile exhibits an initial phase of clathrin "assembly" at the pit, followed by a very short "maturation" phase, and finally a drop in intensity corresponding to the "scission and release" of the CCV. The maturation phase accounts for only ~15% of the entire span of development, while the assembly phase takes more than 40% of the span. Such a segregation in the intensity profile is consistent with the 'constant curvature model', rather than constant surface area model, which entails a short assembly and very long maturation phases (Avinoam et al., 2015). Moreover, membrane bending dynamics contributes to faster CCP development when following constant curvature model (Scott et al., 2017). That would explain the shorter average lifetime of clathrin foci in *Arabidopsis* (figure 2C). Also the intensity profile confirms the consistency in CCP development between protoplast system and organ systems of *Arabidopsis*.

Ultrastructural analysis of CCSs at the PM clearly shows the absence of large clathrin lattices or plaques that develop into vesicles. The observations of various CCP developmental stages suggest that the predominant mode membrane bending in *Arabidopsis* follows the 'constant curvature model' (figure 1I). This also surprisingly shows that CCP development in *Arabidopsis* closely resembles mammalian systems rather than high-turgor pressure system like yeast, as the clathrin polymerisation energy predominantly remodels the membrane. However, the involvement of actin forces in membrane bending could not be eliminated and this needs to be carefully tested.

3.2.3 Cortical actin forms main and subsidiary filaments and not polymerised foci at the endocytic spot

Bending the membrane during clathrin pit invagination requires the action of lots of forces. Several membrane-bending proteins, that retain the curvature, have been identified in non-plant systems. However actin is the major contributor as a working force actin against high

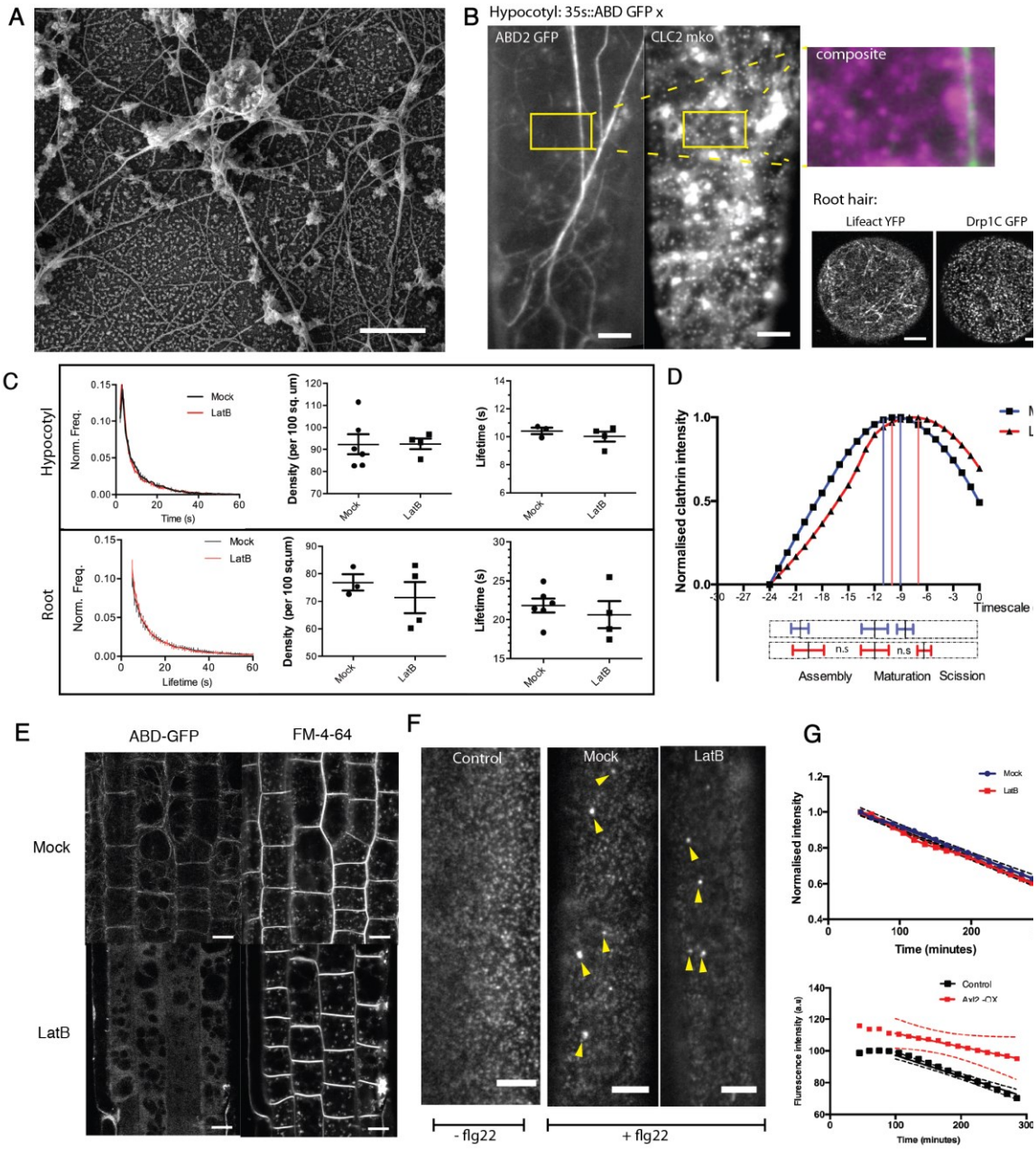

Figure 2: Localization and endocytic function of actin

Ultrastructural analysis of actin cytoskeletal network in unroofed protoplasts (A) and TIRF microscopic observation of cortical actin network *in vivo* in epidermal cells. Scale bar: 0.5 um (B) reveal main and subsidiary filaments of actin and the lack of foci.

B) Imaging cortical actin and the endocytic foci: (on the left) dual-colour TIRF image of Hypocotyl epidermal cell. *p35S::ABD2-GFP* x *p35S::CLC2-mKO* transgenic line marking the filamentous actin network and the endocytic foci formed by clathrin. (on the right) Also shown is the composite of the inset marked. Scale bars: 5 um; (on the bottom) Confocal airy scan image of the root hair cell. *pRPS5A::Lifeact-YFP* transgenic line marking the filamentous network of actin and *DRP1CC:: DRP1C-GFP* transgenic line marking the endocytic foci. Note that actin does not form foci at the endocytic spot in both the hypocotyl and root hair cells. Scale bars: 4 um (see also supplementary figure S2B).

C) Effect of LatB on clathrin foci at the PM compared - in root and hypocotyl epidermal cells. pCLC2::*CLC2-GFP* line was imaged by TIRF microscope and a time-series recording the foci dynamics was obtained. 3 hypocotyls for mock condition - 3534, 3761 and 3587 trajectories, and 4 hypocotyls for LatB condition – 3191, 2519, 4452 and 2457 trajectories were analysed. 6 roots for DMSO (mock) condition - 5890, 4812, 5694, 8255, 8340 and 6793 trajectories, and 4 roots for LatB treated condition - 6503, 5746, 6665 and 6600 trajectories were analysed. See also supplementary table 1 for other markers. Top row contains the plots of measurements of lifetime distribution, average lifetime and density of clathrin foci at the PM of hypocotyl

epidermal cells after LatB (10 um; 1 h); the bottom row, the same of the root epidermis (10 uM; 15 min). Note that there is no significant difference of any of the measurement. Two-sided unpaired T tests were made. Average lifetimes:: hypocotyl p=0.43;root p= 0.52. Average density: hypocotyl p=0.48;root p=0.97.
D) CCP developmental profile after LatB treatment. Line used: *pCLC2*::*CLC2-GFP*. Root epidermal cells were treated with LatB for 15 min. The plot represents intensity time course of CCPs marked by CLC2-GFP. Trajectories that have the lifetimes between 17-24 s in 6 control roots (101, 72, 97, 118, 185 and 99 trajectories from each root) and 4 treated roots (68, 140, 117 and 106 trajectories from each root) were analysed. The extrapolation lines mark the maturation phase. The bottom bar plot represents the phase transitions computed individually from the trajectories of each root. The dotted bars represent the whole time scale of CCP development; the solid lines with error bars mark the mean ± SD of the transition point between phases. Note that there is no significant change in the length of the assembly or the maturation phase after LatB treatment. One-sided Mann-Whitney U test - for assembly p=0.44 – for maturation p=0.08.
E) Internalisation of FM4-64 in root meristem of *Fim1-GFP* line after 20 uM LatB treatment for 30 min. Note that the FM4-64 internalisation occurs uninhibited; at least 10 seedlings per condition; Scale bars: 10 um (see also supplementary figures S2D and D; and supplementary movie 1).
F) Late endosomal formation. VAEM images of hypocotyl cell with PM and LE localised receptor, FLS2 are shown. Line used: *FLS2-GFP* x *ARA7-RFP*. After pretreatment with mock DMSO or 10 uM LatB (1.5 h) along with flg22 10 uM (last 0.5 h), FLS2 internalisation was followed for an h; 9 hypocotyls were imaged per condition. Control condition with no flg22 treatment is also shown. Note that FLS2 reaches the endosomes irrespective of depolymerisation of actin with LatB following flg22 stimulation; however in the absence of flg22, no endosomal localisation of FLS2 is observed. Scale bars: 5 um.
G) Test for PIN2 endocytic rate. (Top) Rate of PIN2 endocytosis over time after actin perturbation. The dots represent the mean intensity and the dotted lines represent the error with 95% CI – shown after 45 min of LatB treatment (10 uM; 45 min) compared to the mock. PIN2 internalisation rate after LatB treatment remains the same; LMER - random effects for position; χ^2- 2.5923; df=1; p=0.107; 5 seedlings per condition; all the cells in the root meristem were considered; 2 independent experiments. (Bottom) Positive control for the test of PIN2 endocytic rate: Rate of PIN2 endocytosis over time. The dots represent the mean intensity and the dotted lines represent the error with 95% CI – shown after induced Auxlin-LIKE2 overexpression for 24 h (AXL2-OX) compared to uninduced condition. PIN2 internalisation rate after AXL2-OX is reduced; LMER - random effects for position; χ^2 =78.095; df=1; p < 2.2e-16 ***; 4 seedlings per condition; all the cells in the root meristem were considered; 2 independent experiments.

The arrangement of cortical actin with preserved spatial resolution could be observed in the replica of the protoplasts (figure 2A). Actin forms thick main filaments and several thinner subsidiary filaments close to the plasma membrane. Although deeper inside the cell, actin exhibits a much more complicated network (supplementary figure S2A) along with the endomembrane structures. In addition, the dynamics of actin and its localisation at the plasma membrane need to be studied carefully.

TIRF is a powerful technique that could be used to study dynamic events that are close to the cell surface. Structure and localisation of cortical actin including its dynamics need to be characterized in order to understand its mechanism of action. The cortical actin filaments in the entire multicellular organ system as visualized under TIRF using *ABD2-GFP* marker line, is shown in (figure 2 B). Hypocotyl epidermal cells and the root hair cells - both show filamentous network of cortical actin consisting of thick main filament that is stationary and numerous branches of dynamic subsidiary filaments (Staiger et al., 2009); but there is no concrete focus of polymerisation that could potentially co-localise with endocytic spots at the plasma membrane. This is not consistent with yeast and some mammalian systems where CCP invagination and proper vesicle formation has been shown to be facilitated by actin polymerization. Different marker lines – *Lifeact-YFP*, *ABD2-GFP* and *mTalin-GFP* were tested and none of them revealed actin foci at the plasma membrane but consistently

revealed dynamic filaments close to the membrane (supplementary figure 2B). This also complements the observation made in protoplasts.

Plant cells form a clear endocytic focus marked by endocytic machinery proteins like clathrin – CLC2 and dynamin – DRP1C in the plasma membrane (figure 2B). But there are no foci of actin polymerisation that could mark the same at the plasma membrane.

3.2.4 Actin is not mandatory for CCV formation

The absence of actin foci at the plasma membrane is intriguing. Actin polymerization energy is a potential driving force for the clathrin pit development against the membrane tension/turgor pressure. This necessitates a thorough analysis of clathrin pit development and endocytosis, and the role of actin in it.

In order to empirically study the importance of actin in the different stages of CCV formation – initiation, invagination and scission, we perturbed actin by drug treatments to stabilize the filaments using Jasplakinolide or to depolymerize completely using LatrunculinB (LatB). We used TIRF microscopy to directly visualize the endocytic events at the plasma membrane of root and hypocotyl epidermal cells. The CCP developmental dynamics was observed by three different markers of the endocytotic machinery, that functions at different stages of endocytic pit development: TPLATE adaptor, clathrin (CLC2) and Dynamin (DRP1C). We observed no obvious change in the lifetime distribution of the clathrin foci after 10 uM LatB and 500 nM Jasp treatments for 1 h in hypocotyl and 15 min in roots (figure 2C and supplementary table1). The CCVs marked by CLC2-mKO could still form and fall off the plasma membrane, despite the spiky actin filaments (an extreme structural abnormality occurring due to prolonged Jasp treatment) after 10 uM Jasp treatment for 1 h (supplementary movie 2) or LatB (data not shown). This shows that there is no spike in arrested pits or abortive pits at the PM despite actin perturbation. In addition, we observed no differences in the density and the lifetimes of the foci at the PM after the treatments. The average lifetime of the clathrin foci was measured to be ~21 s with an average density of 0.9/sq.um in root epidermal cells; and the same was ~10.5 s with 0.76/sq.um density in hypocotyl. There was no significant changes in the measurements LatB and Jasp treatments– as shown in figure 2C and supplementary table 1, suggesting that there is no change in the rate of endocytosis after actin perturbation. All the marker lines that have varying functions at the endocytic focus show consistent results.

Then we checked the effect of actin perturbation directly on the CCP development. As proven in several models, membrane invagination during the CCP development is facilitated by actin. Therefore, we checked for significant delay in assembly and maturation phases in developing pits after actin depolymerisation. Consistent to our previous observations, we observed no significant change in the intensity profile or the average duration of any of the developmental phases after LatB treatment in roots (10 uM, 15 min). Importantly, there was no increase in the duration of the assembly or maturation period, when the invagination of the pit occurs (figure 2D). All these results suggest that depolymerizing or stabilizing actin has no inhibitory effect on CCP initiation, maturation or scission, in extension, the rate of endocytosis. This is dissimilar to mammalian systems with high membrane tension, *Dictyostelium* and particularly to high turgor pressure system like yeast, where actin

perturbation causes arrest of CCP development at the plasma membrane (Basu et al., 2014; Boulant et al., 2011; Brady et al., 2010; Watanabe et al., 2013).

In addition to direct studies of the dynamics of the endocytic machinery, we tested the productivity of the pits. That is, we studied the internalisation potential of the cell in the absence of a functional actin. We looked at the bulk uptake of the plasma membrane using the dye FM4-64 and at RME after ligand stimulation. Uptake of the dye FM4-64 in the roots showed that endocytosis still occurs and the endocytosed vesicles do reach the EEs after actin perturbation. Internalisation of FM4-64 dyed membrane was tested in root epidermal cells after LatB and Jasp treatments. There was no inhibition of endocytosis. Effects of LatB 20 uM, 30 min (figure 2E) and Jasp 5 uM, 60 min (supplementary figure S2C) on FM4-64 dye internalisation are shown; however effects of LatB 10 uM - 30 min and 60 min had similar effects (data not shown). The internalization of the dye could be observed clearly even after complete depolymerized state of actin filaments or spiky state of the actin filaments (as visualized by actin marker lines). The effect of actin perturbation on RME in hypocotyls was tested by flagellin (flg22) uptake through its receptor – FLS2. On application of flg22 (cargo), its receptor FLS2 gets endocytosed and could be visualized in ARA7 labeled endosomes after 40 min (Beck et al., 2012). After LatB treatment (10 uM), endocytosis of the receptor still occurred and the receptors reached the expected endosomes (figure 2D).

However the implications of loss of actin on endocytotic rate of cargoes needs to be analysed. Therefore, we directly followed the endocytosis of a cargo - PIN2, an auxin transporter after actin depolymerisation. PIN2 is an apically localised plasma membrane protein in root epidermal cells, which gets constitutively recycled. PIN2 was tagged with a photo convertible Dendra and then the entire population of PIN2 in the root was photo converted. The loss of photo-converted PIN2 membrane signal was followed over time, which denotes the rate of its endocytosis. There was no significant change in the endocytic rate of PIN2 from the plasma membrane in LatB (10 uM) treated roots compared to mock, as shown in figure 2E (top). In fact, the rates of endocytosis of PIN2 were very similar between the conditions for the observed 3 h. However we managed to significantly decrease the endocytic rate after AUXILIN-LIKE2 overexpression – a positive inhibitor of endocytosis (figure 2E - bottom), as we previously described in (Adamowski et al., 2018)

In summary, there is no arrest of CCPs or a decrease in the endocytotic rate on actin perturbation. Concomitantly, there is no dense actin network around a developing CCP aiding its invagination or scission. FM4-64 stained plasma membrane gets internalized and the rate of PIN2 endocytosis remains unchanged. This is consistent with studies in *Chara*, a more primitive plant model (Klima and Foissner, 2008). This shows that actin is not mandatory for the CCP development and subsequent endocytosis in *Arabidopsis* and likely many species *in planta,* in spite of high turgor pressure counteracting the endocytic energetics in the cells (Jarvis. et al., 2000). All these studies prove that the membrane remodeling by continuous clathrin polymerisation, as featured by 'constant curvature model', contributes to pit invagination with no requirement of actin.

3.2.5 Actin is essential for maintaining the dynamics of the EE/TGN and efficient down-stream trafficking events

Though actin is not functional at the developing endocytic pit, its role post-endocytosis could be relevant. Vesicular trafficking and Early Endosome (EE) formation are the post-endocytotic events that require active transport with high spatial and temporal control. Each cell has several tens of Golgi apparatus along with the trans-golgi network fused with EE/TGN. They are transported around the cell along the actin network.

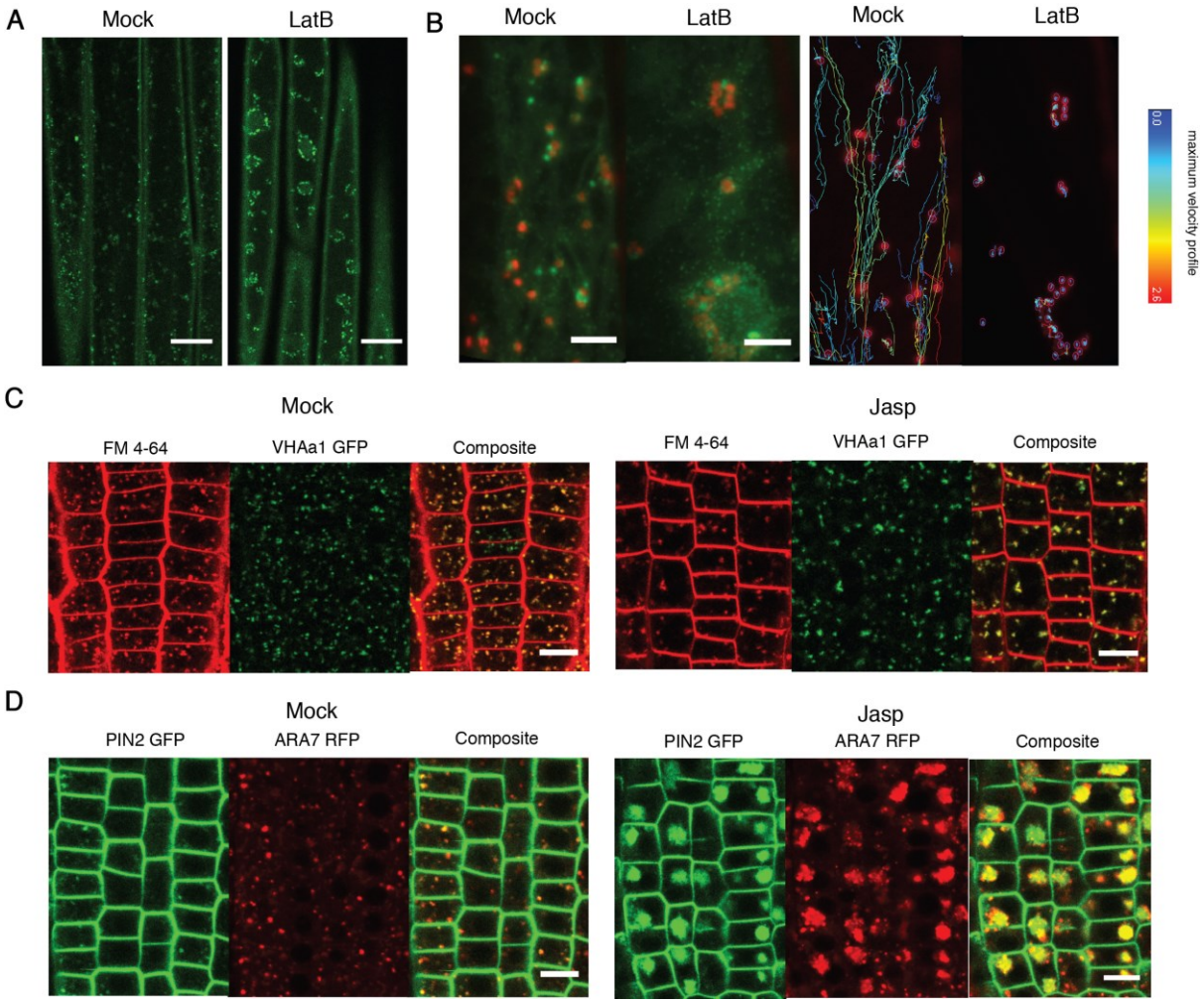

Figure 3: Lack of actin dynamics results in defective trafficking

A) and B) Clustering of EE/TGN observed in hypocotyl . A) shows confocal images of EE/TGN (CLC2-GFP) aggregated after 10 uM LatB treatment for 1 h. 5 hypocotyls per condition. Scale bars: 15 um B) shows VAEM images of aggregated Golgi (ST-RFP) together with EE/TGN (CLC2-GFP) (on the left) due to loss of dynamics. The dynamics of EE/TGN is shown by obtaining the velocity profile of Golgi apparatus (on the right) before and after LatB treatment (10 uM; 1 h). At least 15 cells per condition. Scale bars: 5 um (see also the supplementary movie 2 and 3).

C) Uptake of FM4-64 dye and its localization after 5 uM Jasp treatment for 30 min. Confocal images of co-localisation of FM4-64 with the EE/TGN marker VHA-a1-GFP are shown in root meristem. 7 roots per condition. Scale bars: 10 um.

D) Down-stream PIN2 trafficking. Confocal images of PIN2-GFP co-localised with the Late endosomal marker – ARA7-RFP are shown in root meristem before and after 5 uM Jasp treatment for 5.5 h. 8 roots per condition. Scale bars: 10 um.

The EE/TGN system, marked by clathrin, continuously forms at and detaches from the trans-side of the Golgi apparatus (Kang et al., 2011). Thus EE/TGN system in general is highly dynamic (supplementary movie 2).

Upon depolymerising or stabilizing the actin filaments, we could observe a complete halt in the dynamics of the Golgi apparatus (marked by ST-RFP) and the EE/TGN system (marked by CLC2-GFP) resulting in local aggregation, as opposed to equal spreading of these organelles. The loss of dynamicity of the EE/TGN after LatB is shown in supplementary movie 3. The tracks of the Golgi apparatus with the velocity profile coded are shown in figure 3B (right half). As a result, the EE/TGN marked by clathrin could be clearly seen lining up together, probably in the inter-vacuolar space along the ER. The pattern could be seen after LatB treatment (10 uM; 1 h) in figure 3A and B. But in the control normal condition, one could observe them uniformly spread throughout the cell.

Though endocytosis is normal upon actin perturbation as described earlier, the EE/TGN system is disorganised due to the lack of dynamicity. In this case, one would expect the downstream targeting events to be impaired. Interestingly, the endocytosed FM4-64 dye still reaches the agglomerated EE/TGN at the trans-side of the Golgi apparatus. Figure 3C shows the internalised dye reaching the VHA-a1 marked EE/TGN compartment after 30min Jasp (5 uM) treatment (also after LatB, data not shown). And one would expect an overall retardation or mistargeting of proteins during downstream events. As expected, mislocalisation of PIN2 signal was observed after 5.5 h of Jasp (5uM) treatment. Huge amount of PIN2 was stuck in late endosomal compartments – marked by ARA7 (figure 3D), pointing towards potential impairment in PIN2 trafficking in degradative pathway. In spite of observing normal PIN2 endocytosis (figure 2G) until ~5 h of actin depolymerized condition, the amount of PIN2 that reaches the vacuole was reported to be less in Kleine-Vehn et al., 2008. This points towards mistargeting or slowed trafficking of proteins post-endocytosis, as reflected by PIN2 stuck in aggregated LE, when actin dynamics is hindered. This proves that lack of functional dynamic actin leads to mistrafficking of proteins.

Actin based motility of the organelles, which is the fundamental feature of the cell, is essential for maintaining the integrity of the organelles themselves. The loss of normal dynamicity of the EE/TGN system and the resultant agglomeration, and overall impairment of trafficking of proteins are the main implications of loss of actin.

3.2.6 Actin network brings the endocytosed CCVs and the EE together

Loss of actin and its dynamics resulted in defective trafficking. Therefore action of actin in actual trafficking events – such as post-endocytic vesicle trafficking and early endosomal movements - needs to be closely studied. The dynamics of actin subsidiary filaments orchestrating the movement of EE/TGN is observed clearly in the cortical region (supplementary movie 2). However the importance and the relevance of their dynamicity is unknown. We took a closer look at endocytosis and the endomembrane system, and monitored the fast trafficking events that occur closer to the plasma membrane in the hypocotyl epidermal cells.

The CCVs and the EE /TGN were followed at deeper angles to TIRF angle. On following the Golgi (marked by ST-RFP) and the CCVs along with the EE/TGN marked by CLC2-GFP, we

observed two distinct sets of events. Firstly, the EE/TGN together with the Golgi moving along the actin network could be observed to pick up the endocytosed CCV (scissioned and released from PM) as shown in supplementary movie 4 and 5, and figure 4A. The moving EE picks up the endocytosed CCVs close to the PM, and aggregates to fuse to endosomal body. Importantly, the fast-moving, uncoated vesicles could not be always followed until the endosomal stage. Therefore, we simply followed the CCV tracks that has a lifetime longer than 5s that ended in a 'defined area' encompassing an active Early Endosome (1.5 um x 1.5 um) ie. Endocytosed CCVs that vanish due to uncoating/fusion.

However, there are several tracks that do not end at an active EE area. The (%) tracks that 'selectively end' in the defined area among all the tracks that cross the area is shown in figure 4B. We could clearly see that in the 'Endosomal' area encompassing an active EE, there is an increase in the % of CCV tracks ending, compared to the 'Control' area with no EE (figure 4B left); meaning that Early Endosomes are actively traversing along actin collecting the CCVs. Adaptor molecules are important for a successful endocytic event. Not all clathrin foci contain TPLATE molecules (Gadeyne et al., 2014). Therefore we checked if there is

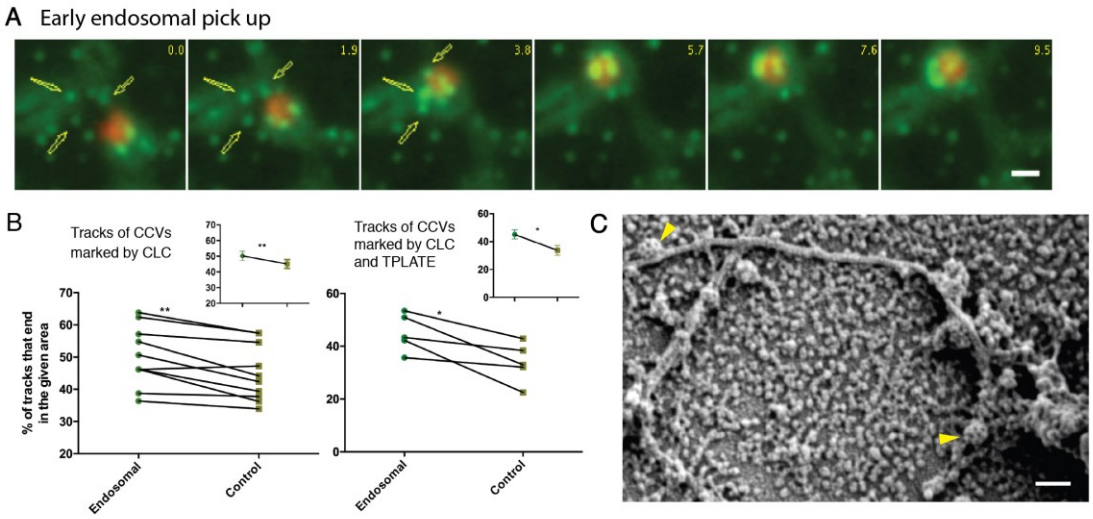

Figure 4: Role of actin in EE formation

A) Early endosomal formation by CCV collection onto the EE/TGN compartment. Sequential VAEM imaging was performed on the line *p35S::ST-RFP* x *pCLC2::CLC2-GFP* in hypocotyl epidermal cells. The movement of the Golgi apparatus together with the EE/TGN towards endocytosed CCVs, and subsequent collection of the CCVs on its trans-side containing the EE/TGN are shown. The time interval between frames is 1.9 s. Scale bar: 1 um. See also supplementary movie 5.

B) Number of CCVs picked up by EE. CCVs were imaged by sequential VAEM imaging of root epidermal cells. Fraction of CCV tracks that vanish within the specified area (1.5 um x 1.5 um) around an active EE was computed. An 'active EE' is signified by the presence of the dynamic EE/TGN body (marked by CLC2-RFP). Area around an active EE track is represented 'Endosomal'; Area around a mis-localised track is represented 'control'. All the CCV tracks that pass through the specified area were followed and the fraction of the tracks that end in the specified area was computed. In the left, the tracks of CCVs marked by CLC2-RFP were followed. On the right, the tracks of CCVs marked by both TPLATE-GFP and CLC2-RFP were followed. In a given cell, hundreds of Endosomal and control track areas were marked to obtain the count of CCV tracks that end in the area. Each dot represents the mean fraction value from a single cell. Line: *pRPS5A*::*CLC2-RFP*. 10 cells were analysed; one cell/root. Note that the number of tracks of CCVs ending in the specified area increases in the presence of an active EE within that area (Endosomal condition), in comparison to the area where there is no EE (control). Paired One-sided T test p=0.0015. Line: *pLAT52::TPLATE-GFP x pCLC2::CLC2-RFP* . 5 cells analysed. Paired two-sided T test p=0.03.

C) CCVs moving along actin filament. Ultra-structural SEM analysis of protoplasts reveals fully developed CCVs lined upon an actin filament. The arrows point the CCVs. Scale bar: 100 nm.

drastic increase/decrease in selectivity of the CCVs reaching the EE based on the presence of the adaptor TPLATE in the CCVs. The observation held true for the particular CCV sub-population that acquired TPLATE adaptor (CLC2-RFP+TPLATE-GFP) – figure 4B (right) as much for the entire population of CCVs (marked by CLC2-RFP) – figure 4A. This means that EE selectivity in picking up the CCVs is not biased upon the functionality of the adaptor. It is also to be noted that EE also remain static at times in a normal cell. Similarly, in the static state, the CCVs that are close by reach the EE to fuse. This could be clearly seen in supplementary movie 7. Together these events mark the very first evidence of EE formation through collection and fusion of endocytosed CCVs *in planta*. We also observed the dynamics of actin subsidiary filaments and the clathrin coated pits and vesicles. There appears to be a spatial and temporal correlation between the appearance of a small branch of an actin subsidiary filament (not a focus) and the fully formed CCVs pinching off the membrane. The CCV once completely developed, scissions and starts moving away; and they move away as the actin subsidiary filaments appear at the site of scission. There are a few regions in the cell that clearly show this dynamics (supplementary movie 7). In addition, the replica images in protoplasts show some preserved CCVs moving along actin filaments. Fig 4C shows two fully formed CCVs attached to a long actin filament in close proximity to endo membrane structures.

All these results together with the *in vivo* imaging of endocytotic events at the plasma membrane show that actin filaments traffic the CCVs directly from the site of endocytosis. Also, actin directionally transports the EE/TGN compartments to pick up a fraction of CCVs as they move. A model depicting the summary of these is shown in figure 6. Mistrafficking of proteins, as seen in the case of PIN2 (figure 3D), is a probable effect of loss of functional actin. This proves the significance of actin post endocytosis in conferring effectiveness in targeting of proteins to endosomes.

3.2.7 Uncoating is a sequential process

CCVs aggregate and fuse to EE. This process involves the CCV to shed their coat proteins, so as to fuse to the EE (Beck et al., 1992; Sekiya-Kawasaki et al., 2003). This uncoating process is done by a set of 'uncoating machinery proteins' like auxilins and HSC70; and these are known to be inevitable in mammalian and yeast systems. And its appearance at the CCP is tightly correlated with dynamin, meaning that the uncoating machinery is recruited right after vesicle constriction (Gall et al., 2000; Massol et al., 2006; Yim et al., 2010). The exact mechanism of clathrin disassembly once the uncoating factors are recruited was a highly debated question: Does the coat get released all at once, co-operatively or does the uncoating happen bit-by-bit sequentially? It has been proved that the HSC70-Auxilin duo disassemble the coat in rapid co-operative way in yeast and animal cellular systems (Böcking et al., 2011; Krantz et al., 2013). Whereas in plants, we have previously described that AUXILIN-LIKE1, the putative uncoating factor bind to only ~5% of the CCPs at the final stage just before scission. Also the knock out mutants have no strong phenotypes (Adamowski et al., 2018). This means that the uncoating mechanism might not be strongly conserved in plants and there could be an alternative mechanism of disassembly – say, sequential.

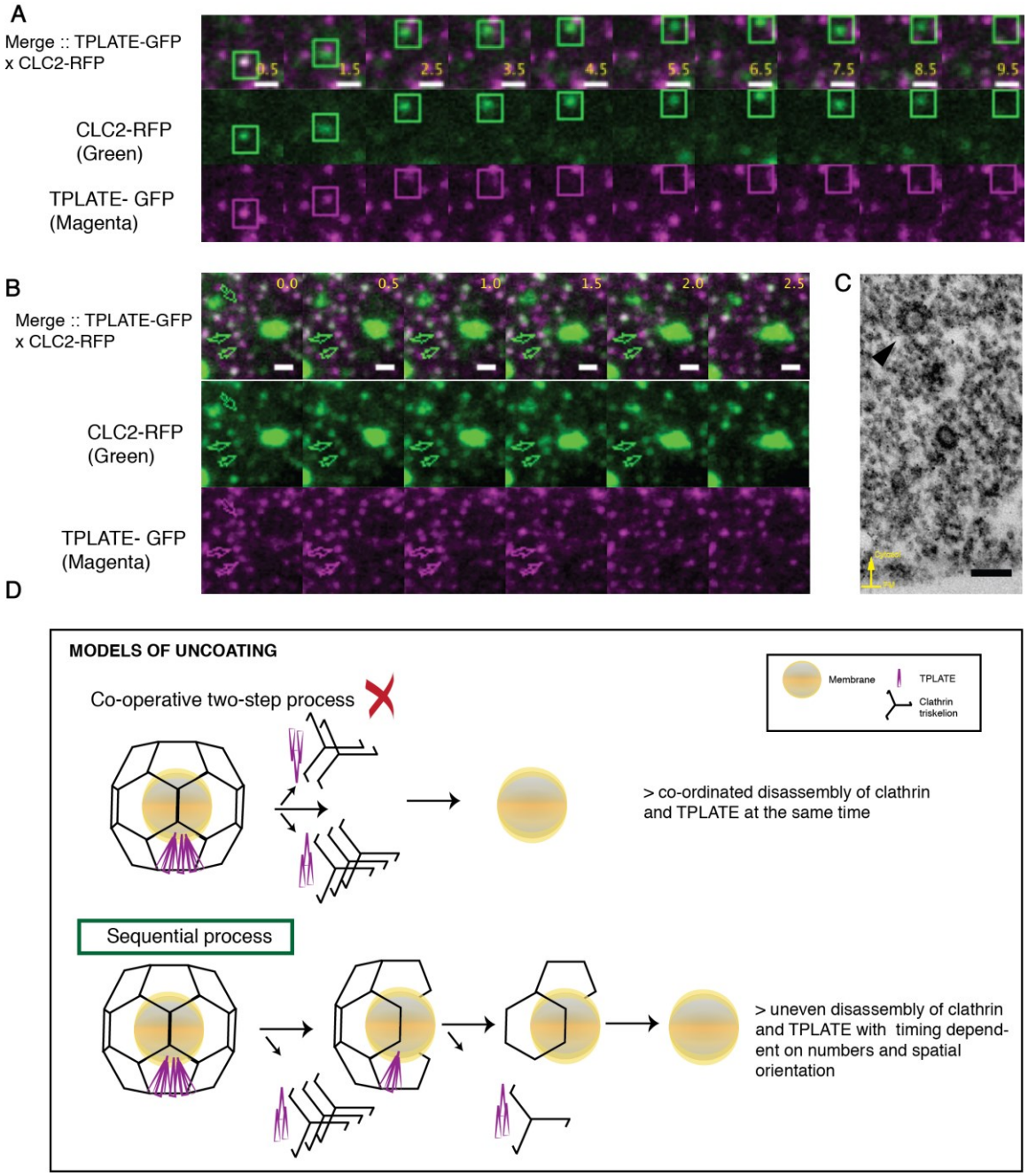

Figure 5: Uncoating is a sequential process

A) Uncoating process in a fully developed CCV. *pLAT52::TPLATE-GFP* x pCLC2::*CLC2-RFP* was imaged sequentially in VAEM mode in hypocotyl epidermal cells. The figure shows the fully developed CCV moving away from the PM after scission. The signal of TPLATE adaptors is lost before that of clathrin coat proteins. The frames are 0.5 s apart. Scale bar: 1 um. See also supplementary movie 8.

B) Uncoating process at the EE/TGN. *pLAT52::TPLATE-GFP* x pCLC2::*CLC2-RFP* was imaged sequentially in VAEM mode in hypocotyl epidermal cells. CLC2 marks both the endocytic foci (smaller dots) and the EE/TGN (bigger structure), whereas TPLATE marks only the endocytic foci. The figure shows fully developed CCVs (marked by arrows) reaching the stationary EE/TGN. The signal of TPLATE adaptors is lost at the EE/TGN compartment. The status of clathrin coat proteins is inconclusive due to the signal from the EE/TGN. The frames are 0.5 s apart. Scale bar: 1 um. See also supplementary movie 9.

C) TEM image of a CCV deeper in the cytosol (black arrowhead) after high-pressure freezing and freeze-substitution. The CCV is in the process of uncoating with partially removed clathrin coat. Scale bar: 100 nm.

D) Models of uncoating process: co-operative disassembly and sequential disassembly models are

proposed; (shown on top) Temporally co-ordinated disassembly of clathrin and TPLATE molecules, where the disassembly of all the molecules occurs all at once is the only outcome for the former model; (shown on bottom) Uneven disassembly of the molecules with TPLATE molecules disappearing before clathrin as a possible outcome for the latter model. Given the observation of uneven disappearance of TPLATE before clathrin, shown in 5A, we reject the first model.

As observed in supplementary movies 4 and 5, the CCVs described to reach the EE/TGN remain coated still contain the clathrin coat protein. Some CCVs obviously can retain the clathrin coat until they reach the EE. This shows that the clathrin coat does not get removed immediately, therefore there is a possibility for the coat to be removed sequentially bit by bit taking much longer time for complete uncoating.

To check if uncoating is a sequential process with intermediates, we followed the CCVs that leave the membrane. We observed two types of events. The CCVs that leave the membrane either or 1) remains coated until immediate fusion into the EE or 2) gets uncoated on the way to an EE. We followed the same events with the TPLATE adapter molecules (TPLATE-GFP) co-localizing with clathrin (CLC2-RFP). In the first type of event in which the CCVs immediately fuse into an EE, both clathrin and TPLATE molecules were still retained until the vesicles reached the EE. However after fusion, the EE compartment did not retain the TPLATE molecules any longer, meaning that the uncoating process had taken place at least partially, but enough to get rid of TPLATE molecules (figure 5B; supplementary movie 8 and 9). Bunches of aggregated partially coated CCVs have been found in endomembrane structures – figure 1H and supplementary figure 1B. This opens the possibility that CCVs could remain partially uncoated at the EE.

In the event that CCVs uncoat midway, we could observe the endocytosed CCVs losing T-plate adaptor first, followed by clathrin – as seen in figure 5A. This happened in 90% cases (18/20 CCVs that was traced leaving the PM with clathrin and TPLATE). In the rest 10%, they vanished together. This means that the disassembly does not happen all at once, in which case all the proteins forming the cage and residing within the cage would be released at once “co-operatively”. Since molecules of TPLATE are lost before clathrin featuring an uneven disassembly scenario, it is conclusive that the uncoating process is majorly “sequential”. A CCV, deeper in the cytosol, in the process of discarding the clathrin coat could be seen in figure 5C.

In summary, uncoating of the CCVs does not happen immediately after scission at the endocytic spot; the clathrin coat is retained for a longer time. The endocytosed vesicles sometimes fuse to the EE before completely losing the coat. They lose their adaptor and the coat proteins after reaching the EE. Together these results show that uncoating of CCVs in plants is a sequential process with intermediates, unlike in yeast and animal cellular systems where the entire coat is shed all-at-once co-operatively. This could be attributed to the fact that auxilin-likes reach only 5% of the pits in *Arabidopsis*, and a possible alternative unknown uncoating machinery to be pre-dominantly functional.

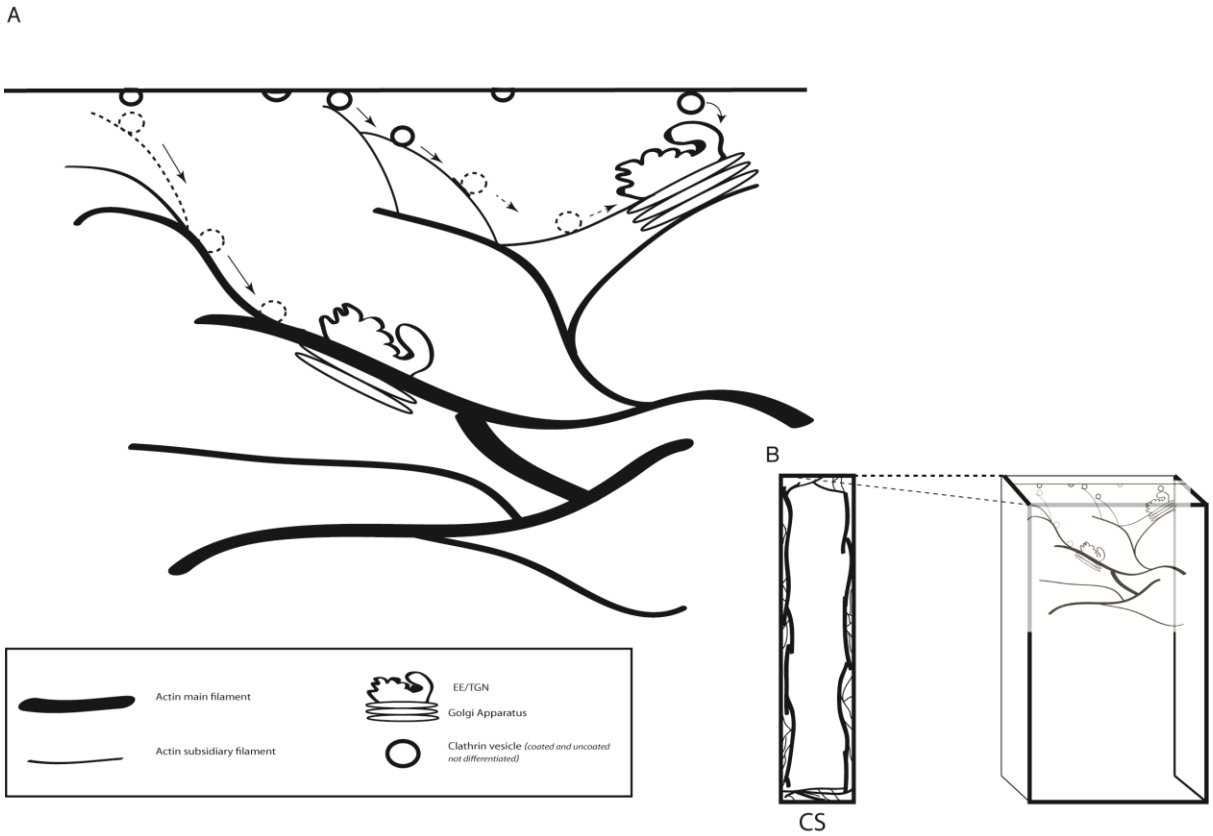

Figure 6: Model for role of actin in post-endocytic trafficking
A) Actin-mediated trafficking of the fully formed CCVs and the EE/TGN compartments. Developing CCPs are devoid of actin structures. Fully developed CCVs are trafficked along the subsidiary filaments to reach the EE/TGN. Parallelly, actin facilitates the pick up of the fully developed CCV by the EE/TGN transported to the site of scission.
B) 3-dimensional representation of actin cytoskeleton and its trafficking events. Cross-Section (CS) of a hypocotyl cell illustrating the cortical actin is shown to the left.

3.3 DISCUSSION

This is the first complete study *in planta* on the fate of the clathrin coated vesicle -starting from the development of the pit at the PM, its transport and eventual fusion to the EE. This includes the uncoating process of the endocytosed CCVs and the role of actin in the transport of these vesicles and endosomes facilitating the fusion events. The studies have been made in complex multi-cellular organs, thus accounting for higher order interactions which otherwise is absent in unicellular system.

3.3.1 Actin independent endocytosis

Endocytosis in high turgor pressure system has been an intriguing phenomenon for many years (Jarvis. et al., 2000), given the unfavourable energetics against the hydrostatic pressure. Though further studies proved the existence of coated pits in such systems, actin has been emphasized to be required for detaching the PM from the cell wall, and further for deforming the membrane locally - all against the turgor (Dmitrieff and Nédélec, 2015; Tweten et al., 2017). However our results in higher plant organ systems conclusively show that there is no change in endocytotic rate upon actin perturbation. This challenges all the models that frame our current understanding on membrane cycling energetics under turgor.

However a simpler explanation might come from studies that uncoupled membrane bending trajectories and clathrin assembly (Bucher et al., 2018; Scott et al., 2017). According to their observations, development of the clathrin pit from a plaque (constant area model) entails actin-mediated membrane bending after the initial assembly of clathrin on flat surfaces; this is the case where actin polymersation counteracts the opposing forces, whereas, continuous bending of membrane by clathrin polymerization (constant curvature model) does not necessarily involve actin. Both the *Arabidopsis* organ and protoplasts systems do exhibit the latter model of pit development. Thus clathrin polymerization energy, in addition to other membrane deforming proteins, might be good enough to counteract the turgor. In addition, studying the bending modulus of the membrane might shed light on plant cellular mechanisms establishing curvature. Lower rigidity could establish lower cost of bending against turgor pressure (Dmitrieff and Nédélec, 2015; Pinot et al., 2014), eventually not requiring actin for pit development.

Alternative approach would be to totally re-organise our current knowledge in unicellular yeast and mammalian cells onto complex multi-cellular systems. It is possible that during the evolution of multi-cellularity, alternate membrane deformation mechanisms co-evolved in accordance to cell-cell adhesion, signaling, polarity etc (Eaton and Martin-Belmonte, 2014). Screening for other membrane modifying proteins and studying their activity would definitely enable us to discern the substitution for actin-mediated membrane deformation.

3.3.2 Characterising different cohorts of CCPs

We observed the endocytic events at the PM; and based on their intensity profile and lifetime distribution, the pits could be categorised into different cohorts. We analysed the entire set of cohorts – including the very short events (5-15 s cohort), which accounted for majority of the detected events. This contributed to a lifetime distribution exhibiting an exponential decay (Johnson and Vert, 2017b). Such a method of analysis eliminates the biases one might get while kymographing these events. This explains the discrepancy in lifetime distribution observed in previous studies (Higaki, 2015; Konopka et al., 2008).
The biological relevance of the short events (at the start of the exponential curve) could be attributed to the exocytotic events, or abortive pits, or even CCPs with a different functionality. We would eventually conduct further studies in plants to understand these cohorts. This would enable us to unequivocally understand the effect of actin perturbation or any other effect on pit developmental.

3.3.3 Active and passive transport of endocytosed CCVs

Trafficking of endocytosed CCVs to the EE is dependent on actin and its dynamics. However what happens during the total absence of actin is hard to explain. The internalised FM4-64 dye surprisingly reaches the EE/TGN compartment despite the actin-perturbed conditions. But what causes the passive collection of internalized CCVs in the EE within the estimated time is inexplicable. 'Brownian movement' of the vesicles to endosomes could possibly be one contributing phenomenon.

Also, what causes the selectivity of some CCVs to reach particular EE or what determines the pick up of some CCVs by a moving EE/TGN system could not be explained. Is it a completely random event? Or spending so much energy in actively moving several tens of EE/TGN system around synchronized with endocytotic and exocytotic events? This remains elusive.

Importantly, how the smaller subsidiary filaments bring the just endocytosed CCVs from the site of endocytosis to the EE is not trivial. Though a spatio-temporal relationship could be observed between the actin filaments and the endocytosis of CCVs, exactly how a CCV is marked for the actin filament and the EE to reach for, is a complex question. Yeast and mammalian systems that does depend on actin for endocytosis obviously has Arp2/3 branching and acto-myosin framework pre-established at the endocytic spot which eventually builds a network of actin for the CCV to move on (Collins et al., 2011; Picco et al., 2015; Toshima et al., 2006; Yarar, 2004). In so many mammalian systems and *in planta*, where actin polymerization is not a pre-requisite for the CCP development, the active transport of the fully formed CCVs from the site of endocytosis is not well-studied. One possibility is the Brownian movement of CCVs until a closer acto-myosin network is hit eventually getting actively transported. The other is the conventional Arp-dependent branching of actin filament from a matured endocytic site, merely transporting the vesicle along the network (Merrifield et al., 1999, 2002). Further studies need to be directed to resolve these possibilities.

3.3.4 The uncoating process

We unexpectedly observed still-coated CCVs reach the EE immediately after scission. Similarly in yeast, sla1 coat protein containing endocytosed vesicles have been observed to fuse to the EE (Toshima et al., 2006). Recently the question: "Is uncoating an all-or-nothing process" is being raised. There are several evidences for competing events of uncoating and coat retention mechanisms, so as to retain a partially coated state for efficient tethering and fusing events of COP vesicles (Schroeter et al., 2016; Trahey and Hay, 2010). Also it has been reported by Massol et al., that 100% of the CCVs had bound auxilins. This suggests functioning of the machinery even post scission. Similar evidences, as on uncoating COP vesicles were unavailable for CCVs. Partially uncoated state of CCVs or questions on the duration of coat retention has not been addressed before. For the first time, we show evidence for a longer retention of clathrin coats as the CCVs reach the EE. This opens a huge scope for coat functions in vesicular-endosomal fusion.

Also, interestingly, HSC70-Auxilin combination of proteins has been shown to disassemble CCVs co-operatively. As Auxilin-likes in plants are not as essential as in other systems and predominant mode of disassembly in plants is sequential, as discussed before, we need to look for alternative uncoating machineries. A thorough study of uncoating process should be made in *Arabidopsis*.

3.4 Experimental model and subject details:

3.4.1 Accession numbers of the genes

The *Arabidopsis thaliana* genes studied and their corresponding accession numbers are listed: Fim1 – AT4G26700, CLC2 - AT2G40060, DRP1C – AT1G14830, Tplate- AT3G01780, VHA-a1 - At2g28520, PIN2 - AT5G57090, FLS2 – AT5G46330, Axl2 - AT4G12770

3.4.2 Plant lines used

All the plant material is of the model organism *Arabidopsis thaliana.*

pCLC2::CLC2-GFP, *pDRP1C::DRP1C-GFP* (Konopka et al., 2008), *pRPS5A::CLC2-RFP* , *pLAT52p::TPLATE-GFP* x *pRPS5A::AP2-RFP*, *pLAT52::TPLATE-GFP* x *pRPS5::CLC2-RFP tplate* (Gadeyne et al., 2014b), *p35S::Fim1-GFP*, *35S::ABD2-GFP* (Wang et al., 2004), *p35S:: mTalin-GFP* (Kost et al., 1998), *p35S::Lifeact-Venus* (Era et al., 2009), *p35S::ST-RFP* x *pCLC2::CLC2-GFP* (Ito et al., 2012), *pVHA-a1::VHA-a1-GFP* (Dettmer et al., 2006), *pFLS2::FLS2-GFP* x *pUBQ10::mRFP ARA7* (Beck et al., 2012)**,** *pPIN2::PIN2-Dendra eir1-1* (Salanenka et al., 2018), *pPIN2::PIN2-GFP* x *p35S::ARA7-mRFP* (Ueda et al., 2004; Xu, 2005; Zhang et al., 2016), *XVE>>Axl2* x *pPIN2::PIN2-Dendra* (Adamowski et al., 2018). *p35S::ABD2-GFP* x *p35S::CLC2-mKO* was generated by crossing *p35S::CLC2-mKO* (Ito et al., 2012; Naramoto et al., 2010) with *p35S::ABD2-GFP*.

3.4.3 Seedling growth conditions

The seedlings were growing in ½ MS Agar medium with 1% (w/v) sucrose at 21°C in a 16 h/8 h day/night cycle for 3 days (unless mentioned) for all the experiments and observations conducted in roots, or in dark for 3 days in case of etiolation of hypocotyl. 7-day-old seedlings have been used for following the endocytic foci in roots of endocytic machinery lines.

3.4.4 Root cell culture – maintenance

Arabidopsis (col-0 WT) root-derived suspension was made from roots by the lab of Eva Kondorosi in Gif-sur-Yvette, France. The suspension culture is maintained in growth medium of pH5.7 containing 4.25 g/l of MS salts (Sigma M5524), 30g/l of sucrose, 0.250mg of 2,4D, 0.015mg of kinetin and 2ml Vitamin B5 stock (100ml stock contains 0.1g nicotininc acid, 0.1g pyridoxine HCl, 1g thiamine HCl. 10g myo-inositol)

3.5 Materials:

Latrunculin B -Sigma Aldrich. Jasplakinolide -Santa Cruz. β-estradiol - Sigma Aldrich. MS powder (Sigma Aldrich). Cellulase (Serva), Macerozyme (Yakult pharmaceuticals). EM grade glutaraldehyde and pioloform - Agar Scientific Ltd. (Stansted, UK). Osmium tetroxide - Electron Microscopy Sciences (Hatfield, PA). Acetone and polyethylene glycol - Merck KGaA (Darmstadt, Germany). picric acid - Fluka GmbH (Buchs, Switzerland). Uranyl acetate was from AL-Labortechnik e.U. (Amstetten, Austria). All remaining chemicals used for metal repica and resin embedding was from Sigma-Aldrich GmbH (Vienna, Austria). Aclar® foil - Ted Pella Inc. (Redding, CA). Aluminium planchettes and sapphire disks - Wohlwend (Sennwald, Switzerland). Cryo-vials - Biozym GmbH (Vienna, Austria). Glass cover slips - Roth (Karlsruhe, Germany). Maxtaform H15 finder grids - Science Services GmbH (München, Germany). Platinum and carbon rods were - Leica Microsystems (Vienna, Austria).

The concentration and timing of treatment are reported in the main text.

3.6 Methods

3.6.1 Protoplast preparation and plating

3 d old cultured cell were used for protoplasting procedure. All the centrifugation steps in this procedure were carried out with no brakes (reduced deceleration). The whole procedure was done at RT. The buffer base for the protoplasts is GM buffer (MS salt powder, 0.17 M glucose, 0.17 M mannitol, pH5.5). 25 ml of cell suspension was centrifuged at 1500rpm for 5 min to remove residual media. The pelleted cells were resuspended with 25 ml of enzyme solution (1% cellulose 16426, 0.2% macerozyme, in GM buffer) made up to 50 ml with GM buffer. The enzymatic digestion of cell wall was carried out for 4 h in dark with gentle rocking. Washing out of the enzymatic solution with GM buffer was carried out with two repetitive centrifugation steps of 5 min each at 1200 rpm. Finally the pellet was resuspended. Then a gradient centrifugation was carried out with Sucrose buffer (4.4 g/l of MS powder and 0.28 M sucrose, pH 5.5) at 800rpm for 7 min to isolate the protoplasts that float from the pelleted cells. Protoplasts were carefully removed with Pasteur pipette with no remnant sucrose. Isolated (undiluted) protoplasts were left at 4°C overnight.

The protoplasts were then plated for further replica and embedding procedures. Round glass coverslips (Ø 12 mm) were coated with carbon to a thickness of 10 nm and treated with Poly-L-Lysine overnight at 4 °C to facilitate cell adhesion; then washed briefly with water to remove excess poly-L-lysine and dried. Protoplasts prepared, as described above, were plated onto the coverslips for 4 h at RT to adhere. Finally a brief spin was made at 800rpm for 5 min to make the protoplasts adhere better.

3.6.2 Metal replica electron microscopy

The protoplasts plated were further processed for metal replica. After brief wash in PBS equilibrated to RT to remove the excess protoplasts, the extraction solution was applied for 4 min at RT: 1% Triton X-100 in PIPES-EGTA-magnesium buffer (PEM; 100 mM PIPES, 1 mM EGTA, 1 mM $MgCl_2$, pH 6.9) plus 1% high-MW polyethylene glycol (PEG; 20 kDa) and 2 µM phalloidin. Samples were then washed in PEM plus 1% PEG three times 1 min each and fixed in 2% GA in PB. After washing in distilled water, samples were treated with 0.1% tannic acid in water (w/v) for 20 min at RT and 0.2% uranyl acetate in water (w/v) for 20 min at RT. Samples were then critical point dried following a procedure described by Svitkina and colleagues (Svitkina et al., 2007). In brief, samples were transferred under water to wire-mesh baskets that fit the chamber of the critical point drying (CPD) device Leica CPD300 (Leica Microsystems). Samples were dehydrated in graded ethanols and transferred to the CPD device where the ethanol was replaced for CO2. After CPD, samples were fixed on SEM specimen mounts by means of carbon conductive adhesive tabs (Ø 12 mm), and gold-coated to a thickness of 5 nm by rotary shadowing at 45° angle using the ACE600 coating device (Leica Microsystems). Samples were then examined in a scanning electron microscope FE-SEM Merlin VP Compact (Zeiss GmbH; Oberkochen, Germany) at 5 kV and In-lens Duo detector.

3.6.3 Resin embedding ultrastructure analysis

Aclar® foil was coated with poly-L-lysine (PLL) overnight at 4 °C. Progenitor cells were prepared as described above and plated onto Aclar® foil allow adhering for 4h at RT. After brief wash in phosphate buffered saline (PBS; 0.1M, 0.9% NaCl, pH 7.4), cells were incubated in one of the following solutions for 30 min at RT: GM buffer plus dimethyl-sulfoxide (DMSO), GM plus LatrunculinB or hyperosmolar buffer. Cells were then fixed in 2% formaldehyde (FA) plus 2.5% glutaraldehyde (GA) and 15% of a saturated solution of picric acid in phosphate buffer (PB; 0.1M, pH 7.4) for 30 min at RT. After brief wash in PB, cells were treated with 0.5% tannic acid in PB (w/v) for 1h at 4 °C, 1% osmium tetroxide in PB (w/v) for 30 min at 4 °C and 1% uranyl-acetate in water (w/v) overnight at 4 °C. Cells were then contrast-enhanced with Walton's lead aspartate for 30 min at 60 °C, dehydrated in graded ethanols and anhydrous acetone, and embedded in epoxy resin (Durcupan™ ACM). Serial ultrathin sections (40-70 nm) were cut with an ultramicrotome UC7 (Leica Microsystems), collected onto Formvar-coated copper slot grids and stained with 1% aqueous uranyl acetate and 0.3% lead citrate. Sections were examined in a Philips Tecnai 10 transmission electron microscope (TEM; Thermo Fisher Scientific GmbH) at 80 kV, equipped with a side-mounted camera MegaView III G3 (Electron Microscopy Soft Imaging Solutions [EMSIS] GmbH; Muenster, Germany). Images were processed with Radius software (EMSIS) and Photoshop (Adobe®) without changing any specific feature within.

3.6.4 High-pressure freezing and freeze-substitution ultrastructure analysis

For high-pressure freezing experiments, 1.4 x 0.05 mm sapphire disks were carbon-coated to a thickness of 10 nm using the high-vacuum coating device ACE600 (Leica Microsystems). The pattern of a Maxtaform H15 finder grid was evaporated onto the disk surface, and the coat was stabilized by baking 2 h at 120 °C. Sapphire disks were incubated overnight in PLL at 4 °C and washed in water. Progenitor cells were prepared as described above and plated onto sapphires allow adhering to the disk surface for 4h at RT. Sapphires were then placed into cup-shaped aluminium planchettes with cavity dimensions of 2 mm inner diameter and 100 µm indentation. Medium equilibrated to RT was added as space filler and anti-freezing agent. The flat side of aluminium planchettes with a 300 µm indentations was used as lid and excess of solution was removed with filter paper. The sandwiched samples were high-pressure frozen instantaneously using the Bal-Tec HPM 010 (Leica Microsystems), transferred to cryovials and stored in liquid nitrogen.

For freeze-substitution, samples were processed in an AFS1 device (Leica Microsystems) with ethanol in the loading chamber and perpetual motion using an agitation module (Reipert et al., 2018). Two substitution cocktails were applied consecutively: (i) 0.1% tannic acid in anhydrous acetone (w/v) and (ii) 1% osmium (w/v) plus 0.2% uranyl acetate (20% stock in methanol; v/v) in anhydrous acetone. 2 ml screw-cap Nalgene® cryovials were used for substitution, filled with 1 ml of cocktail. The sequence for infiltration and stepwise warming was: 24 h incubation in 0.1% tannic acid in acetone at -85 °C, 3 times 10 min wash in acetone at -85 °C, 6 h incubation in 1% osmium plus 0.2% uranyl acetate in acetone at -85 °C, temperature rise 15 °C/h to -60 °C, 4 h incubation at -60 °C, temperature rise 15 °C/h to 4 °C, 1h incubation at 4 °C. Sapphires were removed then from the aluminium planchettes and embedded in epoxy resin (Durcupan® ACM). Serial ultrathin sections (40-70 nm) were cut using an ultramicrotome UC7 (Leica Microsystems) and collected onto Formvar-coated copper slot grids. They were stained with 1% aqueous uranyl acetate for 10 min at RT and

Reynold's lead citrate for 2 min at RT. Sections were examined in a Philips Tecnai 10 TEM at 80 kV, equipped with a MegaView III G3 camera. Images were processed with Radius software.

3.6.5 Treatment conditions

All the treatments were carried out in RT in ½ MS medium containing 1% (w/v) sucrose.
Jasplakinolide and LatrunculinB treatments on the seedlings were carried out dissolving them in dissolved in liquid medium. The lines, concentration and time of treatment were as mentioned in the main text. Throughout subsequent imaging, the seedlings were kept continuously treated – except during FM4-64 uptake experiment.

XVE>> Axl2 x pPIN2::PIN2-Dendra line was experimented with induced over-expression of AUXILIN2. 2-day-old seedlings were chemically induced with 2uM β-estradiol. The seedlings were grown in solid Agar medium in plates for approximately 24h. The seedlings were continuously under chemical induction during subsequent imaging by confocal microscopy.

FM4-64 uptake: For internalisation test, 3-day-old seedlings of corresponding lines were stained with 2 uM FM4-64 dye dissolved in liquid medium. The seedlings were incubated for 2 min, and washed twice; subsequently the roots were imaged at the confocal microscope.

Flagellin uptake: 10 uM flg22 was dissolved in liquid medium. 3-day-old etiolated seedlings were treated in it for 0.5 h before imaging the hypocotyl by VAEM microscopy. Flagellin treatment was continuously present during imaging.

3.6.6 Microscopy

Confocal microscopy
PIN2 endocytic rate test: Photo conversion and imaging of photo converted PIN2-Dendra at the PM was done in Zeiss LSM700 vertical confocal microscope using Objective Plan-Apochromat 20x / NA 0.8 Air and PMT/T-PMT detectors. The whole root expressing PIN2-Dendra was photo converted from green to red by a 2min excitation by UV, directed from a source of mercury arc lamp through a DAPI filter. The growing root was tracked for 4 h with the 'Tip Tracker' software and the loss of intensity of the converted red PIN2-Dendra signal was imaged through all roots in 15 min intervals over different planes of the entire Epidermal tissue layer. The microscopic setup was done as described in von Wangenheim et al., 2017. The processing of the time-lapse images is described in the following section.
Imaging of FM4-64 dye and PIN2 co-localisation with ARA7-RFP and in root meristem, and imaging of CLC2-GFP localisation in etiolated hypocotyl were done with LSM700 inverted confocal microscope using Objective Plan-Apochromat 40x / NA 1.3 water and PMT detector.

Root hairs were imaged with Zeiss LSM880 upright confocal/super resolution microscope using Objective Plan-Apochromat 40x / NA 1.2 water and AiryScan super resolution detector. Post processing of the images was done using Fluorescence Correlation Spectroscopy (FCS) software.

TIRF microscopy

Roots of 7-day-old seedlings or hypocotyls of 3-day-old etiolated seedlings were imaged in Olympus IX83 inverted microscope equipped with a Cell^TIRF module and Hamamatsu EM-CCD C9100-13 camera, using OLYMPUS Uapo N 100x/1.49 Oil TIRF objective at an 1.6X magnification. Dual channel imaging was done sequentially with the mentioned time interval.

Time-lapse imaging in hypocotyl was done on the epidermal cells that are closer to the root-hypocotyl junction, after cutting the cotyledon. In certain cases, imaging was done in deeper angles than TIRF angles-VAEM mode (mentioned in the main text). Time-lapse imaging in root was done in the epidermal cells of the transition zone under TIRF mode (Johnson and Vert, 2017b).

Electron Microscopy:

After protoplasts unroofing and metal replica, the samples were imaged in FE-SEM Merlin VP Compact. An accelerating voltage of 0.5 – 5 kV was applied in high vacuum condition and In-lens duo detector was used for detection.

Following the pre-embedding and sectioning of protoplasts, the protoplasts were imaged at an accelerating voltage of 80kV in TEM-Tecnai10 equipped with OSIS Megaview III camera,.

Processing and quantification

CCSs population analysis:

The classification of the CCSs were done manually by observation and counted for the Histogram analysis. The final plot was done using R.

Quantification of endocytotic foci:

The time lapse images of machinery marker lines to follow the dynamics of endocytic foci were processed with cmeAnalysis particle tracking software published in (Aguet et al., 2013) using Matlab. For specific parameters set in the software refer (Johnson and Vert, 2017a). An ROI was drawn and the trajectories were made for each endocytic focus. For density calculations a ROI of dimensions 10umx10um was drawn and an average density over 100 frames were obtained per root. Trajectories that are shorter than 3s were filtered out for analysis.

The developmental profile of the endocytic foci marked by CLC2-GFP was processed as described in (Loerke et al., 2009). Duration of the developmental phases: Assembly, Maturation and scission/release - were characterized based on the average change of intensity of the several trajectories over time. All the trajectories obtained in a root were further filtered to select only the trajectories corresponding to the average lifetime of each root (which generally varies between 18s-24 s). Then the average CLC2-GFP intensity varying over the considered lifetime was plotted with all their departure time point converging to 0 s. The average Intensity values of CLC2-GFP measured over time in each root were normalised before plotting the intensity profile. The points were connected with a smoothening lowess cuve and the phase transition was marked at the closest the point when the slope of the lowess drops 50% below the minimum slope. Post processing and the final plots were made in graphpadPRISM6.

PIN2 endocytic rate test:
The time series images made were further processed using FIJI ImageJ version2.0.0-rc-67/1.52c. Maximum intensity projection of the different planes of epidermal PIN2 signal was obtained. ROI covering majority of the meristem was drawn. Mean intensity of photo-converted PIN2 signal was measured over time with multimeasure option. Statistical testes were done in R as discussed below. The final plot was made by graphpadPRISM6.

Velocity profile by organelle tracking:
The time-lapse movies made on the movement of Golgi apparatus were processed using the plugin Trackmate in FIJI ImageJ version2.0.0-rc-67/1.52c. LoG detector was used to apply Laplacian of Gaussian filter to the images with an estimated blob diameter if 1um and a threshold of 20. Automatic filter was set on. A simple LAP tracker was selected to track with the following parameters: Linking max distance – 3um; Gap closing max distance – 3um; Gap closing max frame gap – 2. Tracks were profiled according to the maximum velocity exhibited by the organelle.
Post processing, the final plots were made in graphpadPRISM6.

Statistical analysis
Statistical analysis on the data for endocytotic density, lifetime and CCP developmental progression were done using PRISM graphpad6.

Statistical analyses for PIN2 internalisation rate between treatments were carried out using R version 1.1.383. The logistic regression analyses were performed by building Generalised linear mixed models (GLMM). The modeling package lme4 was used for it. The significance of the parameter was tested by comparing to reduced models by likelihood ratio test. The models were further tested for the wellness of the fit by BIC and AIC test of deviance (Bolker et al., 2009). The model assumptions were checked by 1) testing for equal variance of the residuals 2) testing for normality of the residuals and 3) testing the normality of the random effects.

The number of samples and the repetitions of each experiment are all described in the respective figure main text and legends.

3.7 Supplementary Information

Supplementary figure S1
Supplementary figure S2
Supplementary table 1

Supplementary movie 1: **Dynamics of CCVs after actin** p**erturbation**. **Related to: Figure 2.**
The movie shows dynamics of CCVs and actin in in hypocotyl epidermal cells. The marker line *p35S::ABD2-GFP* x *p35S::CLC2-mKO* was imaged in TIRF mode. After prolonged treatment with Jasp – 5 uM for 1 h, actin no more forms filaments; and instead reaches the spiky state. Movie shows the CCVs still forming and getting removed after the treatment comparable to the mock condition. Time interval between the frames is 500 ms. Time label is in seconds. Scale bars: 5 um.

Supplementary movie 2: Actin mediated dynamics of the EE/TGN system.

Actin and the EE/TGN were imaged sequentially in VAEM mode in hypocotyl epidermal cells. *p35S::ABD2-GFP* x *p35S::CLC2-mKO* marker line was used. The EE/TGN marked by CLC2-mKO (bigger structures) could be observed to be constantly moving along the actin filaments marked by ABD2-GFP. Time interval between the frames is 50 0ms. Time label is in seconds. Scale bar: 2 um.

Supplementary movie 3: **Dynamics of the Golgi- EE/TGN after actin perturbation. Related to: Figure 3**
Golgi apparatus and the EE/TGN compartment were imaged sequentially in *p35S::ST-RFP* x *pCLC2*::*CLC2-GFP* marker line in VAEM mode in hypocotyl epidermal cells. ST-RFP marks Golgi apparatus in red and CLC2-GFP marks the EE/TGN in green (bigger structures). After LatB treatment (10 um; 1 h), the dynamicity of Golgi together with the EE/TGN is lost and their resultant aggregation in inter-vacuolar space could be clearly observed. Time interval between the frames is 330 ms. Time label is in seconds. Scale bar: 5 um.

Supplementary movie 4: EE/TGN moving along actin collecting an endocytosed CCV.
Dynamics of actin and EE/TGN was imaged sequentially in the hypocotyl epidermal cells in VAEM mode. *p35S::ABD2-GFP* x *p35S::CLC2-mKO* line marks actin in green, and both CCSs (smaller dots) and EE/TGN (bigger structure) in orange. The CCV (arrowed) is collected by the EE/TGN (boxed) moving along the actin filament – marked by ABD2-GFP. Time interval between the frames is 500 ms. Time label is in seconds. Scale bar: 1.5 um.

Supplementary movie 5: Aggregation of endocytosed CCVs at the EE/TGN. Related to: Figure 4.
Dynamics of Golgi with the EE/TGN compartment and the CCVs were followed in hypocotyl epidermal cells. The marker line *p35S::ST-RFP* x *pCLC2*::*CLC2-GFP* was imaged sequentially in VAEM mode. ST-RFP marks Golgi apparatus in red, and both EE/TGN (bigger structures) and the CCSs (smaller dots) in green. Aggregation of the endocytosed CCVs (marked by arrows) on the trans-side of the Golgi could be observed as the Golgi is moved along the cortical surface. Time interval between the frames is 1890 ms. Time label is in seconds.
Scale bar: 2 um.

Supplementary movie 6: CCV fusion to a stationary EE/TGN. Related to: Figure 4.
p35S::CLC2-mKO marker line was imaged sequentially in VAEM mode in hypocotyl epidermal cells. It marks both the EE/TGN (bigger structures) compartment and the CCSs (smaller dots). The movie shows CCVs being collected into neighboring EE/TGN compartments (arrows) that are stationary. Time interval between the frames is 500 ms. Time label is in seconds. Scale bar: 1 um.

Supplementary movie 7: Removal of CCVs by actin.
The movie shows dynamic actin subsidiary filaments and the CCSs in hypocotyl epidermal cells. *p35S::ABD2-GFP* x *p35S::CLC2-mKO* line that marks actin in green and CCSs in orange, was imaged sequentially in TIRF mode. The spatial and temporal correlation between appearance of actin subsidiary filaments and the disappearance of CCVs could be seen. Time interval between the frames is 500 ms. Time label is in seconds. Scale bar: 1 um.

Supplementary movie 8: Uncoating process of a fully developed CCV. **Related to: Figure 5**.
pLAT52::TPLATE-GFP x *pRPS5A::CLC2-RFP* was imaged sequentially in VAEM mode in hypocotyl epidermal cells. The movie shows the fully developed CCV moving away from the PM after scission. The signal of TPLATE adaptors is lost before that of clathrin coat proteins. Time interval between the frames is 500 ms. Time label is in seconds. Scale bar: 1 um.

Supplementary movie 9: Uncoating process as the CCVs reach the EE/TGN. **Related to: Figure 5**.
pLAT52::TPLATE-GFP x *pRPS5A::CLC2-RFP* was imaged sequentially in VAEM mode in hypocotyl epidermal cells. CLC2 marks both the endocytic foci (smaller dots) and the EE/TGN (bigger structure), whereas TPLATE marks only the endocytic foci. The movie shows fully developed CCVs (marked by arrows) reaching the stationary EE/TGN. The signal of TPLATE adaptors is lost at the EE/TGN compartment. The status of clathrin coat proteins is inconclusive due to the signal from the EE/TGN. Time interval between the frames is 500 ms. Time label is in seconds. Scale bar: 1 um.

Supplementary movie 10: Uncoating process as the EE/TGN collects the CCVs.
pLAT52::TPLATE-GFP x *pRPS5A::CLC2-RFP* was imaged sequentially in VAEM mode in hypocotyl epidermal cells. CLC2-RFP marks both the endocytic foci (smaller dots) and the EE/TGN (bigger structure), whereas TPLATE-GFP marks only the endocytic foci. The movie shows a moving EE/TGN compartment collecting two fully developed

CCVs (boxed). The signal of TPLATE adaptors is lost at the EE/TGN compartment. The status of clathrin coat proteins is inconclusive due to the signal from the EE/TGN. Time interval between the frames is 500 ms. Time label is in seconds. Scale bar: 1 um.

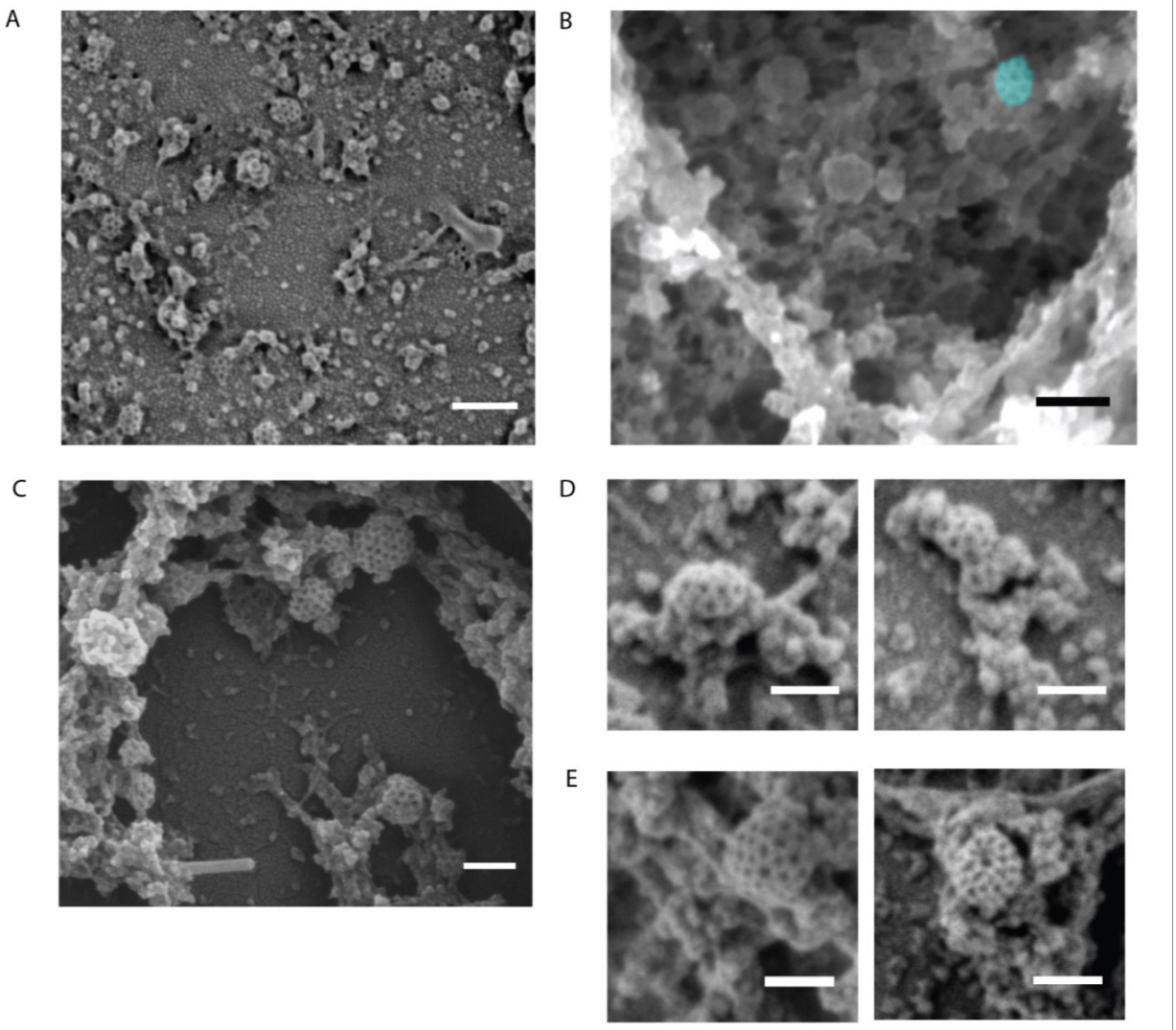

Figure S1. Related to: Figure 1

Refer to: Different populations of clathrin-coated structures found at the Plasma membrane and Endo membranes.

A) CCPs of different population types in varying stages of development at the plasma membrane. Scale bar: 200 nm

B) CCSs found deeper inside the cell is shown in blue.

C) CCPs of distinct population types aggregated at the endo-membrane structure.

D) and E) Arrangement of the CCSs in endomembrane structures. E) Isolated CCSs of huge basket type and F) Multiple-fused CCSs are shown. Scale bars of BCDE are 100 nm

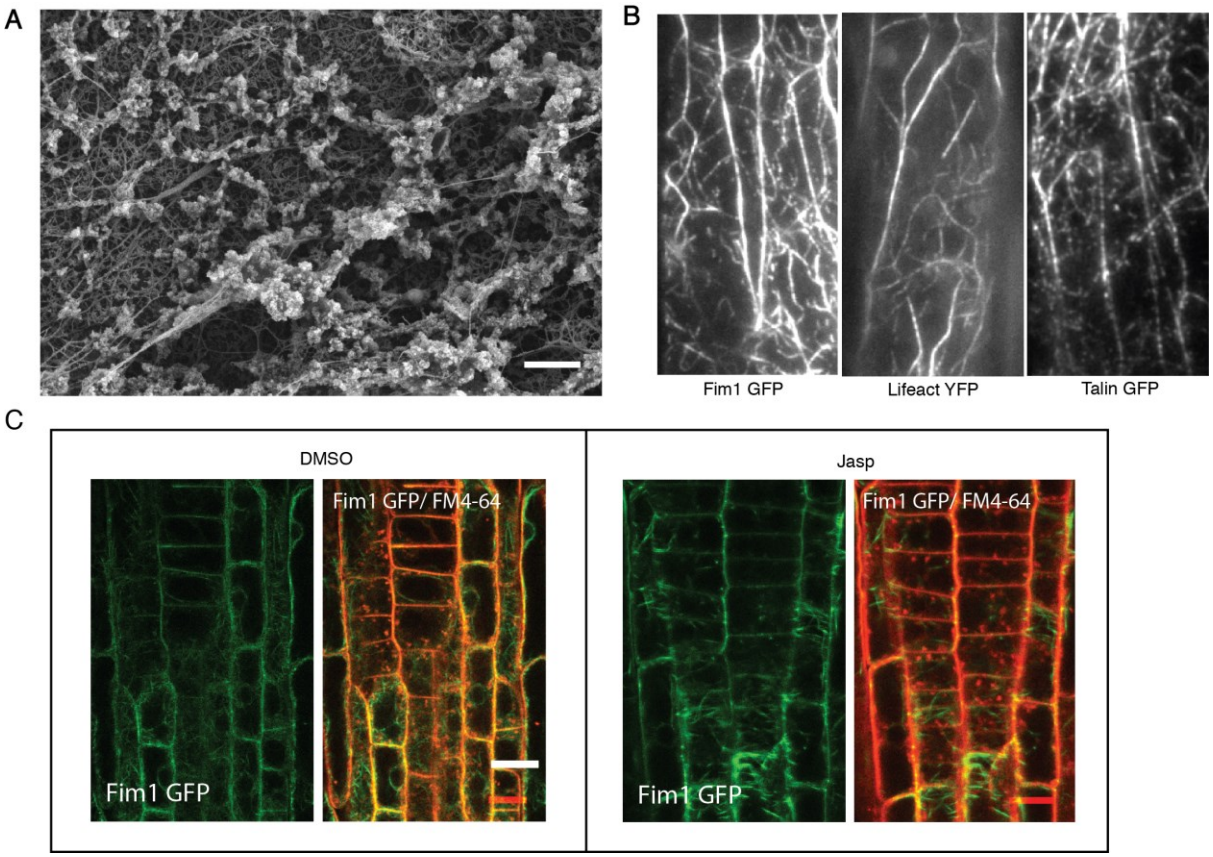

Figure S2. Related to: Figure 2

Refer to: Cortical actin forms main and subsidiary filaments but not thick polymerised focus at the endocytic spot and

Actin is not mandatory for CCV formation thus the endocytotic process remains uninhibited on actin perturbation

A) Ultra structural analysis of actin cytoskeletal network in unroofed protoplasts deeper inside the cell. Cytoskeletal and endo-membranous structures tightly linked along with other cellular components. Scale bar: 0.5 um

B) TIRF image of Hypocotyl epidermal cell. Different marker lines – *p35S::Fim1-GFP*, *35S::Lifeact-YFP* and *35S::mTalin-GFP* - mark the main and subsidiary filaments of cortical actin network. Lack of actin foci is consistent with different actin markers.

C) Internalisation of FM4-64 in root meristem of *Fim1-GFP* line after 5 uM Jasp treatment for 60 min and the mock- DMSO condition; 8 seedlings per condition. Note that the actin is no more filamentous and is spiky after Jasp; FM4-64 dye still gets internalised. The composite of channels is shown. Scale bars: 10 um.

Supplementary table 1:

Effect of LatB (10 uM) and Jasp (500 nM) on CME machinery proteins – CLC2, TPLATE and DRP1C - root and hypocotyl epidermal cells. Roots were treated for 15 min; hypocotyl for 1 h. Unpaired two-sided T tests were performed.

Hypocotyl cells after LatB:

TPLATE-GFP			
	Mean lifetime (s)	Mean density (/100 sq. um)	N cells, # tracks
Mock	9.886 +/- 0.7763	105.9 +/- 16.08	4 cells, 13308 tracks
LatB	9.648 +/- 1.318	93.57 +/- 12.70	4 cells, 15062 tracks
Significance	ns	ns	

DRP1C-GFP			
	Mean lifetime (s)	Mean density (/100 sq. um)	N cells, # tracks
Mock	16.74 +/- 0.6432	84.08 +/- 11.81	3 cells, 11004 tracks
LatB	14.58 +/- 1.571	76.08 +/- 6.843	4 cells, 14654
Significance	ns	ns	

Hypocotyl cells after Jasplakinolide:

TPLATE-GFP			
	Mean lifetime (s)	Mean density (/100 sq. um)	N cells, # tracks
Mock	9.89 +/- 0.7763	105.9 +/- 16.08	4 cells, 13308 tracks
Jasp	10.45 +/- 0.8326	106.6 +/- 12.14	3 cells, 8688 tracks
Significance	ns	ns	

CLC2-GFP			
	Mean lifetime (s)	Mean density (/100 sq. um)	N cells, # tracks
Mock	9.71 +/- 0.7643	67.90 +/- 12.60	4 cells, 8986 tracks

Jasp	9.79 +/- 0.5736	75.86 +/- 11.79	4 cells, 11828 tracks
Significance	ns	ns	

DRP1C-GFP			
	Mean lifetime (s)	Mean density (/100 sq. um)	N cells, # tracks
Mock	12.87 +/- 0.2628	72.57 +/- 4.777	3 cells, 23998 tracks
Jasp	11.96 +/- 0.2449	97.95 +/- 5.144	5 cells, 22303 tracks
Significance	*	***	

Root cells after Jasplakinolide:

TPLATE-GFP			
	Mean lifetime (s)	Mean density (/100 sq. um)	N cells, # tracks
Mock	24.07 +/- 2.694	101.3 +/- 7.479	3 cells, 16675 tracks
Jasp	25.07 +/- 3.876	100.9 +/- 20.68	4 cells, 22388 tracks
Significance	ns	ns	

CLC2-GFP			
	Mean lifetime (s)	Mean density (/100 sq. um)	N cells, # tracks
Mock	21.85 +/- 2.177	92.34 +/- 11.10	6 cells, 39784 tracks
Jasp	24.78 +/- 2.429	86.19 +/- 9.630	5 cells, 31232 tracks
Significance	ns	ns	

DRP1C-GFP			
	Mean lifetime (s)	Mean density (/100 sq. um)	N cells, # tracks
Mock	27.53 +/- 2.649	68.81 +/- 10.99	3 cells, 11613 tracks

Jasp	24.82 +/- 0.9795	46.35 +/- 11.60	4 cells, 14448 tracks
Significance	ns	ns	

3.8 External contributions

TIRF imaging on roots and post-processing of all the data on CME machinery dynamics using cmeAnalysis was done by Alexander Johnson. He also performed the endosomal pick-up analysis using the same.
Walter Kaufmann optimized the protocol for metal replica of protoplasts; and he also did the pre-embedding and TEM analysis.
I would also like to thank Roshan Prizak and Maciek Adamowski for valuable discussions, Matous Glanc and HJ Li for the lines, Vanessa Zheden and Daniel Gutl for the technical support, Barbara Casillas and Lenka Matejovicova for her help with statistics.

4 On deciphering the role of auxin on endocytotic regulation

4.1 Introduction

After the biogenesis, the plant hormone, auxin is directionally transported across tissues, which is termed as Polar Auxin Transport (PAT). This is crucial to for effective spatial and temporal developmental signaling. For efficient PAT in the system, both importers and exporters of auxin in the cell –namely Aux1 and PIN-FORMED proteins or PINs - should be functional at the plasma membrane (PM). Importantly, the polarity of PINs at the PM is essential in determining the direction of auxin flow (Petrasek and Friml, 2009), ensuring streamlined PAT. Therefore, studying the maintenance of polarity of the transporters is relevant in understanding auxin-mediated developmental processes.

Several processes, such as, clustering and limited lateral diffusion are vital for retaining the strict apical/basal polarity of PINs with limited lateral diffusion. In addition, constitutive endocytosis and recycling of PINs are also important. This was shown by expressing a mutant variant of PIN2, namely $PIN2^{Y505A}$-YFP, which has the cargo recognition site for endocytosis mutated. Excessive lateral polarization of PIN2 was observed in such a mutant (Kleine-Vehn et al., 2011). Biochemically, PIN phosphorylation and dephosphorylation switches are essential in polarity maintenance. AGC kinases – PID and WAGs directly phosphorylate PINs at the serine residues. *pid* and *wag* multiple mutants have excessive basal PINs and the over-expressors possess a definitive basal to apical polarity switch; and such changes result in several defective physiological phenotypes. Protein phosphatase (PP2A), which dephosphorylates PID, has been reported play a role in PIN1 polarity. Mutants – *pp2aa1 pp2aa2* and *pp2aa1 pp2aa3* possess a basal to apical polarity switch of PIN1 and apolar PIN2 (Barbosa et al., 2018). Thus, PIN polarity is regulated at multiple levels.

One of the important physiological relevance of polarly transporting auxin is maintaining its differential distribution across cell files. This is important for responses, such as, halotropism, gravitropism and phototropism. Studies show that, for such a differential distribution to occur, PINs and AUX1 should work in consort to produce asymmetric flow of auxin (Galvan-Ampudia et al., 2013; Laxmi et al., 2008; Petrasek and Friml, 2009). Studies have shown that auxin could generally inhibit endocytosis through auxin Binding Protein 1 (ABP1); thus could impose PIN stability at the plasma membrane (PM) (Robert et al., 2010). The asymmetric distribution of auxin is maintained by stabilized PIN2 at the side tending to high auxin accumulation. This has been observed under gravistimulation and salt stress (Abas et al., 2006; Baster et al., 2013; Galvan-ampudia et al., 2013). Under no external stimulus, after prolonged exposure to auxin, loss of PM PINs and subsequent vacuolar trafficking was shown clearly by Baster et al., 2013. In addition, auxin molecules also possess regulatory control over the distribution of PINs. ARF1- AUX/IAA mediated polar targeting of PINs to the outer lateral sides from the basal/apical sides was demonstrated after long-term auxin application (Sauer et al., 2006)

Based on all these studies, it is clear that auxin mediation of polarity of its own exporters is an important aspect of PAT. The complicated part is that auxin imparts two opposite effects on PINs: over long term (>3 h), auxin causes loss of PINs and other cargo proteins from PM; under short-term (<2 h), auxin results in stabilization of PINs at the PM, which is likely due to its ability to inhibit endocytosis. This time-dependent property had been observed by

various different experiments over the decade using different auxin isoforms - mainly 1-Naphthaleneaceticacid (1-NAA or simply, NAA). Some of the notable observations are the following. After 2 h of NAA treatment (5 – 10 uM), in the presence of Brefeldin-A (BFA), less amount of cargo proteins were found accumulated in the BFA body, implying a decrease in the rate of endocytosis. In the same line of evidence, after 30 min of treatment with NAA (10uM), there was less FM4-64 stained membrane in the EE/TGN (Paciorek et al., 2005; Robert et al., 2010). Interestingly, after 3 h of NAA (20uM) treatment, western blot analysis of the microsomal PIN2 fraction revealed a considerable decrease, meaning a loss PIN2 from the membrane (Baster et al., 2013). This was attributed as long-term effect of auxin – where after 3 h of NAA treatment, PIN1 and PIN2 are lost from the PM, whereas until 2 h (short-term), PIN1 and PIN2 are stabilized at the PM.

But interestingly, Abas et al., observed a decrease in the microsomal fraction of PIN2 in earlier times, such as, 2 h of NAA treatment (10uM). This contradicts the results obtained from BFA based experiment that showed inhibition of endocytosis of PIN1 and PIN2 (Abas et al., 2006; Paciorek et al., 2005; Robert et al., 2010). Jasik et al, recently claimed that after NAA application, there are defects in BFA body formation (Jásik et al., 2016). These observations question the regulatory role of auxin upon overall endocytosis, and also particularly of endocytosis of PINs. Also, it is now essential to check if BFA as a tool could be used to test auxin and its effects.

In order to clarify the regulatory controls of auxin on clathrin-mediated endocytosis (CME), we decided to resolve the tools that were being used for endocytosis studies. We primarily used the natural form of auxin, Indole-3-acetic acid (IAA), in our experiments; and for a better comparison, we further used NAA, which has been widely utilised in several key studies, so far. In the presence of high concentrations of either of the isoforms of auxin, we could clearly observe problems in the BFA induced aggregation of endosomes. Moreover, only NAA, and not IAA, interferes with the amount of membrane internalised (FM4-64 stained membrane flow to the Early endosome/Trans-Golgi Network or EE/TGN). But NAA also affects the EE/TGN system in general. Both the isoforms accelerate internalisation of PIN2 even after 5 min of treatment, but not of PIN1 or other membrane proteins. Both the basal constitutive internalisation and accelerated auxin-mediated internalisation of PIN2 occur via CME pathway. However, on a short term, NAA has no influence on the CME machinery proteins at the PM. Hindrance of CME results in altered PIN polarity. This leads to a possible role for auxin in mediating fast polarity changes of PIN2 in a clathrin-mediated way without influencing the overall endocytotic rate of the cell. This direction needs to be further explored in the future.

4.2 Results

4.2.1 Both NAA and IAA interferes with the endosomal aggregation response to Brefeldin-A

The toxin BFA has been used as an important tool so far to check endocytosis by aggregating the endosomes and quantifying the total amount of endocytosed cargo in the aggregate, termed as the BFA body. This is a useful method to analyse endocytic potential of the cell. Recently, based on the visualization of the cargo PIN2 in BFA bodies, Jasik et al., has claimed

that BFA body formation is defective in the presence of NAA (Jasik et al.,2016). This claim questions all the inferences derived so far, that had been based on endocytosis and trafficking of cargoes in BFA bodies. Therefore BFA as tool needs to be thoroughly tested for auxin studies. BFA bodies are aggregations of Golgi apparati, late and early endosomes and the TGN containing cargoes; and it is not enough to merely look at the cargo protein to make a claim about the entire BFA body. We decided to test their claim by visualizing the effect of BFA on the amount of endosomes aggregating after BFA treatment and the subsequent quantification of PIN2 cargo accumulated in the BFA body.

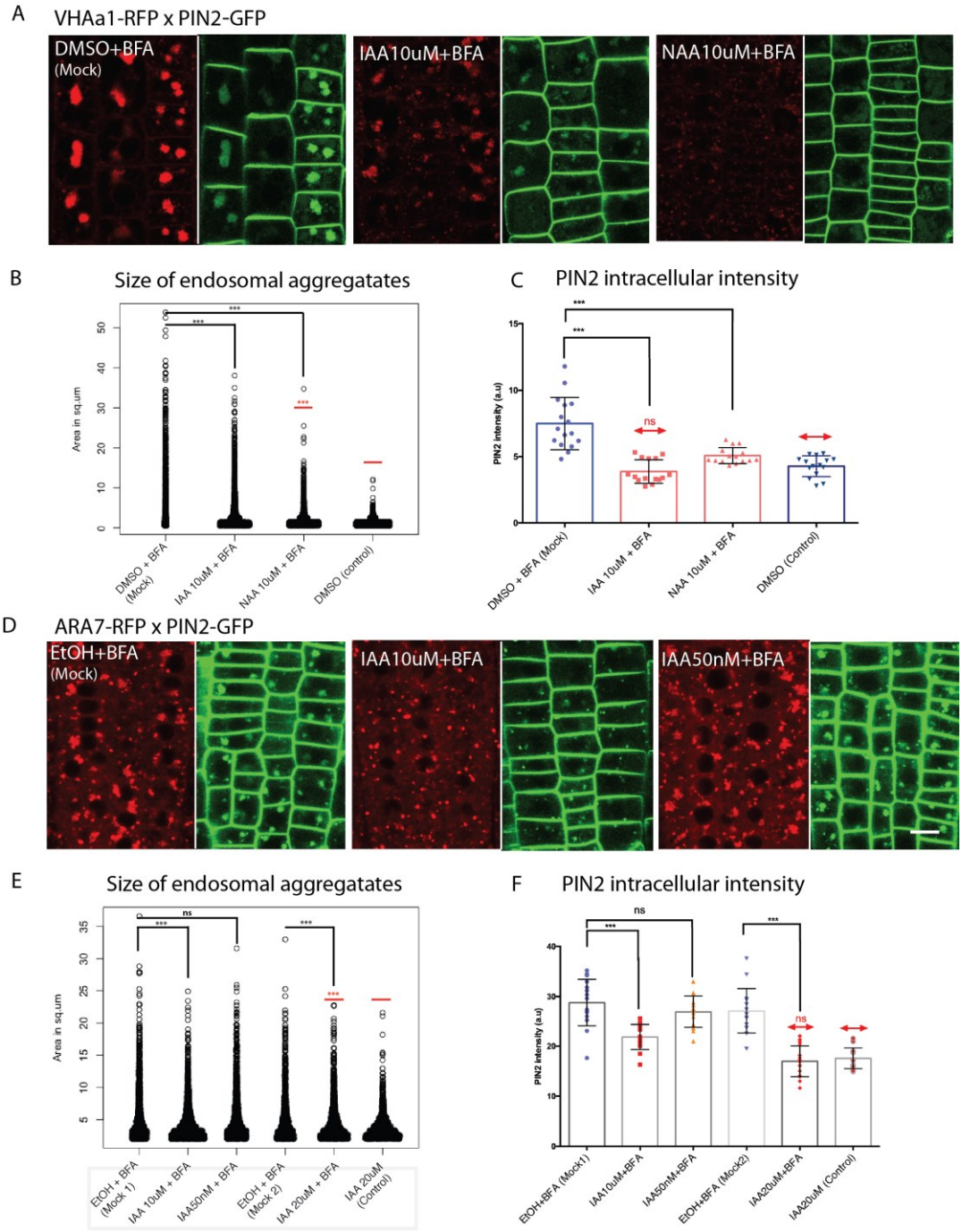

Figure 1: Effect of NAA and IAA on the endosomal aggregation response to BFA
A-F) Live-imaging of BFA body formation in the presence of auxin by confocal microcopy. One could observe an increase in number smaller aggregates in the presence of NAA and IAA with a corresponding decrease in PIN2

intensity **A) BFA body formation**. Imaging of the line *VHA-a1::VHA-a1-RFP x pPIN2::PIN2-GFP* ; 30 min pre-treatment with DMSO (as mock), IAA10uM or NAA10uM, followed by 60 min co-treatment with BFA 37.5 uM; corresponding BFA aggregate size and cargo PIN2 intensity measurements could be seen in B and C respectively. One could observe an increase in number smaller aggregates in the presence of NAA and IAA with a corresponding decrease in PIN2 intensity **B) Endosomal aggregation size.** The Sina plot represents the size of the BFA aggregates in sq.um, formed by VHA-a1-RFP marked EE/TGN structures. Each point is a measurement of an aggregate. 5 roots in each condition and all the epidermal cells in the meristematic zone were measured. A total of 858, 2064, 2220 and 2550 measurements were made for each condition in the order represented. One-sided Mann-Whitney U test were performed. EtOH+BFA (mock)>IAA10uM+BFA p-value<2.2e-16; DMSO+BFA(Mock)>NAA10uM+BFA p-value = 4.34e-15; NAA10uM+BFA>DMSO (Mock) p-value<2.2e-16; Mock>IAA 50nM p-value=0.001282; IAA 20uM+BFA>IAA20uM;p-value = 0.1996. **C) PIN2 visualisation in the aggregate**. The scatter dot plot represents the intracellular intensity of PIN2-GFP in the aggregates. Each dot represents the average value from each root. The bars represent mean with SD. 15 cells per root; 5 roots in each condition; one-sided t test was performed. Mock > IAA10uM+BFA with welch correction for difference of variance p<0.0001; DMSO+BFA > NAA10uM with welch correction for difference of variance p<0.0001; IAA 10uM+BFA > DMSO (Control) p=0.1. **D) BFA body formation.** Imaging of the line *ARA7-RFP x PIN2GFP*; 30 min pre-treatment with Ethanol (control), IAA 10 uM, 20 uM and 50 nM followed by 30 min co-treatment with BFA 50 uM. Throughout the experiment, seedlings were treated with 50 uM CHX. **E) Endosomal aggregation size.** The Sina plot represents the size of the BFA aggregates in sq.um, formed by ARA7-RFP marked LE. 6 roots were used and all the epidermal cells in the meristem were considered. A total of 1122,1552,1397,1048,1197 and1229 measurements were made. One-sided Mann-Whitney U test was performed. EtOH+BFA (Mock)>IAA 10uM+BFA p-value=3.789e-09; EtOH+BFA (mock)>IAA 20uM+BFA p-value = 0.000241; EtOH+BFA (Mock)>IAA 50nM+BFA p-value = 0.2; IAA 20 um<IAA20uM+BFA p-value = 0.001. **F) PIN2 visualisation in the aggregate.** The scatter dot plot represents the intracellular intensity of PIN2-GFP the aggregates. Each dot represents the average value from each root. The bars represent mean with SD. 15 cells per root; at least 6 roots were used. One-sided t test was performed. EtOH (Control) > IAA 20uM+BFA p<0.0001; EtOH (Control) > IAA10uM+BFA with welch correction for difference in variance p<0.0001; IAA20uM > IAA20uM+BFA p=0.26; EtOH+BFA (Mock)>IAA 50 nM+BFA p=0.11. Scale bar: 10 um.

We tested the effects of the both NAA and IAA. Varying concentrations of NAA – 10 uM, 20 uM, and IAA – 50 nM, 10 uM were used to pretreat and further co-treat the seedlings along with BFA. Using the line *VHA-a1*::*VHA-a1-RFP x pPIN2::PIN2-GFP* (EE/TGN visualized together with the cargo protein, PIN2), we observed the aggregating potential of the endosomes and followed the concomitant visualization of the cargoes – see figure 1A-C. The mock condition (with DMSO/EtOH + BFA) had prominent BFA body consisting of a wholesome endosomal aggregation (see VHA-a1 based endosomal aggregation) and corresponding PIN2 cargo visualized within the endosomes. However, after both NAA and IAA 10uM, there was a substantial decrease in the amount of endosomes aggregated, hence a smaller BFA body and correlatively a diminished PIN2 signal emanating form the disaggregated BFA body. The sina plot shows the aggregate size distribution. With higher concentrations of auxin, there is a drastic increase in the smaller bodies of around 3 um2 area - owing to an increase in partially aggregated and disaggregated individual endosomes (Figure 1B and C). This shows that less aggregated the endosomes are in the BFA body, less intense the cargo signal is - primarily due to diffusion of the signal intensity.

The observation was further confirmed by a subsequent experiment with cyclohexamide (CHX) treatment. Under the influence of 10 uM CHX, majorly the PIN2 internalised from the PM and only to a lesser extent the newly synthesized PIN2 gets accumulated in the BFA body. Also PIN2 could be clearly observed to be localised in the ARA7 labeled endosomal structures – see figure S1A. Therefore, using the marker line *ARA7-RFP* x *PIN2-GFP*, we observed the aggregated ARA7 endosomes in the BFA body together with the PIN2 signal in it. We clearly saw a concentration dependent effect of IAA on the endosomal aggregation –

see figure 1D-F. At a higher concentration of IAA – 10 uM, very less number of LE were a part of the BFA body; basically the BFA body size was smaller; concomitantly less PIN2 cargo was observed. However at lower concentration – 50nM, the BFA body remained unaffected with most of the LE aggregating to form BFA bodies (Figure 2E, F). Golgi Apparati are organelles that each cell acquires and their numbers cannot be affected as in the case of EE/TGN. Moreover, they aggregate tightly around the endosomes to form a BFA body (Paciorek et al., 2005); so we tested their aggregation potential after NAA. In the presence of NAA 20 uM, one could clearly observe loosely arranged and disarrayed Golgi apparati (marked by ST-YFP); the ARF1 immuno-labeled and CLC2-GFP marked EE/TGN structures behaved the same way as well. Concomitantly, there was very low PIN2 signal in such disaggregated BFA bodies (Figure S1 B,C). These observations show that disaggregated and smaller BFA bodies correspondingly project lower PIN2 signal intensity. Thus NAA and IAA do not directly regulate the localisation/trafficking of PIN2 and other cargoes; they interfere with the BFA body formation leading to an indirect artifact of lower and diffused cargo signal intensity.

The observations clearly show that both NAA and IAA interfere with the aggregation property of the endosomes, as signified by Jasik et al., 2016. However, it is still not clear how such an effect is being mediated by auxin. Nevertheless, improper formation of BFA bodies in the presence of high concentrations of NAA and IAA disregards BFA as a tool to quantify cargoes within the BFA body; this is because cargo proteins could still be present in the endosomes but they will not be visualised effectively due to disaggregated BFA body. Since reduced cargo signal is merely an artifact of disaggregated BFA body, we need to reevaluate the effect of auxin on endocytosis using different set of tools.

4.2.2 NAA, not IAA affects the EE/TGN system

As it is clear that endocytosis effect of auxin cannot be tested using BFA treatment, we decided to quantify membrane internalisation, as an alternate tool after NAA and IAA treatments. Series of concentrations of auxin was applied; and the flow of FM4-64 stained membrane to the EE was quantified (cytosolic signal intensity) after 30 min of auxin treatment in the epidermal cells of root meristem – see figure 2A-C, figure S2A. From 10uM concentration of NAA on, the effect was significant; and we could detect obvious decrease in internalised FM4-64 signal at the EE/TGN (Figure 2A,C). The signal gets weaker as the concentration of NAA increases (Figure S2A). At 100 uM, there is almost no cytosolic signal (Figure 1A). It is interesting to note that IAA, which is a far powerful molecule and can produce physiological effects at 10nM concentration (Fendrych et al., 2018), had no effect on the amount of FM4-64 internalised even at 10 uM and 100 uM concentrations. FM4-64 stained membrane reaches the EE/TGN with no obvious defects (Figure 2B,C).

To understand the differential effects between IAA and NAA, one needs to contemplate the features of FM4-64 internalisation experiment. Less FM4-64 staining of the EE/TGN after NAA could be attributed to 1) less endocytosis 2) defective trafficking of endocytosed vesicles to EE/TGN or 3) affected EE/TGN. In the cases 2) and 3) were true, it is unwise to use FM4-64 as a tool to study endocytosis. We tested if there are trafficking defects in general, owing to the described effects of NAA on actin (Rahman et al., 2007). If there were trafficking defects, vesicles and endosomes would move less effectively; thus less FM4-64 dye would reach the EE/TGN system. However, there was no obvious trafficking defect

detected after NAA application. The general trafficking of ARA7 marked endosomes in the epidermal cells after 20 uM NAA treatment for 60 min was comparable to control condition – see supplementary video 1.

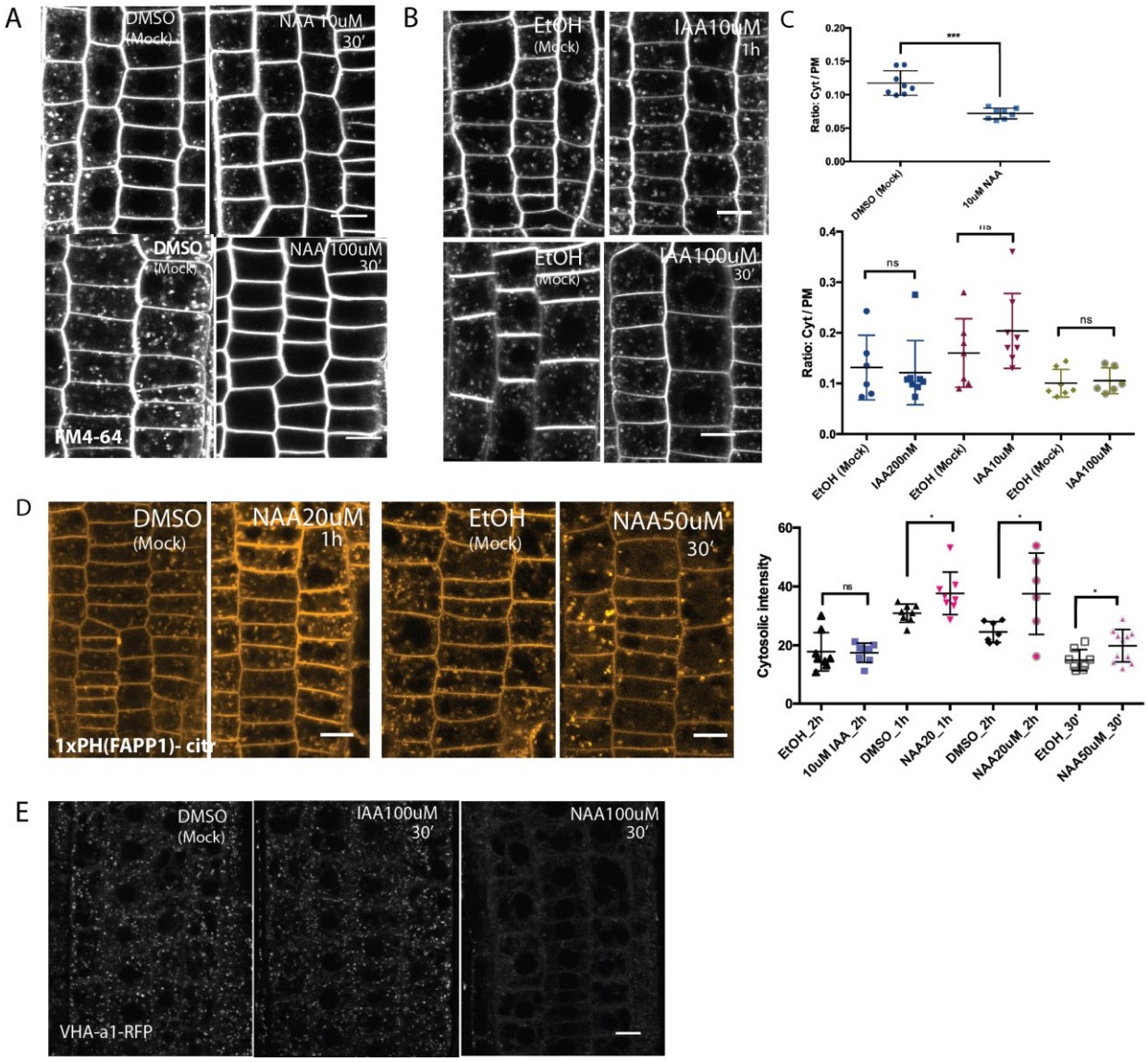

Figure 2: Effects of NAA and IAA on the EE/TGN

A-C) Live imaging by confocal microscopy and quantification of FM4-64 stained membrane at the EE/TGN structures after IAA and NAA treatments **A) FM4-64 staining after NAA.** Roots after treatment for 30 min with 10 uM NAA (top) and 100 uM NAA (bottom) and mock DMSO. Note that there is a decrease in the amount of FM4-64 signal at the EE/TGN already after 10uM NAA. After 100uM NAA treatment there is very little signal. The effects of other concentrations of NAA are shown in supplementary fig S2A. **B) FM4-64 staining after IAA.** Roots after treatment with 200 nM IAA for 1 h (not shown), 10 uM IAA for 1 h (top) and 100 uM IAA for 30 min (bottom) and mock Ethanol. There is no difference in the amount of FM4-64 signal in the EE/TGN after treatment. **C)** Quantification of the amount of FM4-64 signal in the EE/TGN from the experiments described in A and B. Ratio between the mean cytosolic intensity to the mean PM intensity was made in at least 10 cells per root; 10 roots per condition. At the top, quantification of NAA treated roots is shown in scatter dot plot. Each dot represents the average value from each root. The bars represent mean with SD. Two-sided t test was performed $p<0.0001$. At the bottom, quantification of IAA treated roots is shown in scatter dot plot. Each dot represents the average value from each root. The bars represent mean with SD; at least 6 roots each condition; 7 - 10 cells per root; non-parametric Mann-Whitney U two-sided test was performed for EtOH (mock) vs IAA200nM $p=0.929$; Two-sided T test – EtOH (mock) vs IAA10uM $p=0.25$; EtOH (mock) vs IAA100uM $p=0.74$. **D) Quantification of PIns(4)P at the EE/TGN.** Live imaging of the EE/TGN, marked by Ubq:

FAPP1xCITRINE by confocal microscopy. The effect of 20uM NAA (2h treatment) and 50uM NAA (30 min treatment) on PIns(4)P of the EE/TGN is shown. The scatter dot plot of the mean cytosolic intensity of PIns(4)P after 10uM IAA for 2 h, 20uM NAA after 1 h and 2 h, and 50uM NAA after 30 min are shown. Note that there is increase in amount of PIns(4)P at the EE/TGN after NAA, but not IAA treatment. Each dot is the mean intensity of a single root; 8 roots per condition; 8 cells per root were measured. The bars represent the mean with SD. One sided t tests were performed; EtOH_2h (mock) < 10uM IAA_2h p=0.445; DMSO_1h (mock)< NAA20uM_1h p=0.0183 (after welch's correction); DMSO_2h (mock)<NAA 20uM 1h p=0.0348 (after Welch's correction); EtOH30' (mock) < NAA50uM_30' p=0.02. **E) EE/TGN number and distribution after auxin.** Live imaging of the EE/TGN, marked by VHA-a1-RFP by confocal microscopy. The effect of 100 uM NAA and IAA on the EE/TGN is shown. Note that there is a drastic reduction in the number of the EE/TGN structures after high concentration of NAA treatment. The effect of other lower concentrations of NAA is shown in the supplementary figure S2B. Scale bar: 10 um

Then we tested the effects of NAA on the integrity of the endomembrane system. We tested the effect of varying concentrations of NAA – 20, 50, 100 uM - on the size, distribution and composition of the EE/TGN. We observed that at higher concentration of NAA, there was generally less number of EE/TGN structures in the cell. One could clearly see that the EE/TGN, as marked by VHA-a1-RFP, has significantly decreased in number at 100 uM NAA concentration (Figure 2E), which corresponds to decreased FM4-64 signal. Similar to this, Wang et al previously have observed decreased and affected clathrin signal at the EE/TGN after 2,4 D treatment(Wang et al., 2013a). In contrast, IAA even at high concentration such as 100 uM, does not affect the EE/TGN, which is also reflected by the FM4-64 staining. However at lower concentration of NAA - 10 and 50 uM, there were no obvious changes in the number and distribution of the EE/TGN (Figure S2B).

Phosphatidylinositols are the molecules that confer basic identity to the membrane system; and the membrane composition is important for its efficient functionality (Noack and Jaillais, 2017). Therefore we tested if auxin can cause any significant changes to the phosphatidylinositols in the endomembrane system leading to its defective functionality. It was reported before that NAA could alter the phosphatidylinositol-4-monosphosphate (PIns(4)P) and phosphatidylinositol-4,5-bisphosphate (PIns(4,5)P_2) ratio (Ischebeck et al., 2013). In the same line of evidence, we observed an increase in PIns(4)P levels (marked by the biosensor FAPP1-citrine) in the EE/TGN system after 1-h treatment with 20 uM NAA. Consistently, after 30 min of 50 uM NAA treatment, though the number and distribution of EE/TGN structures –marked by VHA-a1-RFP is comparable to the mock condition (Figure S2B), the amount of PIns(4)P level in them is increased – see figure 2D. However, 10 uM IAA even after 2 h of treatment has no effect on the PIns(4)P levels. This is consistent with FM4-64 staining experiments after NAA and IAA. This shows that following the FM4-64 stained membrane flow to the EE/TGN structures is not advisable at higher NAA concentrations, until we explore further the avenues of phosphotidylinsitols influencing EE formation.

In summary, the lipid identity of the EE/TGN system is altered by NAA and not by IAA. Importantly, the number and distribution of the EE/TGN structures are affected solely by higher concentrations of NAA treatment. This is in concordance with lesser FM4-64 staining in the EE/TGN observed after NAA treatment; however the connection between less membrane flow to the endosomes and the offset ratio of phosophotidylinositols in them is not clear. Nevertheless, one could not discard the option that NAA could directly affect endocytosis machinery causing decreased endocytosis. On the other hand, IAA neither affects the EE/TGN system nor interferes with the FM4-64 stained membrane reaching it.

4.2.3 Auxin accelerates PIN2 internalisation from the PM but does not affect other cargoes

NAA has been shown to inhibit internalisation of membrane and cargoes in several studies before. But most of the results have been interpreted based on FM4-64 staining on the endosomes or upon analyzing the total cargo protein after BFA treatment (Paciorek et al., 2005; Robert et al., 2010). Both these techniques have their drawbacks due to various endomembrane defects accompanying high auxin concentrations as shown above. In order to clarify the internalisation potential of auxin, we tested PIN2 cargo first, as it transports auxin and is closely associated to auxin-mediated physiological processes (Adamowski and Friml, 2015).

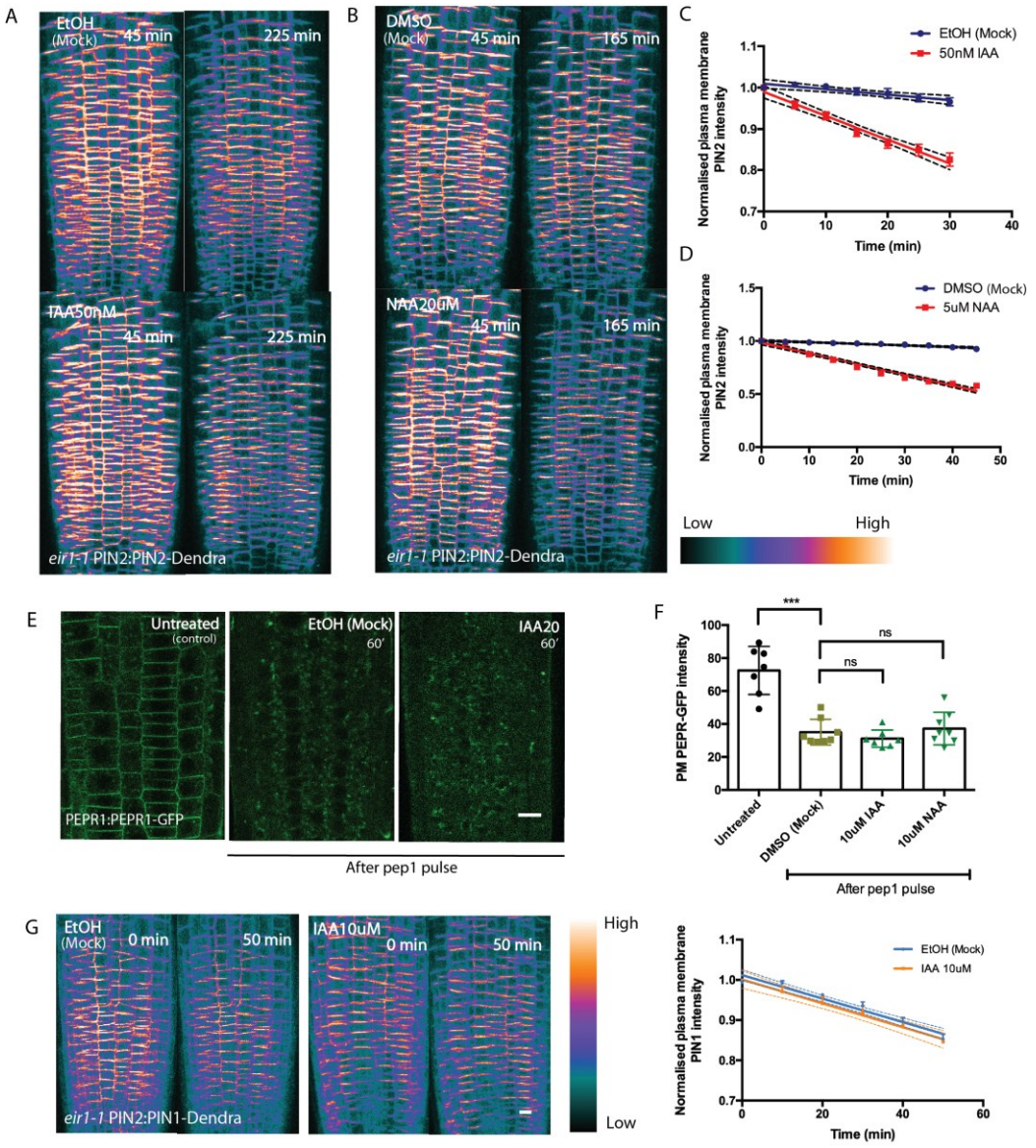

Figure 3: Effect of auxin on internalisation of different cargoes

A –D) **Effect of IAA and NAA on PIN2 internalisation.** Live imaging and quantification of PIN2 at the PM of the root meristem in the photo-converted marker line *eir1-1 pPIN2::PIN2-Dendra* was done by confocal microcopy. Note that PIN2 PM intensity decreases faster over time in the presence of both IAA and NAA compared to mock condition. **A)** Effect of IAA 50 nM was tested on the rate of loss of photo-converted PIN2-Dendra signal from the PM continuously in 15 min intervals after 45 min of application. Regression analysis was performed

by fitting a linear mixed model. 5 roots per condition; all the epidermal cells in the meristem were analysed. The corresponding regression plots could be seen in supplementary figure S3A. And effects of other concentration of IAA – 10uM and 10nm are represented in corresponding regression plots in supplementary figure S3A. **B)** The same was done for 20 uM NAA. And the corresponding regression plot is shown in Supplementary figure S3B together with the effect of 10uM NAA. **C)** Regression plots depicting the PIN2 internalisation rate from the PM. Early effects of IAA 50nM were tested using RootChip - from the time point 0, imaging every 5 min. Regression lines were plotted with the lines depicting 95% CI. 4 roots per condition and all the cells in the meristem were analysed. Regression analysis was performed by fitting a linear mixed model. Slope of PIN2 internalisation rate after IAA treatment is significantly higher than of mock; LMER - random effects for position; χ^2- 69.418; df=1; p=2.2e-16 *** **D)** The same was done for 5 uM NAA. 4 roots per condition and all the cells in the meristem were analysed. Slope of PIN2 internalisation rate after NAA treatment is significantly higher than of mock; LMER - random effects for position; χ^2- 75.878; df=1; p=2.2e-16 *** **E) Effect of auxin on PEPR internalisation**. Roots were pre-treated with 10 uM NAA, 10 uM IAA or DMSO (mock) for 30 min before pep1 treatment (200nM pulse for 1 min) followed by the same post-treatment for 60 min. Internal control is seedlings incubated with DMSO (mock) throughout with no pep1 treatment (Untreated). On the right, the scatter dot plot of the mean PM PEPR intensity is plotted. Each dot represents the mean intensity of a single root. At least 7 seedlings per condition; 20 cells per root. Two-sided Mann-Whitney U test for pep1 pulsed condition: DMSO (mock) vs 10uM IAA p = 0.27; DMSO (mock) vs 10uM NAA p=0.56; One-sided Mann-Whitney U test for Untreated > DMSO (mock), p=0.003. **G) Effect of IAA on PIN1 internalisation.** Live imaging and quantification of PIN1 at the PM of the root meristem in the photo-converted marker line *eir1-1 pPIN2::PIN1-Dendra* was done by confocal microcopy. Note that there is no difference between IAA and EtOH (mock) treatments. Effect of IAA 10 uM was tested on the rate of loss of photo-converted PIN1-Dendra signal from the PM continuously in 10 min interval using Lanchip from time 0 min. Regression analysis was performed by fitting a linear mixed model. On the right, the corresponding regression lines depicting the PIN1 internalisation are plotted and the curves represent 95% CI. At least 5 roots per condition and all the epidermal cells in the meristem were analysed. Slope of PIN2 internalisation rate after 10 uM IAA is equal to that of mock; LMER - random effects for position; χ^2- 0.65; df=1; p=0.42. Scale bar: 10 um.

We used Dendra tagged PIN2 protein and followed the PIN2 signal at the PM of the meristem using confocal microscopy. We photo converted the existing PIN2 in the whole root meristem. After photo-conversion, the newly synthesized PIN2 is not captured in the same imaging channel as the existing PIN2 in the cell. Subsequently, we quantified the loss of PIN2 from the PM continuously, thus obtaining the rate of PIN2 internalisation. The curves signifying the rate of PIN2 loss from the PM could be seen in figure 3. One could observe a clear increase in the rate of PIN2 internalisation from the PM after both NAA and IAA treatments – see figure 3A-D and figure S3A,B. IAA as low as 10 nM and 50 nM could impart a significant increase in PIN2 internalisation rate. Also it is clearly concentration dependent. A concentration of 50 nM is far better at increasing the rate than 10nM (Figure S3A). Other higher concentrations of IAA and NAA have also been tested (Figure S3A,B). We also tested the time scale of the effect. How early can auxin accelerate the internalisation process? We used RootChip technique as means for controlled drug application thereby capturing the early effects of IAA on PIN2 – see figure 3C,D. As early as 5 min after application of both IAA and NAA, one could observe loss of PIN2 from the membrane. However we haven't tested the time points earlier than that.

As we have established that PIN2 internalisation is increased by auxin, we still need to check other auxin-unrelated cargoes, in order to establish an overall internalisation potential of auxin. We tested the clathrin-mediated endocytic rate of PM associated PEPR protein, which is involved in immune response mediated by pep1 peptides, and has no known connection to auxin response (Huffaker et al., 2006; Ortiz-Morea et al., 2016). As shown in the figure 3E and Figure S3 C,D, 1 h after pep1 pulse, there was a substantial endocytosis of PEPR receptors from the PM. We then tested the effect of auxin on endocytosis of PEPR. In the

presence of both NAA – 5 uM and IAA 10 uM – for 60 min, the rate of pep1 mediated endocytosis of PEPR neither decreases nor increases (Figure S3 C,D). We further confirmed the results by pre-treating the seedlings with auxin (10uM NAA and 10uM IAA); after pretreatment, we pulsed in pep1 and then continued incubating the seedlings in NAA/IAA containing medium for 1 h further – see figure 3E,F. The amount of PEPR internalised remained the same as the mock situation. The results confirmed that auxin does not alter rate of PEPR internalisation.

As a final test, another PIN protein – PIN1, which also is a physiologically important auxin exporter, was tested for auxin-mediated internalisation response (Adamowski and Friml, 2015). We used the line – *pPIN2::PIN1-Dendra*, so as, to express PIN1 in the same tissues as PIN2 and to follow only the protein specific effects of auxin. We used a new device called Lanchip to control drug applications in order to capture early internalisation events. As shown in figure 3G, even at a high concentration of IAA –like 10 uM, there was no increase or decrease from the basal constitutive endocytic rate. Very high concentrations have not been tested, as nano-molar concentrations of IAA has been proven to elicit a substantial internalisation response.

Auxin does affect the internalisation process, but possesses specificity. Only PIN2 internalisation is influenced, specifically - accelerated upon auxin application. This could be manifested by controlling, for example, its phosphorylation status (Barbosa et al., 2018). There is no discernable general effect of auxin on internalisation of unrelated proteins, like PEPR or even a closely related protein, its own exporter - PIN1. Furthermore, we need to understand how and why PIN2 internalisation is under such a tight regulation.

4.2.4 Accelerated internalisation of PIN2 by auxin is clathrin-mediated

There are previous evidences indicating that constitutive PIN internalisation – contributing to a basal internalisation rate - is clathrin-mediated (Dhonukshe et al., 2007), we have obtained more quantified evidences for it and further checked if auxin controls the same clathrin-mediated endocytotic pathway to influence PIN2 endocytic rate.

Over-expression of AUXILIN-LIKE1/2 proteins has been shown to inhibit CCP development and drastically decrease the density of CCPs at the PM. This phenomenon halts the endocytosis process (Adamowski et al., 2018). We have used the inducible Auxilin-like2 over-expression line (*XVE>> Axl2 x pPIN2::PIN2-Dendra*) to check PIN2 internalisation process. After about 24 h of induction of Axl2, we could observe a significant decrease in the basal internalisation rate of PIN2. This proves that PIN2 constitutive internalisation process happens in a clathrin-mediated way (Figure 4A).

We further tested if the auxin increases PIN2 internalisation via CME. We applied IAA 10 uM and NAA 5 uM after 24 h AXL2 induction. That is, we hindered CME in the cells and then tested if auxin can still internalise PIN2. We saw that either of the auxins – NAA or IAA, could no longer promote PIN2 internalisation (figure 4B-D); meaning that auxin indeed regulates PIN2 internalisation via CME.

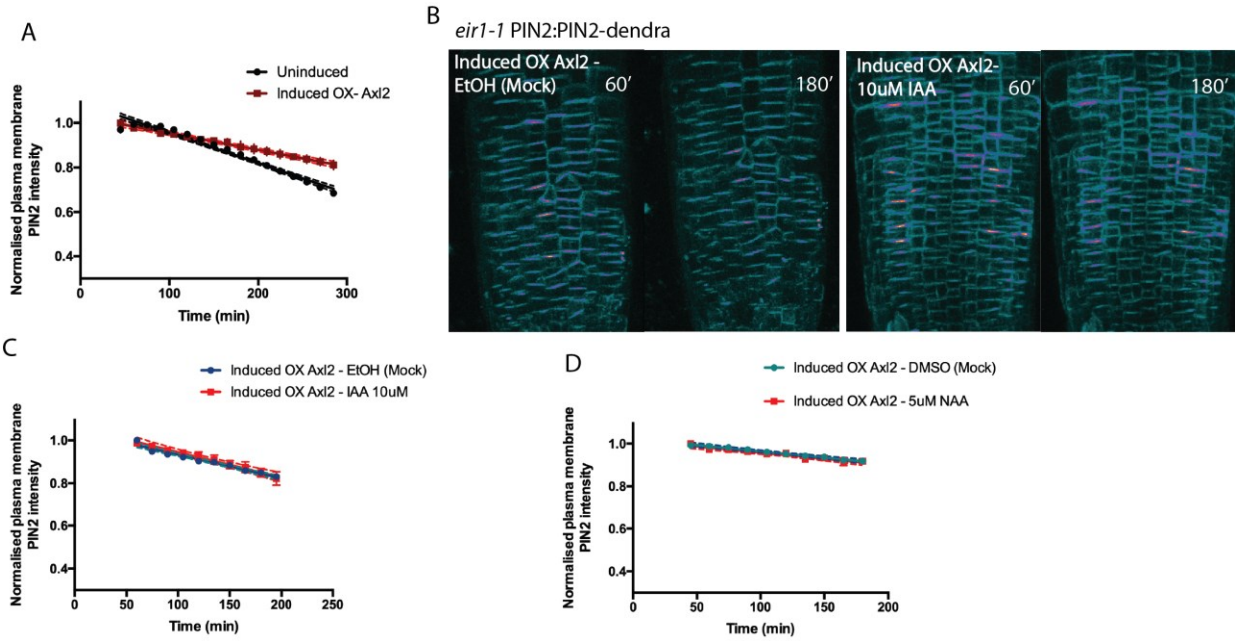

Figure 4: PIN2 internalisation test after inhibition of CME pathway

A) PIN2 internalisation with inhibited CME. Live imaging and quantification of PIN2 at the PM of the root meristem in the photo-converted marker line *eir1-1 pPIN2::PIN2-Dendra x XVE>>Axl2* was done by confocal microcopy. Note that the basal constitutive endocytotic rate was inhibited by inducing AXL2 for 24 h. Following the PM PIN2 intensity continuously in 15-minute interval for the AXL2 induced and uninduced conditions, regression lines were plotted with the curves representing the 95% CI. 4-6 roots per condition; all the epidermal cells in the meristematic zone were measured; N=3. Regression analysis was performed by fitting a linear mixed model. Induced OX-Axl2 condition has lower slope than of uninduced condition; LMER - random effects for position; χ2- 65.82; df=1; p=4.931e-16 ***. **B-D) Effect of auxin after CME inhibition.** The same experimental setup was adopted as described for fig 4A and the effect of 10 uM IAA and 5 uM NAA on PIN2 internalisation was tested after 24 h of AXL2 induction**. B)** Roots depicting the amount PIN2 localised at the PM in AXL2 induced condition (24 h) after Ethanol (mock) and 10 uM IAA treatments. It is to be noted that, after AXL2 induction, auxin cannot accelerate PIN2 internalisation**. C)** Following the PM PIN2 intensity continuously in 15-minute interval in AXL2 induced roots treated with EtOH (mock) and 10 uM IAA, regression lines were plotted with the curves representing the 95% CI. 6 roots per condition; all the epidermal cells in the meristematic zone were measured. Regression analysis was performed by fitting a linear model. Slopes of control and 10uM IAA regression lines are equal; LM; F =0.88; p= 0.34. **D)** Regression plot on PIN2 internalisation after 5uM NAA treatment. Regression analysis was performed by fitting a linear mixed model for 5 roots per condition. Slopes of DMSO (mock) and 5 uM NAA regression lines are equal; LMER - random effects for position; χ2- 0.0027; df=1; p= 0.95.

4.2.5 NAA, over short-term, does not influence the CME machinery

Effects of NAA on clathrin in both the plasma membrane and the endomembrane system have been described before. However under the current light of observations, we decided to further investigate its direct effects on the CME machinery. The endocytic foci at the PM marked by the lines *CLC2-GFP*, *DRP1C-GFP* and *TPLATE-GFP* were investigated. TIRF imaging of the root epidermal cells was done to obtain a time-series consisting of several trajectories of endocytic foci forming and leaving. The density and the lifetime of the foci were analysed.

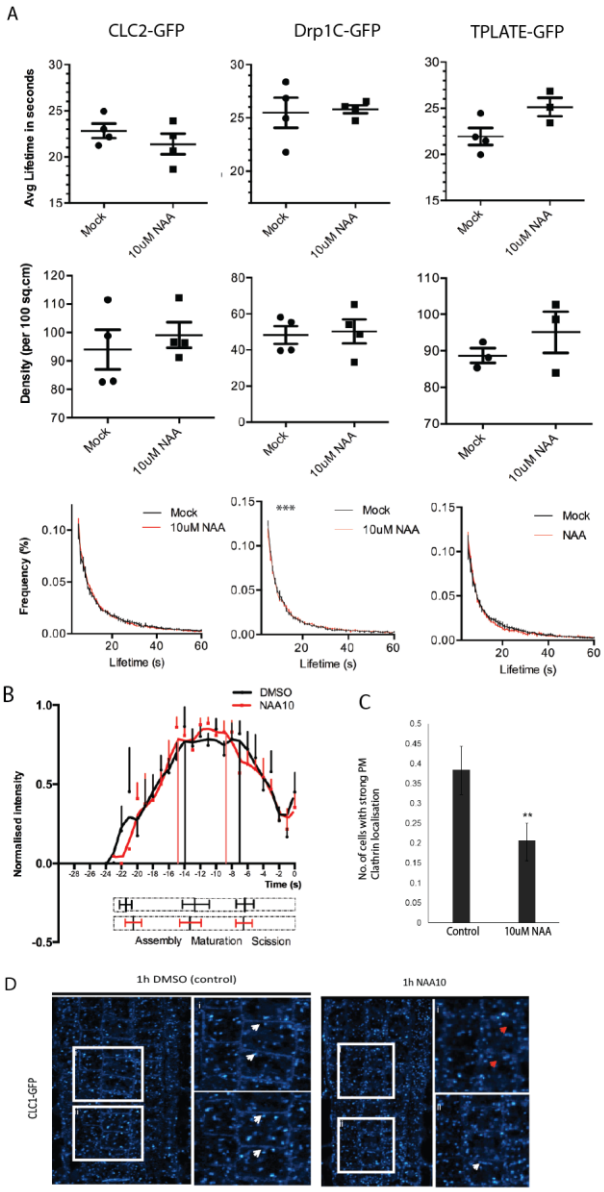

Figure 5: Analysis of clathrin-coated pit development and overall endocytotic rate after NAA treatment

A) Comparative analysis: Average lifetime, Density and lifetime distribution of the clathrin machinery proteins at the endocytic foci between NAA and DMSO (mock) treatments. The dynamics of the machinery proteins marked by CLC2-GFP (first column), DRP1C-GFP (middle column) and TPLATE-GFP (last column) were followed after 10 uM NAA for 15 min. Epidermal cells of 3-4 roots were imaged by TIRF microscopy to obtain time-series of endocytic pit development. All the trajectories over 3s were considered. No of trajectories of CLC2-GFP signal that were analysed - in mock: 4 roots with 5890, 4812,5694 and 8255 trajectories obtained from each - in NAA treated condition: 4 roots analysed with 10465, 7095, 21027 and 8108 trajectories obtained from each. No of trajectories of DRP1C-GFP signal that were analysed - in mock: 4 roots with 4921, 3073,2287and 7898 trajectories obtained from each - in NAA treated condition: 4 roots analysed with 3734, 4330, 9039 and 3505 trajectories obtained from each. No of trajectories of TPLATE-GFP signal that were analysed - in mock: 4 roots with 6949, 6896, 5871, 5745 trajectories obtained from each - in NAA treated condition: 3 roots analysed with 5531, 6047 and 6183 trajectories obtained from each. Plots for Average lifetime, density and normalised frequency distribution of lifetime were obtained for each marker line. In the first row, the scatter dot plot representing the average lifetime of all the trajectories obtained from each root. In the second row, a scatter dot plot representing the average density of foci/100 sq. um observed over time in each root is shown. The bars represent the mean with SEM. In the third row, normalised frequency distribution of all the trajectories per root is shown with the bars representing the SEM.

Statistics: Two-tailed t tests on the average lifetime between mock and NAA treated conditions. There were no significant differences. *CLC2-GFP* - Mock vs 10 um NAA p=0.33; *DRP1C-GFP* - Mock vs 10 uM NAA p=0.83; *TPLATE-GFP* - Mock vs 10 uM NAA p=0.069. Two-tailed T tests on the density between mock and NAA treated conditions. There were no significant differences. *CLC2-GFP* - Mock vs 10 um NAA p=0.65; *DRP1C-GFP* - Mock vs 10 uM NAA p=0.81; *TPLATE-GFP* - Mock vs 10 uM NAA p=0.34. Two-way ANOVA analyses were conducted between mock and NAA treated conditions. Lifetime distribution of DRP1C foci varied significantly. *CLC2-GFP* - Mock vs 10 um NAA p>0.99; *DRP1C-GFP* - Mock vs 10uM NAA p=0.0076**; *TPLATE-GFP* - Mock vs 10uM NAA p>0.99. **B) CCP developmental profile after NAA**. CCP developmental profile classified into Assembly, Maturation and scission/release phases as described Loerke et al., 2009. The mean intensity of CLC2-GFP over time is plotted. Each dot represents the mean intensity of all the trajectories of a given condition at that particular time-point of CCP development (102, 72, 95 and 128 from control; 231, 92, 322 and 138 from NAA condition). Note that there is no drastic differences in developmental phases after NAA **C-D) Long-term effect of NAA on CLC density.** 1h- NAA 10 uM treatment on clathrin at the PM. *p35S:CLC1-GFP* line. D) The root meristem is shown with CLC signal localised to both PM and the EE/TGN in control and NAA treated conditions. White arrows indicate strong CLC1 signal at the PM. Red arrows signal low clathrin signal. Note the loss of PM CLC signal after NAA treatment. C) Number of cells with strong CLC1 signal at the PM was manually counted and a normalised histogram was plotted with the error bars indicating 95% CI. T test p<0.01. N=4.

As represented in the figure 5A, after short-term NAA (10 uM, 15 min) treatment, there was no significant increase or decrease in the average lifetime and the density of the endocytic foci. Though a slight increase in the clathrin foci density and a slight dip in their average lifetime could be observed (but they are insignificant). Also there were no significant changes in the lifetime distribution of the clathrin and TPLATE foci at the PM. But DRP1C behave differently after NAA treatment; nevertheless, the average lifetime stayed the same. In order to understand if NAA could alter the CCP development per se (considering the altered behaviour of drp1C foci), we followed the amount of clathrin molecules (CLC2-GFP intensity) assembling in a pit over time. CCP developmental profile of mock and NAA treated conditions were obtained for all the foci of average lifetime ~22-24 s, and the time frame of the progressing phases - assembly, maturation and scission/release phases were marked in figure 5B, as described by Loerke et al., 2009. After NAA treatment, no significant changes in developmental phases could be observed.

We also checked the long-term effects of NAA on clathrin (CLC-GFP) at the PM (10uM NAA, 1 h). This time we saw a decrease in the CLC signal at the PM, indicating a drop in density of the clathrin foci – see figure 5D. Though this is inconsistent with short-term NAA treatment, it is still consistent with the fact that NAA could potentially alter the endocytotic rate by altering endocytic machinery. However, the observed decrease in intensity alone does not implicate modified endocytotic rate. We do not know about the lifetime of the foci (overall rate of endocytosis= Density of CCPs/Average lifetime of the foci). The PM was too affected to focus and capture the foci dynamics by TIRF after 1 h NAA treatment. Due to such technical difficulties, further analysis of endocytic foci could not be performed. Therefore, the effects of long-term NAA treatment on endocytic rate could not be confirmed by TIRF microscopic observation.

In summary, NAA over short-term does not affect the clathrin foci dynamics and has no effect on the clathrin-pit development. However, after longer treatment, NAA causes a decrease in density of clathrin foci at the PM, which could potentially suggest an alteration in endocytotic rate. As previously shown, FM4-64 membrane internalisation rate decreases, but PIN2 endocytic rate increases after NAA treatment. Due to such contradictions, it is unclear as to how NAA regulates endocytosis.

4.2.6 Clathrin-mediated endocytosis maintains the apical polarity of PIN2

It is clear that auxin influences the endocytic rate of PIN2 and also could influence the overall endocytic rate of the cell by modifying the endocytic machinery. Additionally, phosphorylation status of PINs has been proven to be relevant to efficiency of its endocytosis; in addition to maintaining its polarity (Barbosa et al., 2018). Se we checked if such sensitive and tight regulatory controls over CME are significant for PIN2 polarity maintenance in the cells.

To study that, we employed the same tool as described before. After Axl2 over-expression for 24 h, we observed PIN2 localisation in the cells. PIN2 polarity was completely disturbed. In normal conditions, the outer lateral membrane is devoid of PINs, with a clear apical localisation. However, with the lack of endocytic control, PIN2 was completely spread along the entire lateral surface area of the membrane. In addition to such an apolar localisation of

PIN2, indicated by the low polarity index values in the figure, one could observe that there is generally more PIN2 in the membrane (Figure 6A).

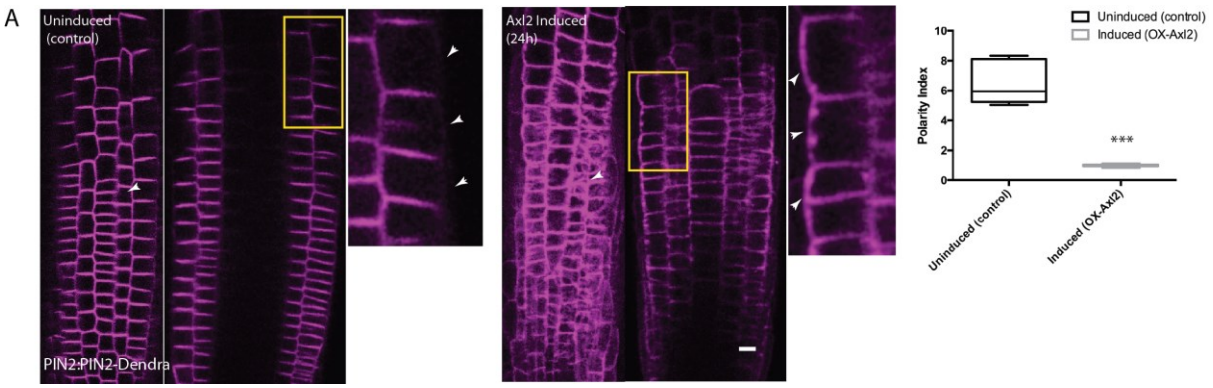

Figure 6: Role of CME in PIN2 polarity maintenance
A) PIN2 polarity after endocytosis inhibition. Line used: *XVE>> Axl2 x pPIN2::PIN2-Dendra eir1-1*. The roots were induced to over-express Axl2 for at least 16 h before imaging. Two planes per root in AXL2 induced and uninduced conditions are displayed. The first image in each condition shows the front view of the root; note the excessive PIN2 localised in the frontal sides of the PM after induction (white arrows). The second image displayed shows the middle of the root. The lateral localisation of PIN2 (also projected in an inset) could be seen clearly, as indicated by arrows. B] PIN2 polarity index after AXL2 induction. 5 roots per condition; 10 cells per root; 3 independent experiments. Cells on the outer lateral sides were quantified. Polarity index = Apical PIN2 intensity/Lateral PIN2 intensity. Two-sided Mann-Whitney U test was performed $p<0.0001$ ***. Scale bar: 20 uM.

In conclusion, clathrin-mediated endocytic regulation of PIN2 maintains its polarity in the cell. Importantly, if and how the polarity of PIN2 varies with respect to time and concentration of auxin is not clearly laid out. Auxin and its down-stream regulatory control of endocytotic rate of PIN2 is potential topic to explore.

4.3 Discussion

We have explored the effects of auxins – NAA and IAA on clathrin-mediated endocytosis. During the initial course of the study, we have shown varying effects of high concentrations of auxin on the endomembrane system. This renders the tools like BFA, which mediates aggregation of the endosomes, and FM4-64 dye, which reaches the EE/TGN and the LE, inappropriate to study auxin. NAA does not alter the endocytic machinery at early time points and has no influence on CCP developmental rate. However, NAA, and IAA even at extremely low concentrations such as 10 nM, can promote PIN2 endocytosis. Notably, endocytosis of other cargoes remains unaltered. All in all, clathrin-mediated endocytotic regulation of PIN2 is essential for maintaining the PIN2 polarity; therefore role of auxin in influencing PIN2 endocytosis could be to impart fast changes to its polarity.

BFA body formation requires aggregation of endosomes and other endomembrane organelles; and auxin, by some means, interferes with this process. This could happen due to variation in the property of the endosomes, such as PIns(4)P ratio or reduction in the number of functional endosomes. Our systematic analysis of the BFA body formation confirms the observations made by Jásik et al., 2016. Nevertheless, it is unwise to further

make conclusions about cargoes in BFA bodies while there are excessive amounts of NAA or IAA in the system. Any conclusions about the amount of cargoes in the BFA body in such conditions have to be revisited. Basically, reduced amount of PINs or any cargo -internalised from the PM or newly synthesized observed within the BFA body cannot be attributed to any direct effect of auxin. They are merely artifacts of disaggregated BFA bodies.

Auxin-mediated endocytotic regulation of PIN2 has been associated to several physiological responses: gravitropism, Hhalotropism, phototropism etc. (Abas et al., 2006; Galvan-Ampudia et al., 2013; Yu et al., 2016). And these responses require an asymmetric localisation of PIN2, which likely directs the auxin flow to one side, leaving the other side auxin-deficient. The highly explored response is Gravitropism. PIN2 is stabilized for around 2 h on the lower side (the gravity vector is perpendicular), where the auxin concentration is surplus. Whereas the other side has increased PIN2 degradation and reduced auxin level promoting cell division. So far, the claim had been that the stabilization of PIN2 in auxin-surplus side is due to inhibitory effect of auxin on endocytosis. Under the current light of evidences, we have to revisit the results.

Gravitropism response is complex and there are possibly many regulatory controls happening - notably, hormonal cross-talks and calcium responses (Bizet et al., 2018; Löfke et al., 2013). One such documented case is the asymmetric distribution of Giberellic acid (GA). Higher level of GA, similar to auxin, is also found at the lower side of the root. Importantly, GA induces retromer-mediated recycling of PIN2 to the plasma membrane; also retromer mutants have defective gravitropic response (Kleine-Vehn et al., 2008; Salanenka et al., 2018). Lack of GA induces degradation of PIN2 (Salanenka et al., 2018). On the other hand, higher NAA levels independently promotes loss of PINs from the PM and degradation (Baster et al., 2013). All of this together with our current results could produce a working model where, auxin and Giberellin that accumulate at the lower side stabilise PINs: while auxin promotes PIN2 endocytosis, GA increases retromer recycling of PIN2 back to the PM. On the upper side, lack of GA induces PIN2 degradation.

Fast response of auxin in stopping the root growth was recently reported to occur through TIR1/AFB–AUX/IAA co-receptor complex in a non-transcriptional way. A similar ‘rapid’ effect of low concentration of IAA in promoting PIN2 endocytosis might also involve the TIR1/AFB – AUX/IAA receptor complex. Role of this co-receptor signaling pathway in auxin mediated PIN2 endocytosis is one the promising directions to study.

4.4 Experimental model and subject details

4.4.1 Accession numbers of the genes

The *Arabidopsis thaliana* genes studied and their corresponding accession numbers are listed: ARA7 – AT4G19640, CLC2 - AT2G40060, DRP1C – AT1G14830, Tplate- AT3G01780, VHA-a1 - At2g28520, PIN2 - AT5G57090, Axl2 - AT4G12770

4.4.2 Plant material used

All the plant material is of the model organism *Arabidopsis thaliana.*

pCLC2::CLC2-GFP and pDRP1C::DRP1C-GFP (Konopka et al., 2008), *p35S::CLC1-GFP* (Wang et al., 2013a), *pLAT52::TPLATE-GFP* x *RPS5A::AP2-RFP* (Gadeyne et al., 2014b), *p35S::N-ST-YFP* (Grebe et al., 2003)**,** *pPIN2::PIN2-Dendra eir1-1* (Salanenka et al., 2018), *pPIN2::PIN2-GFP* x *p35S::ARA7- mRFP* (Ueda et al., 2004; Xu, 2005; Zhang et al., 2016), *UBQ10::CITRINE-1xPH(FAPP1*) (Simon et al., 2014), *PEPR1::PEPR1-GFP pepr1 pepr2* (Ortiz-Morea et al., 2016); *XVE>> Axl2 x pPIN2::PIN2-Dendra eir1-1* (Adamowski et al., 2018); *VHA-a1::VHA-a1-RFP* x *pPIN2::PIN2-GFP eir1-1* was made by crossing *VHA-a1::VHA-a1-RFP* (Dettmer et al., 2006) and *eir1-1 pPIN2::PIN2-GFP* (Xu and Scheres, 2005).

4.4.3 Chemicals used

pep1 peptide sequence : ATKVKAKQRGKEKVSSGRPGQHN (Ortiz-Morea et al., 2016) was commercially synthesized from EZbiolab; dissolved in water. Indole 3- Acetic Acid or IAA - Duchefa Biochemie (Cat no.I0901.0025); dissolved in EtOH or DMSO. 1-Naphthalene Acetic Acid or NAA - Sigma-Aldrich (Cat no. N0640-100G); dissolved in DMSO. Anti Rabbit Arf1 antibody - agrisera AS08325.

4.4.4 Seedling growth conditions

The seedlings were growing in ½MS Agar medium with 1% (w/v) sucrose at 21°C in a 16 h/8 h day/night cycle for 3-4 days for all the experiments. 7-day-old seedlings have been used for following the endocytic foci in roots of endocytic machinery lines.

4.5 Methods

4.5.1 Treatment conditions

All the treatments were carried out in RT in ½ MS medium containing 1% (w/v) sucrose. Except for the PIN2-Dendra experiments where the treatments and imaging were done continuously mounted with drugs dissolved in ½MS solid medium containing 1% Agar.

XVE>> Axl2 x pPIN2::PIN2-Dendra was analysed after induced over-expression of AXL2. 2-day-old seedlings were chemically induced with 2 uM β-estradiol. The seedlings were grown in solid Agar medium in plates overnight for approximately 24 h. The seedlings were continuously under chemical induction during subsequent imaging by confocal microscopy.
FM4-64 uptake: For internalisation test, 3-day-old seedlings of corresponding lines were stained with 2uM FM4-64 dye dissolved in liquid medium. The seedlings were incubated for 2 min, and washed twice; subsequently the roots were imaged at the confocal microscope.

The rest of the details are specified in the figure legends.

4.5.2 Immuno staining

For immuno staining of the roots, we used the InsituPro VSi robot as described in (Sauer et al., 2006). The treatment conditions are reported in the main test. The following antibodies were used: rabbit anti-Arf1 1:500 dilution, rabbit anti-PIN2 1:1000 dilution (Abas et al., 2006).

4.5.3 Microscopy

Confocal microscopy

PIN2 endocytic rate test: Photo conversion and imaging of photo converted PIN2-Dendra at the PM was done in Zeiss LSM700 vertical confocal microscope using Objective Plan-Apochromat 20x / NA 0.8 Air and PMT/T-PMT detectors. The whole root expressing PIN2 Dendra was photo converted from green to red by a 2min excitation by UV, directed from a source of mercury arc lamp through a DAPI filter. The growing root was tracked with the 'Tip Tracker' software as described by (von Wangenheim et al., 2017). The processing of the time-lapse images is described in the following section.

For controlling the treatment environment, the roots were grown in RootChip and imaged at required time points, specifically time points immediately after the flow of drug, as described by Fendrych et al., 2018. Alternatively to RootChip, we also used the device Lanchip. Lanchip was designed to allow immediate drug application without alterations in the focusing plane of the sample. The Lanchip consists of a cylindrical well; a permeable polyester membrane insert and a nylon mesh in between. The cylindrical well was constructed by the local machine shop; it consists of a cover glass at the bottom of the well and a notch on the edge to fit exactly the commercial permeable polyester membrane insert (Corning). Before mounting, a piece of nylon mesh was cut and placed on the surface of the polyester membrane of the insert and then a drop of ½ MS liquid medium was injected on the top, which spread evenly. 4-day-old seedlings were mounted on the surface of the nylon mesh on the insert. The insert with the nylon mesh and seedlings were placed inside of the cylinder well and clipped tightly to the notch on the top of the cylindrical well. Afterwards, the mounted Lanchip was mounted onto the vertical confocal microscope. The drug was injected with a mini plastic pipette into the insert right before imaging.

Imaging of experiments corresponding to FM4-64 internalisation, BFA treatments, PIns(4)P quantifications and VHA-a1-RFP distribution were done with LSM700 inverted confocal microscope using Plan-Apochromat 40x / NA 1.3 water objective and PMT detector. Imaging for PEPR-GFP internalisation was done with LSM880 inverted confocal microscope using Plan-Apochromat 40x / NA 1.2 Water objective and GaAsP PMT detector.

TIRF microscopy

Roots of 7-day-old seedlings were imaged in Olympus IX83 inverted microscope equipped with a Cell^TIRF module and Hamamatsu EM-CCD C9100-13 camera, using OLYMPUS Uapo N 100x/1.49 Oil TIRF objective at 1.6X magnification. Dual channel imaging was done sequentially with the mentioned time interval.

Time-lapse imaging in root was done in the epidermal cells of the transition zone in TIRF mode (Johnson and Vert, 2017b).

4.5.4 Processing and quantification

Quantification of endosomal aggregation size:

The size of the ARA7 and VHA-a1 endosome aggregation were calculated for determining the BFA body size. FIJI ImageJ version2.0.0-rc-67/1.52c was used. 'Threshold' adjustment was applied on the images. The thresholding widow was set to lower threshold values to filter out everything in the background but the aggregates. 'Watershed' processing was further made to emphasize the separation of structures. 'Particle analysis' was performed on the filtered and processed images. Threshold on size was set to filter out the individual

endosomes (3-50 sq um including the point spread from confocal imaging). 'Outlines' option was selected to obtain a final file with all the detected aggregates and their corresponding sizes.

Quantification of endocytotic foci at the PM:
The time lapse images of machinery marker lines to follow the dynamics of endocytic foci were processed with cmeAnalysis particle tracking software published in (Aguet et al., 2013) using Matlab. For specific parameters set in the software refer (Johnson and Vert, 2017). An ROI was drawn and the trajectories were made for each endocytic focus. For density calculations a ROI of dimensions 10umx10um was drawn and an average density over 100 frames were obtained per root.

The developmental profile of the endocytic foci marked by CLC2-GFP was processed as described in (Loerke et al., 2009). Duration of the developmental phases: Assembly, Maturation and scission/release - were characterized based on the average change of intensity of the several trajectories over time. All the trajectories obtained in a root were further filtered to select only the trajectories corresponding to the average lifetime of each root (which generally varies between 18s-24s). Then the average CLC2-GFP intensity varying over the considered lifetime was plotted with all their departure time point converging to 0s. The average Intensity values of CLC2-GFP measured over time in each root were normalised before plotting the intensity profile. The points were connected with a smootheining lowess cuve and the phase transition was marked at the closest the point when the slope of the lowess drops 50% below the minimum slope. Post processing and the final plots were made in graphpadPRISM6.

PIN2 endocytotic rate test:
The time series images made were further processed using FIJI ImageJ version2.0.0-rc-67/1.52c. Maximum intensity projection of the different planes of epidermal PIN2 signal was obtained. ROI covering majority of the meristem was drawn. Mean intensity of photo-converted PIN2 signal was measured over time with multimeasure option. Statistical testes were done in R as discussed below. The final plot was made by PRISM graphpad 6.

Miscellaneous quantifications with ImageJ:
PM and/or cytosolic signal intensity measurements for analysing PEPR-GFP localisation, FM4-64 staining, and PIN2 visualisation in the aggregates were done by drawing free-hand lines and polygons in the individual cells and measuring the mean intensity values.

Statistical analysis:
Statistical analyses for PIN2 internalisation rate between treatments were carried out using R version 1.1.383. The logistic regression analyses were performed by building Generalised linear mixed models (GLMM). The modeling package lme4 was used for it. The significance of the parameter was tested by comparing to reduced models by likelihood ratio test. The models were further tested for the wellness of the fit by BIC and AIC test of deviance (Bolker et al., 2009). The model assumptions were checked by 1) testing for equal variance of the residuals 2) testing for normality of the residuals and 3) testing the normality of the random effects.

The endosomal aggregation size was analysed in R. The statistical tests for all the other experiments were made in PRISM graphpad 6.

4.6 Supplementary information

Supplementary figure S1
Supplementary figure S2
Supplementary figure S3
Supplementary movie1: **Effect of NAA on endosomal movement**. Roots were treated with the following drugs for 60 min and the endosomal movements were observed by confocal microscopy. 4s time lapse movies were made to follow the endosomal movements. Positive control: belbbistatin 500 uM; DMSO (mock); NAA 20 uM; 6 roots each condition; 2 independent experiments.

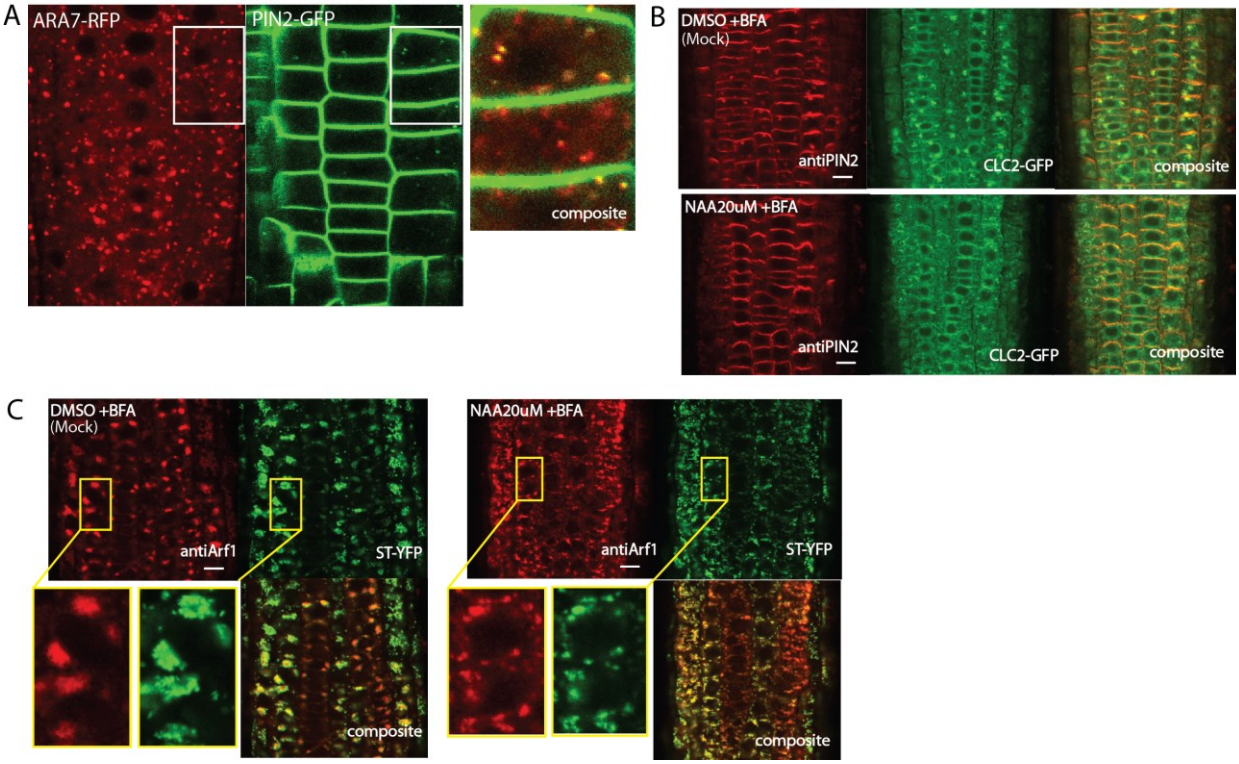

Supplementary figure S1: Effect of auxin on BFA body formation
A) Localisation of PIN2 in Late endosomal structures. Live imaging of the line *ARA7-RFP x PIN2-GFP*. **B)** Immunolabeling of the cargo PIN2 in the BFA body. EE/TGN marker line CLC2-GFP was pre-treated with 20uM NAA or with DMSO (mock) followed by a co-treatment with 50 uM BFA, and then immunolabeled by PIN2 antibody. Note that, after 20 uM NAA, the BFA body consisting of EE/TGN (CLC2-GFP) is very loosely packed with very small, disaggregated compartments; and correspondingly there is less observable PIN2 in the bodies. 8 roots per condition were analysed. Scale bar: 10 um. **C)** Immunolabeling of the EE/TGN by Arf1 antibody to visualize BFA body. Golgi marker line ST-YFP was pre-treated with 20 uM NAA or with DMSO (mock) followed by a co-treatment with 50 uM BFA, and then immunolabeled by Arf1. Note that the BFA body consisting of the arrangement of Golgi apparati (ST-YFP) and EE/TGN structures (Arf1 immunolabel) is loosely packed after NAA 20 um. 8 roots per condition were analysed. Scale bar 10 um.

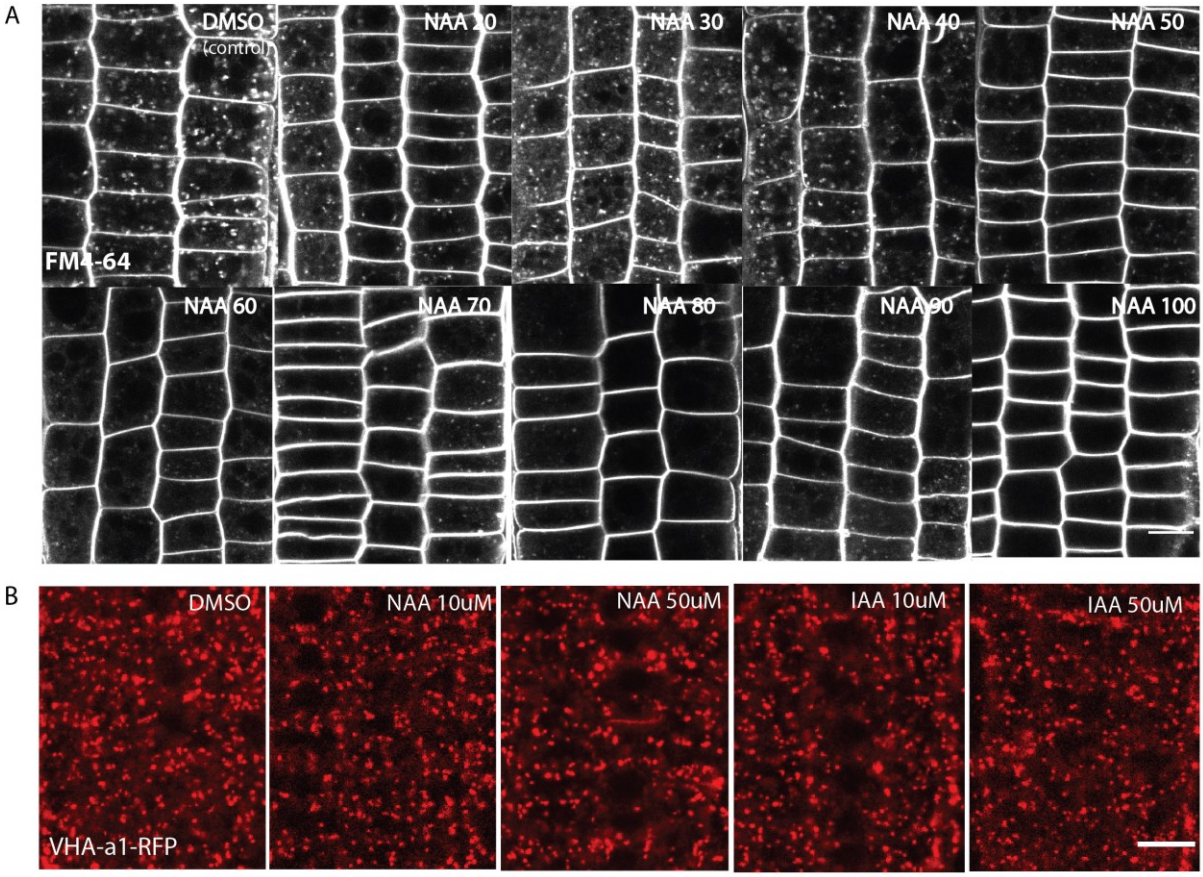

Supplementary figure S2: Effects of NAA and IAA on the EE/TGN

A) FM4-64 staining analysis after NAA. Live imaging by confocal microscopy and quantification of FM4-64 stained membrane at the EE/TGN structures after NAA treatment. The roots were pre-treated for 30 min with varying concentrations of NAA from 20 -100 uM followed by FM4-64 staining; 10 roots each condition. Note that there is less and less FM4-64 stain as the concentration of NAA increases. 10 roots per condition were analysed. **B)** Analysis of EE/ TGN number and size after NAA and IAA. Live imaging of EE/TGN structures, marked by VHA-a1-RFP, after NAA treatment. Varying concentrations of NAA and IAA were applied for 30 min, and the number and sizes of the EE/TGN structures were observed. Note that there is no observable change. At least 7 roots per condition. Scale bar: 10 um.

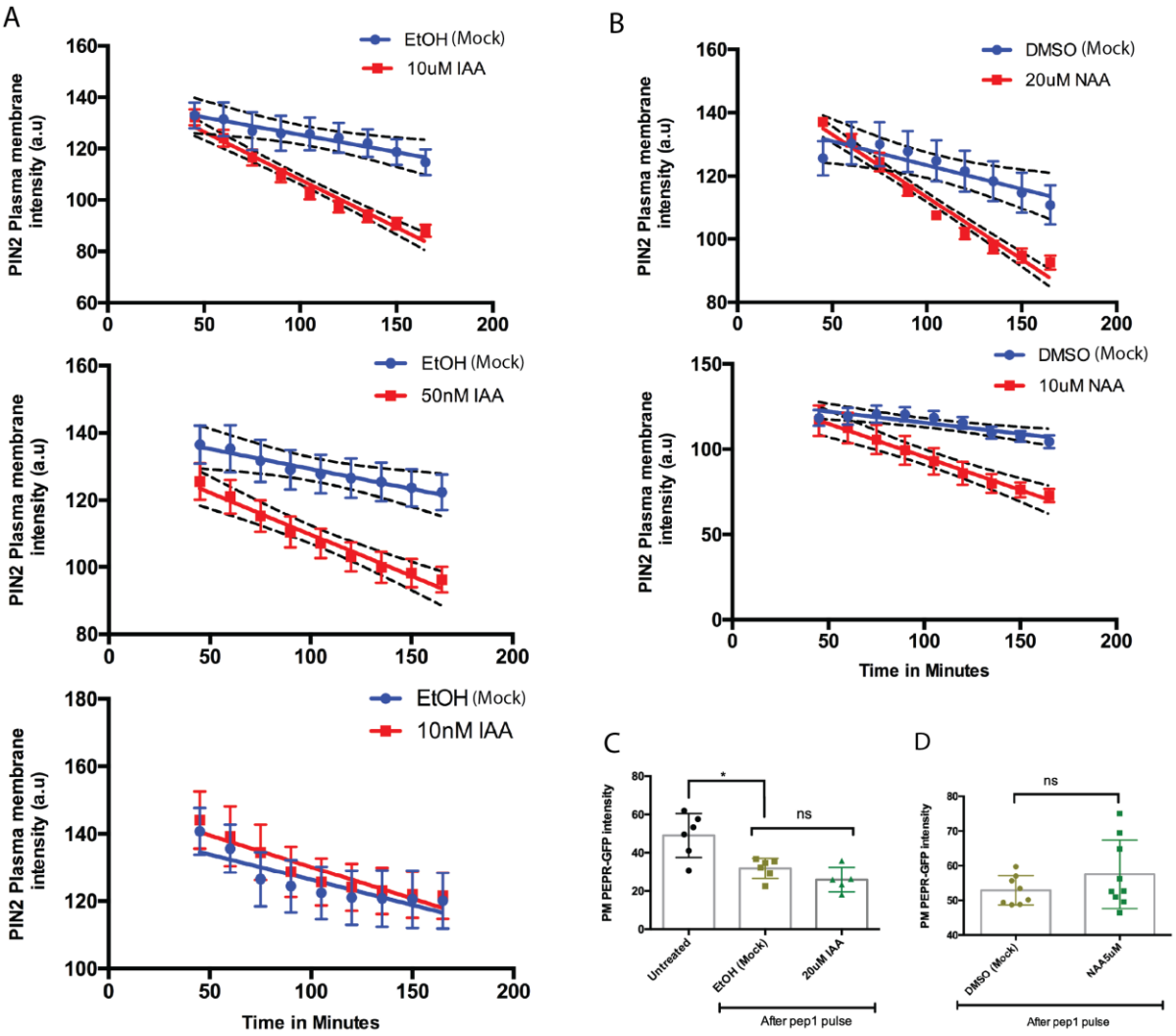

Supplementary figure S3: Effect of auxin on internalisation of different cargoes

A-B) Effect of IAA (A) and NAA (B) on PIN2 internalisation. Live imaging and quantification of PIN2 at the PM of the root meristem in the photo-converted marker line *eir1-1 pPIN2::PIN2-Dendra* was done by confocal microcopy. Note that PIN2 PM intensity decreases faster over time in the presence of both IAA and NAA compared to mock condition. Effect of IAA and NAA along with their respective controls was tested for the rate of loss of photo-converted PIN2-Dendra signal from the PM continuously in 15 min intervals after 45 min of application. Regression analysis was performed by fitting a linear mixed model. Regression lines were plotted with the lines depicting 95% CI. For the test of 10 uM IAA, at least 5 roots were analysed. IAA 10uM slope is significantly higher than of mock; LMER - random effects for position; χ^2- 96.703; p=2.2e-16 ***. For the test of 50 nM IAA, 3 roots per condition were analysed per condition. IAA 50 nm slope is significantly higher than of control; LMER - random effects for position; χ^2- 56.897; p=4.594e-14 ***. For the test of 10nM IAA, at least 5 roots were analysed per condition. IAA 10 nm slope is significantly higher than of mock; LMER - random effects for position; χ^2- 15.70; p=7.187e-05 ***. For the test of 20 uM NAA, at least 5 roots were analysed per condition. NAA 20 uM slope is significantly higher than of mock; LMER - random effects for position; χ^2- 62.216 ; p=3.078e-15 ***. For the test of 10uM NAA, at least 3 roots were analysed per condition. NAA10 uM slope is significantly higher than of mock; LMER - random effects for position; χ^2- 50.17 ; p=1.41e-12 ***. **C)** Effect of auxin on PEPR internalisation is shown. Roots were pep1 treated (200 nM pulse for 1 min) followed by the NAA or IAA treatment with corresponding control treatments. Internal control is seedlings with no pep1 treatment (Untreated). . Scatter dot plot of average PM intensity of roots are shown. Each dot represents the mean intensity of a single root after treatment. Note that auxin treatment does not make any difference. For the experiment with IAA 20 uM at least 5 roots were analysed per condition; 10 cells per root; EtOH (mock) vs IAA 20 uM two-tailed Mann-Whitney U test; p=0.24; Untreated (control)>EtOH (mock) one tailed Mann-Whitney U test; p=0.01. For the experiment with IAA 20 uM NAA 5 uM: at least 8 roots per condition; 10 cells per root; DMSO vs NAA5uM two-tailed Mann-Whitney U test; p=0.41

4.7 External contributions

Imaging and analysis of NAA effect on FM4-64 internalisation was done by Shutang Tan and Lesia Rodriguez. Imaging for auxin's effect on BFA body formation using *VHA-a1-RFP x PIN2-GFP* was done by Shutang Tan. Shutang Tan did imaging for the effect of 100uM NAA and IAA on VHA-a1-RFP. Imaging for the effect of auxin on ARA7-GFP endosomal movement was done by Huibin Han. R script for PIN2 endocytic analysis and CCP developmental analysis were done by Barbara Casillas-Perez. Imaging and post-processing of the dynamics of CME machinery proteins were done by Alexander Johnson. Imaging and analysis on the long-tern effect of NAA on CLC1 was done by Ellie Himschoot.

I would like to thank Matous Glanc and Lanxin Li for helping me set up the PIN2-Dendra experiment; Maciek Adamowski and Matyas Fendrych for all the valuable discussions; Eugenia Russinova for sharing the lines.

5 Conclusion and future prospects

The goal of the thesis was to study different aspects of CME utilising various techniques. Using TAP-MS, we obtained several interactors of clathrin, some of which were functional at the PM potentially regulating CME. Axl1 appears at the end of the lifetime of the CCP very much like other uncoating co-factors observed in animal and yeast systems. However, loss of function of *axl1/2* was not lethal, meaning Auxilin might not be the major co-factor of the uncoating machinery. Moreover, the HSC70 - auxilin/auxilin orthologues co-operatively disassemble clathrin molecules in other systems (Krantz et al., 2013). However, in *Arabidopsis*, we do not observe such a mode of disassembly. The CCVs are observed to remain coated for a longer duration as well. This contradicts the existing model. A comprehensive study on the HSC70-AXL1/2 activity on Arabidopsis CCVs should be done further to get a better resolution of the uncoating process. Based on the results, we might need to look for alternative co-factors, or even alternative uncoating machinery. In addition, the other CLC interactors that were identified, - CAP1 (and its homologue ECA4) and SH3P2 should be characterised to identify its role in CCV formation.

Using TIRF/VAEM techniques we looked at the dynamics of CME machinery proteins at the PM. Such data was critical in identifying the changes in the endocytic machinery, such as density and lifetime of the foci. Using this technique, we observed the effects of over-expression of Auxilin where we could distinctly detect the absence of clathrin foci and very short-lived TPLATE foci at the PM possibly due to abortion of endocytic foci. This explains heavily inhibited endocytosis of membrane, as well as the cargo, PIN2, after induction of Axl1/2 over-expression in cells. Thus we created a cell-biological tool to hinder endocytosis in a controlled way: *XVE>> Axl1/2*.

Using the same techniques we analysed the clathrin pit developmental profile and membrane remodeling dynamics. Analysing the clathrin intensity-time course data at the PM, we deciphered the phases in pit development: Initiation, Maturation and Scission/Release. The average lifetime of clathrin foci was generally shorter compared to other systems: ~ 20 s (Kaksonen and Roux, 2018). When we looked at the seggregation of phase changes, we observed a very long assembly phase - accounting for 45% of the total developmental span of the pit, and a very short maturation phase - 15%. Such a developmental profile signifies the mode of CCP development to follow ‘constant curvature model’, where the membrane remodeling occurs as clathrin polymerises. This means that clathrin polymerisation energy is the major contributor of membrane modification during invagination. This analysis was further complemented by ultrastructural analysis of CCSs at the PM. For the first time in Arabidopsis system, we applied unroofing- metal replica technique and directly observed different populations of CCSs in both the PM and the endomembrane systems. On staging the development of the highly occurring hexagonal pits, we saw a constant radius of curvature across different stages of developing pits, confirming that the common mode of CCP development follows the ‘constant curvature model’.

This poses the question if actin is ever necessary for CCP development; given clathrin polymerisation energy is the major driving force for membrane remodeling. Actin was not polymerizing to form a focus at the endocytic spot aiding the pit development. FM4-64 membrane internalisation and rate of PIN2 internalisation were normal after complete

depolymerisation of actin. In addition there were no changes in the density and lifetimes of the CME machinery proteins at the PM upon actin perturbation. All these observations point towards the fact that actin is not required for CCP development and endocytosis in plants. This however goes against all the existing models of CCP development of high turgor pressure systems where actin-pulling force remodels the membrane for invagination. It is clear that plants have evolved different ways to handle the turgor pressure. Therefore, it is critical that we look for alternative membrane modifiers like Drp and other BAR domain proteins, and clearly resolve their functionality at the PM.

Auxin has been long speculated to inhibit CME through actin stabilization (Murphy and Peer, 2012). Given the fact that actin is not involved in endocytosis; we looked for an alternative mode of regulation of endocytosis by auxin. Moreover the common tools that have used to study endocytosis – FM4-64 staining of the EE/TGN and visualization of endocytosed cargoes by forming BFA body - are not effective in the presence of auxin for reasons unknown still. Both IAA and NAA interfere with the BFA body formation resulting in reduced PIN accumulation, leading to an artifact. Therefore we used an alternative way that does not involve endosomal visualization. We checked if the rate of loss of cargoes from the PM is affected in the presence of auxin. We saw a big increase in rate of endocytosis of PIN2 very rapidly (~ 5 min) at already 50 nM concentration. Interestingly, both IAA and NAA did not modify endocytosis of other cargoes like PEPR and PIN1. This shows that auxin does not inhibit endocytosis, as inferred before using BFA treatments. In contrary, auxin accelerates PIN2 endocytosis. However we are not sure why such a tight control over PIN2 endocytosis regulation exists. We do know that inhibition of CME results in modified PIN2 polarity. Therefore we have planned to look at the changes in PIN2 polarity with respect to CME machinery proteins after auxin treatment - using high-resolution microscopic techniques like SIM.

We have explored the aspects of plant endocytosis, which were left unstudied, by utilising multiple techniques. Major conclusion is that plants do possess differently evolved strategies to perform efficient endocytosis; high turgor pressure combined with muti-cellularity has possibly been the driving evolutionary pressure. This has opened new avenues to explore further.

6 References

Abas, L., Benjamins, R., Malenica, N., Paciorek, T.T., Wiřniewska, J., Moulinier-Anzola, J.C., Sieberer, T., Friml, J., and Luschnig, C. (2006). Intracellular trafficking and proteolysis of the Arabidopsis auxin-efflux facilitator PIN2 are involved in root gravitropism. Nat. Cell Biol. **8**: 249–256.

Adamowski, M. and Friml, J. (2015). PIN-Dependent Auxin Transport: Action, Regulation, and Evolution. Plant Cell Online **27**: 20–32.

Adamowski, M., Narasimhan, M., Kania, U., Glanc, M., De Jaeger, G., and Friml, J. (2018). A Functional Study of AUXILIN-LIKE1 and 2, Two Putative Clathrin Uncoating Factors in Arabidopsis. Plant Cell **30**: tpc.00785.2017.

Aghamohammadzadeh, S. and Ayscough, K.R. (2009). Differential requirements for actin during yeast and mammalian endocytosis. Nat. Cell Biol. **11**: 1039–1042.

Aguet, F., Antonescu, C.N., Mettlen, M., Schmid, S.L., and Danuser, G. (2013). Advances in analysis of low signal-to-noise images link dynamin and AP2 to the functions of an endocytic checkpoint. Dev. Cell **26**: 279–291.

Ahle, S. and Ungewickell, E. (1990). Auxilin, a newly identified clathrin associated protein in coated vesicles fron bovine brain. J. Cell Biol **111**: 19–29.

Ahn, G. et al. (2017). SH3P2 plays a crucial role at the step of membrane tubulation during cell plate formation in plants. Plant Cell: tpc.00108.2017.

Asai, T., Tena, G., Plotnikova, J., Willmann, M.R., Chiu, W.L., Gomez-Gomez, L., Boller, T., Ausubel, F.M., and Sheen, J. (2002). Map kinase signalling cascade in Arabidopsis innate immunity. Nature **415**: 977–983.

Avinoam, O., Schorb, M., Beese, C.J., Briggs, J.A.G., and Kaksonen, M. (2015). Endocytic sites mature by continuous bending and remodeling of the clathrin coat. Science (80-.). **348**: 1369–1372.

Baral, A., Shruthi, K.S., and Mathew, M.K. (2015). Vesicular trafficking and salinity responses in plants. IUBMB Life **67**: 677–686.

Barberon, M., Dubeaux, G., Kolb, C., Isono, E., Zelazny, E., and Vert, G. (2014). Polarization of IRON-REGULATED TRANSPORTER 1 (IRT1) to the plant-soil interface plays crucial role in metal homeostasis. Proc. Natl. Acad. Sci. **111**: 8293–8298.

Barberon, M., Zelazny, E., Robert, S., Conéjéro, G., Curie, C., Friml, J., and Vert, G. (2011). Monoubiquitin-dependent endocytosis of the transporter controls iron uptake in plants. Proc. Natl. Acad. Sci. U. S. A. **108**: e450–e458.

Barbez, E. et al. (2012). A novel putative auxin carrier family regulates intracellular auxin homeostasis in plants. Nature **485**: 119–122.

Barbosa, I.C.R., Hammes, U.Z., and Schwechheimer, C. (2018). Activation and Polarity Control of PIN-FORMED Auxin Transporters by Phosphorylation. Trends Plant Sci. **23**: 523–538.

Barroso-González, J., Machado, J.D., García-Expósito, L., and Valenzuela-Fernández, A. (2009). Moesin regulates the trafficking of nascent clathrin-coated vesicles. J. Biol. Chem. **284**: 2419–2434.

Barth, M. (2004). Identification and functional characterization of Arabidopsis AP180, a binding partner of plant C-adaptin. J. Cell Sci. **117**: 2051–2062.

Bashline, L., Li, S., Zhu, X., and Gu, Y. (2015). The TWD40-2 protein and the AP2 complex cooperate in the clathrin-mediated endocytosis of cellulose synthase to regulate cellulose biosynthesis. Proc. Natl. Acad. Sci. **112**: 12870–12875.

Baster, P., Robert, S., Kleine-Vehn, J., Vanneste, S., Kania, U., Grunewald, W., De Rybel, B., Beeckman, T., and Friml, J. (2013). SCFTIR1/AFB-auxin signalling regulates PIN vacuolar trafficking and auxin fluxes during root gravitropism. EMBO J. **32**: 260–274.

Basu, R., Munteanu, E.L., and Chang, F. (2014). Role of turgor pressure in endocytosis in fission yeast. Mol. Biol. Cell **25**: 679–687.

Beck, K.A., Chang, M., Brodsky, F.M., and Keen, J.H. (1992). Clathrin assembly protein AP-2 induces aggregation of membrane vesicles: A possible role for AP-2 in endosome formation. J. Cell Biol. **119**: 787–796.

Beck, M., Zhou, J., Faulkner, C., MacLean, D., and Robatzek, S. (2012). Spatio-Temporal Cellular Dynamics of the *Arabidopsis* Flagellin Receptor Reveal Activation Status-Dependent Endosomal Sorting. Plant Cell **24**: 4205–4219.

Beevers, L. (1996). Clathrin-Coated Vesicles in Plants. Int. Rev. Cytol. **Volume 167**: 1–35.

Belda-Palazon, B. et al. (2016). FYVE1/FREE1 Interacts with the PYL4 ABA Receptor and Mediates Its Delivery to the Vacuolar Degradation Pathway. Plant Cell **28**: 2291–2311.

Benková, E., Michniewicz, M., Sauer, M., Teichmann, T., Seifertová, D., Jürgens, G., and Friml, J. (2003). Local, Efflux-Dependent Auxin Gradients as a Common Module for Plant Organ Formation. Cell **115**: 591–602.

Bizet, F., Pereda-loth, V., Chauvet, H., Gérard, J., Eche, B., Girousse, C., Courtade, M., Perbal, G., and Legué, V. (2018). Both gravistimulation onset and removal trigger an increase of cytoplasmic free calcium in statocytes of roots grown in microgravity.: 1–10.

Böcking, T., Aguet, F., Harrison, S.C., and Kirchhausen, T. (2011). Single-molecule analysis of a molecular disassemblase reveals the mechanism of Hsc70-driven clathrin uncoating. Nat. Struct. Mol. Biol. **18**: 295–301.

Bolker, B.M., Brooks, M.E., Clark, C.J., Geange, S.W., Poulsen, J.R., Stevens, M.H.H., and White, J.S.S. (2009). Generalized linear mixed models: a practical guide for ecology and evolution. Trends Ecol. Evol. **24**: 127–135.

Bonnett, H.T. and Newcomb, E.H. (1966). Coated vesicles and other cytoplasmic components of growing root hairs of radish. Protoplasma **62**: 59–75.

Boucrot, E., Ferreira, A.P.A., Almeida-Souza, L., Debard, S., Vallis, Y., Howard, G., Bertot, L., Sauvonnet, N., and McMahon, H.T. (2014). Endophilin marks and controls a clathrin-independent endocytic pathway. Nature **517**: 460–465.

Boulant, S., Kural, C., Zeeh, J.C., Ubelmann, F., and Kirchhausen, T. (2011). Actin dynamics counteract membrane tension during clathrin-mediated endocytosis. Nat. Cell Biol. **13**: 1124–1132.

Boutté, Y., Frescatada-Rosa, M., Men, S., Chow, C.-M., Ebine, K., Gustavsson, A., Johansson, L., Ueda, T., Moore, I., Jürgens, G., and Grebe, M. (2010). Endocytosis restricts Arabidopsis KNOLLE syntaxin to the cell division plane during late cytokinesis. EMBO J. **29**: 546–558.

Brach, T., Godlee, C., Moeller-Hansen, I., Boeke, D., and Kaksonen, M. (2014). The initiation of clathrin-mediated endocytosis is mechanistically highly flexible. Curr. Biol. **24**: 548–554.

Brady, R.J., Damer, C.K., Heuser, J.E., and O'Halloran, T.J. (2010). Regulation of Hip1r by epsin controls the temporal and spatial coupling of actin filaments to clathrin-coated pits. J. Cell Sci. **123**: 3652–3661.

Bucher, D., Frey, F., Sochacki, K.A., Kummer, S., Bergeest, J.P., Godinez, W.J., Kräusslich, H.G., Rohr, K., Taraska, J.W., Schwarz, U.S., and Boulant, S. (2018). Clathrin-Adaptor ratio and membrane tension regulate the flat-To-curved transition of the clathrin coat during endocytosis. Nat. Commun. **9**: 1–13.

Buser, C. and Drubin, D.G. (2013). Ultrastructural imaging of endocytic sites in saccharomyces cerevisiae by transmission electron microscopy and immunolabeling. Microsc. Microanal. **19**: 381–392.

Buxbaum, E. and Woodman, P.G. (1995). Selective action of uncoating ATPase towards clathrin-coated vesicles from brain. J. Cell Sci. **108 (Pt 3**: 1295–306.

Carlsson, A.E. (2018). Membrane bending by actin polymerization. Curr. Opin. Cell Biol. **50**: 1–7.

Carlsson, A.E. and Bayly, P. V. (2014). Force generation by endocytic actin patches in budding yeast. Biophys. J. **106**: 1596–1606.

Cheng, Y., Boll, W., Kirchhausen, T., Harrison, S.C., and Walz, T. (2007). Cryo-electron Tomography of Clathrin-coated Vesicles: Structural Implications for Coat Assembly. J. Mol. Biol. **365**: 892–899.

Chinchilla, D., Zipfel, C., Robatzek, S., Kemmerling, B., Nürnberger, T., Jones, J.D.G., Felix, G., and Boller, T. (2007). A flagellin-induced complex of the receptor FLS2 and BAK1 initiates plant defence. Nature **448**: 497–500.

Chisholm, S.T., Coaker, G., Day, B., and Staskawicz, B.J. (2006). Host-microbe interactions: Shaping the evolution of the plant immune response. Cell **124**: 803–814.

Cocucci, E., Aguet, F., Boulant, S., and Kirchhausen, T. (2012). The first five seconds in the life of a clathrin-coated pit. Cell **150**: 495–507.

Colaneri, A.C., Tunc-ozdemir, M., Huang, J.P., and Jones, A.M. (2014). Growth attenuation under saline stress is mediated by the heterotrimeric G protein complex Growth attenuation under saline stress is mediated by the heterotrimeric G protein complex.

Coleman, J. and Evans, D. (1987). Structure and molecular organization of higher plant coated vesicles. J. Cell Sci. **57**.

Coleman, J., Evans, D., Hawes, C., Horsley, D., and Cole, L. (1987). Structure and molecular organization of higher plant coated vesicles. Electrophoresis **57**.

Collings, D.A., Gebbie, L.K., Howles, P.A., Hurley, U.A., Birch, R.J., Cork, A.H., Hocart, C.H., Arioli, T., and Williamson, R.E. (2008). Arabidopsis dynamin-like protein DRP1A: A null mutant with widespread defects in endocytosis, cellulose synthesis, cytokinesis, and cell expansion. J. Exp. Bot. **59**: 361–376.

Collins, A., Warrington, A., Taylor, K.A., and Svitkina, T. (2011). Structural organization of the actin cytoskeleton at sites of clathrin-mediated endocytosis. Curr. Biol. **21**: 1167–1175.

Cremona, O., Di Paolo, G., Wenk, M.R., Lüthi, A., Kim, W.T., Takei, K., Daniell, L., Nemoto, Y., Shears, S.B., Flavell, R.A., McCormick, D.A., and De Camilli, P. (1999). Essential role of phosphoinositide metabolism in synaptic vesicle recycling. Cell **99**: 179–188.

Dawson, J.C., Legg, J.A., and Machesky, L.M. (2006). Bar domain proteins: a role in tubulation, scission and actin assembly in clathrin-mediated endocytosis. Trends Cell Biol. **16**: 493–498.

Dettmer, J., Hong-Hermesdorf, A., Stierhof, Y.-D., and Schumacher, K. (2006). Vacuolar H+-ATPase Activity Is Required for Endocytic and Secretory Traf cking in Arabidopsis. Plant Cell **18**: 715–730.

Dhonukshe, P., Aniento, F., Hwang, I., Robinson, D.G., Mravec, J., Stierhof, Y.D., and Friml, J. (2007). Clathrin-Mediated Constitutive Endocytosis of PIN Auxin Efflux Carriers in Arabidopsis. Curr. Biol. **17**: 520–527.

Di Rubbo, S. et al. (2013). The Clathrin Adaptor Complex AP-2 Mediates Endocytosis of BRASSINOSTEROID INSENSITIVE1 in Arabidopsis. Plant Cell **25**: 2986–2997.

Ding, J., Segarra, V.A., Chen, S., Cai, H., Lemmon, S.K., and Ferro-Novick, S. (2015). Auxilin facilitates membrane traffic in the early secretory pathway. Mol. Biol. Cell **27**: 1–36.

Dmitrieff, S. and Nédélec, F. (2015). Membrane Mechanics of Endocytosis in Cells with Turgor. PLoS Comput. Biol. **11**: 1–23.

Doohan, M.E. and Palevitz, B.A. (1980). Microtubules and coated vesicles in guard-cell protoplasts of Allium cepa L. Planta **149**: 389–401.

Du, Y., Tejos, R., Beck, M., Himschoot, E., Li, H., Robatzek, S., Vanneste, S., and Friml, J. (2013). Salicylic acid interferes with clathrin-mediated endocytic protein trafficking. Proc. Natl. Acad. Sci. **110**: 7946–7951.

Eaton, S. and Martin-Belmonte, F. (2014). Cargo sorting in the endocytic pathway: A key regulator of cell polarity and tissue dynamics. Cold Spring Harb. Perspect. Biol. **6**.

Emons, A.M.C. and Traas, J.A. (1986). Coated pits and coated vesicles on the plasma membrane of plant cells. Eur. J. Cell Biol. **41**: 57–64.

Era, A., Tominaga, M., Ebine, K., Awai, C., Saito, C., Ishizaki, K., Yamato, K.T., Kohchi, T., Nakano, A., and Ueda, T. (2009). Application of lifeact reveals F-actin dynamics in arabidopsis thaliana and the liverwort, marchantia polymorpha. Plant Cell Physiol. **50**: 1041–1048.

Fan, L., Hao, H., Xue, Y., Zhang, L., Song, K., Ding, Z., Botella, M.A., Wang, H., and Lin, J. (2013). Dynamic analysis of Arabidopsis AP2 subunit reveals a key role in clathrin-mediated endocytosis and plant development. Development **140**: 3826–3837.

Fan, L., Li, R., Pan, J., Ding, Z., and Lin, J. (2015). Endocytosis and its regulation in plants. Trends Plant Sci. **20**: 388–397.

Fendrych, M., Akhmanova, M., Merrin, J., Glanc, M., Hagihara, S., Takahashi, K., Uchida, N., Torii, K.U., and Friml, J. (2018). Rapid and reversible root growth inhibition by TIR1 auxin signalling. Nat. Plants **4**: 453–459.

Feraru, E., Paciorek, T., Feraru, M.I., Zwiewka, M., De Groodt, R., De Rycke, R., Kleine-Vehn, J., and Friml, J. (2010). The AP-3 Adaptin Mediates the Biogenesis and Function of Lytic Vacuoles in Arabidopsis. Plant Cell **22**: 2812–2824.

Fowke, L.C. (1980). Ultrastructural aspects of coated vesicles in tobacco protoplasts.

Frank, M., Egile, C., Dyachok, J., Djakovic, S., Nolasco, M., Li, R., and Smith, L.G. (2004). Activation of Arp2/3 complex-dependent actin polymerization by plant proteins distantly related to Scar/WAVE. Proc. Natl. Acad. Sci. **101**: 16379–16384.

Friml, J. (2004). A PINOID-Dependent Binary Switch in Apical-Basal PIN Polar Targeting Directs Auxin Efflux. Science (80-.). **306**: 862–865.

Fuji, K., Shirakawa, M., Shimono, Y., Kunieda, T., Fukao, Y., Koumoto, Y., Takahashi, H., Hara-Nishimura, I., and Shimada, T. (2016). The Adaptor Complex AP-4 Regulates Vacuolar Protein Sorting at the trans-Golgi Network by Interacting with VACUOLAR SORTING RECEPTOR1. Plant Physiol. **170**: 211–219.

Fujimoto, L.M., Roth, R., Heuser, J.E., and Schmid, S.L. (2000). Actin assembly plays a variable, but not obligatory role in receptor-mediated endocytosis in mammalian cells. Traffic **1**: 161–171.

Fujimoto, M., Arimura, S. -i., Ueda, T., Takanashi, H., Hayashi, Y., Nakano, A., and Tsutsumi, N. (2010). Arabidopsis dynamin-related proteins DRP2B and DRP1A participate together in clathrin-coated vesicle formation during endocytosis. Proc. Natl. Acad. Sci. **107**: 6094–6099.

Gadeyne, A. et al. (2014). The TPLATE adaptor complex drives clathrin-mediated endocytosis in plants. Cell **156**: 691–704.

Gall, W.E., Higginbotham, M.A., Chen, C.Y., Ingram, M.F., Cyr, D.M., and Graham, T.R. (2000). The auxilin-like phosphoprotein Swa2p, is required for clathrin function in yeast. Curr. Biol. **10**: 1349–1358.

Galvan-ampudia, C.S., Julkowska, M.M., Darwish, E., Gandullo, J., and Korver, R.A. (2013). Halotropism Is a Response of Plant Roots to Avoid a Saline Environment Halotropism Is a Response of Plant Roots to Avoid a Saline Environment. Curbio **23**: 2044–2050.

Galvan-Ampudia, C.S., Julkowska, M.M., Darwish, E., Gandullo, J., Korver, R.A., Brunoud, G., Haring, M.A., Munnik, T., Vernoux, T., and Testerink, C. (2013). Halotropism is a response of plant roots to avoid a saline environment. Curr. Biol. **23**: 2044–2050.

Galway, M.E., Rennie, P.J., and Fowke, L.C. (1993). Ultrastructure of the endocytotic pathway in glutaraldehyde-fixed and high-pressure frozen/freeze-substituted protoplasts of white spruce (Picea glauca). J. Cell Sci. **106 (Pt 3**: 847–858.

Gao, B., Biosca, J., Craig, E.A., Greene, L.E., and Eisenberg, E. (1991). Uncoating of coated vesicles by yeast hsp70 proteins. J. Biol. Chem. **266**: 19565–19571.

Gilliland, L.U., Kandasamy, M.K., Pawloski, L.C., and Meagher, R.B. (2002). Both vegetative and reproductive actin isovariants complement the stunted root hair phenotype of the Arabidopsis act2-1 mutation. Plant Physiol. **130**: 2199–2209.

Gilliland, L.U., Pawloski, L.C., Kandasamy, M.K., and Meagher, R.B. (2003). \textbackslashtextitArabidopsis actin gene ACT7 plays an essential role in germination and root growth. Plant J. Cell Mol. Biol. **33**: 319–328.

Girao, H., Geli, M.I., and Idrissi, F.Z. (2008). Actin in the endocytic pathway: From yeast to mammals. FEBS Lett. **582**: 2112–2119.

Godlee, C. and Kaksonen, M. (2013). From uncertain beginnings: Initiation mechanisms of clathrin-mediated endocytosis. J. Cell Biol. **203**: 717–725.

Golomb, L., Abu-Abied, M., Belausov, E., and Sadot, E. (2008). Different subcellular localizations and functions of Arabidopsis myosin VIII. BMC Plant Biol. **8**: 1–13.

Goode, B.L., Eskin, J.A., and Wendland, B. (2014). Actin and endocytosis in budding yeast. Genetics **199**: 315–358.

Greener, T., Zhao, X., Nojima, H., Eisenberg, E., and Greene, L.E. (2000). Role of cyclin G-associated kinase in uncoating clathrin-coated vesicles from non-neuronal cells. J. Biol. Chem. **275**: 1365–1370.

Grove, J., Metcalf, D.J., Knight, A.E., Wavre-Shapton, S.T., Sun, T., Protonotarios, E.D., Griffin, L.D., Lippincott-Schwartz, J., and Marsh, M. (2014). Flat clathrin lattices: stable features of the plasma membrane. Mol. Biol. Cell **25**: 3581–3594.

Hawes, C. and Martin, B. (1986). Deep etching of plant cells: Cytoskeleton and coated pits. Cell Biol. Int. Rep. **10**: 985–992.

Henne, W.M., Boucrot, E., Meinecke, M., Evergren, E., Vallis, Y., Mittal, R., and McMahon, H.T. (2010). FCHo proteins are nucleators of Clathrin-Mediated endocytosis. Science (80-.). **328**: 1281–1284.

Heuser, J. and Kirchhausen, T. (1985). Deep-etch views of clathrin assemblies. J. Ultrastruct. Res. Mol. Struct. Res. **92**: 1–27.

Higaki, T. (2015). Real-time Imaging of Plant Cell Surface Dynamics with Variable-angle Epifluorescence Microscopy Video Link. J. Vis. Exp: 1–6.

Huffaker, A., Pearce, G., and Ryan, C.A. (2006). An endogenous peptide signal in Arabidopsis activates components of the innate immune response. Proc. Natl. Acad. Sci. **103**: 10098–10103.

Hurley, J.H. and Hinshaw, J.E. (2012). Dynamin: Membrane scission meets physics. Curr. Biol. **22**: R1047–R1048.

Idrissi, F.Z., Grötsch, H., Fernández-Golbano, I.M., Presciatto-Baschong, C., Riezman, H., and Geli, M.I. (2008). Distinct acto/myosin-I structures associate with endocytic profiles at the plasma membrane. J. Cell Biol. **180**: 1219–1232.

Irani, N.G. et al. (2012). Fluorescent castasterone reveals BRI1 signaling from the plasma membrane. Nat. Chem. Biol. **8**: 583–589.

Ischebeck, T. et al. (2013). Phosphatidylinositol 4,5-Bisphosphate Influences PIN Polarization by Controlling Clathrin-Mediated Membrane Trafficking in Arabidopsis. Plant Cell **25**: 4894–4911.

Ito, E., Fujimoto, M., Ebine, K., Uemura, T., Ueda, T., and Nakano, A. (2012). Dynamic behavior of clathrin in Arabidopsis thaliana unveiled by live imaging. Plant J. **69**: 204–216.

Jarvis., M.C., Fricke, W., Jarvis, M.C., and Brett, C.T. (2000). Turgor pressure, membrane tension and the control of exocytosis in higher plants. Plant. Cell Environ. **23**: 999–1003.

Jásik, J. and Schmelzer, E. (2014). Internalized and newly synthesized Arabidopsis PIN-FORMED2 pass through Brefeldin A compartments: A new insight into intracellular dynamics of the protein by using the photoconvertible fluorescence protein Dendra2 as a tag. Mol. Plant **7**: 1578–1581.

Jásik, J., Bokor, B., Stuchlík, S., Mičieta, K., Turňa, J., and Schmelzer, E. (2016). Effects of auxins on PIN-FORMED2(PIN2) dynamics are not mediated by inhibiting PIN2 endocytosis. Plant Physiol. **172**: pp.00563.2016.

Jiang, R.F., Greener, T., Barouch, W., Greene, L., and Eisenberg, E. (1997). Interaction of auxilin with the molecular chaperone, Hsc70. J. Biol. Chem. **272**: 6141–6145.

Johnson, A. and Vert, G. (2017a). Single Event Resolution of Plant Plasma Membrane Protein Endocytosis by TIRF Microscopy. Front. Plant Sci. **8**: 1–11.

Kadlecova, Z., Spielman, S.J., Loerke, D., Mohanakrishnan, A., Reed, D.K., and Schmid, S.L. (2017). Regulation of clathrin-mediated endocytosis by hierarchical allosteric activation of AP2. J. Cell Biol. **216**: 167–179.

Kaksonen, M. and Roux, A. (2018). Mechanisms of clathrin-mediated endocytosis. Nat. Rev. Mol. Cell Biol. **19**: 313–326.

Kaksonen, M., Toret, C.P., and Drubin, D.G. (2005). A modular design for the clathrin- and actin-mediated endocytosis machinery. Cell **123**: 305–320.

Kang, B.H., Busse, J.S., Dickey, C., Rancour, D.M., and Bednarek, S.Y. (2001). The arabidopsis cell plate-associated dynamin-like protein, ADL1Ap, is required for multiple stages of plant growth and development. Plant Physiol. **126**: 47–68.

Kang, B.H., Nielsen, E., Preuss, M.L., Mastronarde, D., and Staehelin, L.A. (2011). Electron Tomography of RabA4b- and PI-4K??1-Labeled Trans Golgi Network Compartments in Arabidopsis. Traffic **12**: 313–329.

Kang, B.H., Rancour, D.M., and Bednarek, S.Y. (2003). The dynamin-like protein ADL1C is essential for plasma membrane maintenance during pollen maturation. Plant J. **35**: 1–15.

Karimi, M., Inzé, D., and Depicker, A. (2002). GATEWAY^{TM} vectors for Agrobacterium-mediated plant transformation. Trends Plant Sci. **7**: 193–195.

Kelly, B.T., Graham, S.C., Liska, N., Dannhauser, P.N., Höning, S., Ungewickell, E.J., and Owen, D.J. (2014). AP2 controls clathrin polymerization with a membrane-activated switch. Science (80-.). **345**: 459–463.

Khaled, S. Ben, Postma, J., and Robatzek, S. (2015). A Moving View: Subcellular Trafficking Processes in Pattern Recognition Receptor– Triggered Plant Immunity. Annu. Rev. Phytopathol **53**: 379–402.

Kim, S.Y., Xu, Z.-Y., Song, K., Kim, D.H., Kang, H., Reichardt, I., Sohn, E.J., Friml, J., Juergens, G., and Hwang, I. (2013). Adaptor Protein Complex 2-Mediated Endocytosis Is Crucial for Male Reproductive Organ Development in Arabidopsis. Plant Cell **25**: 2970–2985.

Kirchhausen, T. (2000). Tomas Kirchhausen. Blood: 699–727.

Kirchhausen, T. (2009). Imaging endocytic clathrin structures in living cells. Trends Cell Biol. **19**: 596–605.

Kirsch, T. and Beevers, L. (1993). Uncoating of clathrin-coated vesicles by uncoating ATPase from developing peas. Plant Physiol. **103**: 205–212.

Kitakura, S., Vanneste, S., Robert, S., Löfke, C., Teichmann, T., Tanaka, H., and Friml, J. (2011). Clathrin Mediates Endocytosis and Polar Distribution of PIN Auxin Transporters in *Arabidopsis*. Plant Cell **23**: 1920–1931.

Kleine-Vehn, J. et al. (2011). Recycling, clustering, and endocytosis jointly maintain PIN auxin carrier polarity at the plasma membrane. Mol. Syst. Biol. **7**: 1–13.

Kleine-Vehn, J., Leitner, J., Zwiewka, M., Sauer, M., Abas, L., Luschnig, C., and Friml, J. (2008). Differential degradation of PIN2 auxin efflux carrier by retromer-dependent vacuolar targeting. Proc. Natl. Acad. Sci. **105**: 17812–17817.

Klima, A. and Foissner, I. (2008). FM dyes label sterol-rich plasma membrane domains and are internalized independently of the cytoskeleton in characean internodal cells. Plant Cell Physiol. **49**: 1508–1521.

Kolb, C., Nagel, M.-K., Kalinowska, K., Hagmann, J., Ichikawa, M., Anzenberger, F., Alkofer, A., Sato, M.H., Braun, P., and Isono, E. (2015). FYVE1 Is Essential for Vacuole Biogenesis and Intracellular Trafficking in Arabidopsis. Plant Physiol. **167**: 1361–1373.

Konopka, C.A. and Bednarek, S.Y. (2008). Variable-angle epifluorescence microscopy: A new way to look at protein dynamics in the plant cell cortex. Plant J. **53**: 186–196.

Konopka, C.A., Backues, S.K., and Bednarek, S.Y. (2008). Dynamics of Arabidopsis Dynamin-Related Protein 1C and a Clathrin Light Chain at the Plasma Membrane. Plant Cell Online **20**: 1363–1380.

Kost, B., Spielhofer, P., and Chua, N.H. (1998). A GFP-mouse talin fusion protein labels plant actin filaments in vivo and visualizes the actin cytoskeleton in growing pollen tubes. Plant J. **16**: 393–401.

Kotchoni, S.O., Zakharova, T., Mallery, E.L., Le, J., El-Assal, S.E.-D., and Szymanski, D.B. (2009). The Association of the Arabidopsis Actin-Related Protein2/3 Complex with Cell Membranes Is Linked to Its Assembly Status But Not Its Activation. Plant Physiol. **151**: 2095–2109.

Krantz, K.C., Puchalla, J., Thapa, R., Kobayashi, C., Bisher, M., Viehweg, J., Carr, C.M., and Rye, H.S. (2013). Clathrin coat disassembly by the yeast hsc70/Ssa1p and auxilin/Swa2p proteins observed by single-particle burst analysis spectroscopy. J. Biol. Chem. **288**: 26721–26730.

Kukulski, W., Schorb, M., Kaksonen, M., and Briggs, J.A.G. (2012). Plasma membrane reshaping during endocytosis is revealed by time-resolved electron tomography. Cell **150**: 508–520.

Kural, C., Tacheva-Grigorova, S.K., Boulant, S., Cocucci, E., Baust, T., Duarte, D., and Kirchhausen, T. (2012). Dynamics of Intracellular Clathrin/AP1- and Clathrin/AP3-Containing Carriers. Cell Rep. **2**: 1111–1119.

Lam, B.C., Sage, T.L., Bianchi, F., and Blumwald, E. (2001). Role of SH3 domain-containing proteins in clathrin-mediated vesicle trafficking in Arabidopsis. Plant Cell **13**: 2499–512.

Lampe, M., Vassilopoulos, S., and Merrifield, C. (2016). Clathrin coated pits, plaques and adhesion. J. Struct. Biol. **196**: 48–56.

Lauber, M.H., Waizenegger, I., Steinmann, T., Schwarz, H., Mayer, U., Hwang, I., Lukowitz, W., Jürgens, G., Entwicklungsgenetik, L., Tübingen, U., Tübingen, D.-, and Republic, F. (1997). KNOLLE Protein Is a Cytokinesis-specific Syntaxin. Cell **139**: 1485–1493.

Laxmi, A., Pan, J., Morsy, M., and Chen, R. (2008). Light plays an essential role in intracellular distribution of auxin efflux carrier PIN2 in Arabidopsis thaliana. PLoS One **3**: 1–11.

Lemière, J. and Berro, J. (2018). Adaptation of actin dynamics and membrane tension control for yeast endocytosis J. Lemière.

Leyton-Puig, D., Isogai, T., Argenzio, E., Van Den Broek, B., Klarenbeek, J., Janssen, H., Jalink, K., and Innocenti, M. (2017). Flat clathrin lattices are dynamic actin-controlled hubs for clathrin-mediated endocytosis and signalling of specific receptors. Nat. Commun. **8**: 1–14.

Li, D. et al. (2015). Extended-resolution structured illumination imaging of endocytic and cytoskeletal dynamics. Science (80-.). **349**.

Li, Y. (2004). Arabidopsis NAP and PIR Regulate Actin-Based Cell Morphogenesis and Multiple Developmental Processes. Plant Physiol. **136**: 3616–3627.

Lin, W.-Y., Huang, T.-K., and Chiou, T.-J. (2013). NITROGEN LIMITATION ADAPTATION, a Target of MicroRNA827, Mediates Degradation of Plasma Membrane-Localized Phosphate Transporters to Maintain Phosphate Homeostasis in Arabidopsis. Plant Cell **25**: 4061–4074.

Livak, K.J. and Schmittgen, T.D. (2001). Analysis of Relative Gene Expression Data Using Real-Time Quantitative PCR and the $2^{-\Delta\Delta CT}$ Method. Methods **25**: 402–408.

Loerke, D., Mettlen, M., Yarar, D., Jaqaman, K., Jaqaman, H., Danuser, G., and Schmid, S.L. (2009). Cargo and Dynamin Regulate Clathrin-Coated Pit Maturation. PLoS Biol. **7**.

Löfke, C., Zwiewka, M., Heilmann, I., Van Montagu, M.C.E., Teichmann, T., and Friml, J. (2013). Asymmetric gibberellin signaling regulates vacuolar trafficking of PIN auxin transporters during root gravitropism. Proc. Natl. Acad. Sci. **110**: 3627–3632.

Luu, D.T., Martiniãre, A., Sorieul, M., Runions, J., and Maurel, C. (2012). Fluorescence recovery after photobleaching reveals high cycling dynamics of plasma membrane aquaporins in Arabidopsis roots under salt stress. Plant J. **69**: 894–905.

Makihara, M., Watanabe, T., Usukura, E., Kaibuchi, K., Narita, A., Tanaka, N., and Usukura, J. (2016). A new approach for the direct visualization of the membrane cytoskeleton in cryo-electron microscopy: A comparative study with freeze-etching electron microscopy. Microscopy **65**: 488–498.

Marhavý, P., Bielach, A., Abas, L., Abuzeineh, A., Duclercq, J., Tanaka, H., Pařezová, M., Petrášek, J., Friml, J., Kleine-Vehn, J., and Benková, E. (2011). Cytokinin Modulates Endocytic Trafficking of PIN1 Auxin Efflux Carrier to Control Plant Organogenesis. Dev. Cell **21**: 796–804.

Massol, R.H., Boll, W., Griffin, A.M., and Kirchhausen, T. (2006). A burst of auxilin recruitment determines the onset of clathrin-coated vesicle uncoating. Proc. Natl. Acad. Sci. **103**: 10265–10270.

Massol, R.H., Boll, W., Griffin, A.M., and Kirchhausen, T. (2006). A burst of auxilin recruitment determines the onset of clathrin-coated vesicle uncoating. Proc. Natl. Acad. Sci. U. S. A. **103**: 10265–70.

Mbengue, M., Bourdais, G., Gervasi, F., Beck, M., Zhou, J., Spallek, T., Bartels, S., Boller, T., Ueda, T., Kuhn, H., and Robatzek, S. (2016). Clathrin-dependent endocytosis is required for immunity mediated by pattern recognition receptor kinases. Proc. Natl. Acad. Sci. **113**: 11034–11039.

Mcmahon, H.T. and Boucrot, E. (2011). Molecular mechanism and physiological functions of clathrin-mediated endocytosis. Nat. Publ. Gr. **12**: 517–533.

McMahon, H.T. and Boucrot, E. (2011). Molecular mechanism and physiological functions of clathrin-mediated endocytosis. Nat. Rev. Mol. Cell Biol. **12**: 517–533.

Merrifield, C.J., Feldman, M.E., Wan, L., and Almers, W. (2002). Imaging actin and dynamin recruitment during invagination of single clathrin-coated pits. Nat. Cell Biol. **4**: 691–698.

Merrifield, C.J., Moss, S.E., Ballestrem, C., Imhof, B. a, Giese, G., Wunderlich, I., and Almers, W. (1999). Endocytic vesicles move at the tips of actin tails in cultured mast cells. Nat. Cell Biol. **1**: 72–4.

Merrifield, C.J., Qualmann, B., Kessels, M.M., and Almers, W. (2004). Neural Wiskott Aldrich Syndrome Protein (N-WASP) and the Arp 2/3 complex are recruited to sites of clathrin-mediated endocytosis in cultured fibroblasts. Eur. J. Cell Biol. **83**: 13–18.

Mersey, B.G., Griffing, L.R., Rennie, P.J., Fowke, L.C., Mersey, B.G., Griffing, L.R., Rennie, P.J., and Fowke, L.C. (1985). The isolation of coated vesicles from protoplasts of soybean. Planta **163**: 317–327.

Mettlen, M. and Danuser, G. (2014). C 1977).: 1–15.

Miller, S.E., Mathiasen, S., Bright, N.A., Pierre, F., Kelly, B.T., Kladt, N., Schauss, A., Merrifield, C.J., Stamou, D., Höning, S., and Owen, D.J. (2015). CALM Regulates Clathrin-Coated Vesicle Size and Maturation by Directly Sensing and Driving Membrane Curvature. Dev. Cell **33**: 163–175.

Mravec, J. et al. (2009). Subcellular homeostasis of phytohormone auxin is mediated by the ER-localized PIN5 transporter. Nature **459**: 1136–1140.

Murphy, A.S. and Peer, W.A. (2012). Vesicle trafficking: ROP-RIC roundabout. Curr. Biol. **22**: 576–578.

Nagel, M.-K., Kalinowska, K., Vogel, K., Reynolds, G.D., Wu, Z., Anzenberger, F., Ichikawa, M., Tsutsumi, C., Sato, M.H., Kuster, B., Bednarek, S.Y., and Isono, E. (2017). *Arabidopsis* SH3P2 is an ubiquitin-binding protein that functions together with ESCRT-I and the deubiquitylating enzyme AMSH3. Proc. Natl. Acad. Sci.: 201710866.

Naramoto, S., Kleine-Vehn, J., Robert, S., Fujimoto, M., Dainobu, T., Paciorek, T., Ueda, T., Nakano, A., Van Montagu, M.C.E., Fukuda, H., and Friml, J. (2010). ADP-ribosylation factor machinery mediates endocytosis in plant cells. Proc. Natl. Acad. Sci. **107**: 21890–21895.

Nishimura, T., Yokota, E., Wada, T., Shimmen, T., and Okada, K. (2003). An Arabidopsis ACT2 Dominant-Negative Mutation, which Disturbs F-actin Polymerization, Reveals its Distinctive Function in Root Development. Plant Cell Physiol. **44**: 1131–1140.

Noack, L.C. and Jaillais, Y. (2017). Precision targeting by phosphoinositides: how PIs direct endomembrane trafficking in plants. Curr. Opin. Plant Biol. **40**: 22–33.

Ortiz-Morea, F.A. et al. (2016). Danger-associated peptide signaling in *Arabidopsis* requires clathrin. Proc. Natl. Acad. Sci. **113**: 11028–11033.

Paciorek, T., Zažímalová, E., Ruthardt, N., Petrášek, J., Stierhof, Y.D., Kleine-Vehn, J., Morris, D.A., Emans, N., Jürgens, G., Geldner, N., and Friml, J. (2005). Auxin inhibits endocytosis and promotes its own efflux from cells. Nature **435**: 1251–1256.

Palmer, S.E., Smaczynska-de Rooij, I.I., Marklew, C.J., Allwood, E.G., Mishra, R., Johnson, S., Goldberg, M.W., and Ayscough, K.R. (2015). A dynamin-actin interaction is required for vesicle scission during endocytosis in yeast. Curr. Biol. **25**: 868–878.

Park, M., Song, K., Reichardt, I., Kim, H., Mayer, U., Stierhof, Y.-D., Hwang, I., and Jurgens, G. (2013). Arabidopsis mu-adaptin subunit AP1M of adaptor protein complex 1 mediates late secretory and vacuolar traffic and is required for growth. Proc. Natl. Acad. Sci. **110**: 10318–10323.

Pawlowski, N. (2010). Dynamin self-assembly and the vesicle scission mechanism: How dynamin oligomers cleave the membrane neck of clathrin-coated pits during endocytosis. BioEssays **32**: 1033–1039.

Petrasek, J. and Friml, J. (2009). Auxin transport routes in plant development. Development **136**: 2675–2688.

Picco, A. and Kaksonen, M. (2018). Quantitative imaging of clathrin-mediated endocytosis. Curr. Opin. Cell Biol. **53**: 105–110.

Picco, A., Mund, M., Ries, J., Nédélec, F., and Kaksonen, M. (2015). Visualizing the functional architecture of the endocytic machinery. Elife **2015**: 1–29.

Pinot, M., Vanni, S., Pagnotta, S., Lacas-Gervais, S., Payet, L.A., Ferreira, T., Gautier, R., Goud, B., Antonny, B., and Barelli, H. (2014). Polyunsaturated phospholipids facilitate membrane deformation and fission by endocytic proteins. Science (80-.). **345**: 693–697.

Prasad, K., Barouch, W., Greene, L., and Eisenberg, E. (1993). A protein cofactor is required for uncoating of clathrin baskets by uncoating ATPase. J. Biol. Chem. **268**: 23758–23761.

Puthenveedu, M.A. and von Zastrow, M. (2006). Cargo Regulates Clathrin-Coated Pit Dynamics. Cell **127**: 113–124.

Rahman, A., Bannigan, A., Sulaman, W., Pechter, P., Blancaflor, E.B., and Baskin, T.I. (2007). Auxin, actin and growth of the Arabidopsis thaliana primary root. Plant J. **50**: 514–528.

Reddy, A.S. and Day, I.S. (2001). Analysis of the myosins encoded in the recently completed Arabidopsis thaliana genome sequence. Genome Biol. **2**: RESEARCH0024.

Renard, H.-F. et al. (2014). Endophilin-A2 functions in membrane scission in clathrin-independent endocytosis. Nature **517**: 493–496.

Richter, S., Kientz, M., Brumm, S., Nielsen, M.E., Park, M., Gavidia, R., Krause, C., Voss, U., Beckmann, H., Mayer, U., Stierhof, Y.D., and Jürgens, G. (2014). Delivery of endocytosed proteins to the cell-division plane requires change of pathway from recycling to secretion. Elife **2014**: 1–16.

Robert, S. et al. (2010). ABP1 mediates auxin inhibition of clathrin-dependent endocytosis in arabidopsis. Cell **143**: 111–121.

Robinson, D.G. and Pimpl, P. (2014). Clathrin and post-Golgi trafficking: A very complicated issue. Trends Plant Sci. **19**: 134–139.

Roux, A. (2014). Reaching a consensus on the mechanism of dynamin? F1000Prime Rep. **6**: 8–11.

Salanenka, Y., Verstraeten, I., Löfke, C., Tabata, K., Naramoto, S., Glanc, M., and Friml, J. (2018). Gibberellin DELLA signaling targets the retromer complex to redirect protein trafficking to the plasma membrane. Proc. Natl. Acad. Sci.: 201721760.

Saleem, M., Morlot, S., Hohendahl, A., Manzi, J., Lenz, M., and Roux, A. (2015). A balance between membrane elasticity and polymerization energy sets the shape of spherical clathrin coats. Nat. Commun. **6**.

Sauer, M., Balla, J., Luschnig, C., Wis, J., and Reinöhl, V. (2006). regulation of PIN polarity Canalization of auxin flow by Aux / IAA-ARF-dependent feedback regulation of PIN polarity. Genes Dev. **20**: 2902–2911.

Sauer, M., Paciorek, T., Benková, E., and Friml, J. (2006). Immunocytochemical techniques for whole-mount *in situ* protein localization in plants. Nat. Protoc. **1**: 98–103.

Scheuring, D., Viotti, C., Kruger, F., Kunzl, F., Sturm, S., Bubeck, J., Hillmer, S., Frigerio, L., Robinson, D.G., Pimpl, P., and Schumacher, K. (2011). Multivesicular Bodies Mature from the Trans-Golgi Network/Early Endosome in Arabidopsis. Plant Cell Online **23**: 3463–3481.

Schroeter, S., Beckmann, S., and Schmitt, H.D. (2016). Coat/Tether Interactions—Exception or Rule? Front. Cell Dev. Biol. **4**.

Scott, B.L. et al. (2017). Membrane bending begins at any stage of clathrin-coat assembly and defines endocytic dynamics. bioRxiv: 1–11.

Sekiya-Kawasaki, M., Groen, A.C., Cope, M.J.T.V., Kaksonen, M., Watson, H.A., Zhang, C., Shokat, K.M., Wendland, B., McDonald, K.L., McCaffery, J.M., and Drubin, D.G. (2003). Dynamic phosphoregulation of the cortical actin cytoskeleton and endocytic machinery revealed by real-time chemical genetic analysis. J. Cell Biol. **162**: 765–772.

Shinohara, N., Taylor, C., and Leyser, O. (2013). Strigolactone Can Promote or Inhibit Shoot Branching by Triggering Rapid Depletion of the Auxin Efflux Protein PIN1 from the Plasma Membrane. PLoS Biol. **11**.

Simon, M.L.A., Platre, M.P., Assil, S., Van Wijk, R., Chen, W.Y., Chory, J., Dreux, M., Munnik, T., and Jaillais, Y. (2014). A multi-colour/multi-affinity marker set to visualize phosphoinositide dynamics in Arabidopsis. Plant J. **77**: 322–337.

Skruzny, M. et al. (2015). An Organized Co-assembly of Clathrin Adaptors Is Essential for Endocytosis. Dev. Cell **33**: 150–162.

Sochacki, K.A. and Taraska, J.W. (2018). From Flat to Curved Clathrin: Controlling a Plastic Ratchet. Trends Cell Biol.: 1–16.

Song, K., Jang, M., Kim, S.Y., Lee, G., Lee, G.-J., Kim, D.H., Lee, Y., Cho, W., and Hwang, I. (2012). An A/ENTH Domain-Containing Protein Functions as an Adaptor for Clathrin-Coated Vesicles on the Growing Cell Plate in Arabidopsis Root Cells. Plant Physiol. **159**: 1013–1025.

Sousa, R. and Lafer, E.M. (2015). The role of molecular chaperones in clathrin mediated vesicular trafficking. Front. Mol. Biosci. **2**: 26.

Staiger, C.J., Sheahan, M.B., Khurana, P., Wang, X., McCurdy, D.W., and Blanchoin, L. (2009). Actin filament dynamics are dominated by rapid growth and severing activity in the Arabidopsis cortical array. J. Cell Biol. **184**: 269–280.

Stefano, G., Renna, L., Wormsbaecher, C., Gamble, J., Zienkiewicz, K., and Brandizzi, F. (2018). Plant Endocytosis Requires the ER Membrane-Anchored Proteins VAP27-1 and VAP27-3. Cell Rep. **23**: 2299–2307.

Suetsugu, N., Kagawa, T., Wada, M., and Corporation, T. (2005). An Auxilin-Like J-Domain Protein , JAC1 , Regulates Phototropin-Mediated Chloroplast Movement. Plant Physiol. **139**: 151–162.

Sun, Y., Leong, N.T., Wong, T., and Drubin, D.G. (2015). A Pan1/End3/Sla1 complex links Arp2/3-mediated actin assembly to sites of clathrin-mediated endocytosis. Mol. Biol. Cell **26**: 3841–3856.

Swarup, R. and Péret, B. (2012). AUX/LAX family of auxin influx carriers—an overview. Front. Plant Sci. **3**: 1–11.

Takano, J., Miwa, K., Yuan, L., von Wiren, N., and Fujiwara, T. (2005). Endocytosis and degradation of BOR1, a boron transporter of Arabidopsis thaliana, regulated by boron availability. Proc. Natl. Acad. Sci. **102**: 12276–12281.

Tanaka, H., Kitakura, S., Rakusová, H., Uemura, T., Feraru, M.I., de Rycke, R., Robert, S., Kakimoto, T., and Friml, J. (2013). Cell Polarity and Patterning by PIN Trafficking through Early Endosomal Compartments in Arabidopsis thaliana. PLoS Genet. **9**.

Tanchak, M.A., Griffing, L.R., Mersey, B.G., and Fowke, L.C. (1984). Endocytosis of cationized ferritin by coated vesicles of soybean protoplasts. Planta **162**: 481–486.

Tanchak, M.A., Rennie, P.J., and Fowke, L.C. (1988). Ultrastructure of the partially coated reticulum and dictyosomes during endocytosis by soybean protoplasts. Planta **175**: 433–441.

Taylor, M.J., Perrais, D., and Merrifield, C.J. (2011). A high precision survey of the molecular dynamics of mammalian clathrin-mediated endocytosis. PLoS Biol. **9**.

Toshima, J.Y., Toshima, J., Kaksonen, M., Martin, A.C., King, D.S., and Drubin, D.G. (2006). Spatial dynamics of receptor-mediated endocytic trafficking in budding yeast revealed by using fluorescent -factor derivatives. Proc. Natl. Acad. Sci. **103**: 5793–5798.

Trahey, M. and Hay, J.C. (2010). Transport vesicle uncoating: it's later than you think. F1000 Biol. Rep. **2**: 1–6.

Tweten, D.J., Bayly, P. V., and Carlsson, A.E. (2017). Actin growth profile in clathrin-mediated endocytosis. Phys. Rev. E **95**: 052414.

Ueda, T., Uemura, T., Sato, M.H., and Nakano, A. (2004). Functional differentiation of endosomes in Arabidopsis cells. Plant J. **40**: 783–789.

Ungewickell, E., Ungewickell, H., Holstein, S.E.H., Linder, R., Prasad, K., Barouch, W., Martin, B., Greene, L.E., and Eisenberg, E. (1995). Role of auxilin in uncoating clathrin-coated vesicles. Nature **378**: 632–635.

Usukura, E., Narita, A., Yagi, A., Ito, S., and Usukura, J. (2016). An Unroofing Method to Observe the Cytoskeleton Directly at Molecular Resolution Using Atomic Force Microscopy. Sci. Rep. **6**: 1–10.

Van Damme, D., Coutuer, S., De Rycke, R., Bouget, F.-Y., Inze, D., and Geelen, D. (2006). Somatic Cytokinesis and Pollen Maturation in Arabidopsis Depend on TPLATE, Which Has Domains Similar to Coat Proteins. Plant Cell Online **18**: 3502–3518.

Van Leene, J. et al. (2014). An improved toolbox to unravel the plant cellular machinery by tandem affinity purification of Arabidopsis protein complexes. Nat. Protoc. **10**: 169–187.

Vassilopoulos, S. et al. (2014). Actin scaffolding by clathrin heavy chain is required for skeletal muscle sarcomere organization. J. Cell Biol. **205**: 377–393.

Von Wangenheim, D., Hauschild, R., Fendrych, M., Barone, V., Benková, E., and Friml, J. (2017). Live tracking of moving samples in confocal microscopy for vertically grown roots. Elife **6**.

Wang, C. et al. (2016). Differential Regulation of Clathrin and Its Adaptor Proteins during Membrane Recruitment for Endocytosis. Plant Physiol. **171**: 215–229.

Wang, C., Yan, X., Chen, Q., Jiang, N., Fu, W., Ma, B., Liu, J., Li, C., Bednarek, S.Y., and Pan, J. (2013a). Clathrin Light Chains Regulate Clathrin-Mediated Trafficking, Auxin Signaling, and Development in Arabidopsis. Plant Cell **25**: 499–516.

Wang, J.-G., Li, S., Zhao, X.-Y., Zhou, L.-Z., Huang, G.-Q., Feng, C., and Zhang, Y. (2013b). HAPLESS13, the Arabidopsis 1 Adaptin, Is Essential for Protein Sorting at the trans-Golgi Network/Early Endosome. Plant Physiol. **162**: 1897–1910.

Wang, Q., Zhao, Y., Luo, W., Li, R., He, Q., Fang, X., Michele, R.D., Ast, C., von Wiren, N., and Lin, J. (2013b). Single-particle analysis reveals shutoff control of the Arabidopsis ammonium transporter AMT1;3 by clustering and internalization. Proc. Natl. Acad. Sci. **110**: 13204–13209.

Wang, X., Cai, Y., Wang, H., Zeng, Y., Zhuang, X., Li, B., and Jiang, L. (2014). Trans-Golgi Network-Located AP1 Gamma Adaptins Mediate Dileucine Motif-Directed Vacuolar Targeting in Arabidopsis. Plant Cell **26**: 4102–4118.

Wang, Y.S., Motes, C.M., Mohamalawari, D.R., and Blancaflor, E.B. (2004). Green fluorescent protein fusions to Arabidopsis Fimbrin 1 for spatio-temporal imaging of F-actin dynamics in roots. Cell Motil. Cytoskeleton **59**: 79–93.

Watanabe, S., Rost, B.R., Camacho-Pérez, M., Davis, M.W., Söhl-Kielczynski, B., Rosenmund, C., and Jorgensen, E.M. (2013). Ultrafast endocytosis at mouse hippocampal synapses. Nature **504**: 242–247.

Watanabe, S., Trimbuch, T., Camacho-Pérez, M., Rost, B.R., Brokowski, B., Söhl-Kielczynski, B., Felies, A., Davis, M.W., Rosenmund, C., and Jorgensen, E.M. (2014). Clathrin regenerates synaptic vesicles from endosomes. Nature **515**: 228–233.

Whitford, R. et al. (2012). GOLVEN Secretory Peptides Regulate Auxin Carrier Turnover during Plant Gravitropic Responses. Dev. Cell **22**: 678–685.

Widhalm, J.R., Ducluzeau, A.L., Buller, N.E., Elowsky, C.G., Olsen, L.J., and Basset, G.J.C. (2012). Phylloquinone (vitamin K1) biosynthesis in plants: Two peroxisomal thioesterases of lactobacillales origin hydrolyze 1,4-dihydroxy-2-naphthoyl-coa. Plant J. **71**: 205–215.

Xing, Y., Böcking, T., Wolf, M., Grigorieff, N., Kirchhausen, T., and Harrison, S.C. (2010). Structure of clathrin coat with bound Hsc70 and auxilin: mechanism of Hsc70-facilitated disassembly. EMBO J. **29**: 655–665.

Xu, J. (2005). Dissection of Arabidopsis ADP-RIBOSYLATION FACTOR 1 Function in Epidermal Cell Polarity. Plant Cell Online **17**: 525–536.

Xu, J. and Scheres, B. (2005). Dissection of Arabidopsis ADP-RIBOSYLATION FACTOR 1 Function in Epidermal Cell Polarity. Cell **17**: 525–536.

Yamaoka, S., Shimono, Y., Shirakawa, M., Fukao, Y., Kawase, T., Hatsugai, N., Tamura, K., Shimada, T., and Hara-Nishimura, I. (2013). Identification and Dynamics of Arabidopsis Adaptor Protein-2 Complex and Its Involvement in Floral Organ Development. Plant Cell **25**: 2958–2969.

Yang, Y., Xiong, D., Pipathsouk, A., Weiner, O.D., and Wu, M. (2017). Clathrin Assembly Defines the Onset and Geometry of Cortical Patterning. Dev. Cell **43**: 507–521.e4.

Yarar, D. (2004). A Dynamic Actin Cytoskeleton Functions at Multiple Stages of Clathrin-mediated Endocytosis. Mol. Biol. Cell **16**: 964–975.

Yim, Y.-I., Sun, T., Wu, L.-G., Raimondi, A., De Camilli, P., Eisenberg, E., and Greene, L.E. (2010). Endocytosis and clathrin-uncoating defects at synapses of auxilin knockout mice. Proc. Natl. Acad. Sci. **107**: 4412–4417.

Yoshinari, A., Fujimoto, M., Ueda, T., Inada, N., Naito, S., and Takano, J. (2016). DRP1-dependent endocytosis is essential for polar localization and boron-induced degradation of the borate transporter BOR1 in arabidopsis thaliana. Plant Cell Physiol. **57**: 1985–2000.

Yu, Q., Zhang, Y., Wang, J., Yan, X., Wang, C., Xu, J., and Pan, J. (2016). Clathrin-Mediated Auxin Efflux and Maxima Regulate Hypocotyl Hook Formation and Light-Stimulated Hook Opening in Arabidopsis. Mol. Plant **9**: 101–112.

Yuan, L., Loque, D., Kojima, S., Rauch, S., Ishiyama, K., Inoue, E., Takahashi, H., and von Wiren, N. (2007). The Organization of High-Affinity Ammonium Uptake in Arabidopsis Roots Depends on the Spatial Arrangement and Biochemical Properties of AMT1-Type Transporters. Plant Cell Online **19**: 2636–2652.

Žárský, V. (2016). Clathrin in plant defense signaling and execution. Proc. Natl. Acad. Sci. **113**: 10745–10747.

Zhang, C. et al. (2016). Endosidin2 targets conserved exocyst complex subunit EXO70 to inhibit exocytosis. Proc. Natl. Acad. Sci. **113**: E41–E50.

Zhang, Y., Persson, S., Hirst, J., Robinson, M.S., van Damme, D., and Sánchez-Rodríguez, C. (2015). Change your Tplate, change your fate: Plant CME and beyond. Trends Plant Sci. **20**: 41–48.

Zhao, X., Greener, T., Al-Hasani, H., Cushman, S.W., Eisenberg, E., and Greene, L.E. (2001). Expression of auxilin or AP180 inhibits endocytosis by mislocalizing clathrin: evidence for formation of nascent pits containing AP1 or AP2 but not clathrin. J. Cell Sci. **114**: 353–365.

Zhao, Y., Yan, A., Feijó, J.A., Furutani, M., Takenawa, T., Hwang, I., Fu, Y., and Yang, Z. (2010). Phosphoinositides Regulate Clathrin-Dependent Endocytosis at the Tip of Pollen Tubes in *Arabidopsis* and Tobacco. Plant Cell **22**: 4031–4044.

Zhuang, X., Cui, Y., Gao, C., and Jiang, L. (2015). Endocytic and autophagic pathways crosstalk in plants. Curr. Opin. Plant Biol. **28**: 39–47.

Zhuang, X., Wang, H., Lam, S.K., Gao, C., Wang, X., Cai, Y., and Jiang, L. (2013). A BAR-Domain Protein SH3P2, Which Binds to Phosphatidylinositol 3-Phosphate and ATG8, Regulates Autophagosome Formation in Arabidopsis. Plant Cell **25**: 4596–4615.

Zoncu, R., Perera, R.M., Sebastian, R., Nakatsu, F., Chen, H., Balla, T., Ayala, G., Toomre, D., and De Camilli, P. V. (2007). Loss of endocytic clathrin-coated pits upon acute depletion of phosphatidylinositol 4,5-bisphosphate. Proc. Natl. Acad. Sci. **104**: 3793–3798.

Zouhar, J. and Sauer, M. (2014). Helping Hands for Budding Prospects: ENTH/ANTH/VHS Accessory Proteins in Endocytosis, Vacuolar Transport, and Secretion. Plant Cell **26**: 1–13.

Zouhar, J. and Sauer, M. (2014). Helping Hands for Budding Prospects: ENTH/ANTH/VHS Accessory Proteins in Endocytosis, Vacuolar Transport, and Secretion. Plant Cell Online **26**: 4232–4244.

Zwiewka, M., Nodzyński, T., Robert, S., Vanneste, S., and Friml, J. (2015). Osmotic Stress Modulates the Balance between Exocytosis and Clathrin-Mediated Endocytosis in Arabidopsis thaliana. Mol. Plant **8**: 1175–1187.